

Probabilistic approach for fatigue evaluation of welded connections with application to road steel bridges

THÈSE N° 6827 (2015)

PRÉSENTÉE LE 18 DÉCEMBRE 2015

À LA FACULTÉ DE L'ENVIRONNEMENT NATUREL, ARCHITECTURAL ET CONSTRUIT
LABORATOIRE DE LA CONSTRUCTION MÉTALLIQUE
PROGRAMME DOCTORAL EN GÉNIE CIVIL ET ENVIRONNEMENT

ÉCOLE POLYTECHNIQUE FÉDÉRALE DE LAUSANNE

POUR L'OBTENTION DU GRADE DE DOCTEUR ÈS SCIENCES

PAR

Luca D'ANGELO

acceptée sur proposition du jury:

Prof. E. Brühwiler, président du jury
Prof. A. Nussbaumer, directeur de thèse
Prof. M. H. Faber, rapporteur
Prof. M. Vormwald, rapporteur
Prof. B. Sudret, rapporteur



ÉCOLE POLYTECHNIQUE
FÉDÉRALE DE LAUSANNE

Suisse
2015

As you will find in multivariable calculus,
there is often a number of solutions
for any given problem.
— John Nash

a Lina, Alberto e Dario

Acknowledgements

I would like to express my gratitude to Professor Alain Nussbaumer, director of my thesis, for his expert advice through this challenging project and for numerous constructive discussions on a wide range of topics. He gave me the possibility to do my research at ICOM, in a very motivating work environment, and to participate to several conferences and workshops around the world.

I wish to express my sincere thanks to Professor Michael Faber for hosting me 6 weeks at the Civil Engineering department of Technical University of Denmark and for fruitful exchanges of ideas we had during my stay.

I would like to thank Swiss Federal Roads Office (FEDRO) for funding this thesis, which was part of the project AGB 2010/003 "Simulations de trafic intégrant la détermination d'indices de performance structurale".

I would also like to thank Professor Eugen Brühwiler, president of the examining committee and I express my gratitude to the examining committee members for their comments and feedbacks on my thesis work: Professor Michael Faber, Technical University of Denmark; Professor Bruno Sudret, Swiss Federal School Zurich; Professor Michael Vormwald, TU Darmstadt.

Finally I want to express my deepest gratitude to my parents for the strong support and encouragement they provided during my school career, which started 26 years ago.

Lausanne, December 18, 2015

L. D.

Abstract

Fatigue is the third cause for damage of steel structures, while it ranks as first cause for damage of steel bridges. In fatigue analysis of steel bridges the consideration of welded joints is demanded. Traditional fatigue analysis of welded joints under variable amplitude loadings is based on the nominal stress approach, wherein constant amplitude (CA) characteristic S-N curves are used in combination with modified Miner's linear damage accumulation rule. CA characteristic S-N curves, which related the nominal applied stress range, S , to the p -quantile of fatigue life, N , are obtained from fatigue tests at constant stress amplitudes.

In current standards CA characteristic S-N curves are estimated by fitting a linear regression to the experimental failure data points; this approach has several limitations: 1) Run-out test results are neglected; 2) A constant amplitude fatigue limit (CAFL) is somewhat arbitrarily fixed at a given number of cycles; 3) CA characteristic S-N curves are based on fatigue scatter at $2 \cdot 10^6$ cycles, resulting in lack of accuracy in high-cycle fatigue (HCF) region ($N > 5 \cdot 10^6$). Furthermore, use of modified Miner's rule is also affected by limitations: 1) The S-N curve reduced slope, m_2 , used for stress range cycles below the CAFL, has not been sufficiently justified by means of variable amplitude (VA) fatigue test results; 2) Assuming the critical value of damage sum, D_c , equal to unity could lead to inaccurate consideration of load history effects. Limitations mentioned above may substantially affect the accuracy of results when the combination of CA characteristic S-N curves with modified Miner's rule is used in fatigue assessment of existing bridges as well as in fatigue design of new ones.

Many authors proposed to overcome the limitations related to the CA S-N curves by using Maximum Likelihood (ML) method to fit a random CAFL non-linear model to experimental data points (failures and run-outs). Nevertheless, this approach does not give explicit method to compute p -quantile S-N curve from ML estimate of model parameters. Furthermore, since the fitted model is non-linear, the direct comparison with current standards is not straightforward. Concerning the limitations related to use of modified Miner's rule, many research works were carried out to investigate on the damage effect of stress range cycles below the CAFL as well as on the choice of the critical value of damage sum. However, these works only provide general trends and do not present a rigorous statistical approach which allows to overcome

shortcomings of modified Miner's rule.

This thesis provides a rigorous probabilistic approach for estimation of: 1) Characteristic S-N curves for CA and VA fatigue loadings; and 2) Critical damage sum parameter, used in Miner's rule. The new probabilistic approach also includes: 1) A new framework for fatigue reliability assessment of existing bridges; and 2) A new framework for re-calibration of fatigue design partial safety factors. The novel contributions of the presented approach consists in: 1) Using Monte-Carlo Simulations (MCS) method for determining true CA characteristic S-N curve, after having estimated CA S-N model parameters with ML method; 2) Using a new scheme which combines MCS and ML methods and uses VA experimental results to estimate the VA S-N curve reduced slope as well as the critical damage sum random parameter; 3) Giving more insight into realistic bridge fatigue reliability indexes, by defining a new framework which computes probability of fatigue failure event as joint probability of CAFL exceeding event and critical damage accumulation event; and 4) Improving the confidence in fatigue design of new bridges, by revising Eurocode formats for fatigue design of structures and associated partial safety factors.

The application to three study cases of ML-MCS approach for estimation of CA S-N curves and the comparison with current standards, allowed for identifying inaccurate definition of fatigue strength in current standards, especially in high cycle fatigue (HCF) region. Moreover, the application to two study cases of ML-MCS approach for estimation of m_2 and D_c parameters and the comparison with current standards, revealed an inadequate definition of damage accumulation mechanism in application of Miner's rule using current standards. The application of reliability analysis framework to the Venoge bridge study case showed the inaccuracy of Eurocode-based assessment of fatigue reliability index, during the 100 year-design life of the bridge. The issue related to the importance of the choice of target reliability index was also addressed for this study case. The revision of Eurocode formats for fatigue design of structures for two fatigue sensitive details, explained the inexactness of hypothesis of considering the same partial resistance factors for all verification formats and showed that Eurocode design format based on CAFL is highly unsafe.

Key words: fatigue reliability, S-N curves, steel bridges, Monte-Carlo Simulations, Maximum Likelihood, reliability index, partial safety factors

Résumé

Pour les structures en acier, la fatigue se trouve être la troisième cause principale d'endommagement ; elle se classe même comme la première cause d'endommagement des ponts en acier. Lors de l'analyse à la fatigue des ponts en acier, il est demandé d'effectuer la vérification des détails soudés. L'approche traditionnelle de l'analyse à la fatigue des assemblages soudés est celle de la contrainte nominale, laquelle utilise les courbes S-N caractéristiques à amplitude constante en combinaison de la règle de cumul linéaire des dommages selon la loi de Miner modifiée. Les courbes S-N caractéristiques, qui décrivent la relation entre la différence de contrainte nominale appliquée, S , et le quantile p de la durée de vie en nombre de cycles, N , sont obtenues à partir d'essais de fatigue à amplitude constante.

Dans les normes, les courbes S-N sont obtenues en ajustant une régression linéaire sur les points expérimentaux de rupture ; cette approche est affectée par plusieurs limitations : 1) Les points de non-rupture sont négligés ; 2) Une limite de fatigue à amplitude constante (CAFL) est fixée arbitrairement à un certain nombre de cycles ; 3) Les courbes S-N caractéristiques sont basées sur la dispersion de la durée de vie à $2 \cdot 10^6$ cycles, en résulte un manque de précision dans la région à grand nombre de cycles. De plus, l'utilisation de la règle de Miner modifiée est également affectée par les limitations suivantes : 1) L'utilisation de la courbe S-N avec une pente réduite, m_2 , pour les cycles de différences de contraintes inférieures à la CAFL n'a pas été suffisamment justifiée à l'aide de résultats expérimentaux sous charges à amplitude variable ; 2) L'hypothèse d'une valeur critique du cumul des dommages, D_c , égale à 1.0 pourrait amener à une considération inexacte des effets liés à l'histoire des charges. Les limitations mentionnées ci-dessus peuvent affecter sensiblement la précision des résultats lorsque la combinaison des courbes S-N caractéristiques avec la règle de Miner modifiée est utilisée pour l'évaluation à la fatigue des ponts existants ainsi que pour le dimensionnement à la fatigue des nouveaux ponts.

Différents auteurs ont proposé de surmonter les limitations liées aux courbes S-N à amplitude constante en utilisant la méthode "Maximum Likelihood" (ML) pour ajuster un modèle non linéaire avec CAFL aléatoire aux données expérimentales (ruptures et non-ruptures). Néanmoins, cette approche ne donne pas de méthode explicite pour calculer les quantiles p de

la courbe S-N à partir des estimations ML des paramètres du modèle. En outre, puisque le modèle ajusté n'est pas linéaire, la comparaison avec les normes existantes ne s'effectue pas directement. Concernant les limitations liées à l'utilisation de la règle de Miner modifiée, de nombreux travaux de recherche ont été effectués pour étudier l'effet des cycles situés au-dessous de la CAFL sur le processus d'endommagement. Cependant, ces travaux ne fournissent que des tendances générales et ne présentent pas une approche statistique rigoureuse permettant de surmonter les limitations de la loi de Miner modifiée.

Cette thèse propose une approche probabiliste rigoureuse pour l'estimation : 1) Des courbes S-N caractéristiques pour des charges de fatigue à amplitude constante et variable ; 2) De la valeur critique du cumul de dommage (règle de Miner). La nouvelle approche probabiliste comprend également : 1) Une nouvelle méthodologie pour l'estimation de la fiabilité en fatigue des ponts existants ; 2) Une nouvelle méthodologie pour la re-calibration des facteurs de sécurité partiels en fatigue. Les contributions originales de cette approche sont : 1) Utiliser des Simulations de Monte-Carlo (MCS) pour déterminer la vraie courbe S-N caractéristique à amplitude constante après avoir estimé les paramètres du modèle avec la méthode ML ; 2) Utiliser un nouveau schéma qui combine les méthodes MCS et ML et qui utilise les données expérimentales à amplitude variable pour estimer la pente réduite de la courbe S-N, m_2 , et la valeur critique de cumul de dommage, D_c ; 3) Apporter un éclairage sur les indices de fiabilité des ponts, en définissant une nouvelle méthodologie qui permet de calculer la probabilité de rupture par fatigue comme probabilité conjointe de l'événement de dépassement de la CAFL et de l'événement d'accumulation de dommage critique ; 4) Améliorer la confiance dans le dimensionnement en fatigue des nouveaux ponts, en révisant les formats de vérification des normes Eurocodes pour les structures et les facteurs de sécurité partiels associés à la fatigue.

L'application à trois cas d'études de l'approche ML-MCS pour l'estimation des courbes S-N à amplitude constante et la comparaison avec les normes actuelles a permis d'identifier une définition inexacte de la résistance en fatigue, en particulier dans la zone à grand nombre de cycles. En outre, l'application à deux cas d'études de l'approche ML-MCS pour l'estimation des paramètres m_2 et D_c et la comparaison avec les normes actuelles a révélé une définition insuffisante du mécanisme d'accumulation de dommage dans l'application de la règle de Miner. L'application de la méthodologie de fiabilité au cas d'étude du pont de la Venoge a montré l'inexactitude des normes Eurocodes dans l'évaluation de l'indice de fiabilité en fatigue, pour une durée de vie nominale de 100 ans. La question liée à l'importance du choix de la valeur cible de l'indice de fiabilité s'est également posée pour ce cas d'étude. La révision des formats des normes Eurocodes pour deux détails sensibles à la fatigue, a montré que l'hypothèse de considérer les mêmes facteurs partiels de résistance pour tous les formats de vérification est inexacte et aussi que le format pour un dimensionnement en fatigue basé sur la CAFL n'est

pas du tout du côté de la sécurité.

Mots clefs : fiabilité en fatigue, courbes S-N, ponts en acier, Simulations de Monte-Carlo, Maximum Likelihood, indice de fiabilité, facteurs partiels de sécurité

Sommario

La fatica é la terza causa di danno delle strutture in acciaio mentre si colloca al primo posto nella classifica delle cause di danno dei ponti in acciaio. L'analisi a fatica dei ponti in acciaio richiede la verifica delle giunzioni saldate. L'approccio tradizionale di verifica a fatica delle giunzioni saldate é quello della tensione nominale, che consiste nell'utilizzare le curve caratteristiche S-N per carichi ad ampiezza costante insieme alla regola di cumulo lineare del danno, secondo la regola di Miner modificata. Le curve S-N, che descrivono la relazione tra la differenza nominale di tensione applicata, S , e il quantile p della vita a fatica in numero di cicli, N , sono ottenute mediante prove sperimentali a fatica effettuate con carichi ad ampiezza costante.

Nelle norme attuali le curve caratteristiche S-N sono ottenute mediante regressione lineare sull'insieme dei punti sperimentali di rottura. Quest'approccio é caratterizzato da diversi limiti: 1) I punti di non-rottura non sono presi in considerazione; 2) Il limite di fatica ad ampiezza costante (CAFL) viene fissato arbitrariamente ad un determinato numero di cicli; 3) Le curve S-N caratteristiche vengono calcolate sulla base della dispersione della vita a fatica a 2 milioni di cicli, con conseguente difetto di precisione nella zona ad alto numero di cicli. Inoltre la regola di Miner modificata é caratterizzata dai seguenti limiti: 1) L'utilizzo della curva S-N con una pendenza ridotta, m_2 , per cicli con differenza di tensione inferiore alla CAFL, non é stato sufficientemente giustificato mediante l'uso di risultati sperimentali; 2) L'utilizzo di un valore critico del danno accumulato uguale a 1.0 potrebbe portare ad una valutazione inesatta degli effetti legati alla storia dei carichi. I limiti menzionati sopra influenzano fortemente l'accuratezza dei risultati allorché le curve S-N caratteristiche sono utilizzate insieme alla regola di Miner per la verifica a fatica di ponti esistenti o per la progettazione a fatica di nuovi ponti.

Diversi autori hanno proposto di risolvere i problemi legati all'utilizzo delle curve S-N proposte nelle norme, utilizzando il metodo di Massima Verosimiglianza per effettuare il fitting di un modello lineare con limite di fatica aleatorio su un insieme completo di punti sperimentali (che include sia punti di rottura che di non-rottura). Tuttavia quest'approccio non fornisce un metodo esplicito per calcolare i quantili p della vita a fatica a partire dalle stime di massima

verosimiglianza dei parametri del modello S-N. Inoltre, poiché il modello S-N di regressione non è lineare, non è possibile effettuare un confronto diretto con le curve S-N delle norme attuali. Riguardo le limitazioni legate all'utilizzo della regola di Miner modificata, esistono numerosi studi di ricerca focalizzati sull'effetto dei cicli con differenza di tensione inferiore al limite di fatica sul cumulo di danno. Tuttavia questi studi danno solo delle indicazioni qualitative e non forniscono un approccio statistico rigoroso che permetta di superare le limitazioni legate all'utilizzo della regola di Miner modificata.

Questa tesi propone un nuovo metodo probabilistico che permette di stimare: 1) Le curve caratteristiche S-N per carichi di fatica ad ampiezza costante e variabile; 2) Il valore critico del danno accumulato da utilizzare nella regola di Miner. Il nuovo metodo comprende anche: 1) Una nuova metodologia per la verifica a fatica dei ponti esistenti; 2) Una nuova metodologia per la ricalibrazione dei fattori parziali di sicurezza a fatica. Il contributo originale di questa tesi consiste nei seguenti punti: 1) Utilizzo del metodo Monte Carlo per la stima delle curve caratteristiche S-N dopo aver determinato i parametri del modello S-N mediante il metodo di Massima Verosimiglianza; 2) Utilizzo di un nuovo schema che combina il metodo Monte Carlo e il metodo di Massima Verosimiglianza e che utilizza i risultati sperimentali delle prove a fatica effettuate con carichi ad ampiezza variabile, per stimare la pendenza ridotta della curva S-N e il valore critico del danno accumulato; 3) Definizione di una nuova metodologia che permette di calcolare la probabilità di rottura a fatica come probabilità congiunta di eccedenza del limite di fatica e del cumulo critico di danno, migliorando l'accuratezza della stima degli indici di affidabilità dei ponti; 4) Miglioramento dell'affidabilità nella progettazione a fatica dei nuovi ponti mediante la revisione delle norme europee e dei fattori parziali di sicurezza associati alla fatica.

L'applicazione del nuovo metodo per la stima delle curve caratteristiche S-N a tre casi di studio e il confronto con le norme attuali ha svelato una definizione inaccurata della resistenza a fatica, in particolare nella zona ad alto numero di cicli. Inoltre l'applicazione del nuovo metodo per la stima dei parametri della regola di Miner a due casi di studio ed il confronto con le norme attuali ha rivelato una definizione insufficiente del meccanismo di cumulo del danno nell'applicazione della regola di Miner. L'applicazione della metodologia per la valutazione dei ponti esistenti al caso del ponte sulla Venoge ha mostrato l'inesattezza delle norme europee nel calcolo dell'indice di affidabilità a fatica, nel corso della durata di vita nominale di 100 anni. Inoltre la questione legata alla scelta del valore di target dell'indice di affidabilità è stata analizzata per lo stesso caso di studio. La revisione dei format delle norme europee per la progettazione a fatica, per due dettagli tipici, ha mostrato che l'ipotesi di considerare gli stessi fattori parziali di sicurezza per tutti i format di verifica è inesatta e che nelle norme europee attuali il format di progettazione a fatica basato sul limite di fatica risulta fortemente rischioso.

Parole chiave: affidabilità strutturale a fatica, curve S-N, ponti in acciaio, metodo Monte Carlo, metodo di Massima Verosimiglianza, indice di affidabilità, fattori parziali di sicurezza

Contents

Acknowledgements	i
Abstract (English/Français/Italiano)	iii
List of figures	xvii
List of tables	xxi
Nomenclature and definitions	xxiii
1 Introduction	1
1.1 Background: fatigue of welded joints	1
1.1.1 CA S-N curves	2
1.1.2 Cycle counting methods	3
1.1.3 Damage accumulation	3
1.2 Problem statement	5
1.3 Objectives	6
1.4 Structure of the thesis	6
2 S-N curves for constant amplitude loadings	9
2.1 Introduction	9
2.2 Eurocode statistical approach for estimation of S-N curves	12
2.3 New probabilistic approach	14
2.3.1 CA S-N stochastic model	14
2.3.2 ML estimation of model parameters	17
2.3.3 MCS estimation of p-quantile S-N curve	17
2.3.4 Mean stress effect	20
2.4 Study cases	20
2.4.1 Cover plate	21
2.4.2 In-plane gusset	21
2.5 Results	25
	xiii

Contents

2.5.1	S-N curves – Cover plate	27
2.5.2	S-N curves – In-plane gusset	29
2.6	Conclusions and discussion	36
3	S-N curves for variable amplitude loadings	39
3.1	Introduction	39
3.2	New probabilistic approach	44
3.2.1	ML-MCS estimation of VA S-N stochastic model	45
3.3	Study cases	49
3.3.1	Cover Plate	49
3.3.2	In-plane gusset	49
3.4	Results	52
3.5	Conclusions and discussion	70
4	Fatigue reliability assessment of existing bridges	73
4.1	Introduction	73
4.2	New framework for fatigue reliability analysis	75
4.3	Study case	78
4.3.1	Traffic analysis	80
4.3.2	Fatigue resistance models	82
4.3.3	Resolution of reliability problem $P(E_1^*)$	83
4.3.4	Resolution of reliability problem $P(E_2)$	85
4.4	Results	88
4.4.1	Event E_1^* : Critical damage accumulation	88
4.4.2	Event E_2 : CAFL exceedance	91
4.4.3	Event $E_1 \cap E_2$: fatigue failure	94
4.5	Conclusions and discussion	99
5	Calibration of fatigue partial safety factors	103
5.1	Introduction	103
5.2	New framework for partial safety factor calibration	107
5.2.1	Verification scheme 1: based on CAFL	108
5.2.2	Verification scheme 2: based on CA equivalent stress range	110
5.2.3	Verification scheme 3: based on damage accumulation	112
5.3	Study cases	114
5.4	Results	117
5.4.1	Example of fatigue design based on verification scheme 3	120
5.5	Conclusions and discussion	123

6	Conclusions	127
6.1	General conclusions	128
6.2	Future works	129
A	Confidence and prediction bounds for fatigue S-N curves	135
A.1	Confidence intervals	136
A.2	Large sample confidence intervals	136
A.2.1	Confidence interval for the mean	136
A.2.2	Confidence interval for the standard deviation	138
A.3	Confidence intervals of S-N curves - IIW approach	138
A.4	Prediction intervals	141
A.5	Prediction intervals of S-N curves - Eurocode approach	141
A.6	Discussion	142
A.6.1	Numerical example	143
B	Matlab Toolboxes	145
B.1	Toolbox TB1	146
B.2	Toolbox TB2	147
B.3	Toolbox TB3	148
	Bibliography	155
	Curriculum Vitae	157

List of Figures

1.1	VA S-N curves	4
1.2	Structure of the thesis	7
2.1	Eurocode statistical approach for estimation of S-N curves	14
2.2	Median CA S-N curve with model parameters (case of $V = \mathcal{N}$)	15
2.3	ML-MCS-based median, 0.05 quantile and linearized 0.05 quantile S-N curves	19
2.4	Cover plate detail	22
2.5	In-plane gusset detail	22
2.6	Cover plate, ML-MCS-based S-N curves	30
2.7	Cover plate with size effect correction, ML-MCS-based S-N curves	30
2.8	Cover plate, Comment. to Eurocode3-based S-N curves	31
2.9	Cover plate with size effect correction, Comment. to Eurocode3-based S-N curves	31
2.10	Cover plate, characteristic S-N curves	32
2.11	Cover plate, with size effect correction, characteristic S-N curves	32
2.12	In-plane gusset, ML-MCS-based S-N curves	33
2.13	In-plane gusset, Comment. to Eurocode3-based S-N curves	33
2.14	In-plane gusset, characteristic S-N curves	34
2.15	Influence of the aleatory uncertainty of the fatigue life and of the CAFL, cover-plate	35
2.16	Influence of the aleatory uncertainty of the fatigue life and of the CAFL, in-plane gusset	35
3.1	Exceedance diagrams for Weibull spectrum with k shape factor. (a) Concave upward spectrum; (b) Concave downward spectrum	43
3.2	ML-MCS-based VA characteristic S-N curve and re-scaled VA characteristic S-N curve	47
3.3	Cover plate, pdf of VA neg. log-Likelihood, no cut-off / $D_c = \mathcal{W}$	55
3.4	Cover plate, Probability plot of VA neg. log-Likelihood, no cut-off / $D_c = \mathcal{W}$	55
3.5	In-plane gusset, pdf of VA neg. log-Likelihood, no cut-off / $D_c = \log \mathcal{N}$	56
3.6	In-plane gusset, Probability plot of VA neg. log-Likelihood, no cut-off / $D_c = \log \mathcal{N}$	56

List of Figures

3.7	Cover plate, pdf of the parameter μ_D , no cut-off / $D_c = \mathcal{W}$	57
3.8	Cover plate, Probability plot of the parameter μ_D , no cut-off / $D_c = \mathcal{W}$	57
3.9	In-plane gusset, pdf of the parameter μ_D , no cut-off / $D_c = \log \mathcal{N}$	58
3.10	In-plane gusset, Probabiltiy plot of the parameter μ_D , no cut-off / $D_c = \log \mathcal{N}$	58
3.11	Cover plate, pdf of the parameter σ_D , no cut-off / $D_c = \mathcal{W}$	59
3.12	Cover plate, Probability plot of the parameter σ_D , no cut-off / $D_c = \mathcal{W}$	59
3.13	In-plane gusset, pdf of the parameter σ_D , no cut-off / $D_c = \log \mathcal{N}$	60
3.14	In-plane gusset, Probability plot of the parameter σ_D , no cut-off / $D_c = \log \mathcal{N}$	60
3.15	Cover plate, negative log-Likelihood plot, no cut-off	61
3.16	Cover plate, negative log-Likelihood notched box plot, no cut-off / $D_c = \mathcal{W}$	61
3.17	In-plane gusset, negative log-Likelihood plot, no cut-off	62
3.18	In-plane gusset, negative log-Likelihood notched box plot, no cut-off / $D_c = \log \mathcal{N}$	62
3.19	Cover plate, MCS-ML characteristic VA S-N curve, no cut-off / $D_c = \mathcal{W}$	66
3.20	Cover plate, characteristic VA S-N curves, no cut-off / $D_c = \mathcal{W}$	66
3.21	In-plane gusset, MCS-ML characteristic VA S-N curve, no cut-off / $D_c = \log \mathcal{N}$	67
3.22	In-plane gusset, characteristic VA S-N curves	67
3.23	Bubble diagram, characteristic damage sums	69
3.24	Cover plate, D_c distribution with outlier disqualification	70
4.1	The Venoge bridge, Ecublens (Switzerland)	78
4.2	In-plane view and elevation of the Venoge bridge	79
4.3	Lane configuration on the Venoge bridge	79
4.4	The critical detail: welded cover plate	79
4.5	Influence line for nominal stress S_n at the critical section, 1 ton crossing axle	80
4.6	Heavy traffic observations ($GTW > 10$ tons)	81
4.7	Empirical pdf of observed yearly GTWs	82
4.8	Observed weekly sum of m-power stress ranges	90
4.9	Probability plot of observed weekly sum of m-power stress ranges	90
4.10	Observed weekly maximum stress ranges	91
4.11	Return level plot of the weekly maximum stress range	92
4.12	Probability plot of z_p	93
4.13	Quantile plot of z_p	93
4.14	Evolution of reliability index β over the design life	94
4.15	Weekly damage growth: Scenarios 1 and 2	96
4.16	Evolution of reliability index β over the design life, considering traffic growth	96
4.17	MCS data histogram and density map for t=100 years. No traffic growth	97
4.18	MCS data histogram and density map for t=100 years. Traffic growth scenario 2	97

4.19 MCS plot for t=100 years. No traffic growth	98
4.20 MCS plot for t=100 years. Traffic growth scenario 2	98
5.1 Relation between characteristic values, design values and partial safety factors	105
5.2 Resistance partial safety factor, verification schemes 1 and 2	109
5.3 Resistance partial safety factor, verification scheme 3	110
5.4 Rayleigh loading spectra, cover plate	113
5.5 Illustration of γ – characteristic return period plot	115
5.6 Return level plot, cover plate, verification scheme 1	118
5.7 Comparison of VA design S-N curves for verification scheme 3, cover plate . . .	119
5.8 Comparison of VA design S-N curves for verification scheme 3, in-plane gusset	119
5.9 Loading model: (a) Stress range spectrum; (b) Traffic composition according to 2006 WIM measurements	121
5.10 Comparison of design values of n_{veh} for verification scheme 3	122
5.11 Relationship between design fatigue life and traffic volume, in-plane gusset . .	122
5.12 Fatigue design verification chart	125
6.1 Bi-linear S-N curve without CAFL	133
A.1 Student's T probability density function	137
A.2 Chi-squared probability density function	139

List of Tables

2.1	Cover plate, CA experimental data-set	23
2.2	In-plane gusset, CA experimental data-set	24
2.3	Cover plate, CA S-N model parameters	26
2.4	Cover plate, CA S-N model corr. matrix, ($V = \mathcal{N}$) case	26
2.5	Cover plate with size effect correction, CA S-N model parameters	26
2.6	Cover plate with size effect correction, CA S-N model corr. matrix, ($V = \mathcal{N}$) case	26
2.7	In-plane gusset, CA S-N model parameters	27
2.8	In-plane gusset, CA S-N model correlation matrix, ($V = \mathcal{N}$) case	27
3.1	Cover plate, VA experimental data-set	50
3.2	In-plane gusset, VA experimental data-set	51
3.3	Sensitivity study on ML-MCS scheme parameters, Cover plate, <i>no cut-off</i> / $D_c = \mathcal{W}$	52
3.4	Cover plate, VA S-N curve parameters	53
3.5	Cover plate, VA S-N model correlation matrix, <i>no cut-off</i> / $D_c = \mathcal{W}$	53
3.6	In-plane gusset, VA S-N curve parameters	53
3.7	In-plane gusset, VA S-N model correlation matrix, <i>no cut-off</i> / $D_c = \log \mathcal{N}$	53
3.8	Cover plate, D_c distributions. Shaded red pdf is the pdf of $\log \mathcal{N}(0, 0.3)$ distrib.	63
3.9	In-plane gusset, D_c distributions. Shaded red pdf is the pdf of $\log \mathcal{N}(0, 0.3)$ distrib.	64
3.10	Characteristic VA S-N curves	68
3.11	Cover plate, outlier disqualification	69
3.12	Cover plate, outlier disqualification: models comparison	70
4.1	Scheme for calculation of β reliability index	83
4.2	Calculation of β_1 : Eurocode S-N model	89
4.3	Calculation of β_1 : Eurocode vs ML-MCS	89
4.4	Calculation of β_2 : Eurocode vs ML-MCS	92
4.5	Calculation of β reliability index	95
5.1	Recommended values for γ_{Mf} , by assuming $\gamma_{Ff} = 1$ (Table 3.1 of [24])	107
5.2	VA S-N model parameters	114

List of Tables

5.3 Resistance partial safety factors and related characteristic return periods ($\gamma_{Ff} =$
1.0) 117

5.4 Comparison of design values for verification schemes 1 and 2 118

A.1 Numerical table 142

Nomenclature and definitions

a	Crack length
$\mathcal{A}(t)$	Crossing axle time history
C	Intercept of generic CA S-N curve in log(S-N) plane (material constant)
$\underline{\underline{c}}$	CA and VA S-N model correlation matrix
CA	Constant Amplitude
CAFL	Constant Amplitude Fatigue Limit
cdf	Cumulative distribution function
c_v	Coefficient of variation
C_1	Proportionality constant in Paris Law
D	Damage sum at failure
d	Observed damage sum at the end of the experimental test
D_c	Critical damage sum (random variable)
$d_{c,5}$	Characteristic value of critical damage sum, corresponding to the median of D_c
D_d	Accumulated damage over the bridge design life
E_c	Characteristic value of action effect
E_1	Critical damage accumulation event
E_1^*	Critical damage accumulation conditioned to CAFL exceeding (conditioned event)
E_2	CAFL exceeding event
EN3	Eurocode 3
EV	Extreme Value probability distribution

Nomenclature and definitions

FAT	Fatigue strength in MPa at $2 \cdot 10^6$ cycles, according to characteristic S-N curve
FE	Finite elements
FL	Finite life: $N < 5 \cdot 10^6$ cycles, convention according to Eurocode
FLS	Fatigue limit state
FORM	First order reliability method
f_Y	Probability density function of random variable Y
F_Y	Cumulative distribution function of random variable Y
\mathcal{G}	Gumbel distribution
GEV	Generalized Extreme Value probability distribution
GTW	Gross Total Weight
$g(\underline{X})$	Limit state function for basic random vector \underline{X}
$H(\cdot)$	Unit step function
HCF	High cycle fatigue: $N \geq 5 \cdot 10^6$ cycles
$\underline{I}(\underline{\theta})$	Fisher information matrix for parameter vector equal to $\underline{\theta}$
k	Shape parameter of Weibull stress range loading spectrum. The spectrum is concave downward for $k < 1$ and it is concave upward for $k > 1$.
knee point	In a CA S-N curve it is the intersection point between the S-N curve and the CAFL; in a VA S-N curve it is the intersection point between the S-N curve having slope equal to m_1 and the S-N curve having slope m_2
K	Stress intensity factor
log(S-N) plane	S-N plane in which both S axis and N axis are plotted in log scale
$L(\underline{\theta})$	Sample likelihood for model parameter vector equal to $\underline{\theta}$
LEFM	Linear Elastic Fracture Mechanics
LS	Least Squares
m	Slope of generic CA S-N curve in log(S-N) plane (< 0)
MCS	Monte-Carlo simulations
ML	Maximum Likelihood
M_k	Geometric correction factor in Paris Law

m_0	Intercept of the CA S-N curve, in the log(S-N) plane
m_1	Slope of the CA S-N curve, in the log(S-N) plane
m'_1	Slope of the CA S-N curve below the knee point, in the log(S-N) plane, for CA S-N bi-linear model without CAFL
m_2	Slope of the VA S-N curve below the CAFL, in the log(S-N) plane
n	Number of stress range cycles applied to the analysed detail
N	Number of stress range cycles to the end of the test
$\log \mathcal{N}$	Log-Normal probability distribution
\mathcal{N}	Normal probability distribution
n_d	Design value of allowed number of cycles which can be applied to analysed detail
n_f	Number of failures
n_r	Number of run-outs
$nLL(\underline{\theta})$	Negative log-likelihood for model parameter vector equal to $\underline{\theta}$
n_{veh}	Design value of allowed number of vehicles
n_1	Number of cycles applied to the analysed detail, with stress range higher than the CAFL
n_2	Number of cycles applied to the analysed detail, with stress range lower than the CAFL
\mathcal{O}	Objective function in MCS scheme for estimation of CA characteristic S-N curves
pdf	Probability density function
P_f	Probability of failure
P_f^t	Target probability of failure
PLR	Profile Likelihood Ratio
p -quantile	Referred to a S-N curve, it indicates the curve which realizes $p \cdot 100\%$ probability of failure
$P_s = 1 - P_f$	Probability of survival
R	Stress ratio
R_c	Characteristic value of resistance

Nomenclature and definitions

$R_d(\mu_{R_d}, \sigma_{R_d})$	Sum of m-power stress ranges over design life (random variable)
RFL RMC	Root mean cube Random Fatigue Limit
r.m.s	Root mean square of stress range spectrum: $\sqrt{\sum(S_i/n)}$
run-out	Number of cycles reached without failure of the specimen at the end of the test, either because the time limits for the test were reached or because other parts of the tested specimen failed
$R_w(\mu_{R_w}, \sigma_{R_w})$	Weekly sum of m-power stress ranges (random variable)
S	Nominal applied stress range
\mathcal{S}	Sample standard deviation
S_c	Characteristic fatigue strength at $2 \cdot 10^6$ cycles
S_{co}	Cut-off stress range
$S_{E,2}$	Equivalent CA stress range at $2 \cdot 10^6$ cycles
S_{max}	Maximum stress range
$S_{max,c}$	Characteristic value of maximum stress range
S_n	Nominal stress
SORM	Second order reliability method
$t_{\alpha,n}$	Inverse of Student's t cdf for probability equal to $\alpha\%$ and n degrees of freedom
V	Natural logarithm of the CAFL (random variable)
VA	Variable Amplitude
$\nu_{.05}$	Characteristic value of the log-CAFL, corresponding to 95% exceeding probability
w	Importance factor
\mathcal{W}	Weibull distribution
WIM	Weigh in motion
$W(\gamma)$	Objective function in framework for calibration of partial safety factors
x_c	Natural logarithm of characteristic fatigue strength, at $2 \cdot 10^6$ cycles
$x_{c_{LS}}$	LS estimate of fatigue strength at $2 \cdot 10^6$ cycles
X_k	Natural logarithm of the stress range at the knee point

$(x_i, y_i) _{i=1 \dots n_{tot}}$	CA fatigue data-set
z	Design factor in fatigue design and limit state equations
$z_p(\tau, \phi, \xi)$	Return level of maximum stress range, following a $GEV(\tau, \phi, \xi)$ probability distribution
α	Confidence level
β	Reliability index associated to the fatigue failure event
β_t	Target reliability index
β_1	Reliability index associated to the critical damage accumulation event
β_2	Reliability index associated to the CAFL exceeding event
γ_F	Partial safety factor for loading
γ_{Ff}	Fatigue partial safety factor for loading
γ_M	Partial safety factor for resistance
γ_{Mf}	Fatigue partial safety factor for resistance
δ	Binary variable which is equal to 1 for a failure and to 0 for a run-out
$\Delta m = m_1 - m_2$	Slope difference, in the log(S-N) plane
ΔK	Difference between the stress intensity factor at the upper and lower limit stresses of the loading cycle
ϵ	Error term in S-N model
η	Number of simulations
η_F	Number of simulations which realize failure condition
η_{iter}, η_{res}	Parameters which define the number of simulations in ML-MCS scheme for estimation of VA S-N model
η_{sam}	Number of simulations in MCS scheme for estimation of CA characteristic S-N curves
θ	CA S-N model vector
Θ	VA S-N model vector
λ_R	Scale parameter of Rayleigh stress range loading spectrum
μ_D	Location parameter of critical damage probability distribution, D_c
μ_V	Location parameter of log-CAFL probability distribution
σ	Logarithm of the scale parameter of log-life probability distribution

Nomenclature and definitions

σ_V	Logarithm of the scale parameter of log-CAFL probability distribution
σ_D	Scale parameter of critical damage probability distribution, D_c
$\underline{\underline{\Sigma}}$	VA S-N model covariance matrix
$\underline{\underline{\rho}}$	CA S-N model correlation matrix
$\rho_{S_{max}}, \rho_{S_{E,2}}, \rho_{n_{tot}}$	Characteristic return periods of S_{max} , $S_{E,2}$ and n_{tot}
ϕ	Standardized normal pdf
ϕ_d	Load dynamic amplification factor
Φ	Standardized normal cdf
$(\omega_t, y_t) _{t=1 \dots n_{ts}}$	VA fatigue data-set
ς	Percentage of stress range cycles of a loading spectrum, which exceeds the characteristic value of CAFL

1 Introduction

1.1 Background: fatigue of welded joints

Fatigue is defined as a mechanism of failure of a structural member due to the formation and growth of cracks under the effect of repeated stresses [33].

First studies on fatigue date back to the second half of 19th century, when Wöhler published the results of his fatigue tests on railway axles [80]. Studies on welded joints started only after the second World War, when welding started to become a major production process.

Fatigue cracks appear near the regions where the local stress is much higher than the nominal stress; these regions are called stress concentrators. When the stress concentrators lead to fatigue cracking they are called crack initiators.

Fatigue can be classified according to: 1) Type of crack initiators: holes, notches, material structure discontinuities, welds; 2) Form in which fatigue occurs: mechanical, thermo-mechanical, corrosion, creep, fretting, rolling contact [72]; and 3) Duration: low-cycle, high-cycle. Fatigue verification of road steel bridges under the long term effect of traffic asks for consideration of high-cycle mechanical fatigue of welded joints.

The prevention of fatigue failure requires designing fatigue sensitive structure with a sufficient fatigue strength. However, fatigue strength is not a constant material property, like limit of elasticity for example. For an assigned detail geometry the fatigue strength can be calculated by using linear elastic fracture mechanics (LEFM) [79]. Use of LEFM includes several assumptions on the cracking process, which could largely affect the final results.

For this reason, the fatigue verification of structures subjected to variable amplitude (VA) loadings is generally performed by using constant amplitude (CA) S-N curves (which relate the nominal applied stress range, S , to the number of cycles to failure, N), in combination with a cycle-counting algorithm and a damage accumulation rule. The fatigue verification problems can be simplified, by keeping all the stress range cycles below the constant amplitude fatigue

limit (CAFL): in this case only the combination of CA S-N curves with a cycle-counting algorithm is needed. However, this type of fatigue verification is over-conservative and may lead to un-necessary heavy structures (in case of fatigue design of new structures), or to un-necessary and expensive inspections (in case of fatigue assessment of existing structures).

1.1.1 CA S-N curves

CA S-N curves are estimated by means of CA experimental fatigue tests. Due to the randomness of fatigue life, statistical evaluation of experimental results is needed. In order to estimate the median S-N curve the experimental failure points are generally fitted with following linear regression:

$$\log(N) = C + m \cdot \log(S) \quad , \text{ for } S > \text{CAFL} \quad (1.1)$$

where C and m are material constantsⁱ.

Characteristic S-N curve is then estimated by translating the median S-N curve proportionally to the fatigue life scatter at $2 \cdot 10^6$ cycles.

LEFM can be used to show the validity of Equation 1.1.

The fatigue failure process can be divided in three phases: 1) Crack initiation; 2) Stable crack propagation; and 3) Unstable crack propagation, which is very limited in time. The stress field near the crack tip can be expressed by using the stress intensity factor:

$$K = M_k \cdot S_n \cdot \sqrt{\pi a} \quad (1.2)$$

where S_n is the nominal stress, M_k is the geometrical correction factor, and a is the crack size. In 1963 Paris and Erdogan [57] proposed to relate the stress intensity range to the crack propagation rate according to the idea that fatigue crack propagation phenomenon must depend on the stress field around the crack tip:

$$\frac{da}{dN} = C_1 (\Delta K)^{-m} \quad (1.3)$$

where C_1 is a material constants and ΔK is the difference between the stress intensity factor at the upper and lower limit stresses of the loading cycle. In welded joints, the crack initiation phase is almost non existent (fatigue cracks usually initiate at weld toe, where sharp defects can be regarded as small cracks) and the entire fatigue life can be taken by the stable propagation phase. Under this assumption, the Paris Law (Equation 1.3) can be applied to all fatigue life of

ⁱContrary to common practice, in this thesis negative m is used, in order to have correct definition of S-N curve in analytic geometry

welded joints; thus inserting Equation 1.2 in Equation 1.3, gives:

$$\int_{a_1}^{a_2} \frac{da}{(M_k \sqrt{\pi a})^m} = C_1 \cdot S^{-m} \cdot N \quad (1.4)$$

where S is the nominal stress range.

Equation 1.4 confirms that, for a given type of joint and constant values of a_1 and a_2 , the relationship between S and N is linear in the $\log(S-N)$ plane:

$$S^{-m} \cdot N = \text{constant} \quad (1.5)$$

1.1.2 Cycle counting methods

Cycle counting methods allow breaking down a complex load history in simple load cycles, which can be easily applied to CA S-N curves for fatigue evaluation. A realistic counting algorithm should take in account all the stress strain closed hysteresis loops, which are contained in the loading history.

In 1974 Endo et al. [22] proposed the rain-flow method. Its name originates from the fact that the stress history is expressed by using rain-flow on a pagoda roof while the stress ranges are counted by the ranges of the rain-flow. This method allows to count all the closed hysteresis loops and it is by far the most largely used cycle counting algorithm. Various other methods have been also proposed (peak method [1], range method [1], range pair method [65]) but they are affected by the limitation of giving inaccurate evaluation of closed hysteresis loops.

1.1.3 Damage accumulation

Damage accumulation rules are used in combination with a fatigue load spectrum and a CA S-N curve, in order to assess fatigue life of a critical detail. The most widely used damage accumulation rule is the Miner's linear rule [53], which predicts the number of cycles to fatigue failure by assuming that the damage caused by one stress range cycle of VA loading is the same as the one caused by the same stress range in CA loading:

$$\sum_{i=1}^{n_{tot}} \frac{n_i}{N_i} = 1 \quad (1.6)$$

where n_i is the number of cycles corresponding to the stress range S_i and N_i is the number of cycles to failure corresponding to the stress range S_i , according to the CA S-N curve.

If the CA S-N curve has been estimated for a fully reversed CA loading, then the mean VA stress has to be corrected; the modified Goodman law [28] is conventionally used for this purpose.

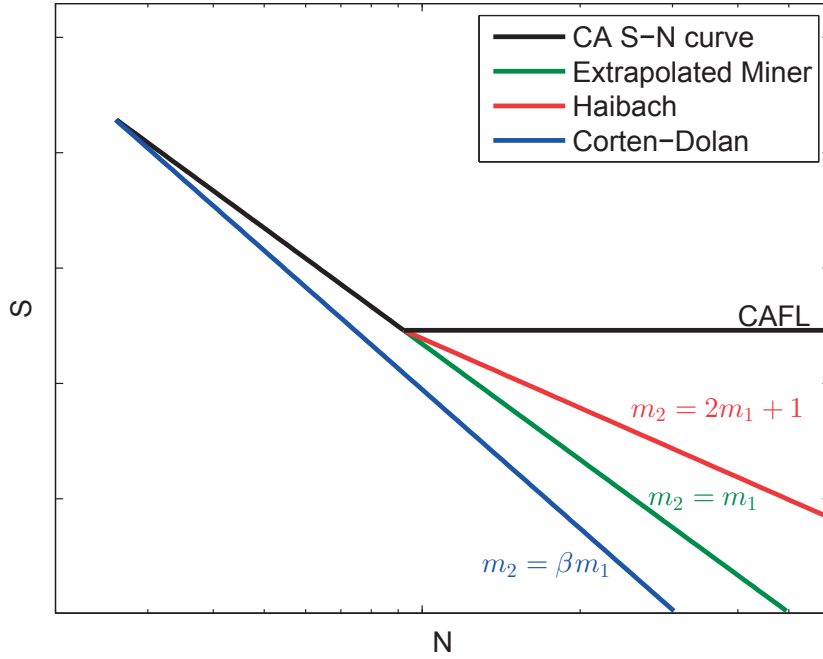


Figure 1.1: VA S-N curves

The main shortcomings of the Miner's rule are: 1) The fatigue damage given by cycles below the CAFL is not considered; 2) The effects related to VA load history on fatigue damage are not considered as well; these effects are all related to the crack closure mechanism [20].

Many modifications of Miner's rule have been proposed in order to overcome its first shortcoming [43] (see Figure 1.1). The most largely used rule is the Haibach's rule [36], which considers a S-N curve with a reduced slope, $m_2 = 2m_1 + 1$ below the CAFL. This rule gives a good estimation of fatigue life when the percentage of stress range cycles below CAFL is large. The second shortcoming of Miner's rule is still an unclear point. In most cases the Miner's rule (Equation 1.6) is not valid because load sequence effects cause significant deviation from the CA crack propagation rate, resulting in a value of the critical damage sum at failure, D_c , which is not equal to unity. Many authors have analysed the influence of load sequence on Miner's rule in welded joints, but without providing a rigorous method for its modification. This topic is discussed more in details in the Introduction of Chapter 3.

1.2 Problem statement

Reliable fatigue verification of road steel bridges and in particular of welded joints, requires realistic assessment of fatigue resistance S-N curves as well as realistic consideration of damage accumulation.

In current standards [24], [40], [2], characteristic CA S-N curves are determined by fitting a linear regression to experimental failure points, disregarding run-outs and somewhat arbitrarily fixing the CAFL at a given number of cycles. Moreover, the fatigue life scatter in the high cycle fatigue (HCF) region ($N > 5 \cdot 10^6$) is not modeled properly. CA characteristic S-N curves are conventionally used in combination with modified Miner's rule, which results in un-realistic consideration of load history effects.

Limitations mentioned above may heavily affect the accuracy of results when the combination of characteristic CA S-N curves with modified Miner's rule (Miner's rule with Haibach's modification) is used in fatigue design of new bridges or in fatigue assessment of existing bridges.

Linear regression analysis and modified Miner's rule do not provide accurate definition of the stochastic VA S-N model (which includes probability distributions of S-N curve parameters and of critical damage sum parameters). This limitation can lead to inaccurate computation of reliability indexes when fatigue reliability analysis of existing bridges is carried out for: 1) Assessment of the remaining fatigue life; 2) Planning of inspections; and 3) Planning of repair interventions.

In structural codes the fatigue design is carried out by using design equations which compare resistance and loading terms. In design equations the uncertainty on loading and resistance terms is considered in a semi-probabilistic model, further simplified, by introducing partial safety factors. Limitations related to VA S-N model may lead to inaccurate calibration of fatigue partial safety factors, resulting in inaccurate design of new bridges.

Based on the discussion above it is clear that a rigorous statistical approach is needed for estimation of stochastic VA S-N models from experimental CA and VA fatigue test results. Advances in VA S-N model estimation will give more insight into realistic fatigue reliability indexes and into reliable calibration of partial safety factors for fatigue design.

1.3 Objectives

The main aim of this study is to provide a novel probabilistic approach which allows to re-define both S-N curves and critical damage sum parameter, by using experimental CA and VA fatigue test results.

The objectives are as follows:

- To provide a new probabilistic approach for estimation of CA S-N curve random parameters and for assessment of true p -quantiles of CA S-N curves;
- To provide a new probabilistic approach for estimation of VA S-N stochastic model parameters;
- To provide a new framework for fatigue reliability assessment of existing bridges, in which the probability of having fatigue failure is computed as joint probability of having critical damage accumulation and CAFL exceedance;
- To provide a new framework for calibration of partial safety factors for fatigue design.

1.4 Structure of the thesis

The structure of this thesis is shown in Figure 1.2, which also illustrates the relationships between topics. The state of art of each topic is presented at beginning of the related Chapter.

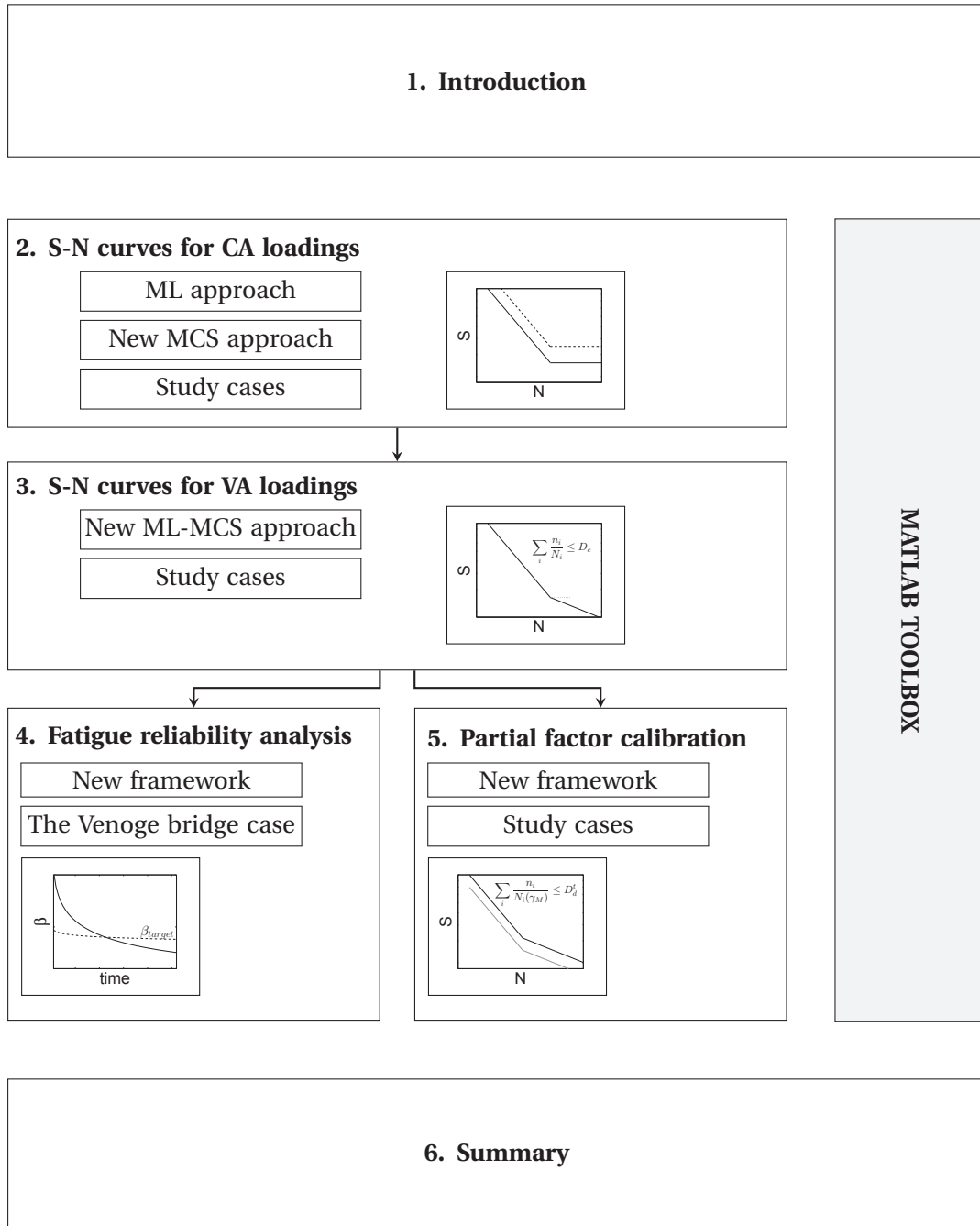


Figure 1.2: Structure of the thesis

2 S-N curves for constant amplitude loadings

2.1 Introduction

Traditional fatigue analysis of welded components under VA loadings is based on the nominal stress approach, where the verification can be based on CAFL or on damage accumulation. Within the two verifications above, the choice of CA fatigue strength curve is of primary importance.

Fatigue strength of welded components is expressed in terms of characteristic S-N curves, which give the fatigue life, N , at each stress range, S , for a certain survival probability, P_s (typically 95%), on the basis of a certain confidence level on the S-N curve parameters (typically 75%). S-N curves are based on experimental tests; however, due to the inherent randomness in the fatigue life, a statistical treatment of experimental data-sets is required.

Median S-N curveⁱ ($P_s = 50\%$) in current Eurocode standards [29] is derived by fitting a linear regression which has a slope of $m_1 = -3$ to the failure data, using a least squares (LS) analysis procedure. Characteristic S-N curve is then derived by translating the median S-N curve on the lower 5% prediction bound, at 2 million cycles; the CAFL is arbitrarily assumed at 5 million cyclesⁱⁱ. The linear regression used disregards run-out data and arbitrarily fixes the CAFL at 5 million cycles, which is unrealistic and neglects important information from experimental observations. Further, to deduce the characteristic S-N curve, one shifts the median curve and thus assumes the fatigue data-set to be homoscedastic. The limitation of LS analysis procedure, connected to run-outs omission in estimation of S-N curves, may be overcome by using Maximum Likelihood (ML) method.

ⁱMedian is preferred here instead of Mean, as different probability distributions than Normal will be used to represent fatigue life randomness

ⁱⁱThis value has been originally taken as a compromise between $2 \cdot 10^6$, proven to be too low in some studies, and 10^7 , seen as too conservative even if shown in some studies

In [70], Spindel and Haibach used ML method to estimate S-N curves for a generic fatigue data-set containing both failures and run-outs. CAFL was not included in the model and it was assumed at 2 million cycles.

In [55], Nelson used ML method to include run-outs in S-N curve estimation of a nickel base super-alloy; Nelson modeled the mean and the standard deviation of the fatigue life as functions of the stress range but the CAFL was not included in the model.

In [56] Nelson proposed several models which included the CAFL.

In [58] Pascual et al. proposed a 5-parameter random fatigue limit (RFL) model that fitted a non-linear S-N curve with a random CAFL to a complete fatigue data-set, using ML method. Median S-N curve and standard deviation parameters expressed the randomness in the fatigue life, while the randomness in the CAFL was expressed by the location and the scale parameters of a generic location-scale probability family. Median and characteristic S-N curves with profile likelihood ratio (PLR)-based confidence bounds were generated using a ML approach.

In [45], Lassen et al. fitted RFL model from Pascual to two experimental data-sets of a plate with fillet welded attachments. Lassen et al. observed that: 1) The RFL method-based 90% confidence interval of the median of CAFL distribution did not include the Eurocode CAFL (median value); 2) The RFL method-based 90% confidence interval of the median of CAFL included the BS5400 CAFL (median value) and the RFL model-based 0.025 quantile S-N curve was in good agreement with BS5400 F-class S-N curve for stress ranges higher than 150MPa; 3) At stress ranges lower than 150 MPa the non linear RFL model-based 0.025 quantile S-N curve predicted fatigue lives that were up to 10 times longer than the predictions made by the F-class S-N curve. Confidence level of 0.025 quantile S-N curve was not indicated.

In Part 3 of the JCSS PMC [41], a ML-based approach is recommended for the estimation of SN-curves parameters: a linear S-N model is fitted to both failure and run-out experimental points and uncertainty related to the parameter fit is estimated by using the Hessian of the log-Likelihood function. It is not specified if the CAFL has to be considered as a random variable whose parameters are included in the model parameter vector or if it has to be considered as a deterministic value which is arbitrarily assumed at a fixed number of cycles. Recommended approach also does not specify how to relate the uncertainty on the parameter fit to the uncertainty on the fatigue life quantiles.

The existence of the CAFL is still an object of dispute; Sonsino [68] proposes a CA bi-linear S-N curve where stress range cycles below the knee point are accounted with a slope $m'_1 = -22$. The knee point is arbitrarily fixed at $N = 10^7$. The slope $m'_1 = -22$ is also arbitrarily fixed in order to have 10% constant stress range decrease with respect to the $\log(N)$ axis for each order of magnitude. The lack of the experimental results in the HCF region and the related high scatter of fatigue life in this region does not allow to provide experimental validation to the CA bi-linear S-N model. For this reason the choice of a CA S-N model including random CAFL

seems to be the most realistic choice allowing for correct interpretation of experimental results in HCF region.

The RFL model proposed by Pascual, allows to overcome limitations of current Eurocode approach but it does not give explicit method to derive the true p -quantile S-N curve from ML estimate of CA S-N stochastic model parameters. Furthermore, the RFL model-based median S-N curve is not linear and direct comparison with current standards is not straightforward. In this Chapter a novel approach, based on ML method and on Monte-Carlo Simulations (MCS) method, is proposed for estimation of median and characteristic S-N curves under CA fatigue loadings. A linear S-N model is fitted to a complete fatigue experimental data-set, using ML method. CAFL is modeled as a random variable whose parameters are included in the CA S-N model parameter vector. The covariance matrix of the model parameter vector is estimated by inverting the observed Fisher information matrix. The true 0.05 quantile S-N curve (corresponding to a probability of failure, $P_f = 5\%$) is estimated by using MCS method. The novel contribution of this approach is summarized in following points:

- Linear S-N model with random CAFL is fitted directly to experimental data;
- p -quantiles of S-N curve are estimated using MCS method. MCS-based p -quantiles correspond to the true $(100 \cdot p\%)$ probability of failure and not to the nominal $(100 \cdot p\%)$ probability of failure with a α -confidence level (as for the case of RFL model);
- Linearization of ML-MCS-based characteristic S-N curves allows to make direct comparison with current standards.

The ML-MCS approach which is presented in this work was implemented in `CAestimation` and `CAquantiles` modules of Matlab [49] Toolbox TB1 (see Appendix B).

The Chapter is organized as follows:

- in Section 2.2 the statistical analysis procedure for estimation of characteristic S-N curves, based on the Eurocode 3 background documentation, is recalled;
- in Section 2.3 the ML-MCS approach for estimation of characteristic S-N curves is presented;
- in Section 2.4 the application of the ML-MCS approach on three study cases is presented;
- in Section 2.5 results of analysis of considered study cases are presented;
- in Section 2.6 results are discussed.

2.2 Eurocode statistical approach for estimation of S-N curves

In this Section an overview is given of the statistical estimation of characteristic S-N curves, according to Eurocode 3 commentary document [29].

The median S-N curve is estimated by carrying out a LS fit analysis on the experimental data-set $(x_i, y_i) |_{i=1, \dots, n_{fail}}$, where x_i is the base 10 logarithm of the applied nominal stress range, y_i is the base 10 logarithm of the observed number of cycles to failure, and n_{fail} is the total number of failed specimens (see Figure 2.1 (a)). Observed results having a fatigue life at failure higher than $5 \cdot 10^6$ cycles are considered as run-outs and hence they are not included in the analysis.

The equation of the median S-N curve is the following:

$$\log(N) = m_{0_{LS}} + m_{1_{LS}} \cdot \log(S) \quad (2.1)$$

where $m_{0_{LS}}$ and $m_{1_{LS}}$ are the LS estimators of m_0 and m_1 .

The LS estimator of the log-strength at $2 \cdot 10^6$ cycles is indicated as $x_{c_{LS}}$ (see Figure 2.1 (a)).

By putting $N = 2 \cdot 10^6$ in the Equation 2.1, it follows:

$$\log(2 \cdot 10^6) = m_{0_{LS}} + m_{1_{LS}} \cdot x_{c_{LS}} \quad (2.2)$$

The 95% hyperbolic lower prediction boundⁱⁱⁱ of $Y(x_{c_{LS}})$ is defined as follows (see Figure 2.1 (b)):

$$Y_c = \log(2 \cdot 10^6) + t_{.05, n_{fail}-2} \cdot \mathcal{S} \sqrt{1 + \frac{1}{n_{fail}} + \frac{(x_{c_{LS}} - \bar{x})^2}{S_{xx}}} \quad (2.3)$$

where:

- $t_{.05, n_{fail}-2}$ is the inverse of Student's t cdf for probability equal to 5% and $(n_{fail} - 2)$ degrees of freedom;
- \mathcal{S} is the sample standard deviation;
- $\bar{x} = \left(\sum_{i=1}^{n_{fail}} x_i \right) / n_{fail}$;
- $S_{xx} = \left(\sum_{i=1}^{n_{fail}} (x_i - \bar{x})^2 \right)$.

ⁱⁱⁱsee Section A.4 in Appendix A

2.2. Eurocode statistical approach for estimation of S-N curves

By inserting Equation 2.2 in Equation 2.3, it follows:

$$Y_c = m_{0_{LS}} + m_{1_{LS}} \cdot x_{c_{LS}} + t_{0.05, n_{fail}-2} \cdot \mathcal{S} \sqrt{1 + \frac{1}{n_{fail}} + \frac{(x_{c_{LS}} - \bar{x})^2}{S_{xx}}} \quad (2.4)$$

The characteristic S-N curve is determined by translating the median S-N curve in the point (x_c, Y_c) , as shown in Figure 2.1 (c).

The equation of the characteristic S-N curve is the following:

$$\log(N) = Y_c - m_{1_{LS}} \cdot x_{c_{LS}} + m_{1_{LS}} \cdot \log(S), \quad N \leq 5 \cdot 10^6 \quad (2.5)$$

The CAFL is assumed to start at $5 \cdot 10^6$ cycles (see Figure 2.1 (d)).

By inserting the Equation 2.4 in Equation 2.5, the characteristic S-N curve may be written as:

$$\log(N) = m_{0_{LS}} + t_{0.05, n_{fail}-2} \cdot \mathcal{S} \sqrt{1 + \frac{1}{n_{fail}} + \frac{(x_{c_{LS}} - \bar{x})^2}{S_{xx}}} + m_{1_{LS}} \cdot \log(S), \quad N \leq 5 \cdot 10^6 \quad (2.6)$$

The characteristic value of fatigue resistance at $2 \cdot 10^6$ cycles can be determined by putting $N = 2 \cdot 10^6$ in Equation 2.6:

$$x_c = \frac{\log(2 \cdot 10^6) - m_{0_{LS}} - t_{0.05, n_{fail}-2} \cdot \mathcal{S} \sqrt{1 + \frac{1}{n_{fail}} + \frac{(x_{c_{LS}} - \bar{x})^2}{S_{xx}}}}{m_{1_{LS}}} \quad (2.7)$$

In the Eurocode 3 commentary document [29], the characteristic value of fatigue resistance at $2 \cdot 10^6$ cycles, x_c , is erroneously indicated as *0.95 lower confidence bound*: in fact it has to be considered as *0.95 lower prediction bound* due to the term 1 in the square root of Equation 2.7.

For comparison, in IIW recommendations [40] the characteristic S-N curve is obtained by translating the median S-N curve at the 0.05 quantile of the Y normal distribution, by using the lower bound of the 0.75 two-sided confidence interval of $E(Y)$ and the upper bound of the 0.75 two-sided confidence interval of standard deviation. The median S-N curve is obtained by carrying out a LS analysis of experimental failure points. The CAFL is assumed to start at 10^7 cycles. The difference between the confidence interval concept and the prediction interval concept is discussed more widely in Appendix A.

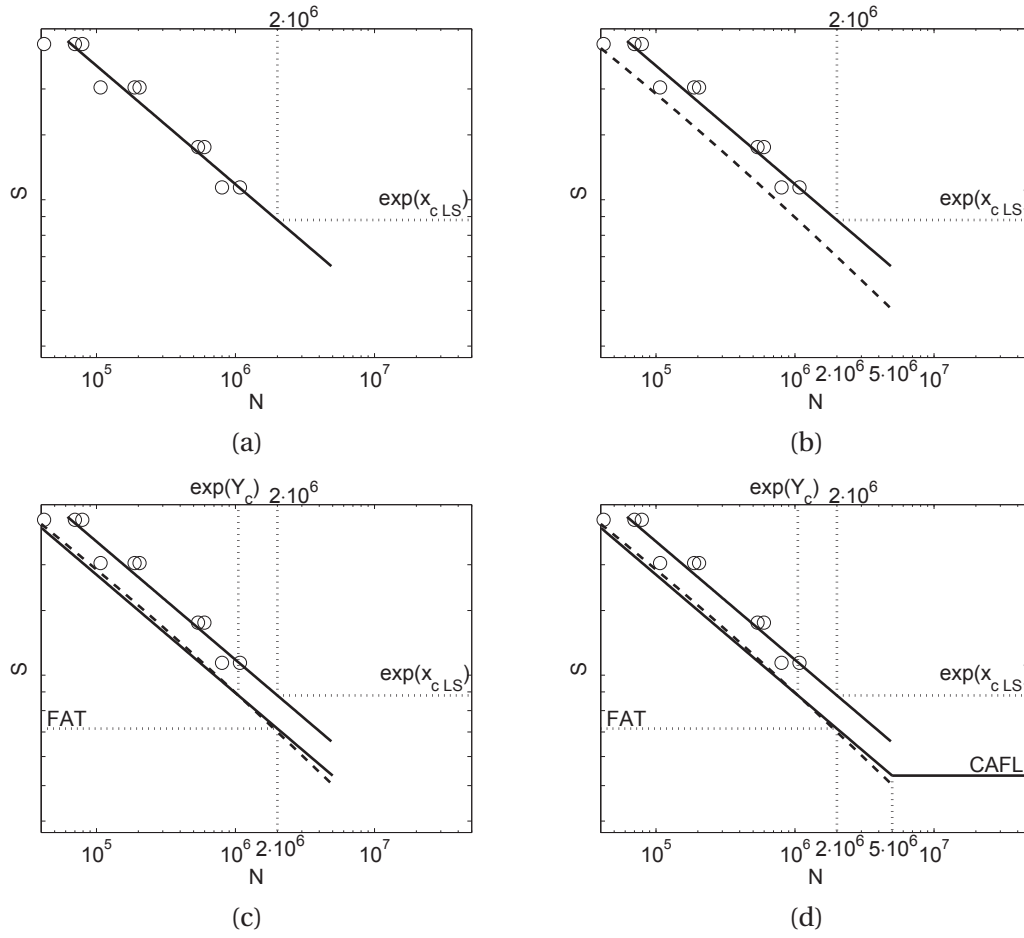


Figure 2.1: Eurocode statistical approach for estimation of S-N curves

2.3 New probabilistic approach

2.3.1 CA S-N stochastic model

The CA S-N stochastic model describes the relationship between the nominal applied stress range, S , and the number of cycles to failure, N , under CA loadings (see Figure 2.2):

$$Y = \frac{m_0 + m_1 X}{H(X - V)} + \epsilon(0, \exp(\sigma)) \quad (2.8)$$

where:

- Y is the natural logarithm^{iv} of the number of cycles, N ;
- X is the natural logarithm of the nominal applied stress range, S ;

^{iv}Natural logarithms are preferred since they are mathematically less heavy to manipulate

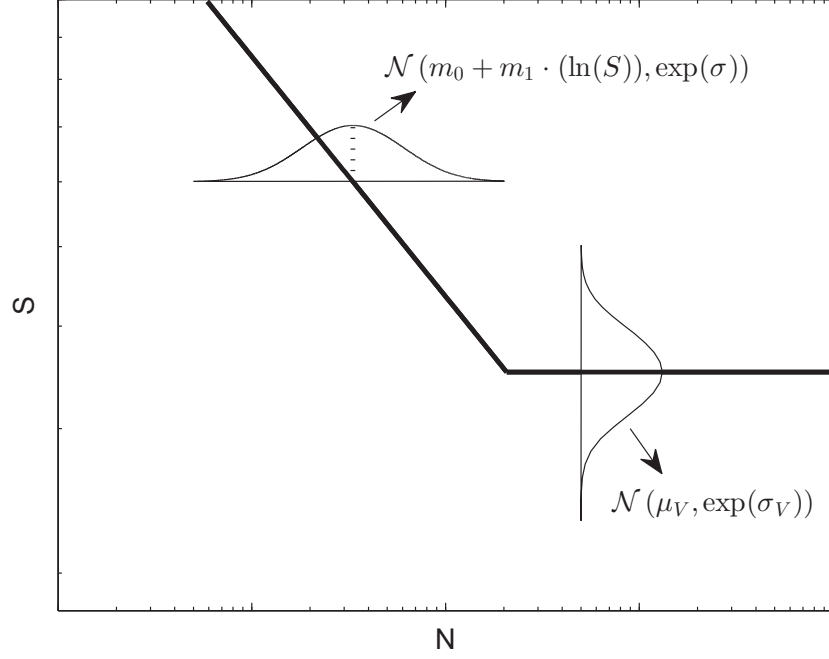


Figure 2.2: Median CA S-N curve with model parameters (case of $V = \mathcal{N}$)

- m_0 is the intercept of the S-N curve in the log(S-N) plane;
- m_1 is the slope of the S-N curve;
- $H(\cdot)$ is the unit step function;
- V is the natural logarithm of the CAFL;
- ϵ is the error term, which is assumed to be normally distributed with mean equal to 0 and standard deviation equal to $\exp(\sigma)$.

$Y|V$ is a random variable following a Normal distribution, with location and scale parameters which are respectively:

$$\mu_{Y|V} = \frac{m_0 + m_1 X}{H(X - V)} \quad (2.9)$$

$$\sigma_{Y|V} = \exp(\sigma) \quad (2.10)$$

V is a random variable following a Normal or an Extreme Value (EV) distribution with location parameter equal to μ_V and scale parameter equal to $\exp(\sigma_V)$. If V has a Normal distribution

Chapter 2. S-N curves for constant amplitude loadings

with parameters μ_V and $\exp(\sigma_V)$, then the CAFL has a log-Normal distribution with parameters μ_V and $\exp(\sigma_V)$; instead if V has an EV distribution with parameters μ_V and $\exp(\sigma_V)$, then the CAFL has a Weibull distribution with parameters $a = \exp(\mu_V)$ and $b = 1/\exp(\sigma_V)$. The probability density function (pdf) of V is given by:

$$f_V(v, \mu_V, \sigma_V) = \frac{1}{\exp(\sigma_V)} \phi_V \left(\frac{v - \mu_V}{\exp(\sigma_V)} \right) \quad (2.11)$$

where $\phi_V(\cdot)$ is either the standardized Normal pdf or the standardized EV pdf. Conditioned on a fixed value of $V \leq x$, $Y|V$ has a conditional pdf given by:

$$f_{Y|V}(m_0, m_1, \sigma; y, x, v) = \frac{1}{\exp(\sigma)} \phi_{Y|V} \left(\frac{y - \left[\frac{m_0 + m_1 x}{H(x - v)} \right]}{\exp(\sigma)} \right) \quad (2.12)$$

where $\phi_{Y|V}$ is either the standardized normal pdf:

$$\phi(z) = \frac{\exp\left(-\frac{1}{2}z^2\right)}{\sqrt{2\pi}} \quad (2.13)$$

or the standardized EV pdf:

$$\phi(z) = \exp(z) \cdot \exp(-\exp(z)) \quad (2.14)$$

The marginal pdf of Y is given by:

$$f_Y(\underline{\theta}; y, x) = \int_{-\infty}^x \frac{1}{\exp(\sigma + \sigma_V)} \phi_{Y|V} \left(\frac{y - \left[\frac{m_0 + m_1 x}{H(x - v)} \right]}{\exp(\sigma)} \right) \phi_V \left(\frac{v - \mu_V}{\exp(\sigma_V)} \right) dv \quad (2.15)$$

where $\underline{\theta}$ is the model parameter vector. f_Y expresses the probability to have a failure at $Y = y$, for an applied log-stress range equal to $\exp(x)$.

Conditioned on a fixed value of $V \leq x$, $Y|V$ has a conditional cdf given by:

$$F_{Y|V}(m_0, m_1, \sigma; y, x, v) = \Phi_{Y|V} \left(\frac{y - \left[\frac{m_0 + m_1 x}{H(x - v)} \right]}{\exp(\sigma)} \right) \quad (2.16)$$

where $\Phi_{Y|V}$ is either the standardized normal cdf or the standardized EV cdf.

The marginal cdf of Y is given by

$$F_Y(\underline{\theta}; y, x) = \int_{-\infty}^x \frac{1}{\exp(\sigma_V)} \Phi_{Y|V} \left(\frac{y - \left\lfloor \frac{m_0 + m_1 x}{H(x-v)} \right\rfloor}{\exp(\sigma)} \right) \phi_V \left(\frac{v - \mu_V}{\exp(\sigma_V)} \right) dv \quad (2.17)$$

and expresses the probability to have a failure for $Y \leq y$, for an applied log-stress range equal to $\exp(x)$. $1 - F_Y$ expresses the probability to have a failure for $Y > y$ and then to have a run-out at $Y = y$. Since there are no closed forms of the marginal pdf and of the marginal cdf of Y , they have to be evaluated numerically.

2.3.2 ML estimation of model parameters

The sample Likelihood for the CA S-N model is the resulting product of the marginal pdfs at failure data points and marginal cdfs at run-out data points. Considering the experimental data-set $(x_i, y_i) |_{i=1, \dots, n_{tot}}$, the sample Likelihood is defined as follows:

$$L(\underline{\theta}) = \prod_{i=1}^{n_{tot}} (f_Y(\underline{\theta}; y_i, x_i))^{\delta_i} \cdot (1 - F_Y(\underline{\theta}; y_i, x_i))^{1-\delta_i} \quad \text{for } \delta_i = \begin{cases} 0 & \text{if } y_i \text{ is a run-out} \\ 1 & \text{if } y_i \text{ is a failure} \end{cases} \quad (2.18)$$

The sample Likelihood, $L(\underline{\theta})$, expresses the probability of observing $(y_1, \dots, y_{n_{tot}})$, at log-stress ranges $(\exp(x_1), \dots, \exp(x_{n_{tot}}))$ for a given model parameter vector, $\underline{\theta}$. The ML estimate $\hat{\underline{\theta}}$ of $\underline{\theta}$ is the model parameter vector which maximizes the sample Likelihood, $L(\underline{\theta})$.

Generally it is easier to work with the negative sample log-Likelihood:

$$nLL(\underline{\theta}) = - \sum_{i=1}^{n_f} \ln(f_Y(\underline{\theta}; y_i, x_i)) - \sum_{i=1}^{n_r} \ln(1 - F_Y(\underline{\theta}; y_i, x_i)) \quad \text{with } \begin{cases} n_f : \text{nb. of failures} \\ n_r : \text{nb. of run-outs} \end{cases} \quad (2.19)$$

Then the ML estimate $\hat{\underline{\theta}}$ of $\underline{\theta}$ is the model parameter vector which minimizes the negative sample log-Likelihood, $nLL(\underline{\theta})$.

2.3.3 MCS estimation of p-quantile S-N curve

Under some regularity conditions, ML estimators have asymptotic normality property [52]: as the sample size increases, the distribution of ML estimators tends to the Normal distribution with mean equal to the true parameter vector being estimated and covariance matrix equal to the inverse of the observed Fisher Information matrix, $\underline{I}(\hat{\underline{\theta}})$.

The Fisher information matrix, $\underline{I}(\underline{\theta})$, is the symmetrical matrix which contains following

entries:

$$\underline{\underline{I}}(\underline{\theta}) = -\frac{\partial^2}{\partial \theta_i \partial \theta_j} L(\underline{\theta}) \quad (2.20)$$

The observed Fisher information matrix^v, $\underline{\underline{I}}(\hat{\underline{\theta}})$, is the Fisher information matrix evaluated at the ML estimate, $\hat{\underline{\theta}}$.

The estimator of the asymptotic covariance matrix is then:

$$\underline{\underline{\rho}} = \underline{\underline{\text{Cov}}}(\underline{\theta}) = \left[\underline{\underline{I}}(\hat{\underline{\theta}}) \right]^{-1} \quad (2.21)$$

Hence under the hypothesis of asymptotic normality of ML estimators, the model parameter vector, $\underline{\theta}$, is multivariate Normal with mean equal to the ML estimate, $\hat{\underline{\theta}}$, and covariance matrix equal to the inverse of the observed Fisher information matrix (Equation 2.21).

In this work the following MCS scheme was designed in order to compute the p -quantile, $y_p(\tilde{x})$, of the fatigue log-life, at the log-stress range, $\exp(\tilde{x})$:

1. The p -value is chosen, with $P_f^t = p$.
2. The parameter η_{sam} (sample size, typically $1 \cdot 10^5$) is chosen.
3. The sample $\underline{\theta}_i |_{i=1 \dots \eta_{sam}}$ is generated from the multivariate normal distribution $\mathcal{N}(\hat{\underline{\theta}}, \underline{\underline{\rho}})$; then, $y(\underline{\theta}_i, \tilde{x}) |_{i=1 \dots \eta_{sam}}$, $\nu(\underline{\theta}_i) |_{i=1 \dots \eta_{sam}}$ are sampled by using the sampled $\underline{\theta}_i |_{i=1 \dots \eta_{sam}}$. The epistemic uncertainty of S-N model parameters is taken into account in the $\underline{\theta}_i |_{i=1 \dots \eta_{sam}}$ sampling, while the aleatory uncertainty of the CAFL and the aleatory uncertainty of the fatigue life are taken into account in the $y(\underline{\theta}_i, \tilde{x}) |_{i=1 \dots \eta_{sam}}$, $\nu(\underline{\theta}_i) |_{i=1 \dots \eta_{sam}}$ sampling.
4. For each element of the sample, the probability $P_{fi}(y_p(\tilde{x}))$ is computed:

$$P_{fi}(y_p(\tilde{x})) = \begin{cases} 0 & \text{if } y(\underline{\theta}_i, \tilde{x}) \geq y_p(\tilde{x}) \quad \text{or} \quad \nu(\underline{\theta}_i) \geq \tilde{x} \\ 1 & \text{if } y(\underline{\theta}_i, \tilde{x}) < y_p(\tilde{x}) \quad \text{and} \quad \nu(\underline{\theta}_i) < \tilde{x} \end{cases}$$

5. Objective function, $\mathcal{O}(y_p(\tilde{x}))$, is built:

$$\mathcal{O}(y_p(\tilde{x})) = \left[\frac{(\sum_{i=1}^{\eta_{sam}} P_{fi}(y_p(\tilde{x})))}{\eta_{sam}} - P_f^t \right]^2$$

^vThe observed Fisher information matrix is computed in `CAestimation` module of Matlab Toolbox TB1 by using the built-in function `hessian(f, v)`, where `f` is the scalar likelihood function and `v` is the ML estimate of model parameter vector

6. p -quantile of the fatigue log-life, at stress range $\exp(\tilde{x})$, is computed by minimizing the objective function, $\mathcal{O}(y_p(\tilde{x}))$:

$$\hat{y}_p(\tilde{x}) = \underset{y_p(\tilde{x})}{\operatorname{argmin}} (\mathcal{O}(y_p(\tilde{x})))$$

The 0.05 quantile S-N curve, obtained with the scheme above, represents ML-based characteristic CA S-N curve. Since ML-based characteristic S-N curve is non-linear (see Figure 2.3), a linearization scheme is proposed here for direct comparison with characteristic S-N curves from standards:

1. A straight line with slope equal to \hat{m}_1 (ML estimate of m_1 parameter) and passing through the true 0.05 quantile of the fatigue life at the maximum tested stress range, is drawn;
2. The line above is intersected with the horizontal line representing the true 0.05 quantile of the CAFL distribution.

The ML-MCS-based linearized characteristic S-N curve is shown in Figure 2.3.

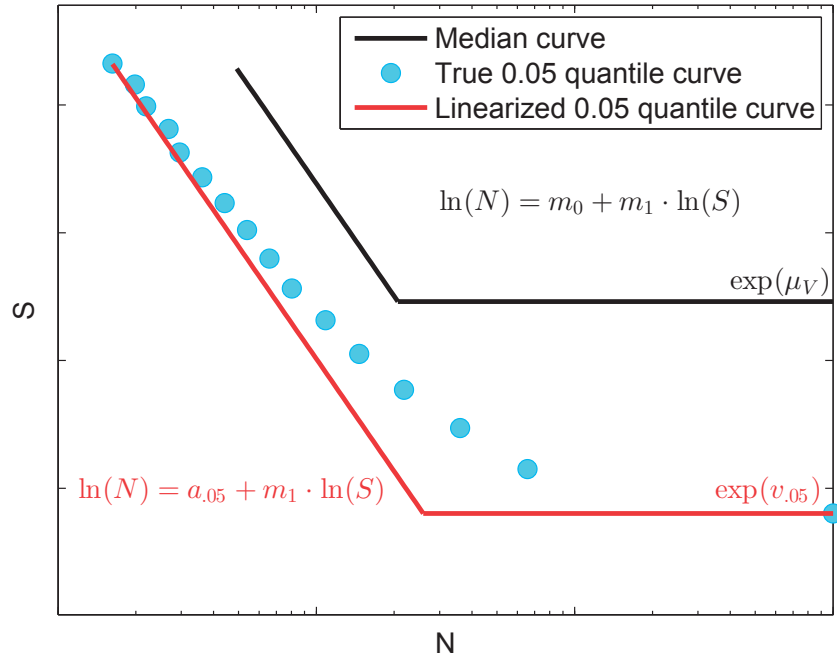


Figure 2.3: ML-MCS-based median, 0.05 quantile and linearized 0.05 quantile S-N curves

2.3.4 Mean stress effect

In the presented ML-MCS approach the effect of mean stress on fatigue strength is not explicitly taken into account by S-N model parameters (see Equation 2.8). The motivation for this choice is given below.

In welded joints, tensile residual stresses are introduced during the cooling process after the welding; these tensile stresses increase the mean stress and they can shorten the associated fatigue life [46]. Under the fatigue loading, a big part of residual stresses quickly relaxes (usually at first application of the maximum stress) [11, 64, 42], although the remaining part is still significant until the end of fatigue life [11, 50]. CA fatigue tests on longitudinal and transverse attachments from Maddox [47], Gurney [34, 35], Sonsino et al. [69], Rörup et al. [63, 62] and Polezhayeva [59] have shown that in as-welded specimens, the compressive part of stress range cycles with stress ratio $-1 \leq R \leq 0$ does not have significant beneficial effect on associated fatigue life, due to the unrelaxed tensile residual stresses. These results supported the choice of not explicitly including the mean stress effect into the S-N stochastic model; minor additional scatter in fatigue life, caused by the above discussed means stress effect, is taken into account by the model error term, $\epsilon(0, \exp(\sigma))$.

For $R \rightarrow -\infty$ (fully compressive cycles) the beneficial effect of the compressive part of stress range cycles is significant [47, 63, 62, 59] and should be taken into account in the formulation of the S-N model; this case was not considered in this study.

2.4 Study cases

The CA S-N stochastic model was fitted to two different fatigue data-sets:

1. From fatigue testing of end-welded cover plate beams, under CA loading (see Section 2.4.1);
2. From fatigue testing of welded in-plane gussets, under CA loading (see Section 2.4.2).

These data-sets are reported, with some differences/errors, in the Commentary to Eurocode 3 [29].

2.4.1 Cover plate

CA experimental data-set for cover plate detail is made of 26 data points from testing of end-welded cover plate beams at CA stress ranges between 27.6 and 55.2MPa [27] (see Table 2.1). The thickness of the beam flange, t_f , is 9.78 mm, while the thickness of the cover-plate, t_c ranges between 13.1 mm and 14.3 mm (see Figure 2.4); the detail is classified as FAT50 (with CAFL=37MPa) according to EN1993-1-9 [29] and IIW recommendations [40] (with CAFL=29 MPa), and as FAT56 (with CAFL=31 MPa) according to AASHTO bridge design specifications [2].

Cover plate with size effect correction

Since the detail considered for CA experimental data-set (FAT50 according to EN1993-1-9) has not the same classification as the detail considered for VA experimental data-set (see Section 3.3, $t_f = t_c = 25.4$ mm, FAT45 according to EN1993-1-9), the observed stress ranges, S_i , are reduced by a factor ($45/50=0.9$) for size effect to be consistent with the VA experimental data-set detail classification. It is noted that the detail is classified as FAT50 (with CAFL=29MPa) according to IIW recommendations [40], where the influence of t_c and t_f is not taken into account, and as FAT40 (with CAFL=18MPa) according to AASHTO bridge design specifications [2], where the influence of t_c and t_f is stronger than in Eurocode standards.

2.4.2 In-plane gusset

CA experimental data-set for in-plane gusset (see Table 2.2 and Figure 2.5) is made of:

- 6 data points from testing of in-plane welded gussets with attachment length, $L = 100$ mm at CA stress ranges between 80 and 160MPa [39];
- 1 data points from testing of in-plane welded gussets with attachment length, $L = 150$ mm at CA stress range equal to 50MPa (ICOM tests, [8]);
- 10 data points from testing of in-plane welded gussets with attachment length, $L = 100$ mm at CA stress ranges between 55 and 140MPa [44];
- 12 data points from testing of in-plane welded gussets with attachment length, $L = 100$ mm at CA stress ranges between 33 and 100MPa [6].

For $L \leq 150$ mm, the detail is classified as FAT40 (with CAFL=31MPa) according to EN1993-1-9 [29], as FAT50 (with CAFL=29MPa) according to IIW recommendations [40], and as FAT56 (with CAFL=31MPa) according to AASHTO bridge design specifications [2].

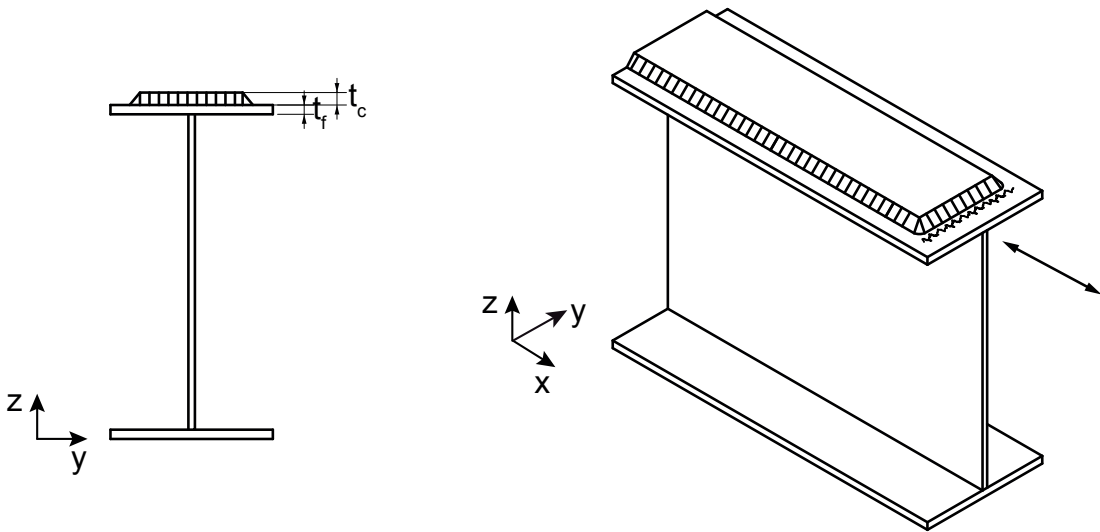


Figure 2.4: Cover plate detail

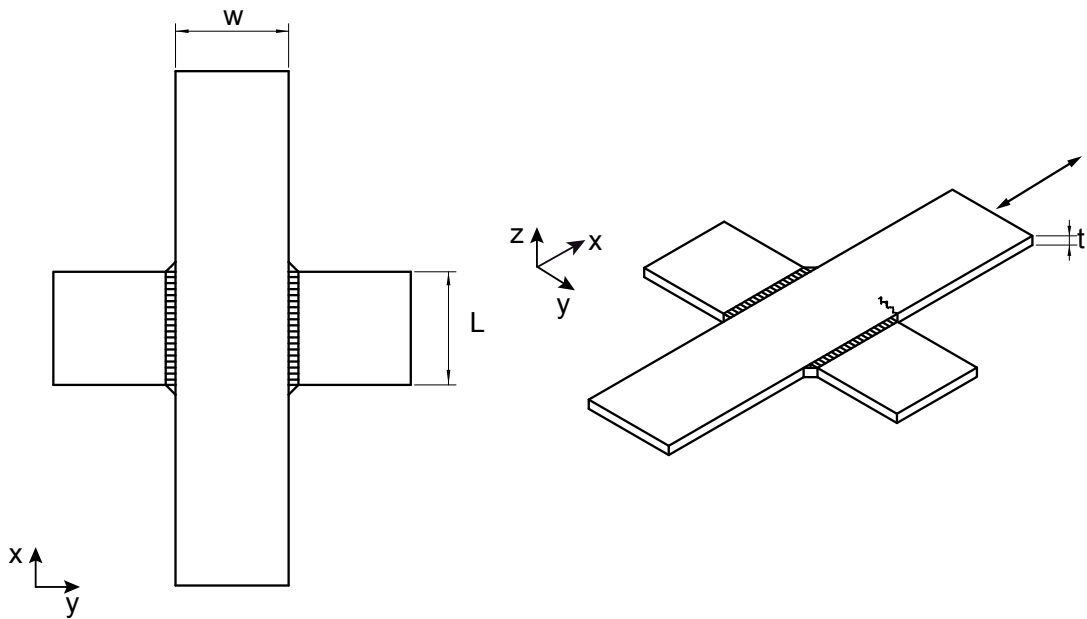


Figure 2.5: In-plane gusset detail

Test series	S [MPa]	N	δ_i	failure location
Fisher (1977)	27.6	100000000	0	-
	27.6	100000000	0	-
	27.6	100000000	0	-
	27.6	100000000	0	-
	31.7	100000000	0	-
	31.7	100000000	0	-
	31.7	100000000	0	-
	31.7	100000000	0	-
	32.4	34930000	1	weld toe
	32.4	37714000	1	weld toe
	34.5	16613000	1	weld toe
	34.5	32506000	1	weld toe
	34.5	8451000	1	weld toe
	34.5	47293000	1	weld toe
	34.5	89314000	0	-
	34.5	89314000	0	-
	41.4	11418000	1	weld toe
	41.4	12158000	1	weld toe
	41.4	4327000	1	weld toe
	41.4	12158000	1	weld toe
	41.4	100000000	0	-
	41.4	100000000	0	-
	55.2	2334000	1	weld toe
	55.2	5006000	1	weld toe
	55.2	4235000	1	weld toe
	55.2	1351300	1	weld toe

Table 2.1: Cover plate, CA experimental data-set. δ_i is a binary variable which is equal to 1 for a failure and to 0 for a run-out

Chapter 2. S-N curves for constant amplitude loadings

Test series	S [MPa]	N	δ_i	failure location
Hirt (1975) L=100mm	80	1922000	1	weld toe
	80	1810000	1	weld toe
	120	514000	1	weld toe
	120	361000	1	weld toe
	160	210000	1	weld toe
	160	199000	1	weld toe
ICOM (2015), L=150mm	50	3800000	1	weld toe
Kondo (2002) L=100mm	140	528000	1	weld toe
	140	252000	1	weld toe
	140	272000	1	weld toe
	100	826000	1	weld toe
	80	1409000	1	weld toe
	80	1431000	1	weld toe
	60	21620000	0	-
	60	5492000	1	weld toe
	60	5144000	1	weld toe
	55	4049000	1	weld toe
Bae (2004) L=150mm	100	387000	1	weld toe
	100	561000	1	weld toe
	100	721000	1	weld toe
	100	787000	1	weld toe
	66	1000000	1	weld toe
	66	1430000	1	weld toe
	66	1710000	1	weld toe
	66	1730000	1	weld toe
	33	13430000	0	-
	33	16600000	0	-
	33	18630000	0	-
	33	23420000	0	-

Table 2.2: In-plane gusset, CA experimental data-set. δ_i is a binary variable which is equal to 1 for a failure and to 0 for a run-out

2.5 Results

The ML estimate and the standard deviation of the CA S-N model vector parameters are shown in:

- Table 2.3 for the cover plate data-set;
- Table 2.5 for the cover plate data-set with size effect correction;
- Table 2.7 for the in-plane gusset data-set.

The value of the negative log-Likelihood at the ML estimate is also shown in the Tables above. In all three data-sets the case ($V = \mathcal{N}$) gives a better fit in terms of sample log-Likelihood, with respect to the case ($V = \text{EV}$). The difference in the sample log-Likelihood is trivial but in any case does not support the case ($V = \text{EV}$) to the detriment of the conventional case ($V = \mathcal{N}$). The size effect correction in the cover plate data-set has small influence on ML estimate of the intercept of the S-N curve, \hat{m}_0 (which drops from 29.02 to 28.66, for the case $V = \mathcal{N}$), while it has quite significant influence on ML estimate of the location parameter of the log-CAFL distribution, μ_V (which drops from 3.56 to 3.45, for the case $V = \mathcal{N}$).

The correlation coefficients $c_{ij} = \rho_{ij} / \sqrt{\rho_{ii}\rho_{jj}}$ of the CA S-N model are shown in:

- Table 2.4 for the cover plate data-set;
- Table 2.6 for the cover plate data-set with size effect correction;
- Table 2.8 for the in-plane gusset data-set.

where the covariance coefficients ρ_{ij} are calculated by inverting the observed Fisher matrix, as explained in Section 2.3.3.

For all three data-sets, the correlation coefficient $c_{m_0 m_1}$ is equal to -1.00, which indicates a perfect negative linear dependency between the intercept of the S-N curve, m_0 , and the slope of the S-N curve, m_1 . For the cover plate data-set and for the cover plate data-set with size effect correction, the correlation coefficient $c_{\mu_V \sigma_V}$ is equal to -0.03, which indicates that there is no linear correlation between the location parameter and the scale parameter of the log-CAFL probability distribution. For the in-plane gusset data-set, the correlation coefficient $c_{\mu_V \sigma_V}$ is equal to -0.62, which indicates a moderate negative linear dependency between the location parameter and the scale parameter of the log-CAFL distribution. For all three data-sets, there is no linear correlation between: 1) The S-N curve variance parameter, σ , and all other parameters; and 2) The S-N curve parameters m_0 , m_1 and the log-CAFL parameters μ_V , σ_V .

Parameter	ML estimate $V = \mathcal{N}$		ML estimate $V = \text{EV}$	
	MLE	St.Dev.	MLE	St.Dev.
m_0	29.017	2.935	29.138	3.002
m_1	-3.416	0.786	-3.448	0.804
σ	-0.544	0.197	-0.540	0.199
μ_V	3.556	0.0577	3.646	0.0679
σ_V	-1.623	0.408	-1.592	0.440
$n\hat{LL}$	24.47		24.74	

Table 2.3: Cover plate, CA S-N model parameters

$$\underline{\underline{c}} = \begin{bmatrix} 1.00 & -1.00 & 0.07 & -0.05 & 0.06 \\ \vdots & 1.00 & -0.07 & 0.05 & -0.06 \\ \vdots & \vdots & 1.00 & -0.04 & 0.04 \\ \vdots & \vdots & \vdots & 1.00 & -0.03 \\ \vdots & \vdots & \vdots & \vdots & 1.00 \end{bmatrix}$$

Table 2.4: Cover plate, CA S-N model corr. matrix, ($V = \mathcal{N}$) case

Parameter	ML estimate $V = \mathcal{N}$		ML estimate $V = \text{EV}$	
	MLE	St.Dev.	MLE	St.Dev.
m_0	28.657	2.852	28.775	2.920
m_1	-3.416	0.786	-3.448	0.804
σ	-0.544	0.197	-0.540	0.199
μ_V	3.451	0.0577	3.540	0.0679
σ_V	-1.623	0.408	-1.592	0.440
$n\hat{LL}$	24.47		24.74	

Table 2.5: Cover plate with size effect correction, CA S-N model parameters

$$\underline{\underline{c}} = \begin{bmatrix} 1.00 & -1.00 & 0.07 & -0.05 & 0.06 \\ \vdots & 1.00 & -0.07 & 0.05 & -0.06 \\ \vdots & \vdots & 1.00 & -0.04 & 0.04 \\ \vdots & \vdots & \vdots & 1.00 & -0.03 \\ \vdots & \vdots & \vdots & \vdots & 1.00 \end{bmatrix}$$

Table 2.6: Cover plate with size effect correction, CA S-N model corr. matrix, ($V = \mathcal{N}$) case

Parameter	ML estimate $V = \mathcal{N}$		ML estimate $V = EV$	
	MLE	St.Dev.	MLE	St.Dev.
m_0	25.770	0.945	25.804	0.954
m_1	-2.666	0.209	-2.674	0.211
σ	-1.048	0.144	-1.048	0.144
μ_V	3.864	0.127	3.966	0.104
σ_V	-1.667	0.498	-1.712	0.590
$n\hat{LL}$	12.34		13.52	

Table 2.7: In-plane gusset, CA S-N model parameters

$$\underline{\underline{c}} = \begin{bmatrix} 1.00 & -1.00 & 0.00 & -0.06 & 0.06 \\ \vdots & 1.00 & -0.00 & 0.05 & -0.06 \\ \vdots & \vdots & 1.00 & -0.00 & 0.00 \\ \vdots & \vdots & \vdots & 1.00 & -0.62 \\ \vdots & \vdots & \vdots & \vdots & 1.00 \end{bmatrix}$$

Table 2.8: In-plane gusset, CA S-N model correlation matrix, ($V = \mathcal{N}$) case

2.5.1 S-N curves – Cover plate

Figure 2.6 shows the ML-MCS-based median S-N curve and ML-MCS-based 0.05 quantile linearized S-N curve, for the cover plate data-set. The non-linear 0.05 quantile S-N curve was computed using the MCS scheme presented in Section 2.3.3, with $\eta_{sam} = 1 \cdot 10^5$; the non-linear 0.05 quantile S-N curve was then linearized as explained in Section 2.3.3: the detail is classified as FAT51, with CAFL=24MPa and knee point at $27 \cdot 10^6$ cycles. Figure 2.8 shows the median S-N curve and the characteristic S-N curve based on the statistical method recommended in Commentary to Eurocode 3 (see Section 2.2), for the cover plate data-set: the detail is classified as FAT47 with CAFL=36MPa assumed to start at $5 \cdot 10^6$ cycles^{vi}. The comparison of the ML-MCS-based 0.05 quantile linearized S-N curve with the characteristic S-N curves from standards, for the cover plate data-set (see Figure 2.10), gives the following information:

- The Commentary to Eurocode3-based S-N curve and the EN1993-1-9 FAT50 S-N curve are almost coincident;
- The estimation of the fatigue strength in the finite life (FL) region ($N < 5 \cdot 10^6$), according

^{vi}The difference between the S-N curve based on Commentary to Eurocode3 and the S-N curve based on Eurocode3 is that the first one is obtained by applying the Eurocode statistical approach to the experimental data-sets considered in this thesis, while the latter one is the S-N curve corresponding to the FAT classification of the considered detail and which is not related to the experimental data-set considered in this thesis

to EN1993-1-9 FAT50 and the IIW FAT50 S-N curves, is slightly over-conservative with respect to the ML-MCS S-N curve: the probability of failure is slightly lower than 5%;

- The estimation of the fatigue strength in the FL region ($N < 5 \cdot 10^6$), according to AASHTO FAT56 S-N curve, is slightly under-conservative with respect to the ML-MCS S-N curve: the probability of failure is slightly higher than 5%;
- The estimation of the CAFL, according to EN3 FAT 50 S-N curve, is highly unsafe: 6 failures point lie below the EN3-based CAFL and the probability of exceeding the EN3-based CAFL is considerably lower than 95%;
- The estimation of the CAFL, according to IIW FAT50 and the AASHTO FAT56 S-N curves, is slightly under-conservative with respect to the ML-MCS S-N curve: the probability of exceeding the IIW-based and the AASHTO-based CAFL is lower than 95%.

Figure 2.7 shows the ML-MCS-based median S-N curve and the ML-MCS-based 0.05 quantile linearized S-N curve, for the cover plate data-set with size effect correction. Due to the reduction of the nominal applied stress ranges, the detail drops from FAT51 to FAT46 and the CAFL drops from 24MPa to 21MPa; the position of the knee point is not affected by the reduction of the nominal applied stress ranges. The same reduction is observed in Commentary to Eurocode 3 document-based characteristic S-N curve (see Figure 2.9). The comparison of the ML-MCS-based 0.05 quantile linearized S-N curves with the characteristic S-N curves from standards, for the cover plate data-set with size effect correction (see Figure 2.11), gives the following information:

- The EN3 Commentary doc.-based and the EN3 FAT50 characteristic S-N curves are almost coincident;
- The estimation of the fatigue strength in the FL region ($N < 5 \cdot 10^6$), according to EN3 FAT 45 S-N curves, is slightly over-conservative with respect to the ML-MCS S-N curve: the probability of failure is slightly lower than 5%;
- The estimation of the fatigue strength in the FL region ($N < 5 \cdot 10^6$), according to IIW FAT 50 characteristic S-N curves, is slightly under-conservative with respect to the ML-MCS S-N curve: the probability of failure is slightly higher than 5%;
- The estimation of the fatigue strength in the FL region ($N < 5 \cdot 10^6$), according to AASHTO FAT40 S-N curve, is considerably over-conservative with respect to the ML-MCS S-N curve: the probability of failure is considerably lower than 5%;

- The estimation of the CAFL, according to EN3 FAT 45 S-N curve, is highly unsafe: 6 failures point lie below the EN3-based CAFL and the probability of exceeding the EN3-based CAFL is considerably lower than 95%;
- The estimation of the CAFL, according to IIW FAT 50 S-N curve, is slightly unsafe: 2 failures point lie below the EN3-based CAFL and the probability of exceeding the IIW-based CAFL is slightly lower than 95%;
- The estimation of the CAFL, according to AASHTO FAT40 S-N curve, is over-conservative with respect to the ML-MCS S-N curve: the probability of exceeding the AASHTO-based CAFL is higher than 95%.

2.5.2 S-N curves – In-plane gusset

Figure 2.12 shows the ML-MCS-based median S-N curve and ML-MCS-based 0.05 quantile linearized S-N curve, for the in-plane gusset data-set: the detail is classified as FAT54, with CAFL=30MPa and knee point at $9.8 \cdot 10^6$ cycles. Figure 2.13 shows the median S-N curve and the characteristic S-N curve based on the statistic method recommended in EN3 Commentary document (see Section 2.2), for the in-plane gusset data-set: the detail is classified as FAT53 with CAFL=38MPa assumed to start at $5 \cdot 10^6$ cycles. The comparison of the ML-MCS-based 0.05 quantile linearized S-N curve with the characteristic S-N curves from standards, for the in-plane gusset data-set (see Figure 2.14), gives the following information:

- The EN3 FAT40 S-N curve is more conservative than the EN3 Commentary doc.-based S-N curve (FAT53);
- The IIW FAT50 S-N curve, the AASHTO FAT56 S-N curve and the ML-MCS-based S-N curve are almost coincident in the FL region ($N < 5 \cdot 10^6$ cycles);
- The estimation of the fatigue strength in the FL region ($N < 5 \cdot 10^6$), according to EN3 FAT 40 S-N curve, is over-conservative with respect to the ML-MCS-based S-N curve: the probability of failure is lower than 5%;
- The AASHTO FAT56 S-N curve, the IIW FAT50 S-N curve and ML-MCS-based S-N curve, give very similar estimation of the CAFL;
- The estimation of the CAFL, according to EN3 Commentary doc.-based S-N curves, is under-conservative with respect to the ML-MCS S-N curve, however no failure points exist to confirm this.

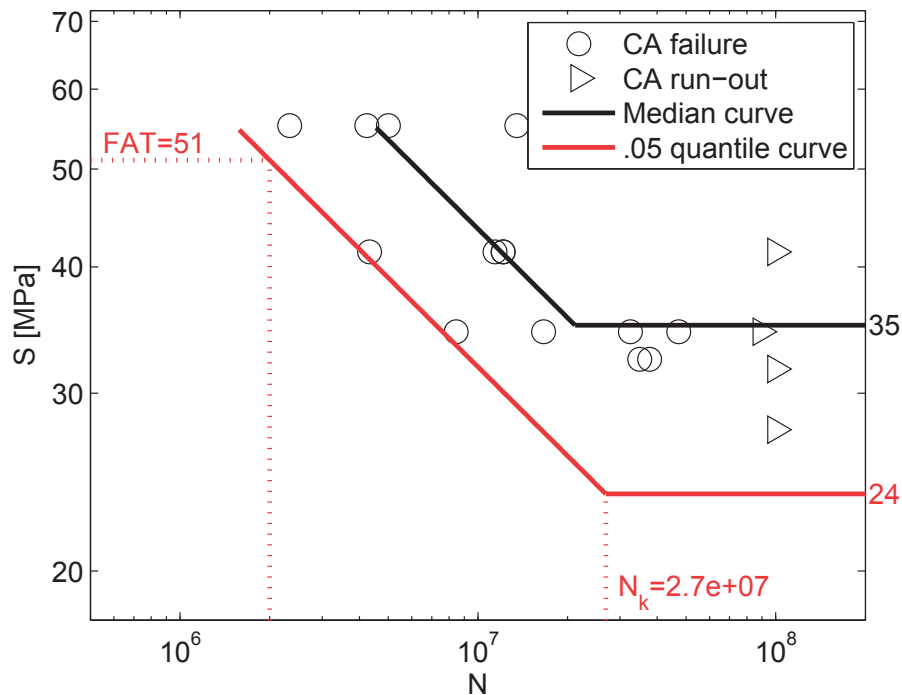


Figure 2.6: Cover plate, ML-MCS-based S-N curves

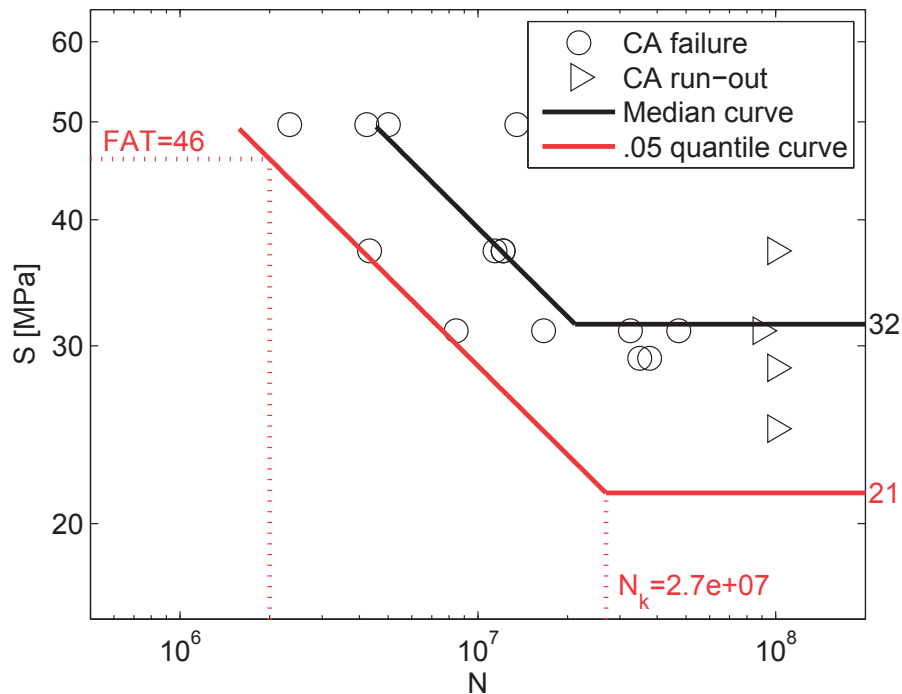


Figure 2.7: Cover plate with size effect correction, ML-MCS-based S-N curves

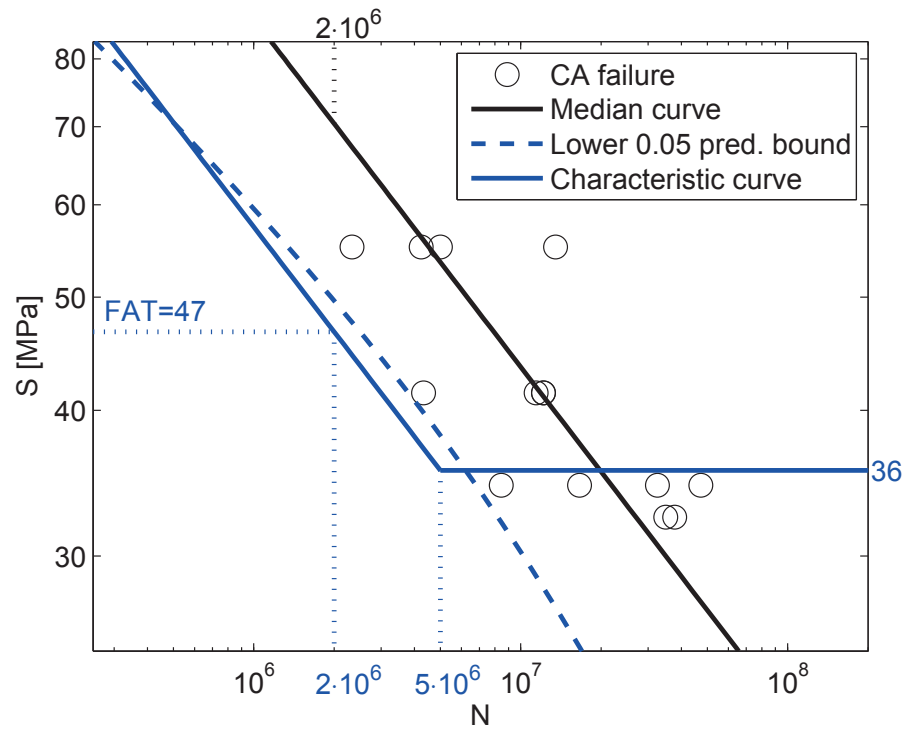


Figure 2.8: Cover plate, Comment. to Eurocode3-based S-N curves

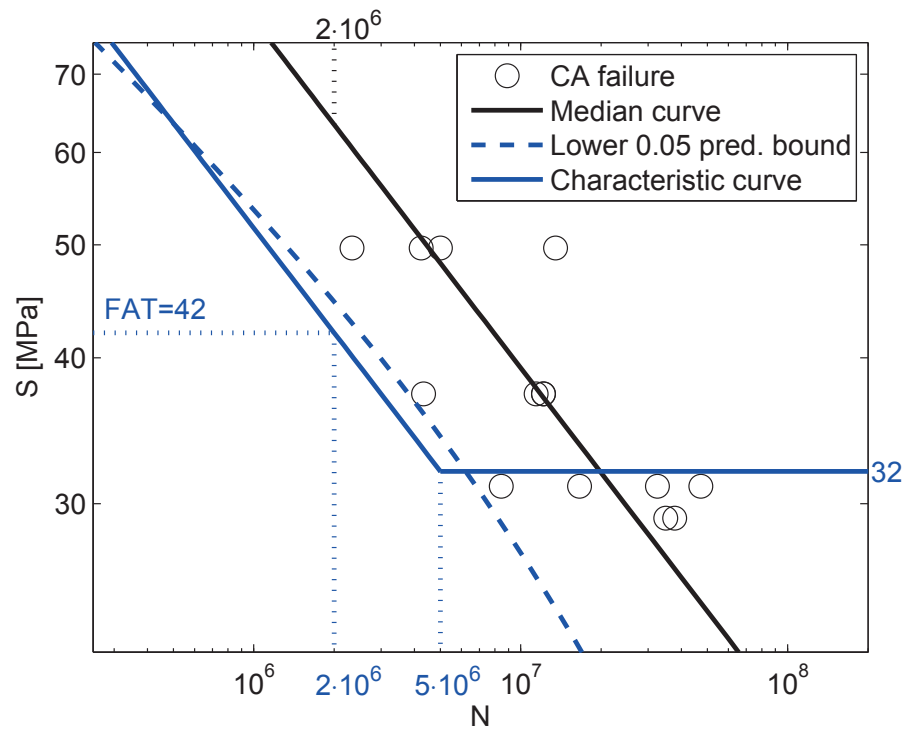


Figure 2.9: Cover plate with size effect correction, Comment. to Eurocode3-based S-N curves

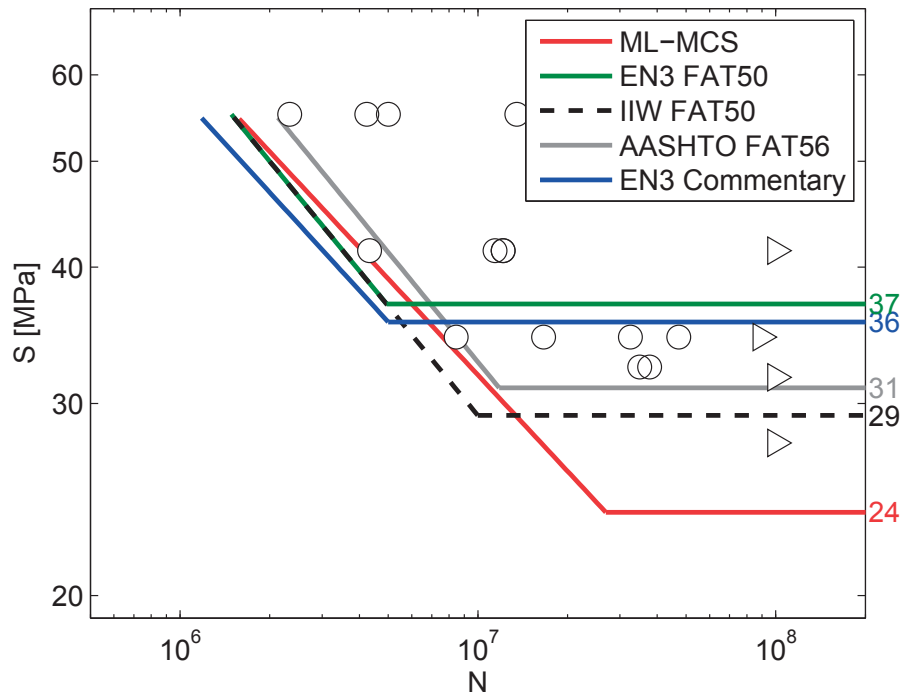


Figure 2.10: Cover plate, characteristic S-N curves

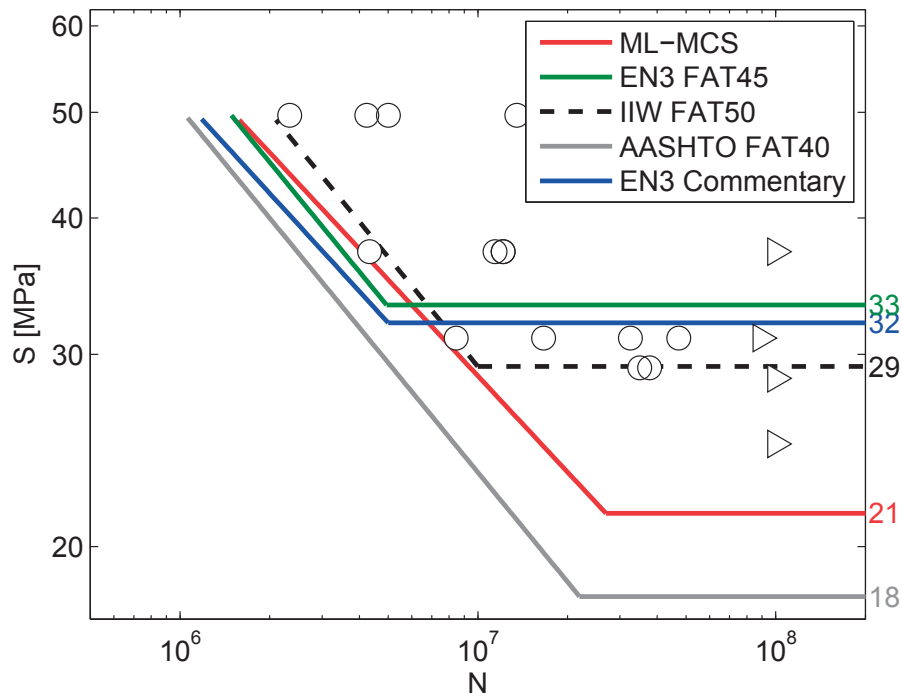


Figure 2.11: Cover plate, with size effect correction, characteristic S-N curves

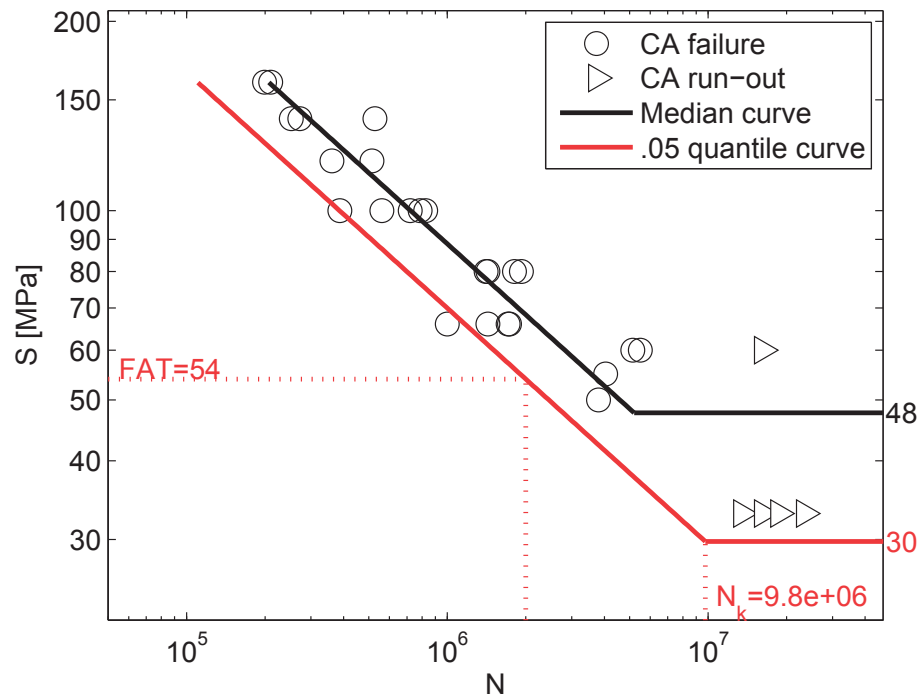


Figure 2.12: In-plane gusset, ML-MCS-based S-N curves

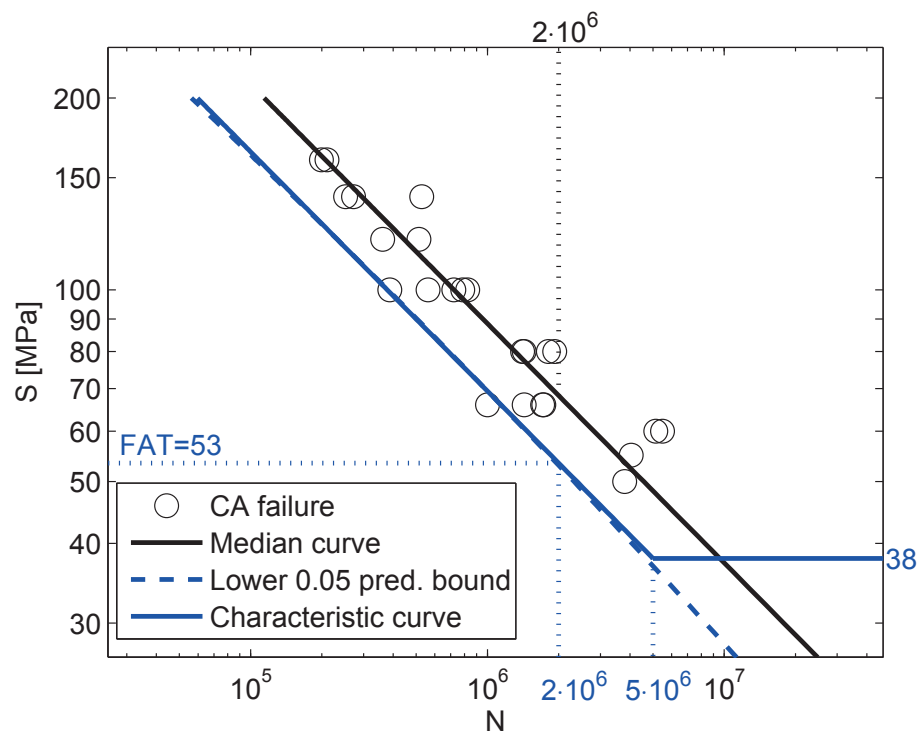


Figure 2.13: In-plane gusset, Comment. to Eurocode3-based S-N curves

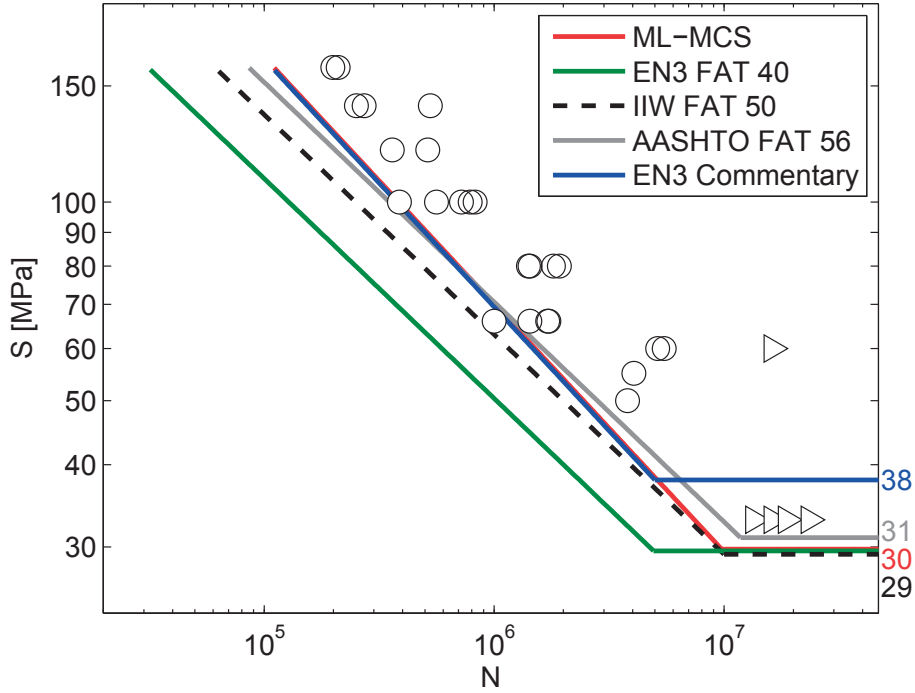


Figure 2.14: In-plane gusset, characteristic S-N curves

It is remarked that the MCS scheme used for estimation of characteristic S-N curves takes into account both: 1) The epistemic uncertainty of S-N model parameters; and 2) The aleatory uncertainty of the CAFL and of the fatigue life.

In order to assess the influence of the aleatory uncertainty following analysis was carried out, by considering the cover-plate and the in-plane gusset data-sets:

1. 10^6 S-N curves were sampled by only considering the epistemic uncertainty of S-N model parameters; two vectors of size $(10^6 \times 1)$ were created by taking from each sampled curve the CAFL and the number of cycle N^* corresponding to the fatigue strength at $2 \cdot 10^6$ cycles according to the median S-N curve ($S = 69.9$ MPa for the cover-plate, while $S = 68.3$ MPa for the in-plane gusset). These vectors were fitted with two log-Normal distributions (CAFL and N^* log-Normal distributions);
2. Step 1 was repeated by considering both the epistemic uncertainty of S-N model parameters and the aleatory uncertainty of the fatigue life and of the CAFL;
3. Log-Normal distributions of the CAFL and of N^* estimated at Step 1 were compared to log-Normal distributions of the CAFL and of N^* estimated at Step 2, in terms of the coefficient of variation.

For the cover-plate, Figure 2.15 shows that: 1) The coefficient of variation of the $N^* = N(S = 69.9\text{MPa})$ distribution significantly increases from 0.46 to 0.86, by taking into account both the epistemic uncertainty of S-N model parameters and the aleatory uncertainty of the fatigue life, with respect to the case where only the epistemic uncertainty of S-N model parameters is considered; and 2) The coefficient of variation of the CAFL distribution notably increases from 0.06 to 0.24, by taking into account both the epistemic uncertainty of S-N model parameters and the aleatory uncertainty of the CAFL, with respect to the case where only the epistemic uncertainty of S-N model parameters is considered. For the in-plane gusset, Figure 2.16 confirms the strong influence of the aleatory uncertainty of the fatigue life and of the aleatory uncertainty of the CAFL, respectively on the $N^* = N(S = 68.3\text{MPa})$ distribution (the coefficient of variation increases from 0.09 to 0.38) and on the CAFL distribution (the coefficient of variation increases from 0.13 to 0.28).

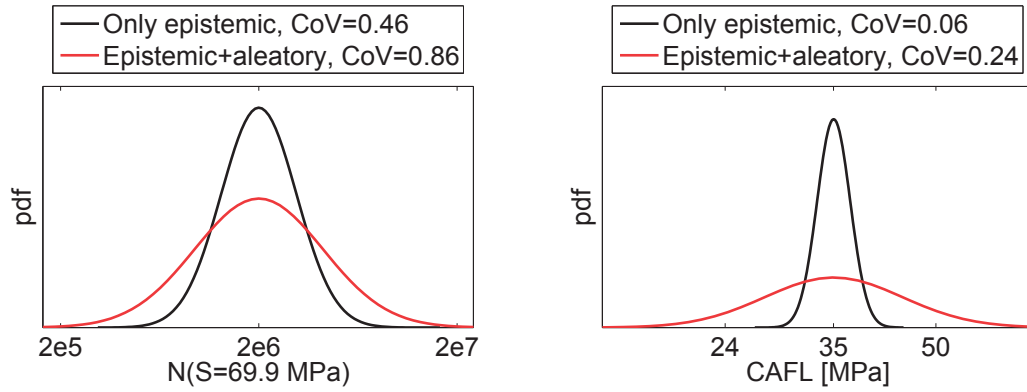


Figure 2.15: Influence of the aleatory uncertainty of the fatigue life and of the CAFL, cover-plate

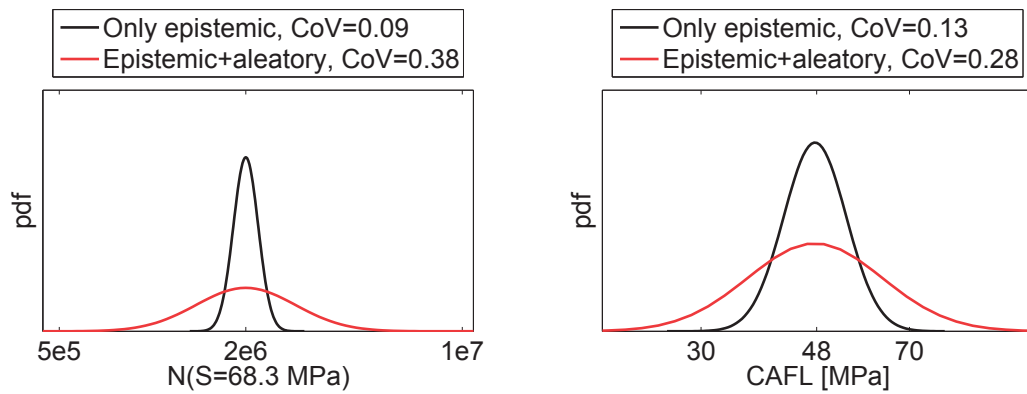


Figure 2.16: Influence of the aleatory uncertainty of the fatigue life and of the CAFL, in-plane gusset

2.6 Conclusions and discussion

In this Chapter a new approach for estimation of CA S-N curves of welded components was presented, with application to three study cases. The new approach was implemented in the Matlab Toolbox TB1 (see Appendix B) allowing for ML fitting of linear S-N model to experimental fatigue data-sets and MCS estimation of true p -quantile S-N curves. The ML-MCS approach-based characteristic S-N curves were linearized for direct comparison with current standards.

The conclusions from this Chapter are as follows:

- The statistical method for evaluation of fatigue S-N curves recommended by Commentary to Eurocode 3 document [29] is affected by several limitations^{vii}: 1) The median S-N curve is estimated by fitting a linear regression to failure data and disregarding run-out data, resulting in loss of information; 2) The characteristic curve is estimated by assuming the fatigue data-set as homoscedastic and by considering the fatigue scatter at $2 \cdot 10^6$ cycles as representative of fatigue scatter at all number of cycles; and 3) The CAFL is arbitrarily assumed to start at $5 \cdot 10^6$ cycles. The ML-MCS approach presented here overcomes these limitations by using run-out data for ML estimation of S-N model, and by including the CAFL and the fatigue scatter in the stochastic model;
- The RFL model proposed by Pascual [58] allows to overcome limitations of Eurocode 3 approach but does not give straightforward method for estimating characteristic S-N curves; the ML-MCS approach presented here allows for computation of true p -quantiles of fatigue life and direct estimation of characteristic S-N curves. Moreover the RFL fitting model is not linear and direct comparison with current standards is not straightforward as for ML-MCS-based S-N curves;
- The estimates of CA S-N stochastic model for all considered data-sets show that the choice of modeling the CAFL as a log-Normal random variable maximizes the sample Likelihood information (see Tables 2.3 and 2.7). In order to make the cover-plate CA data-set consistent with the VA cover plate data-set (used for estimation of VA S-N stochastic model, see Section 3.3), a size effect correction was applied to the cover-plate data-set; also for the cover plate data-set with size correction the choice of modeling the CAFL as a log-normal random variable maximizes the sample Likelihood information (see Table 2.5);

^{vii}The statistical procedures for evaluating S-N curves, recommended in other standards (IIW, AAHSTO), show minor differences with respect to Eurocode recommendations and they are affected by the same limitations.

- The CA S-N model correlation matrix for all considered data-sets shows that there is a perfect negative linear correlation between the intercept and the slope of the S-N curve in the log-S-N plane, while it is realistic to assume that the parameters of the CAFL distribution are independent from the parameters of the S-N curve (see Tables 2.4, 2.6 and 2.8);
- The ML-MCS characteristic S-N curves for all considered data-sets were linearized for direct comparison with current standards. Eurocode 1993-1-9 standards, AASHTO bridge design specifications and IIW recommendations provide estimation of fatigue strength in the FL region ($N < 5 \cdot 10^6$ cycles) which is similar to the estimation based on ML-MCS approach (see Figures 2.10, 2.11 and 2.14).

A larger difference can be observed in the HCF region: for the cover plate data-set, all standards provide unsafe estimation of the CAFL and of the knee point (see Figure 2.10); for the cover plate with size effect correction data-set both Eurocode and AASHTO-based S-N curves provide unsafe estimation of the CAFL and of the knee point (with significant amount of experimental failure points lying below the CAFL), while the AASHTO-based S-N curve provides over-conservative estimation of the CAFL (see Figure 2.11); for the in-plane gussets all standards provide very similar estimation of CAFL (see Figure 2.14);

- The assumption of having the knee point at a number of cycles which increases as the fatigue strength at 2 million cycles decreases (as assumed in AASHTO specifications) seems to be confirmed by estimated ML-MCS S-N curves (cover plate with size effect correction has $FAT = 46$ and knee point at $2.7 \cdot 10^7$ cycles, while the in-plane gusset has $FAT = 54$ and knee point at $9.8 \cdot 10^6$ cycles). This has to be confirmed by further experimental results.

The findings listed above suggest that the limitations included in the current standards could lead to unsafe estimation of fatigue strength, especially in the HCF region. The approach presented in this Chapter constitutes a powerful tool which can be used to re-define current standard S-N curves and relative FAT categories. It has to be noted that use of experimental fatigue data-sets containing significant information in the region between $5 \cdot 10^6$ and 10^8 cycles will reduce the uncertainty on estimation of the CAFL and of the knee point and it will improve the confidence in estimated S-N curves.

3 S-N curves for variable amplitude loadings

3.1 Introduction

Welded joints in road bridges are subjected to VA fatigue loading histories. The fatigue design of new bridges and the fatigue assessment of existing bridges are based on CA S-N curves, used in combination with Miner's rule. CA S-N curves are based on fatigue data from CA experimental tests. According to Miner's rule, following condition has to be verified for fatigue verification:

$$\sum_{i=1}^{n_{tot}} \frac{n_i}{N_i} \leq D_c \quad (3.1)$$

where:

- n_i is the number of cycles corresponding to the applied nominal stress range, S_i ;
- n_{tot} is the total number of stress range cycles;
- N_i is the number of cycles to failure corresponding to S_i ;
- D_c is the critical value of the damage sum.

The first critical aspect in using Miner's rule is how to consider the influence on the fatigue damage of the stress range cycles below the CAFL. In Eurocode standards [24] and in IIW recommendations [40], the CA characteristic S-N curve is bent at the CAFL position from the slope $m_1 = -3$ to the slope $m_2 = -5$; a cut-off limit is fixed at 10^8 cycles. The use of the reduced (flatter) slope $m_2 = -5$ has been proposed by Haibach [36], by assuming a continuously decreasing of the fatigue limit as a function of the linear accumulated damage [37].

According to the Haibach's hypothesis, the standard format of Miner's rule verification (see

Equation 3.1) is replaced by:

$$\sum_{i=1}^{n_{tot1}} \frac{n_i}{N_i} + \sum_{j=1}^{n_{tot2}} \frac{n_j}{N_j} \leq D_c \quad (3.2)$$

where:

- n_i is the number of cycles corresponding to the applied nominal stress range, S_i , with $S_i \geq \text{CAFL}$;
- n_j is the number of cycles corresponding to the applied nominal stress range, S_j , with $S_j < \text{CAFL}$;
- n_{tot1} and n_{tot2} are respectively the total number of stress range cycles above and below the CAFL;
- N_i is the number of cycles to failure corresponding to S_i ;
- N_j is the number of cycles to failure corresponding to S_j .

In AASHTO bridge design specifications [2] the CA S-N curve is extrapolated below the CAFL with no slope change, but a variable amplitude fatigue limit (VAFL) is set at $\text{CAFL}/2$, which is another way of dealing with all stress ranges lower than CAFL contribute less to fatigue damage.

Up to now, the use of the second slope m_2 has not been sufficiently justified by means of VA fatigue test results; at present the influence of the stress range cycles below the CAFL, on the fatigue damage, is still under debate.

Fisher et al. [26] performed fatigue tests of eight large beams with longitudinal attachments and welded cover plates, using different Rayleigh loading spectra with a CAFL^i exceedance rate ranging from 0.1% and 12%. They found that if any of the stress ranges in the loading spectrum exceeded the CAFL, then all cycles contribute to fatigue damage and the one-slope extrapolated S-N curve should be used.

Marquis [48] performed fatigue test of non-load carrying carbon and stainless steel fillet welds, at $R=-1$, using three different concave upwards truncated spectra. He found that the use of the Miner's rule in combination with a bent S-N curve was unsafe, while the use of the extrapolated one-slope S-N curve gave conservative estimate of fatigue damage.

Gurney [33] proposed an alternative approach to assess the influence of small stress range cycles on fatigue damage. VA experimental results were analysed in terms of number of blocks to failure. With different test specimens, the minimum damaging stress range was found by

ⁱCAFL of the characteristic curve of studied detail, according to AASHTO specifications [2]

gradually decreasing the lowest stress range of loading spectra and checking the effect on the number of blocks to failure: if the lowest stress range didn't damage then an increase of blocks to failure was expected. Concave upward spectra having constant relative fatigue damage, $(S_i^{m_1} \cdot n_i / S_{max} \cdot 1.0)$, were used in this type of investigation. The results obtained for as-welded specimens tested with 4 different concave upward spectra, with a peak range at $R=0$, showed that stress range cycles down to 10MPa were fully damaging (suggesting the use of one-slope extrapolated S-N curve).

Zhang and Maddox [81] published results of an investigation of fatigue damage in welded joints under VA loading spectra. Two types of fillet welded connections were tested: 1) longitudinal non-load-carrying in-plane gusset; and 2) longitudinal non-load-carrying fillet welded joint. A concave up stress spectrum, having a relative fatigue damage, $(S_i^{m_1} \cdot n_i / S_{max} \cdot 1.0)$, that increases with decreasing stress ranges, was used in order to make the results of VA tests more sensitive to small stress ranges. The VA test results were analysed using Miner's rule with three different S-N curves: 1) S-N curve with no-slope change; 2) S-N curve with slope change at the CAFL (at 10^7 cycles, according to BS standards); 3) S-N curve with cut-off at the CAFL. Comparison of number of block to failures and damage sums for spectra having different minimum stress ranges, allowed authors to conclude that stress ranges well below the CAFL were fully damaging.

Albrecht et al. [3] reported experimental CA and VA fatigue test results for 192 specimens from different types of welded joints; VA spectra were proportional to real truck traffic histograms which were recorded on several U.S. bridges. VA results were plotted in the CA log(S-N) plane in terms of the RMC stress range of the spectrum $(S_{eq} = (\sum n_i / n_{tot} \cdot S_i^3)^{\frac{1}{3}})$. They found that: 1) VA and CA fatigue test data correlate well in the FL region; 2) When the maximum stress range of the VA spectrum is equal to the CAFL, the equivalent VA stress range is equal to the VA fatigue limit (VAFL in AASHTO bridge design specifications); 3) When the percentage of VA stress range cycles below the CAFL increases, the CA S-N curve gradually bends and approaches the VAFL; and 4) Since the position of the VAFL depends on the type of loading spectrum it is not possible to establish a unique formulation for the VAFL; for loading spectra similar to the truck traffic proportional spectrum, it is safe to fix the VAFL at 50% of the CAFL. In conclusion, studies presented above provide support to the use of one-slope S-N curve for fatigue analysis under VA loadings.

The second critical aspect in using Miner's rule is related to the choice of the critical value of the damage sum, D_c .

Miner and Palmgreen [53] settled D_c to 1.0 by assuming that the fatigue damage corresponding to each stress cycle of a VA loading sequence is the same as that due to the same stress cycle under CA loading sequence. However, many studies have shown that the stress cycles of a VA

loading sequences could be more damaging than the same stress cycles under CA loading, with the result that the Miner's rule can be unsafe in some cases.

In their investigation, Zhang and Maddox [81] considered three types of loading sequences: A) Constant maximum stress; B) Constant mean stress; and C) Constant minimum stress. In order to evaluate the accuracy of Miner's rule by eliminating influence of mean stress, CA S-N curves were assessed by mean of CA experimental tests at constant maximum stress (same condition as the sequence A). Results for both details showed a strong dependence of the damage sum at failure, $\sum n/N$, to the loading sequence: the Miner's rule was highly non conservative for all tests under sequence A ($\sum n/N \leq 0.4$), slightly non conservative for tests under sequence B ($\sum n/N \leq 0.8$), and conservative for tests under sequence C ($\sum n/N \geq 1.3$). Results of fatigue VA tests on 3 types of welded connections (longitudinal non load carrying fillet welds [67, 26, 78, 10, 4, 9], welded cover plates [67], transverse non load carrying fillet welds [30, 9]), under random and block loading spectra, were re-analysed by Gurney [33]. The analysis gave following results: 1) For the longitudinal non-load carrying fillet weld, tested under Rayleigh and Laplace random loading spectra, $\sum n/N$ (computed using BS F mean curve) ranged from 0.14 to 2.89 with a mean of 0.63; 2) For the longitudinal non-load carrying fillet weld, tested under block loading spectra, $\sum n/N$ (computed using BS F mean curve) ranged from 0.71 to 3.65 with a mean of 1.04; 3) For the welded cover plate beams, tested under Rayleigh spectra, $\sum n/N$ (computed using BS G mean curve) ranged from 0.53 to 6.69 with a mean of 1.23; 4) For the transverse non-load carrying fillet weld, tested under block loading spectra, $\sum n/N$ (computed using BS F mean curve) ranged from 0.91 to 12.08 with a mean of 2.50. Results show that the damage sum at failure is highly variable and shall be treated as a random variable.

In his block program investigation, Gurney [33] observed a strong influence of the form of the loading spectrum on the value of damage sum at failure: wide band loading was more damaging than narrow band loadingⁱⁱ. This effect was more significant at $R=-1.0$ than at $R=0$. Gurney also observed that the block program investigation gave values of $\sum n/N$ considerably more optimistic than other fatigue test program involving other types of spectra. Gurney analysed also the influence of loading spectrum parameters on the fatigue strength of as-welded specimens which were tested at constant stress ratio, R . He found that: 1) For concave upwards spectra (see Figure 3.1 (a)), $\sum n/N$ did not depend on the shape parameter k ⁱⁱⁱ; 2) For concave downwards spectra (see Figure 3.1 (b)) having block length smaller than 1000

ⁱⁱAccording to [33] the most reliable method to define spectrum characteristics, in particular the bandwidth, is the Markov transition matrix, which has starting stress levels as row entries and finishing stress levels as column entries: for narrow band loadings all non zero entries are located close to the diagonal, while for wide band loadings non zero entries might be located anywhere. As often loading rates and ramp length are correlated, many authors consider that narrow band loadings correspond to narrow frequency loading histories

ⁱⁱⁱThe shape parameter, k , characterizes the concavity of the loading spectrum (see Figure 3.1). The spectrum is concave upward for $k > 1$ and concave downward for $k < 1$

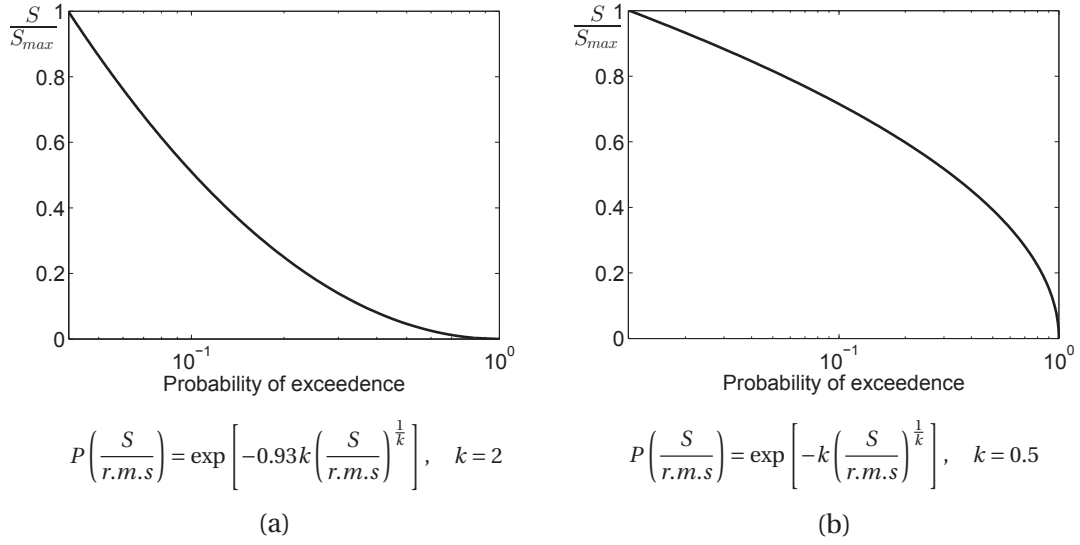


Figure 3.1: Exceedance diagrams for Weibull spectrum with k shape factor. (a) Concave upward spectrum; (b) Concave downward spectrum

cycles, $\sum n/N$ increased with k to a peak and then decreased; instead for concave downwards spectra having block length bigger than 16250 cycles, $\sum n/N$ increased monotonically with k ; 3) For concave downwards spectra, $\sum n/N$ increased with the block length; and 4) The clipping ratio^{iv} had little influence on $\sum n/N$.

Albrecht et al. [5] reviewed previous studies on VA amplitude fatigue in both finite life region and high cycle fatigue region. They proposed a simplified non-linear S-N model which approaches gradually the VAFL, for the fatigue assessment of steel bridges. They observed that the sequence of the blocks of the stress range spectrum, the spectrum size, the spectrum bandwidth and the minimum stress range did not have significant effect on $\sum n/N$.

The investigations listed above give an indication of influence of different VA loading spectrum parameters on the fatigue strength of analysed welded connections; however, these works only provide general trends and do not present a rigorous statistical approach which allows to make inference about the reduce slope, m_2 , and the critical damage sum, D_c . Moreover, they are affected by two substantial limitations: 1) The CA S-N curves used with Miner's rule have inaccurate definition of CAFL and of fatigue life scatter (especially in HCF region); 2) The approach used in these studies is qualitative and does not allow to formally characterize the randomness in the S-N curve variables and in the critical damage sum variable. In this Chapter a ML-MCS approach is proposed for estimation of: 1) Characteristic S-N curve under VA fatigue loadings; and 2) Critical value of damage sum at failure, D_c . The critical

^{iv}The clipping ratio is the ratio between the maximum stress range and the r.m.s. of the process $\left(S_{max}/\sqrt{\sum(S_i)^2/n}\right)$

damage sum is modeled as a random variable whose parameters are included in the VA S-N model parameter vector. The slope of the characteristic S-N curve and the parameters of D_c distributions are estimated by using novel scheme which combines ML and MCS techniques by using the CA S-N stochastic model and the experimental data-set from VA fatigue tests. The novel contribution of this approach is summarized in following points:

- The slope of the S-N curve below the CAFL, m_2 and the critical damage sum D_c are validated by using VA experimental results;
- The effect of the stress range cycles below the CAFL is not arbitrarily assumed but it's represented by the estimated m_2 and D_c ;
- Load sequence, stress ratio, spectrum shape, loading bandwidth and block length effects are represented in the variability of the D_c random variable.

The ML-MCS approach for estimation of VA S-N curves is implemented in VAsamgener and VApstproc modules of Matlab Toolbox TB1 (see Appendix B).

The Chapter is organized as follows:

- in Section 3.2.1 the ML-MCS approach for estimation of VA S-N curves is presented;
- in Section 3.3 the application of the ML-MCS approach on two study cases is presented;
- in Section 3.4 results of analysis of two considered study cases are presented;
- in Section 3.5 results are discussed.

3.2 New probabilistic approach

The VA S-N stochastic model is defined by the S-N curve under VA loadings (Equation 3.3) and by the fatigue failure condition (Equation 3.4):

$$Y = \begin{cases} m_0 + m_1 X + \epsilon(0, \exp(\sigma)), & \text{for } X > V \\ m_0 + V \Delta m + (m_1 - \Delta m) X + \epsilon(0, \exp(\sigma)), & \text{for } X \leq V \end{cases} \quad (3.3)$$

$$\sum_{i=1}^{n_{tot}} \frac{n_i}{\exp(Y(x_i))} = D_c(\mu_D, \sigma_D), \quad \text{if } \max(x_i) > V \quad (3.4)$$

where:

- m_0 and m_1 are the intercept and the slope of the S-N curve, which are defined in the CA S-N stochastic model;
- $\epsilon(0, \exp(\sigma))$ is the error term, which is defined in the CA S-N stochastic model;
- $V(\mu_V, \sigma_V)$ is the natural logarithm of the CAFL, which is defined in the CA S-N stochastic model;
- $\Delta m = m_1 - m_2$, where m_2 is the slope of the S-N curve below the CAFL;
- $D_c(\mu_D, \sigma_D)$ is the critical damage sum.

D_c is a random variable following a log-Normal (conventional choice) or a Weibull distribution with location parameter equal to μ_D and scale parameter equal to σ_D .

The VA S-N stochastic model is defined by the model parameter vector $\underline{\Theta} = (\underline{\theta}, \mu_D, \sigma_D) |_{\Delta m}$ and by the covariance matrix $\underline{\Sigma}(\underline{\Theta})$.

3.2.1 ML-MCS estimation of VA S-N stochastic model

The VA S-N stochastic model is estimated with a novel ML-MCS scheme, using experimental VA fatigue results.

Let denote the VA fatigue data-set as follows:

$$(\omega_t, y_t) |_{t=1 \dots n_{ts}} \quad (3.5)$$

where ω_t is the t^{th} stress range spectrum, y_t is the natural logarithm of number cycles to the end of the t^{th} test and n_{ts} is the total number of tests.

The damage, d_t , associated with the t^{th} test, is:

$$d_t(\underline{\theta}, \Delta m) = \sum_{i=1}^{n_{tot1}} \frac{n_i}{\exp(Y(m_0, m_1, \sigma; x_i))} + \sum_{j=1}^{n_{tot2}} \frac{n_j}{\exp(Y(m_0, m_1, \sigma, V(\mu_V, \sigma_V), \Delta m; x_j))} \quad (3.6)$$

where n_{tot1} and n_{tot2} are respectively the number of stress range cycles above the CAFL and below the CAFL in the spectrum ω_t .

The fatigue failure condition is:

$$d_t(\underline{\theta}, \Delta m) = D_c(\mu_D, \sigma_D) \quad (3.7)$$

where the critical damage sum, D_c , is a random variable following a log-Normal or a Weibull distribution, with parameters μ_D and σ_D .

Following ML-MCS scheme is used to estimate the parameters of VA S-N stochastic model:

1. The experimental VA fatigue data-set is re-simulated η_{res} time. The re-simulated experimental data-set is:

$$(\omega_t, y_t) |_{t=1, \dots, n_{ts} \cdot \eta_{res}}$$

2. One vector $\underline{\tilde{\theta}}_k$ is sampled from the CA S-N stochastic model $\left[\underline{\theta}, \underline{\rho} \right]$; then, one S-N curve is sampled by using the sampled $\underline{\tilde{\theta}}_k$. The epistemic uncertainty of S-N model parameters is taken into account in the $\underline{\tilde{\theta}}_k$ sampling, while the aleatory uncertainty of the CAFL and the aleatory uncertainty of the fatigue life are taken into account in the S-N curve sampling.

For a given value of parameter $\Delta \tilde{m}$ the negative log-Likelihood of the re-simulated sample is computed as follows:

$$nLL_k(\mu_{D_k}, \sigma_{D_k}) |_{\Delta \tilde{m}} = - \sum_{j=1}^{\eta_{res}} \left[\sum_{t=1}^{n_f} \ln(f_D(\mu_{D_k}, \sigma_{D_k}, \Delta \tilde{m}; d_t)) + \sum_{t=1}^{n_r} \ln(1 - F_D(\mu_{D_k}, \sigma_{D_k}, \Delta \tilde{m}; d_t)) \right]$$

where n_f is the number of failures, n_r is the number of run-outs, f_D is the pdf of the random variable D_c and F_D is the cdf of the random variable D_c .

3. ML estimates of parameters μ_D and σ_D are computed by minimizing the negative log-Likelihood of the re-simulated sample:

$$(\hat{\mu}_D, \hat{\sigma}_D)_k = \arg \min_{\mu_{D_k}, \sigma_{D_k}} (nLL_k(\mu_{D_k}, \sigma_{D_k}) |_{\Delta \tilde{m}})$$

4. Steps 1-3 are iterated η_{iter} times.

The $\underline{\underline{G}}$ matrix and the \underline{L} vector are built:

$$\begin{aligned} \underline{\underline{G}} &= [(\underline{\theta})_k \quad (\hat{\mu}_D)_k \quad (\hat{\sigma}_D)_k] |_{\Delta \tilde{m}} \quad \text{for } k = 1, \dots, \eta_{iter} \\ \underline{L} &= [(n\hat{L}L)_k] |_{\Delta \tilde{m}} \quad \text{for } k = 1, \dots, \eta_{iter} \end{aligned}$$

5. Under the assumption of asymptotic normality of ML estimators^v $\hat{\mu}_D, \hat{\sigma}_D, n\hat{L}L$, it is observed that: 1) The matrix $\underline{\underline{G}}$ contains n_{iter} realizations of the multivariate Normal random variable $(\underline{\theta}, \hat{\mu}_D, \hat{\sigma}_D)$; and 2) The vector \underline{L} contains η_{iter} realizations of the Normal random variable $n\hat{L}L$.

For a given value of parameter $\Delta \tilde{m}$, the VA S-N model parameter vector, $\underline{\Theta}$, and the covariance matrix, $\underline{\underline{\Sigma}}(\underline{\Theta})$ are computed as follows:

^vThis hypothesis is verified by using probability plots

$$\underline{\Theta}(\Delta\tilde{m}) = E \left[\underline{G} \right] \Big|_{\Delta\tilde{m}}$$

$$\underline{\Sigma}(\Delta\tilde{m}) = E \left[\left(\underline{G} - E(\underline{G}) \right) \cdot \left(\underline{G} - E(\underline{G}) \right)^T \right] \Big|_{\Delta\tilde{m}}$$

The mean of the $n\hat{L}L$ distribution is indicated as $\overline{n\hat{L}L}$.

6. Steps 1-5 are repeated for different values of $\Delta\tilde{m}$. The ML estimate of the parameter Δm is chosen as the value which minimizes the mean of the $n\hat{L}L$ distribution^{vi}:

$$\Delta\hat{m} = \underset{\Delta\tilde{m}}{\operatorname{argmin}} \left(\overline{n\hat{L}L}(\Delta\tilde{m}) \right)$$

The ML estimate of the VA S-N model parameter vector and the covariance matrix are:

$$\hat{\underline{\Theta}} = \underline{\Theta}(\Delta\hat{m})$$

$$\hat{\underline{\Sigma}} = \underline{\Sigma}(\Delta\hat{m})$$

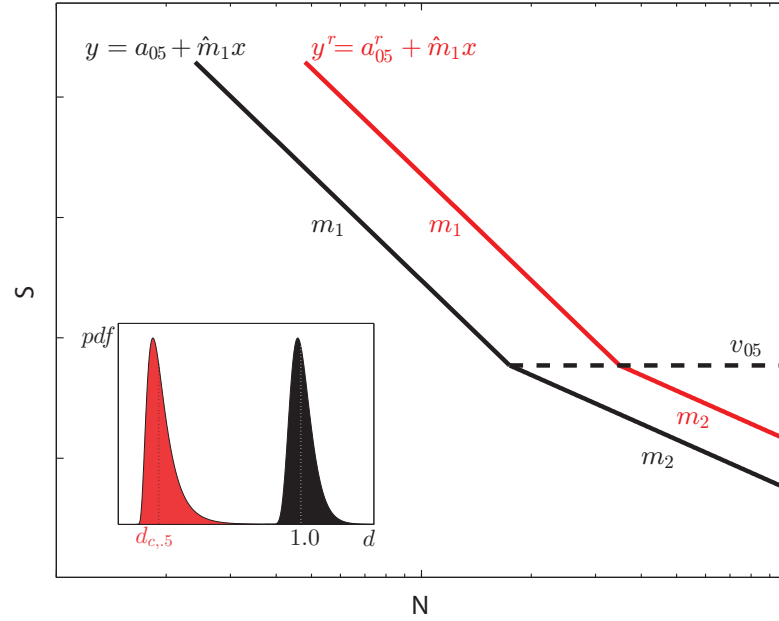


Figure 3.2: ML-MCS-based VA characteristic S-N curve and re-scaled VA characteristic S-N curve

^{vi}The choice of computing different $\Theta(\Delta\tilde{m})$ vectors by assuming different values of $\Delta\tilde{m}$ (steps 1-5) and then to proceed in searching for the value $\Delta\hat{m}$ which minimizes $\overline{n\hat{L}L}(\Delta\hat{m})$ (step 6) was made because the initial choice of including Δm in the model parameter vector did not work in terms of numerical optimization

Chapter 3. S-N curves for variable amplitude loadings

A sensitivity study is performed in order to determine the parameters η_{iter} and η_{res} that have to be used in the ML-MCS scheme described above. Since the $\overline{n\hat{L}L}$ is not a deterministic parameter, the minimum search algorithm includes a Box-plot test to ensure that $\overline{n\hat{L}L}(\Delta\hat{m})$ is lower than $\overline{n\hat{L}L}(\Delta\hat{m} \pm 1)$ at 5% significance level. The ML-MCS based characteristic S-N curve is defined as follows:

$$y_{.05} = \begin{cases} a_{.05} + \hat{m}_1 x, & \text{for } x > \nu_{.05} \\ a_{.05} + \nu_{.05} \Delta\hat{m} + (\hat{m}_1 - \Delta\hat{m})x, & \text{for } x \leq \nu_{.05} \end{cases} \quad (3.8)$$

The characteristic S-N curve in Equation 3.8 has to be used in combination with following damage accumulation rule:

$$\sum_{i=1}^{n_{tot}} \frac{n_i}{\exp(y_{.05}(x_i))} \leq d_{c,.5}, \quad \text{with } d_{c,.5} = F_D^{-1}(0.5, \mu_D, \sigma_D) \quad (3.9)$$

where F_D^{-1} is the inverse of the cdf of the critical damage, D_c .

The ML-MCS-based VA characteristic S-N curve has to be re-scaled for direct comparison with VA characteristic S-N curves from the standards, which consider $d_{c,.5} = 1.0$.

The ML-MCS-based re-scaled VA characteristic S-N curve (see Figure 3.2) is defined as follows:

$$y_{.05}^r = \begin{cases} a_{.05} - \ln(1/d_{c,.5}) + \hat{m}_1 x, & \text{for } x > \nu_{.05} \\ a_{.05} - \ln(1/d_{c,.5}) + \nu_{.05} \Delta\hat{m} + (\hat{m}_1 - \Delta\hat{m})x, & \text{for } x \leq \nu_{.05} \end{cases} \quad (3.10)$$

Three cases are considered for the cut-off stress range, S_{co} : 1) No cut-off stress range; 2) Cut-off stress range at 14.6 MPa, which corresponds to the cut-off stress range of the lowest FAT category in EN 1993-1-9; 3) Cut-off stress range at 50% of the CAFL, according to [76].

3.3 Study cases

The ML-MCS approach was applied on the two fatigue data-sets analysed in Chapter 2.

3.3.1 Cover Plate

VA experimental data-set for cover plate detail is made of 32 data points (see Table 3.1) from testing of end-welded cover plate beam, under 5 different wide-band Rayleigh-type stress range spectra with a block length ranging between 1001 and 10001 cycles [26]. The thickness of the beam flange and of the cover plate is 25.4mm: the detail is classified as FAT45 according to EN1993-1-9 [29], as FAT50 according to IIW recommendations [40], and as FAT 40 (with CAFL=18MPa) according to AASHTO bridge design specifications [2]. The CA S-N stochastic model estimated by using the cover plate CA data-set with size effect correction is used for ML-MCS estimation of VA S-N stochastic model.

3.3.2 In-plane gusset

VA experimental data-set for in-plane gusset detail is made of 21 data points (see Table 3.2) from testing of welded in-plane gussets, under 9 different three-blocks stress range spectra with a block length ranging between 800 and $152 \cdot 10^3$ cycles and constant relative damage ($S_i^{m_1} \cdot n_i / S_{max}$) (ICOM tests, [8]). The attachment length, L , is equal to 150mm: the detail is classified as FAT40 according to EN1993-1-9 [29], as FAT50 according to IIW recommendations [40], and as FAT56 (with CAFL=31MPa) according to AASHTO bridge design specifications [2].

Chapter 3. S-N curves for variable amplitude loadings

S_i [MPa]	n_i				
8				170	
9	73			1200	
10			170	3600	
11	190		1200	1600	
12	237		1700	1300	
13			3500	800	
14	207	73	1300	900	
15			800	200	
16	146		600	100	
17		190	300	60	
18	83		200	60	
19	40	237	100	10	
20			60		
21	16		40		
22		207	20		
23	5		10		
25	2	146			
26				1	670
27					600
28		83			
29	1				300
30		40			200
31			1		
32					100
33		16			
34					60
35					40
36		5			
37					20
38		2			10
51					1
58		1			
$n_{fail} \cdot 10^6 \rightarrow$	> 107.2	120	> 104	> 109	34.7
	> 107.2	120	> 104	> 109	> 34.7
	> 107.2	> 120	> 104	> 109	> 34.7
	> 107.2	> 120	104	> 109	> 34.7
	> 107.2	120			34.7
	> 107.2	120			> 34.7
	> 107.2	> 120			32
	> 107.2	> 120			> 34.7
	> 107.2	> 120			> 34.7

Table 3.1: Cover plate, VA experimental data-set. The column S_i represents the stress ranges of the loading spectrum. The columns n_i represent the number of cycles associated to the stress ranges of the first column; each column of n_i represents a different spectrum. In the lower part of the table, the number of cycles to failure, n_{fail} , are presented; the values which are presented in the same column were obtained under the same loading spectrum. The symbol > is used to indicate a run-out

3.3. Study cases

S_i [MPa]	n_i								
30				3700	29600	15200	6400		$152 \cdot 10^3$
40			2700	1560	12500	6400	2700	$64 \cdot 10^3$	$64 \cdot 10^3$
50		3278	1383	800				$33 \cdot 10^3$	
60	3701	1896	800				800		
70									
80	1562	800				800		$8 \cdot 10^3$	$8 \cdot 10^3$
90									
100	800				800				
$n_{fail} \cdot 10^6 \rightarrow$	1.11	1.61	4.61	> 40.0	6.78	13.2	9.52	3.17	15.08
	1.18	2.43	4.73	10.4	9.64	9.15	> 22.1	3.65	
				14.0			16.1	3.67	
							> 29.6		

Table 3.2: In-plane gusset, VA experimental data-set. The column S_i represents the stress ranges of the loading spectrum. The columns n_i represent the number of cycles associated to the stress ranges of the first column; each column of n_i represents a different spectrum. In the lower part of the table, the number of cycles to failure, n_{fail} , are presented; the values which are presented in the same column were obtained under the same loading spectrum. The symbol > is used to indicate a run-out

3.4 Results

VA S-N models were estimated for the two analysed VA data-sets, using the ML-MCS scheme presented in Section 3.2.1. Three cut-off cases (No cut-off, $S_{co} = 14.6\text{MPa}$, $S_{co} = 0.5 \cdot \text{CAFL}$) and two critical damage sum distributions ($D_c = \log \mathcal{N}$, $D_c = \mathcal{W}$) were considered.

In order to choose the sampling parameters n_{iter} , η_{res} of ML-MCS scheme, a sensitivity study was carried out, using cover plate VA data-set with combination *No cut-off* / $D_c = \mathcal{W}$. For $n_{iter} = [100, 1000, 2000, 5000]$, $\eta_{res} = [10, 50, 100, 200]$, and $\Delta m = \Delta \hat{m} = 8$, the parameter $n\hat{LL}$ was sampled 16 times and $\Delta n\hat{LL} = (\overline{n\hat{LL}_{max}} / \overline{n\hat{LL}_{min}} - 1)$ was computed. Table 3.3 shows that for $\eta_{iter} = 5000$ and $\eta_{res} = 100$, then $\Delta n\hat{LL}$ is lower than 0.2%: for a negative log-Likelihood equal to 1000, the variation in \hat{nLL} is close to unity, which ensures an accurate ML estimation of the Δm parameter for a Δm step equal to 1. The combination $\eta_{iter} = 5000, \eta_{res} = 100$ was chosen for the estimation of VA S-N models.

The ML estimates of parameters $\mu_D, \sigma_D, \Delta m$ and the value of the negative log-Likelihood at ML estimates, for the cover-plate data-set, are shown in Table 3.4. The combination *no cut-off* / $D_c = \mathcal{W}$ gives the best fit in terms of negative log-Likelihood. Between the two cut-off cases, the case $S_{co} = 14.6\text{MPa}$ gives the best fit in terms of negative log-Likelihood. Table 3.5 shows that for the cover plate data-set there is a strong negative linear correlation between the parameters of the critical damage sum, D_c , and that there is no linear correlation between the parameters of the S-N curve and the parameters of the critical damage sum, D_c .

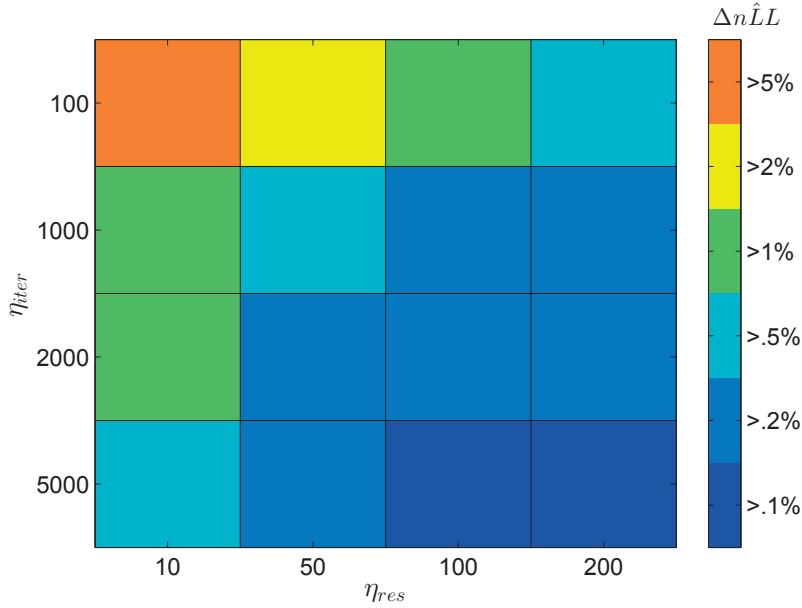


Table 3.3: Sensitivity study on ML-MCS scheme parameters, Cover plate, *no cut-off* / $D_c = \mathcal{W}$

3.4. Results

Cut-off case	/	D_c	\hat{m}_o	\hat{m}_1	$\hat{\sigma}$	$\hat{\mu}_V$	$\hat{\sigma}_V$	$\hat{\mu}_D$	$\hat{\sigma}_D$	$\Delta\hat{m}$	$\overline{n\hat{L}L}$
no cut-off	/	$\log\mathcal{N}_{\mathcal{W}}$	28.65	-3.42	-0.54	3.45	-1.62	0.50	1.46	7	1431
								1.70	1.40	8	1183
14.6MPa	/	$\log\mathcal{N}_{\mathcal{W}}$						0.50	0.87	4	1339
								1.75	1.61	7	1190
0.5·CAFL	/	$\log\mathcal{N}_{\mathcal{W}}$						0.59	1.24	6	1482
								2.13	1.28	8	1324

Table 3.4: Cover plate, VA S-N curve parameters

$$\underline{\underline{c}} = \begin{bmatrix} 1.00 & -1.00 & 0.08 & -0.05 & 0.06 & -0.03 & 0.01 \\ \vdots & 1.00 & -0.07 & 0.05 & -0.06 & 0.02 & 0.01 \\ \vdots & \vdots & 1.00 & -0.04 & 0.04 & 0.02 & 0.00 \\ \vdots & \vdots & \vdots & 1.00 & -0.03 & -0.00 & -0.01 \\ \vdots & \vdots & \vdots & \vdots & 1.00 & 0.03 & -0.00 \\ \vdots & \vdots & \vdots & \vdots & \vdots & 1.00 & -0.71 \\ \vdots & \vdots & \vdots & \vdots & \vdots & \vdots & 1.00 \end{bmatrix}$$

Table 3.5: Cover plate, VA S-N model correlation matrix, *no cut-off* / $D_c = \mathcal{W}$

Cut-off case	/	D_c	\hat{m}_o	\hat{m}_1	$\hat{\sigma}$	$\hat{\mu}_V$	$\hat{\sigma}_V$	$\hat{\mu}_D$	$\hat{\sigma}_D$	$\Delta\hat{m}$	$\overline{n\hat{L}L}$
no cut-off	/	$\log \mathcal{N}_{\mathcal{W}}$	25.77	-2.67	-1.05	3.86	-1.67	-0.31	0.60	5	1009
								1.00	1.48	5	1343
14.6MPa	/	$\log \mathcal{N}_{\mathcal{W}}$						-0.30	0.60	5	1009
								1.00	1.48	5	1343
0.5-CAFL	/	$\log \mathcal{N}_{\mathcal{W}}$						-0.26	0.61	5	1117
								1.07	1.40	5	1486

Table 3.6: In-plane gusset, VA S-N curve parameters

$$\underline{\underline{c}} = \begin{bmatrix} 1.00 & -1.00 & 0.00 & -0.05 & 0.06 & -0.01 & 0.01 \\ \vdots & 1.00 & -0.00 & 0.05 & -0.06 & 0.00 & 0.00 \\ \vdots & \vdots & 1.00 & -0.01 & 0.01 & 0.01 & 0.02 \\ \vdots & \vdots & \vdots & 1.00 & -0.62 & -0.08 & -0.02 \\ \vdots & \vdots & \vdots & \vdots & 1.00 & 0.04 & 0.02 \\ \vdots & \vdots & \vdots & \vdots & \vdots & 1.00 & 0.37 \\ \vdots & \vdots & \vdots & \vdots & \vdots & \vdots & 1.00 \end{bmatrix}$$

Table 3.7: In-plane gusset, VA S-N model correlation matrix, *no cut-off* / $D_c = \log \mathcal{N}$

The ML estimates of parameters $\mu_D, \sigma_D, \Delta m$ and the value of the negative log-Likelihood at ML estimates, for the in-plane gusset data-set, are shown in Table 3.6. The combination (no cut-off/ $D_c = \log \mathcal{N}$) gives the best fit in terms of negative log-Likelihood. Between the two cut-off cases, the case $S_{co} = 14.6 \text{ MPa}$ gives the best fit in terms of negative log-Likelihood. Table 3.7 shows that for the in-plane gusset data-set there is a weak negative linear correlation between the parameters of the critical damage sum, D_c , and there is no linear correlation between the parameters of the S-N curve and the parameters of the critical damage sum, D_c . The assumption of asymptotic normality of $\hat{\mu}_D, \hat{\sigma}_D, n\hat{LL}$ estimators (see step 5 of the ML-MCS approach in Section 3.2.1) is verified by: 1) Comparing the η_{iter} sampled value of $\hat{\mu}_D, \hat{\sigma}_D, n\hat{LL}$ with theoretical normal pdf; and 2) Producing probability plots for the η_{iter} sampled value of $\hat{\mu}_D, \hat{\sigma}_D, n\hat{LL}$. Density plots in Figures 3.3, 3.5, 3.7, 3.9, 3.11, 3.13 and probability plots in Figures 3.4, 3.6, 3.8, 3.10, 3.12, 3.14 support the hypothesis of asymptotic normality of the multivariate vector $(\hat{\mu}_D, \hat{\sigma}_D, n\hat{LL})$ for both the cover-plate data-set and the in-plane gusset data-set.

For the cover plate data-set and no cut-off case, the graph $\overline{n\hat{LL}} - \Delta m$ shows that $D_c = \mathcal{W}$ gives the best fit in terms of Likelihood (see Figure 3.15). The ML estimate of the slope range, $\Delta\hat{m}$, was estimated by producing notched box plots at the four Δm values which gave the four minimum values of $\overline{n\hat{LL}}$. Figure 3.16 shows that box-plot notches at $\Delta m = 8$ and $\Delta m = 9$ overlap, indicating that $\overline{n\hat{LL}}(\Delta m = 9)$ is not significantly lower than $\overline{n\hat{LL}}(\Delta m = 8)$ at the 5% significance level: $\Delta\hat{m} = 8$ is conservatively taken as ML estimate of the slope range.

For the in-plane gusset data-set and no cut-off case, the graph $\overline{n\hat{LL}} - \Delta m$ shows that $D_c = \log \mathcal{N}$ gives the best fit in terms of Likelihood (see Figure 3.17). Figure 3.18 shows that box-plot notches at $\Delta m = 4$ and $\Delta m = 5$ do not overlap, indicating that $\overline{n\hat{LL}}(\Delta m = 5)$ is significantly lower than $\overline{n\hat{LL}}(\Delta m = 4)$ at the 5% significance level: $\Delta\hat{m} = 5$ is taken as ML estimate of the slope range.

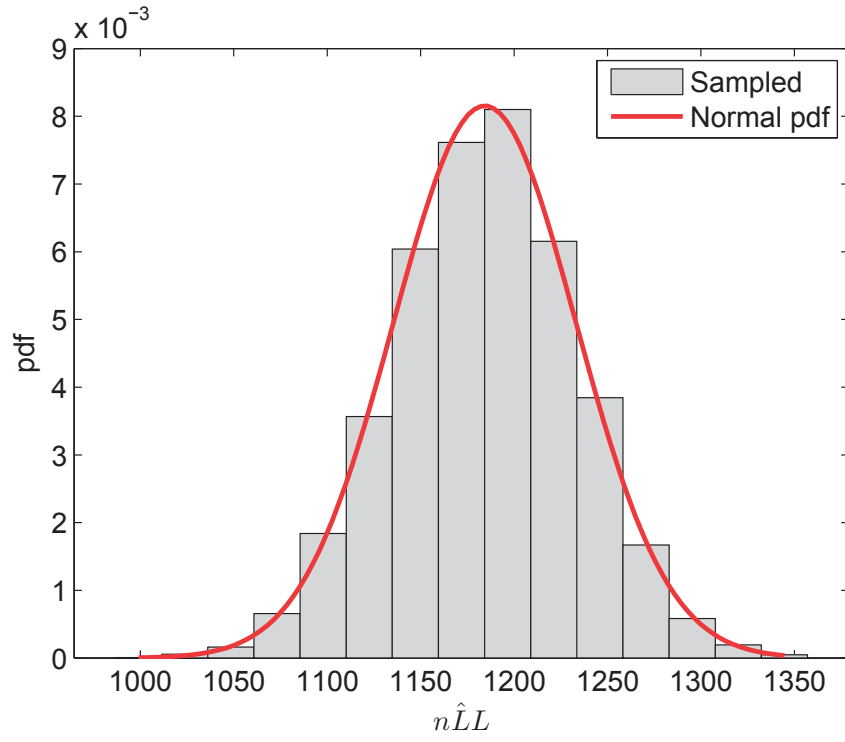


Figure 3.3: Cover plate, pdf of VA neg. log-Likelihood, no cut-off / $D_c = \mathcal{W}$

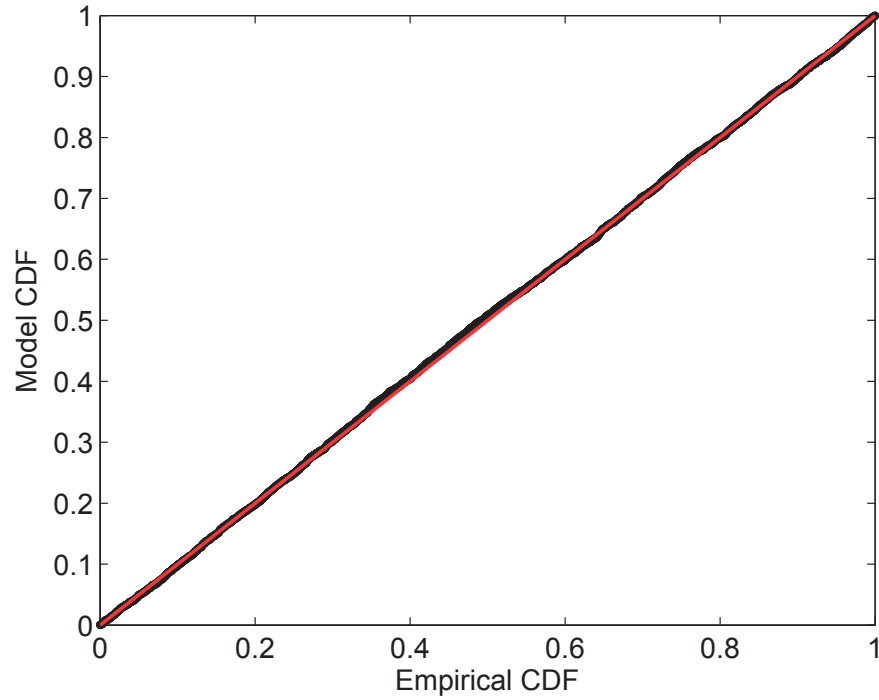


Figure 3.4: Cover plate, Probability plot of VA neg. log-Likelihood, no cut-off / $D_c = \mathcal{W}$

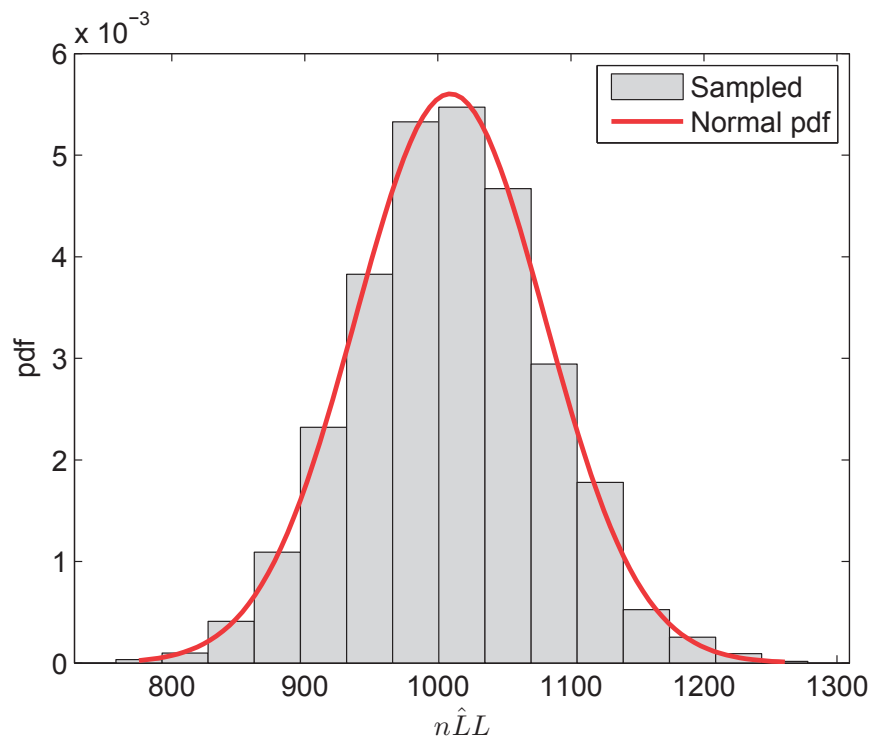


Figure 3.5: In-plane gusset, pdf of VA neg. log-Likelihood, no cut-off / $D_c = \log \mathcal{N}$

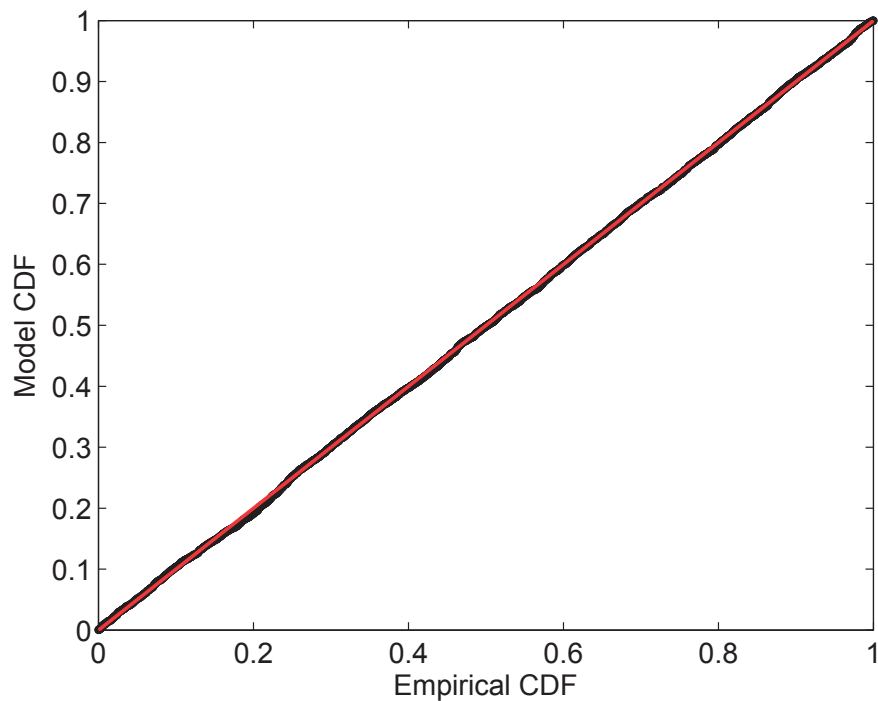


Figure 3.6: In-plane gusset, Probability plot of VA neg. log-Likelihood, no cut-off / $D_c = \log \mathcal{N}$

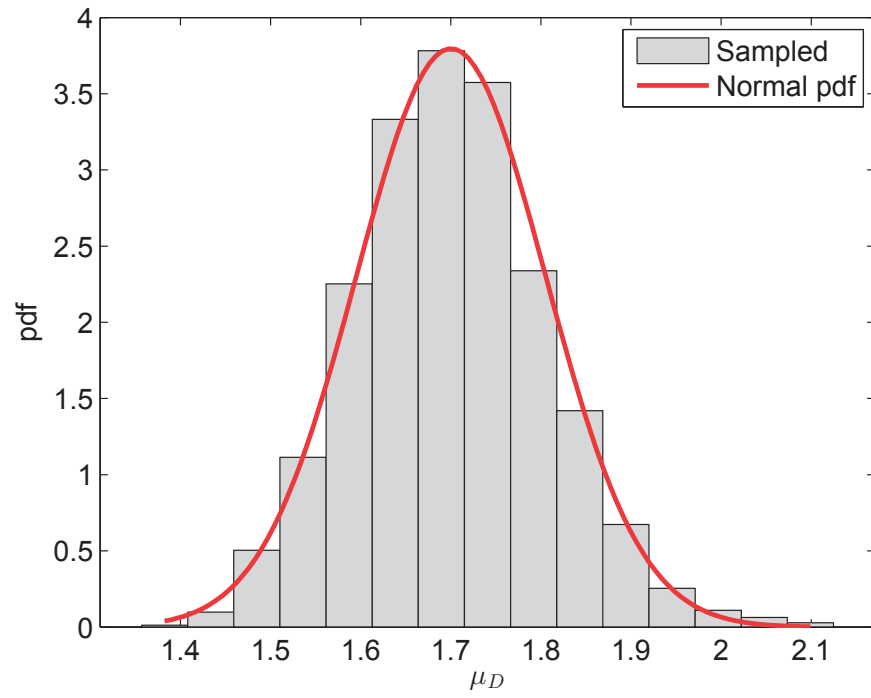


Figure 3.7: Cover plate, pdf of the parameter μ_D , no cut-off / $D_c = \mathcal{W}$

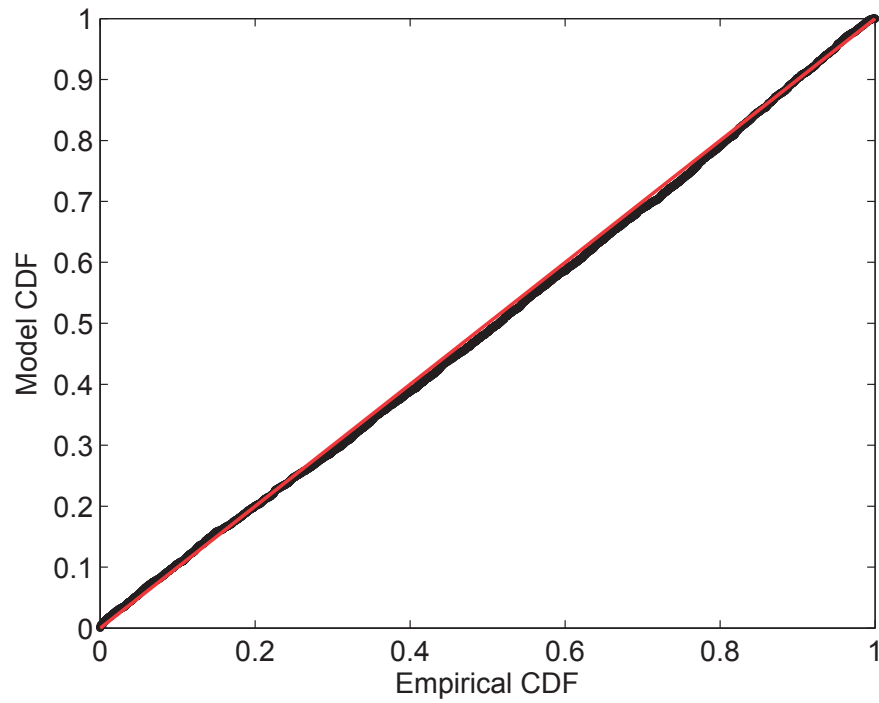


Figure 3.8: Cover plate, Probability plot of the parameter μ_D , no cut-off / $D_c = \mathcal{W}$

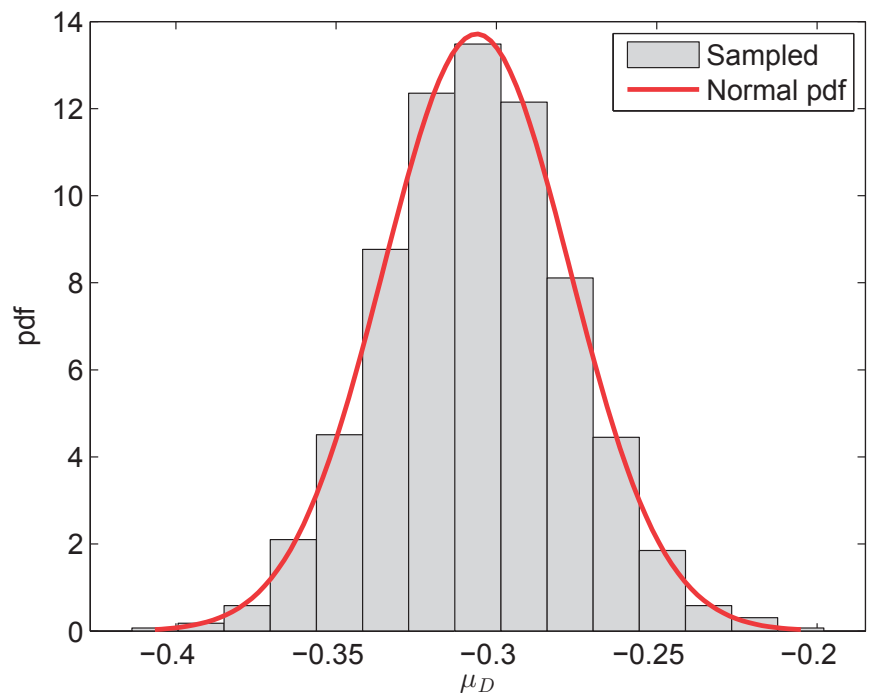


Figure 3.9: In-plane gusset, pdf of the parameter μ_D , no cut-off / $D_c = \log \mathcal{N}$

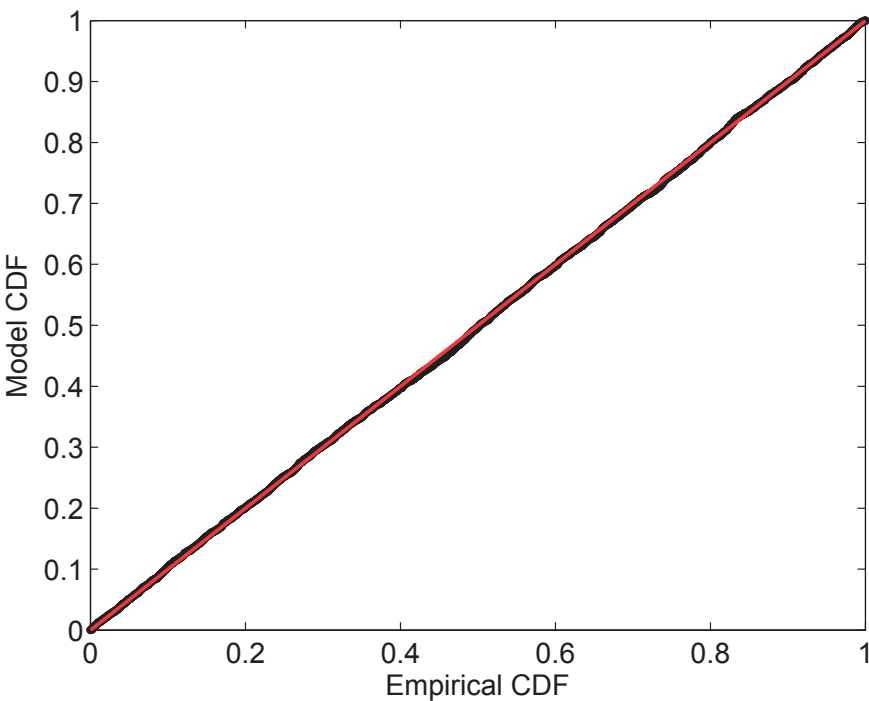


Figure 3.10: In-plane gusset, Probabiltiy plot of the parameter μ_D , no cut-off / $D_c = \log \mathcal{N}$

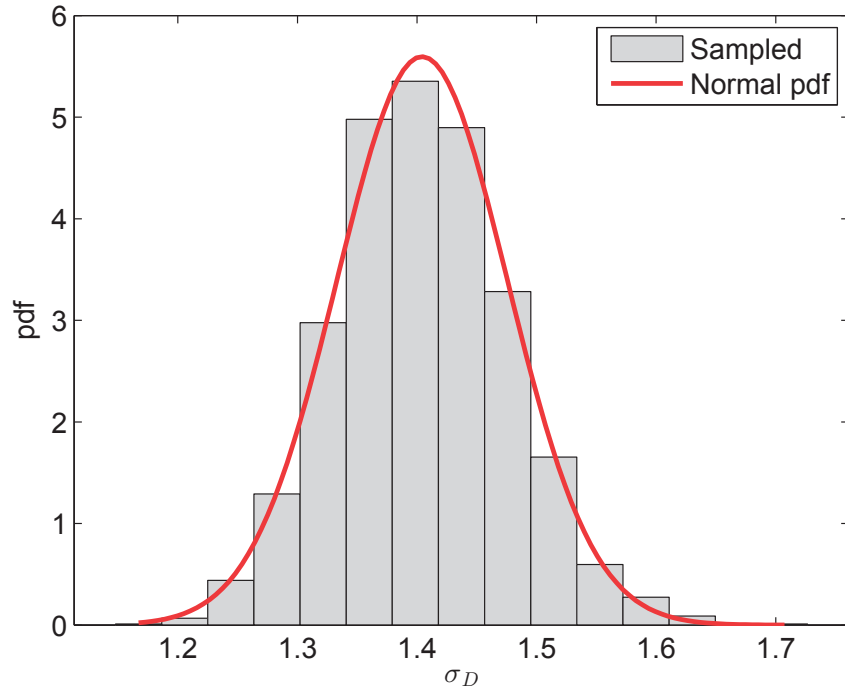


Figure 3.11: Cover plate, pdf of the parameter σ_D , no cut-off / $D_c = \mathcal{W}$

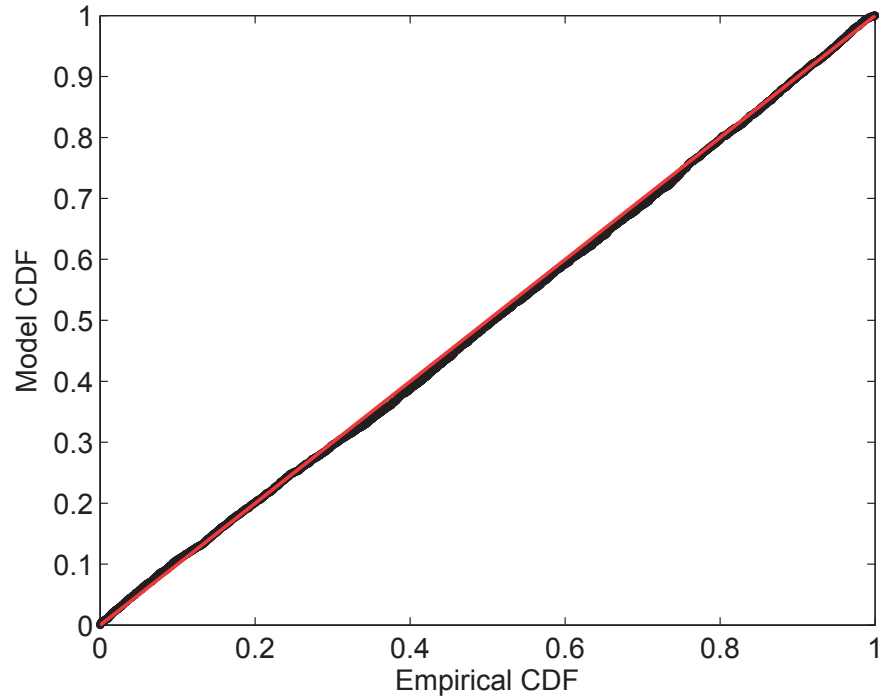


Figure 3.12: Cover plate, Probability plot of the parameter σ_D , no cut-off / $D_c = \mathcal{W}$

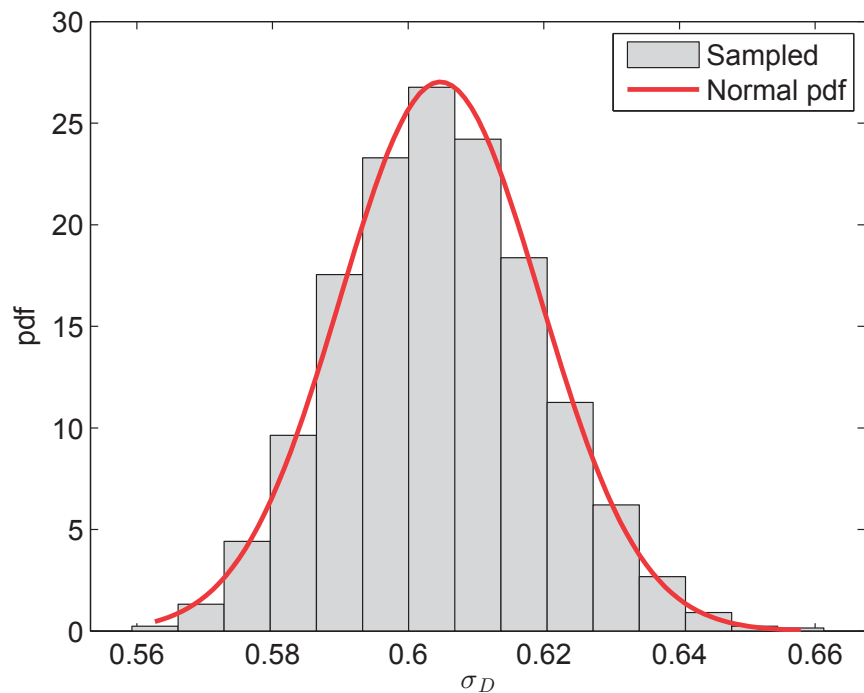


Figure 3.13: In-plane gusset, pdf of the parameter σ_D , no cut-off / $D_c = \log \mathcal{N}$

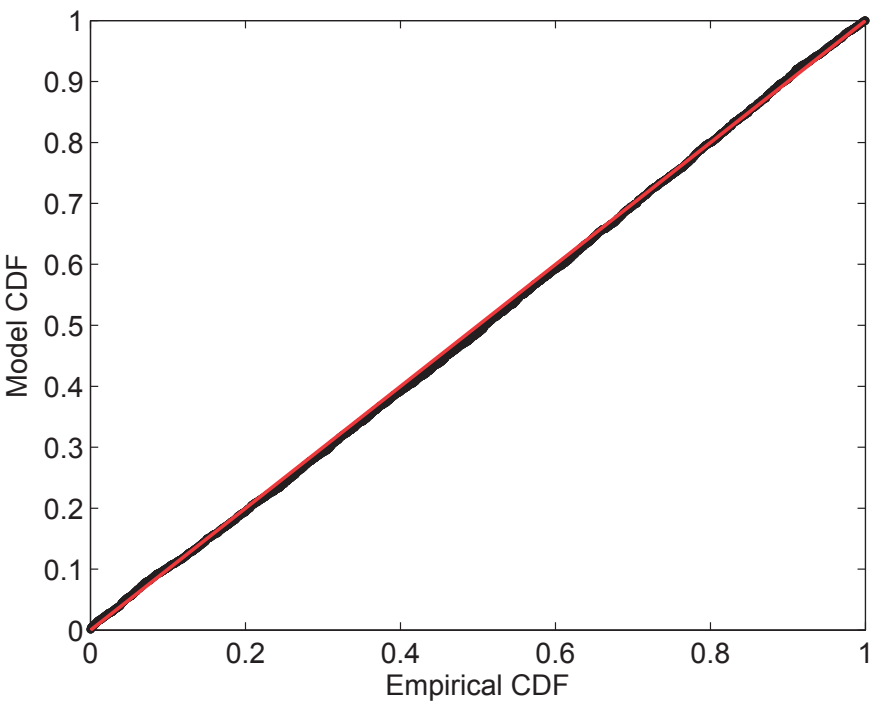


Figure 3.14: In-plane gusset, Probability plot of the parameter σ_D , no cut-off / $D_c = \log \mathcal{N}$

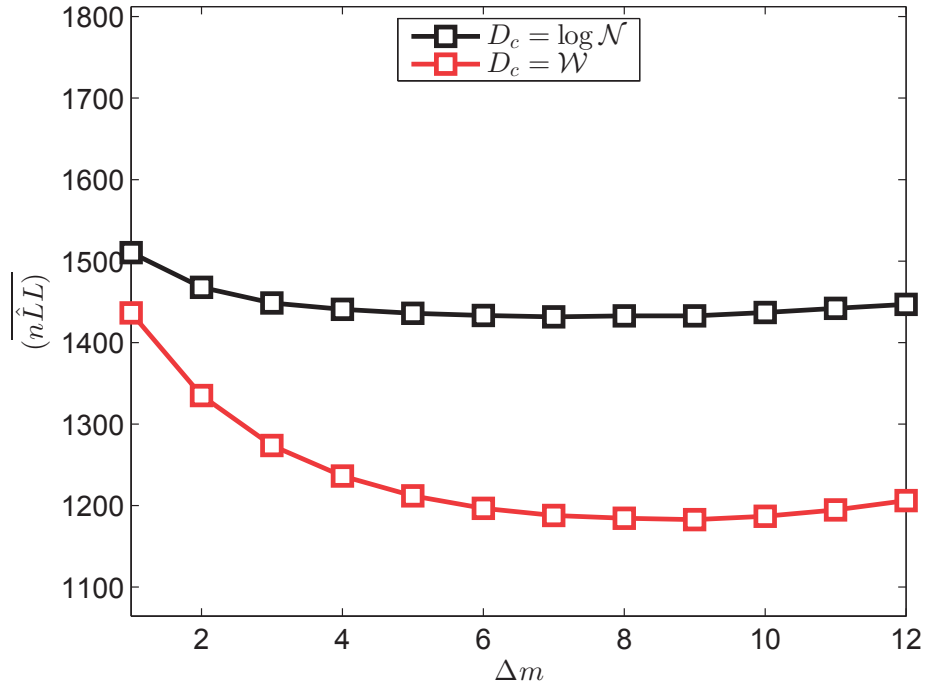
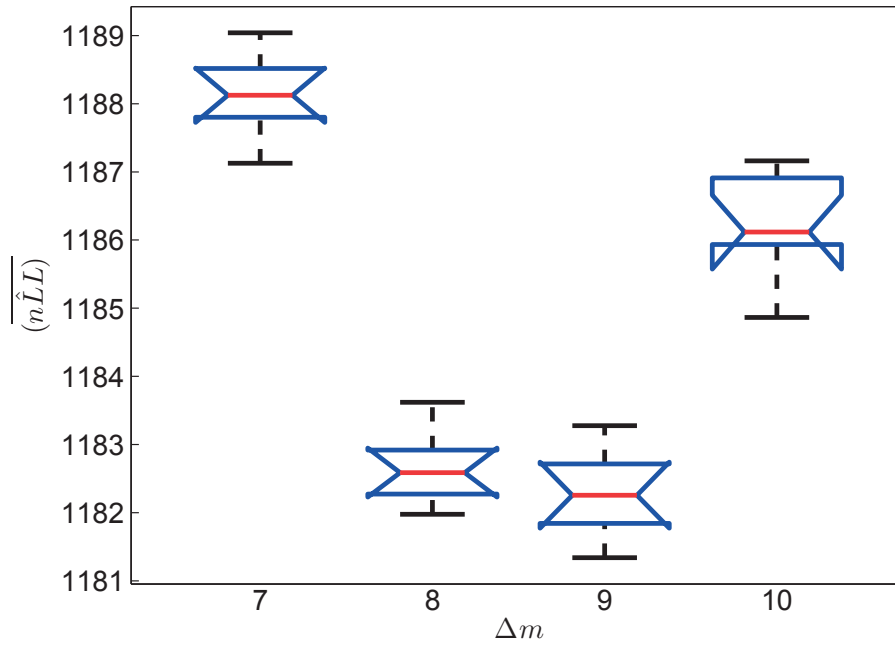


Figure 3.15: Cover plate, negative log-Likelihood plot, no cut-off

Figure 3.16: Cover plate, negative log-Likelihood notched box plot, no cut-off / $D_c = \mathcal{W}$

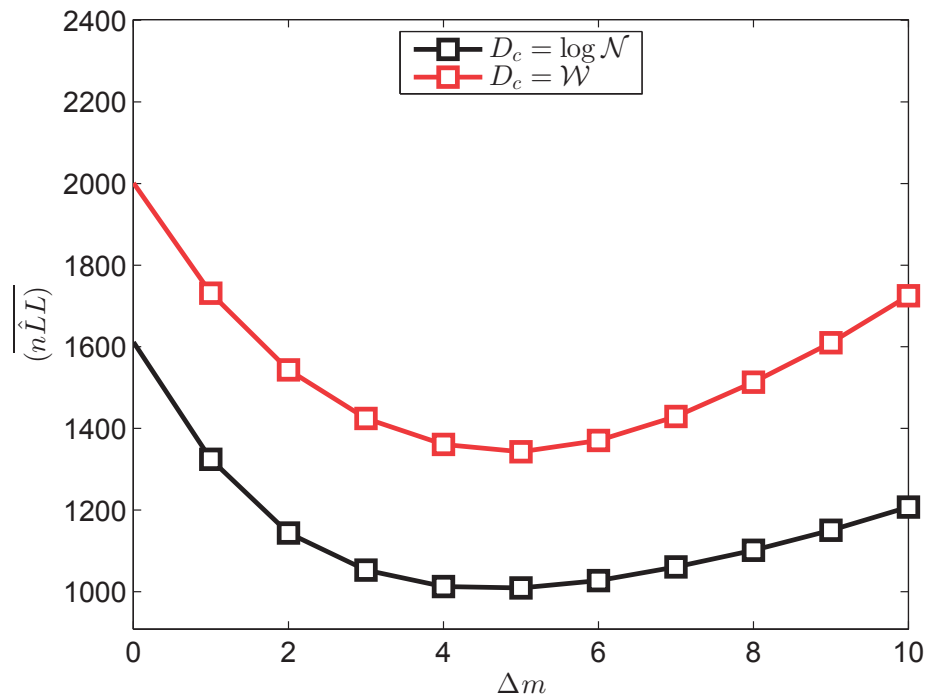


Figure 3.17: In-plane gusset, negative log-Likelihood plot, no cut-off

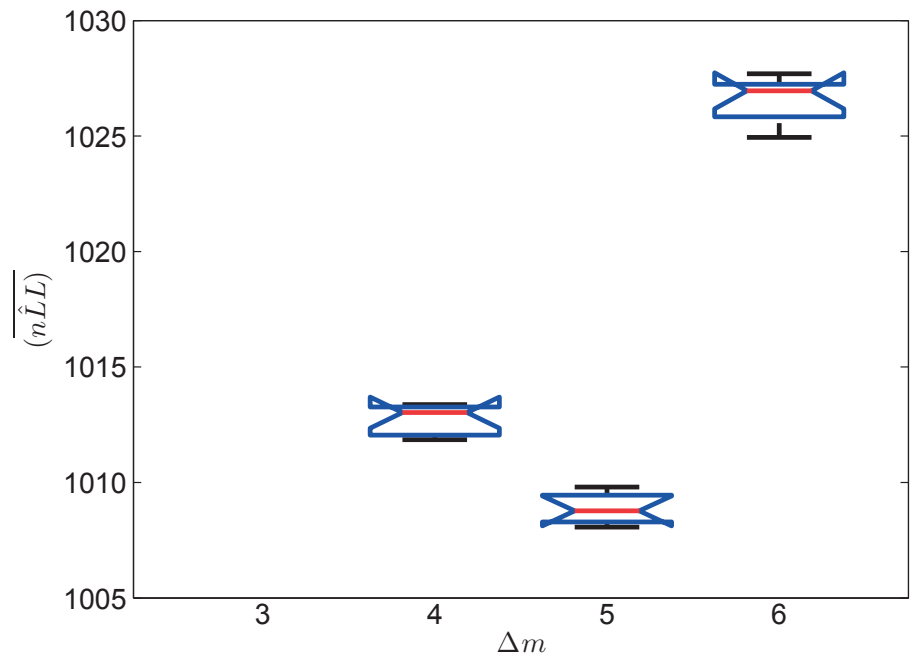


Figure 3.18: In-plane gusset, negative log-Likelihood notched box plot, no cut-off / $D_c = \log \mathcal{N}$

Tables 3.8 and 3.9 show the D_c pdfs, corresponding to the six cut-off / D_c distribution combinations, for the cover-plate data-set and the in-plane gusset data-set respectively. The ML-MCS-based D_c distribution is compared to the conventional $\log \mathcal{N}(0, 0.3)$ damage distribution (red shaded pdf); for each combination, the median value of the ML-MCS-based D_c distribution is also shown.

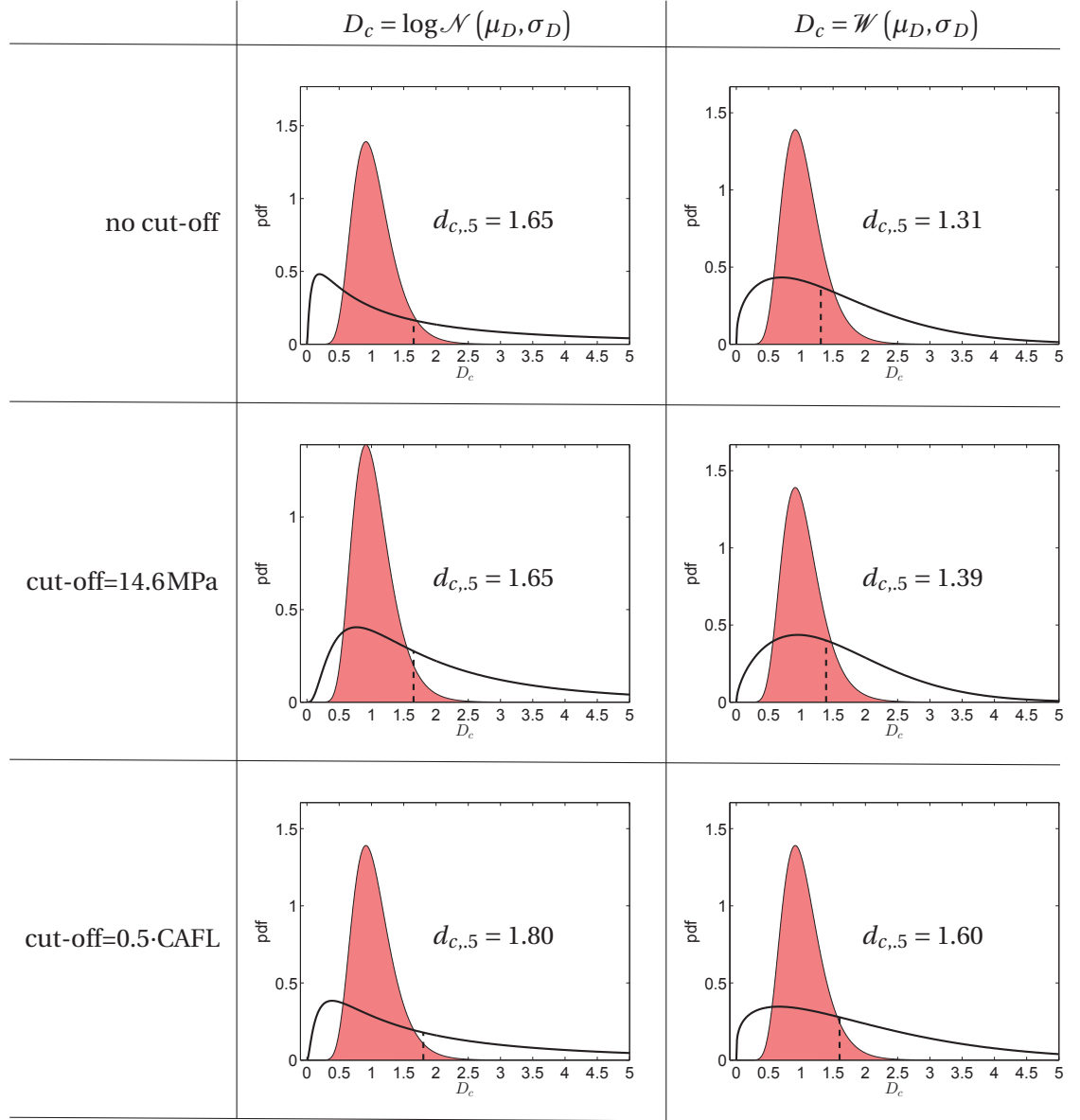


Table 3.8: Cover plate, D_c distributions. Shaded red pdf is the pdf of $\log \mathcal{N}(0, 0.3)$ distrib.

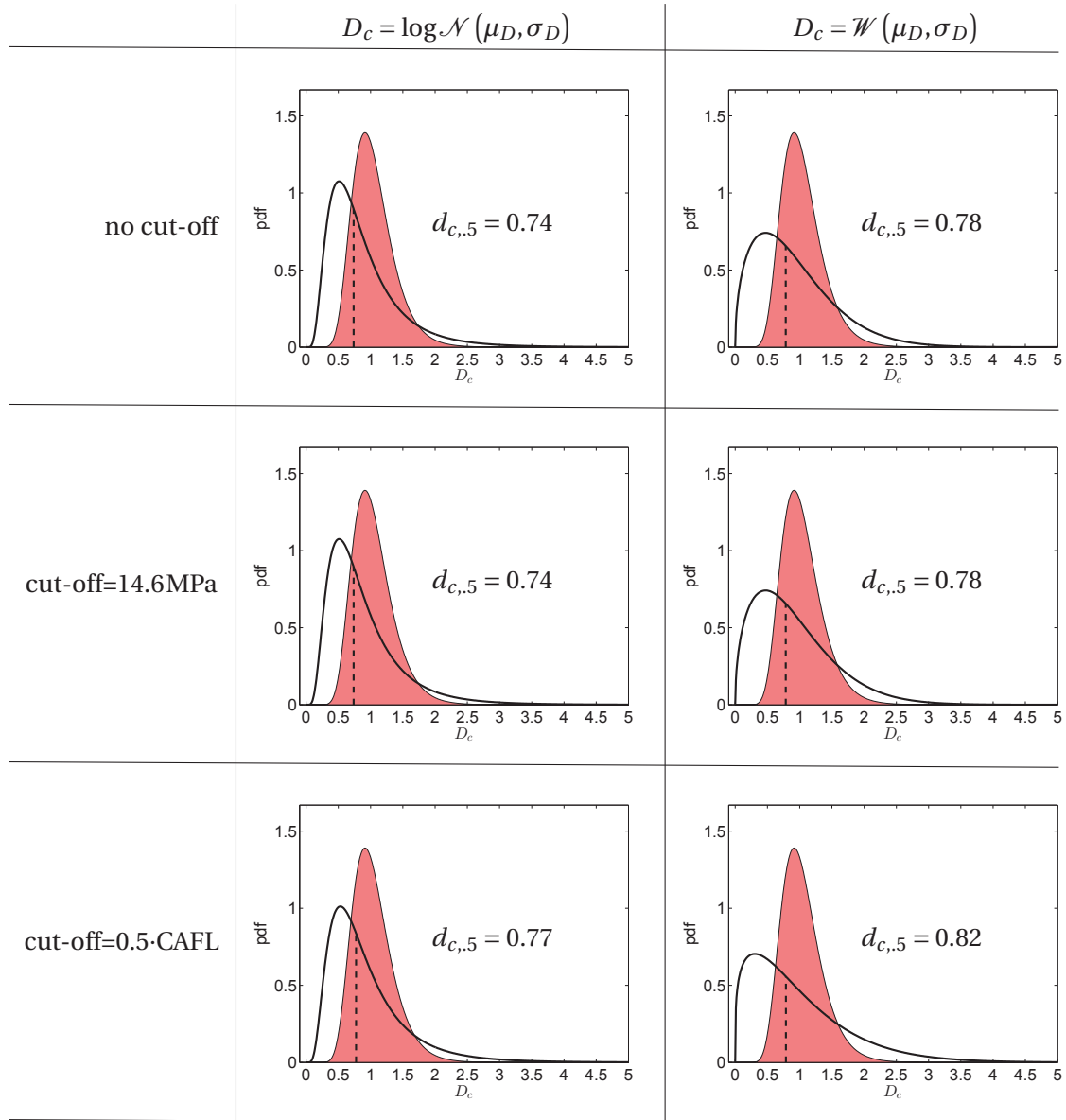


Table 3.9: In-plane gusset, D_c distributions. Shaded red pdf is the pdf of $\log \mathcal{N}(0, 0.3)$ distrib.

Figure 3.19 shows the ML-MCS-based VA characteristic S-N curve for the cover-plate data-set. The combination *no cut-off* / $D_c = \mathcal{W}$, which gave the best ML fit of VA test results, was chosen. The slope m_2 is equal to -11.4 and the median value of the critical damage sum, $d_{c,.5}$, is equal to 1.31. The ML-MCS-based VA S-N curve was re-scaled according to Equation 3.10 for direct comparison with standard VA S-N curves; the comparison in Figure 3.20 gives the following information:

- The AASHTO FAT40 S-N curve is over-conservative with respect to the ML-MCS S-N curve at all stress range levels;

- The EN3 FAT45 S-N curve is slightly over-conservative with respect to the ML-MCS S-N curve at stress ranges between 18MPa (cut-off) and 21MPa (CAFL), and at stress ranges higher than 25MPa;
- The IIW FAT50 and the EN3 FAT45 S-N curves are unsafe below 18MPa (cut-off).

Figure 3.21 shows the ML-MCS-based VA characteristic S-N curve for the in-plane gusset data-set. The combination *no cut-off* / $D_c = \log \mathcal{N}$, which gave the best ML fit of VA test results, was chosen. The slope m_2 is equal to -7.7 and the median value of the critical damage sum, $d_{c,.5}$, is equal to 0.74. The comparison of ML-MCS based re-scaled VA S-N curve with standard VA S-N curves (see Figure 3.22) gives following information:

- The AASHTO FAT56 S-N curve is considerably over-conservative with respect to the ML-MCS S-N curve at stress ranges between 15MPa (cut-off) and 27MPa;
- The EN3 FAT40 S-N curve is considerably over-conservative with respect to the ML-MCS S-N curve at stress ranges higher than 15MPa (cut-off);
- The AASHTO FAT56 and the EN3 FAT40 S-N curves are unsafe below 15MPa (cut-off);
- The IIW FAT50 S-N curve is unsafe at stress ranges lower than 17MPa (cut-off).

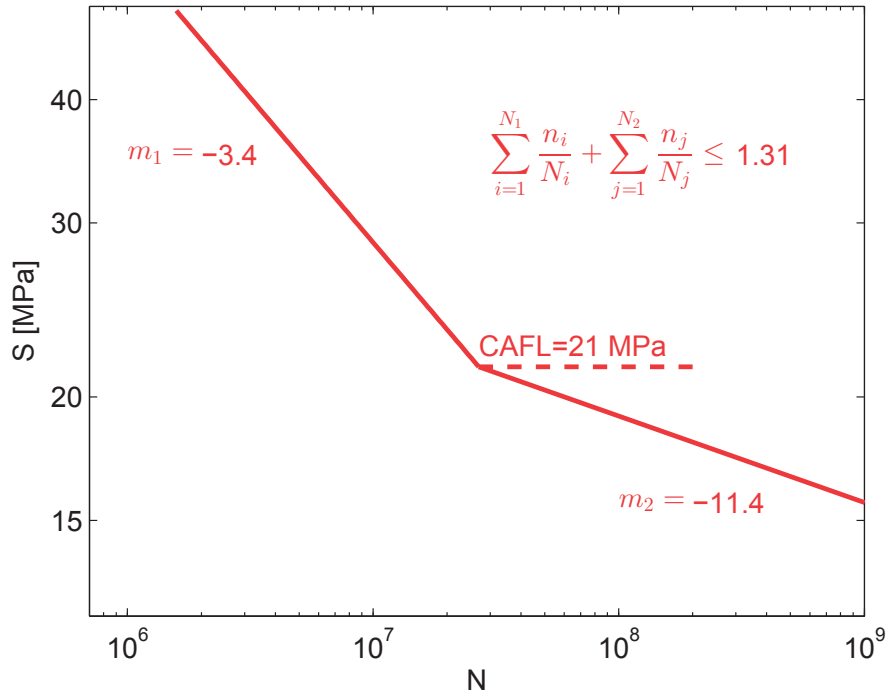


Figure 3.19: Cover plate, MCS-ML characteristic VA S-N curve, no cut-off / $D_c = \mathcal{W}$

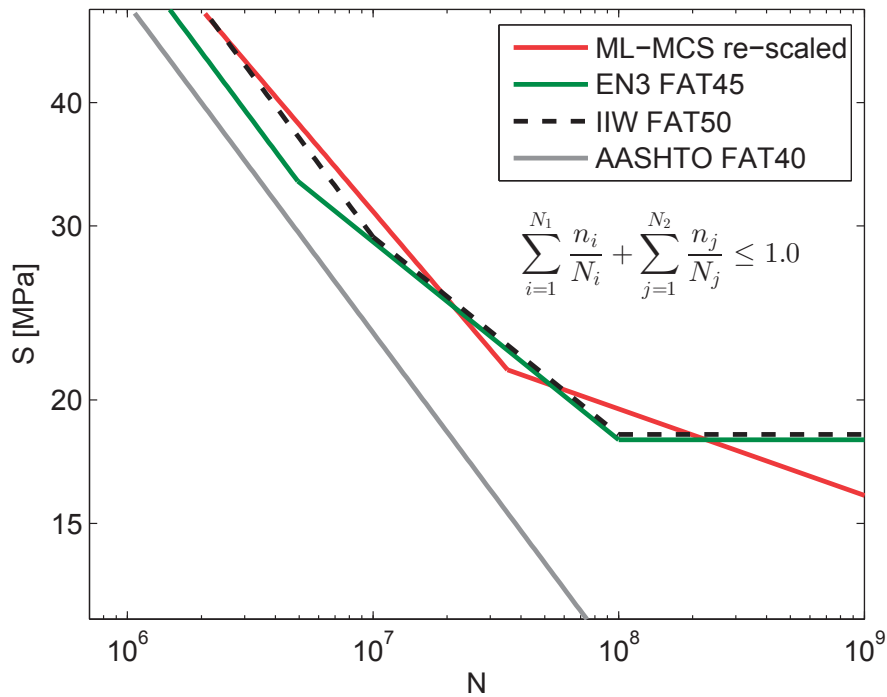


Figure 3.20: Cover plate, characteristic VA S-N curves, no cut-off / $D_c = \mathcal{W}$

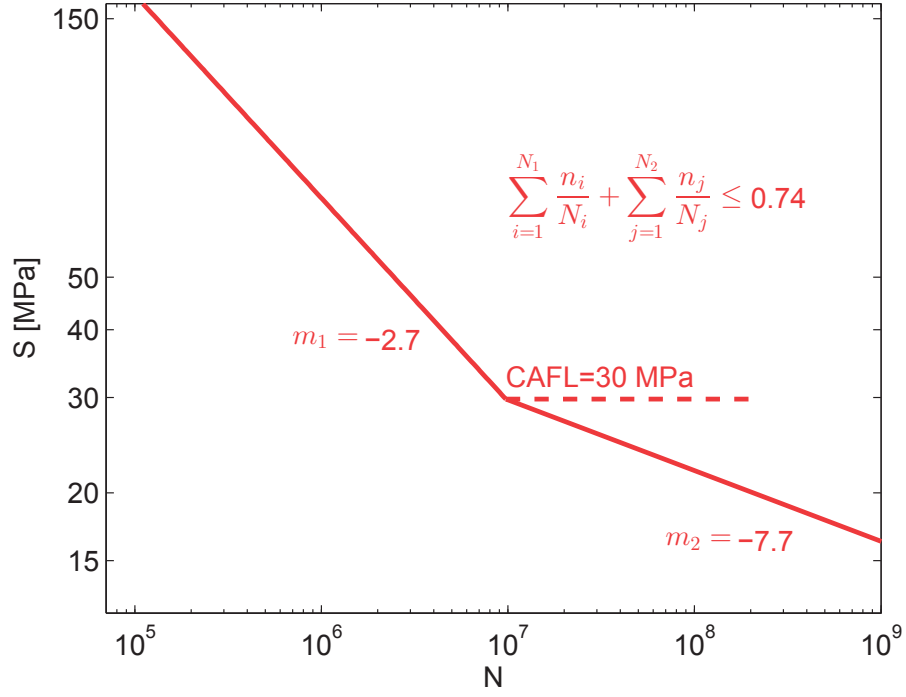
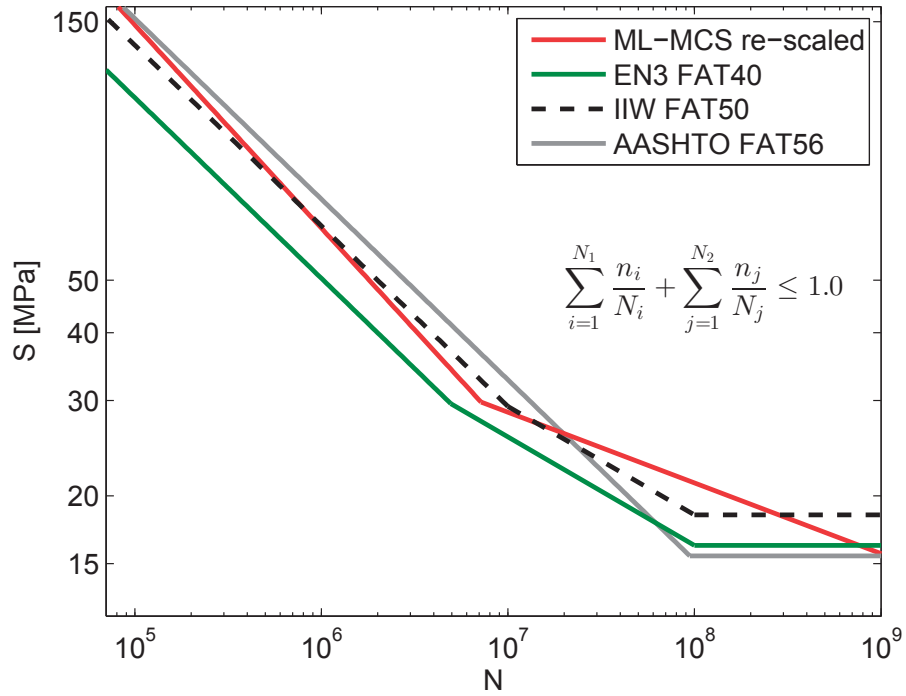
Figure 3.21: In-plane gusset, MCS-ML characteristic VA S-N curve, no cut-off / $D_c = \log \mathcal{N}$ 

Figure 3.22: In-plane gusset, characteristic VA S-N curves

Cover plate				
	FAT [MPa]	CAFL [MPa]	m_1	m_2
ML-MCS	46	21.5	-3.4	-11.4
Eurocode	45	33.2	-3.0	-5.0
IIW	50	29.2	-3.0	-5.0
AASHTO	40	-	-3.0	-
In-plane gusset				
	FAT [MPa]	CAFL [MPa]	m_1	m_2
ML-MCS	54	29.8	-2.7	-7.7
Eurocode	40	29.5	-3.0	-5.0
IIW	50	29.2	-3.0	-5.0
AASHTO	56	-	-3.0	-

Table 3.10: Characteristic VA S-N curves

The ML-MCS-based S-N model provides the best fit of VA experimental points (both failures and run-outs); it is recalled here that each VA experimental point (ϖ_t, n_t) is transformed in damage sum, by mean of the VA S-N curve. In Figures 3.20 and 3.22 the re-scaled ML-MCS characteristic VA S-N curves for cover-plate and in-plane gusset data-sets are compared to VA characteristic S-N curves from standards.

In order to offer to reader another simple way to compare the ML-MCS VA S-N model to VA S-N models from standards, the experimental failure points of both studied data-sets were transformed in damage sums by using ML-MCS characteristic VA S-N curve and characteristic S-N curves from standards (see Table 3.10). Results are compared in Figure 3.23: white "bubbles" represent the damage sum at failure with the size of the bubble being proportional to the frequency of observation, and red circles represent the mean observed damage sum, \bar{d} . Figure 3.23 shows that ML-MCS and IIW models give the most realistic estimates of critical damage sum ($\bar{d} < 2.5$), while Eurocode and AASHTO models give over-conservative estimates of damage sum ($\bar{d} > 3.4$).

It is noted that the "bubble diagram" represents only a fast and simple way to compare different VA S-N models since run-out observations are not considered as well as the variability of VA S-N model parameters. In order to perform a rigorous comparison of different VA S-N models, the ML-MCS scheme presented in Section 3.2.1 should be used.

Disqualification of outliers

When observing failure damage sums for the cover-plate data-set (see first column of Table 3.11), it is evident that the lowest damage sum (third spectrum in Table 3.1, failure at $104 \cdot 10^6$ cycles) lies an abnormal distance from other damage sum values. In order to assess whether this value can be classified as an outlier, the box-plot method was applied to observed failure

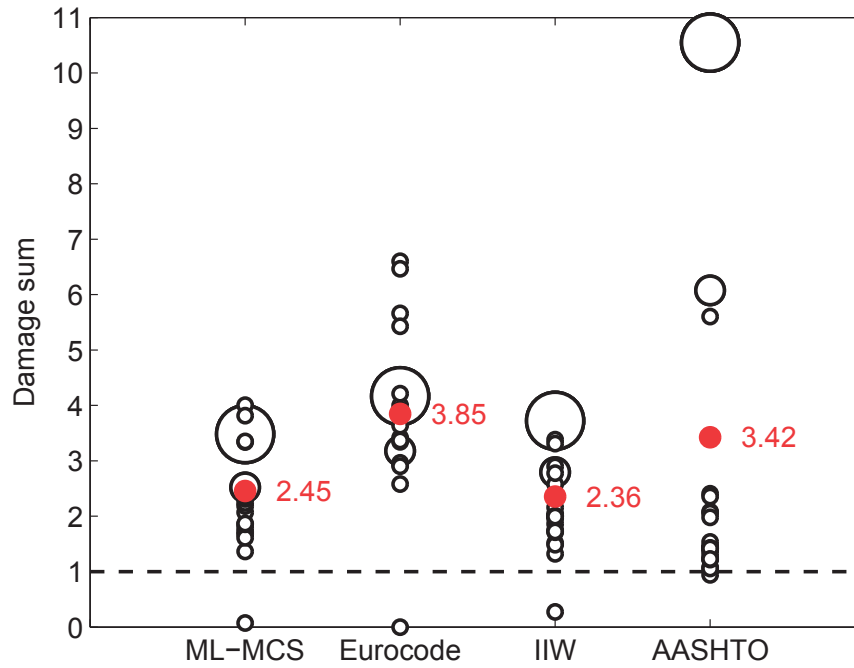


Figure 3.23: Bubble diagram, characteristic damage sums

log-damage sums. Results of the analysis are shown in Table 3.11: since the lowest failure log-damage sum (-2.60) exceeds the lower outer fence (F_{lo}), it can be classified as extreme outlier. The cover-plate VA data-set was re-analysed by neglecting the failure point corresponding to the classified outlier: the ML estimates of parameters of D_c distribution and the ML estimate of slope change, $\hat{\Delta}m$ are shown in Table 3.12. The new ML-MCS-based D_c distribution, with outlier disqualification, is compared to the original ML-MCS-based D_c distribution (without outlier disqualification), in Figure 3.24.

$\log(D)$	Quartiles	Fences
1.25	$Q_3 = 1.25$ $Q_1 = 0.88$ $IQ = 0.36$	$F_{uo} = 2.34$ $F_{ui} = 1.79$ $F_{li} = 0.34$ $F_{lo} = -0.21$
1.25		
1.25		
1.25		
-2.60		
0.92		
0.92		
0.84		

A box plot showing the distribution of log-damage values. The y-axis is labeled 'log-damage' and ranges from -3 to 1. The box plot has a blue box with a red median line at approximately 0.8. Whiskers extend from the box to approximately 0.3 and 1.0. A red cross at the bottom indicates an outlier at -2.60.

Table 3.11: Cover plate, outlier disqualification

Outlier disqualification	Cut-off case	D_c	$\hat{\mu}_D$	$\hat{\sigma}_D$	$\Delta\hat{m}$	$\overline{\hat{n}LL}$
no	no cut-off	\mathcal{W}	1.70	1.40	8	1183
yes	no cut-off	$\log \mathcal{N}$	0.27	0.58	6	934

Table 3.12: Cover plate, outlier disqualification: models comparison

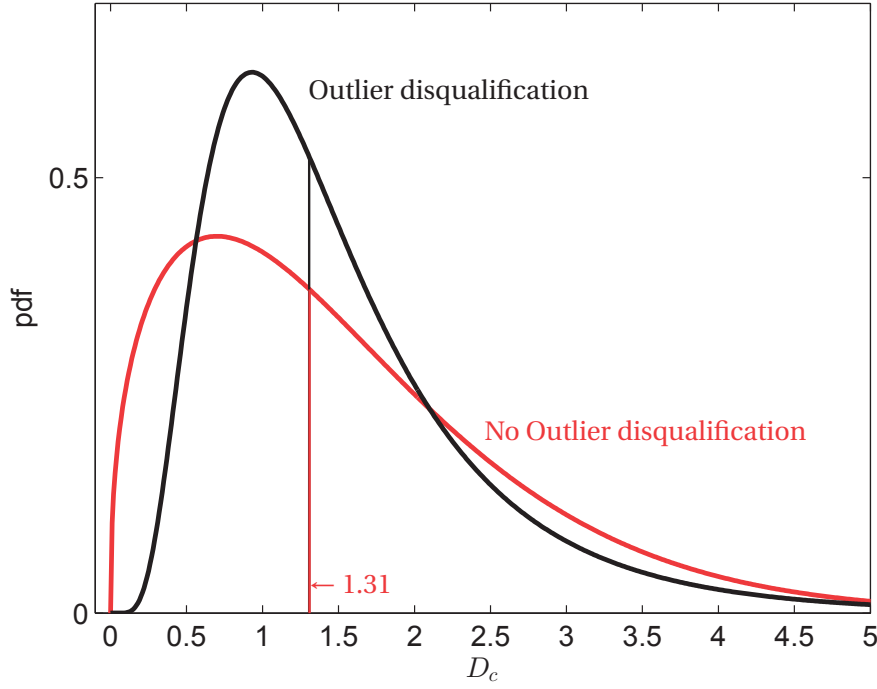


Figure 3.24: Cover plate, D_c distribution with outlier disqualification

3.5 Conclusions and discussion

In this Chapter a new approach was proposed for estimation of VA S-N models of welded joints. The new approach allows to estimate both the VA S-N curve and the critical value of damage sum, which are used in Miner's equation, when the fatigue life of a welded joint under the effect of VA loading is computed. The novel contribution of this approach consists in re-simulating VA experimental fatigue tests and in estimating the S-N curve second slope, m_2 , and the critical damage sum, D_c , with ML method. The new approach was implemented in the Matlab Toolbox TB1 (see Appendix B).

The conclusions from this Chapter are as follows:

- There are two critical aspects which are related to the use of Miner's rule in fatigue assessment of welded components under VA loadings: 1) The choice of the S-N curve

slope, m_2 , below the CAFL; and 2) The choice of the critical value of damage sum, D_c . The ML-MCS approach presented here allows to estimate the S-N curve second slope, m_2 , and the critical damage sum, D_c , on the basis of experimental VA results (including both failures and run-outs), by using the ML-MCS CA S-N stochastic model and without need for any arbitrary assumption;

- The estimates of VA S-N stochastic model for both cover plate and in-plane gusset data-sets (see Tables 3.4 and 3.6) show that the VA S-N curve without stress range cut-off maximizes the Likelihood information: the cases of cut-off at 14.6MPa (lowest Eurocode FAT detail) and cut-off at 0.5·CAFL are not supported by VA experimental results;
- Density plots and probability plots (see Figures 3.4 to 3.14) support the hypothesis of asymptotic normality of estimators $\hat{\mu}_D, \hat{\sigma}_D$ (parameters of critical damage distribution, D_c) and of $n\hat{LL}$ (sampled negative Log-Likelihood), for both cover plate and in-plane gusset data-sets;
- For the cover plate data-set, the graph $\overline{n\hat{LL}} - \Delta m$ shows that $D_c = \mathcal{W}$ with $\Delta\hat{m} = 8$ gives the best fit in terms of Likelihood (see Figure 3.16). However the re-analysis of experimental data using the box-plot method allowed to classify one failure points as a extreme outlier: for the cover plate data-set with outlier disqualification, the graph $\overline{n\hat{LL}} - \Delta m$ shows that $D_c = \log \mathcal{N}$ with $\Delta\hat{m} = 6$ gives the best fit in terms of Likelihood (see Table 3.12). The disqualification of the outlier point does not affect the median value of D_c distribution (which remains equal to 1.31).
For the in-plane gusset data-set, the graph $\overline{n\hat{LL}} - \Delta m$ shows that $D_c = \log \mathcal{N}$ with $\Delta\hat{m} = 5$ gives the best fit in terms of Likelihood (see Figure 3.18);
- The VA S-N model correlation matrix shows that there is no linear correlation between the parameters of the S-N curve and the parameters of the D_c distribution, for both cover plate and in-plane gusset data-sets (see Tables 3.5 and 3.7). This seems to indicate that the location and the scale parameter of D_c are influenced only by the characteristics of loading history and not by the fatigue strength of the studied detail. Further analysis of different fatigue details is needed to confirm this indication;
- For the cover plate data-set, where experimental results were obtained under wide-band Rayleigh type stress range spectra having short block lengths, the median value of D_c is equal to 1.31, while for the in-plane gusset study case, where experimental results were obtained under 3-blocks spectra with stress ranges cycling down from constant maximum stress (no over-loads which could retardate the crack opening), the median value of D_c is equal to 0.74. This seems to indicate that there is a strong influence of

loading characteristics and in particular of load sequence on the critical damage sum distribution, which is coherent with results from [81] and [33];

- The slope range $\Delta m = m_1 - m_2$ is equal to 6 for the cover-plate, while it is equal to 5 for the in-plane gusset: this confirms the existence of a second slope m_2 (in disagreement with results from [26], [48], [81] and [3]) and it seems to indicate that the influence of the loading characteristics on the second slope m_2 is small;
- Re-scaling of ML-MCS characteristic VA S-N curve at $D_c = 1$ allowed for direct comparison of ML-MCS-based VA S-N curves with standard VA S-N curves, showing that S-N curve from AASHTO specification is highly over-conservative for the cover plate data-set at all stress ranges (see Figure 3.20), and that all standard S-N curves (Eurocode, IIW, AASHTO) are slightly over-conservative at stress ranges lower than 30 MPa, for the in-plane gusset data-set (see Figure 3.22);
- ML fit provides support to $D_c = \mathcal{W}$ and to $D_c = \log \mathcal{N}$ respectively for the cover-plate data-set and for the in-plane gusset data-set. This difference is due to the "weakness" of the cover-plate experimental data-set: the disqualification of one extreme outlier of the cover-plate data-set and the re-estimation of the critical damage sum distribution leads to $D_c = \log \mathcal{N}$;
- The "bubble" diagram, representing the characteristic damage sums for both considered data-sets, confirm that the ML-MCS approach gives the most realistic estimates of critical damage sum, together with IIW (see Figure 3.23).

The findings listed above suggest that the ML-MCS approach defined in this Chapter constitutes a powerful tool for re-definition of second slope, m_2 , and of critical damage sum, D_c . The proposed approach was applied on two VA experimental data-sets and validated by using diagnostic plots, Likelihood plots and "bubble" plot.

4 Fatigue reliability assessment of existing bridges

4.1 Introduction

In fatigue life assessment of steel bridges the reliable consideration of extreme loads which lie near the CAFL is of primary importance. In order to accomplish this requirement, three problems need to be adequately solved:

1. Reliable definition of the CAFL and of its variability;
2. Reliable definition of the damage accumulation rule, especially for stress range cycles below the CAFL;
3. Reliable consideration of extreme loads which lie near the CAFL.

The ML-MCS approach, presented in Chapters 2 and 3, provides a solution to problems 1) and 2).

Weigh-In-Motion (WIM) technology provides a powerful tool to face problem 3). Prior to recent years, probabilistic approaches were used to extrapolate short period of recorded data to long return periods (i.e. one recorded week extrapolated to 120 years) [7, 16]; however recent improvements in WIM technology allows to use recorded traffic data of one or more years.ⁱ

Chen et al. [14] proposed a new reliability framework for estimation of fatigue life of suspension bridges under the long-term effect of railway, highway and wind loading. The limit state function was defined by using the daily sum of m -power stress ranges, which were computed by using probabilistic model of railway, highway and wind loading; WIM measurements were

ⁱM. Treacy has shown in his PhD thesis [75] that at least 6 months of record are needed to reliably extrapolate extreme traffic value

used to characterize highway traffic loading history. The fatigue failure probability at fatigue critical locations was based on the critical fatigue damage accumulation event; the CAFL exceedance event was not included in the analysis. The critical value of the damage sum, D_c , was modeled by $\log\mathcal{N}(0, 0.3)$ distribution, and S-N curves were defined according to British standards [74]. The framework was applied on the Tsing Ma suspension bridge in Hong Kong. Guo et al. [32] developed a new approach, integrating WIM data and probabilistic finite element (FE) analysis, for fatigue assessment of steel bridges. The limit state function was based on the critical damage accumulation event, while the CAFL exceedance event was not included in the analysis. S-N curves were defined according to AASHTO bridge design specifications [2] and D_c was modeled by $\log\mathcal{N}(0, 0.3)$ distribution. The approach was applied on the Throgs Neck suspension bridge, connecting the Throgs Neck section of the Bronx in New York city with the Bay Terrace section of Queens.

In both approaches, adopting conventional assumption for definition of S-N curves and of D_c and modeling the CAFL as deterministic value, may yield inaccurate insight into reliability index values and undo the beneficial effect of accurate modeling of the traffic loads as well as of the bridge structure.

D'Angelo et al. [18] provided a fatigue-life reliability assessment of the Venoge highway bridge, on the highway A1 in Switzerland. WIM measurement-based traffic simulation was used to get realistic traffic loading history. The fatigue failure probability at two critical locations was based on the CAFL exceedance event, where the random CAFL was defined according to EN 1993-1-9 [24]. Since the analysis was based only on the CAFL exceedance event, the results could be largely over-conservative. Again, adopting conventional assumption for the definition of S-N curves may yield inaccurate insight into reliability index values.

Sudret et al [71], [31] proposed a probabilistic approach for fatigue life assessment of structures subjected to thermal fatigue. This approach incorporated all kinds of uncertainties affecting the thermal fatigue behavior such as those related to the fatigue strength, to the thermo-mechanical model and to the thermal loading. The proposed probabilistic framework provides an effective tool for computing probability of fatigue failure as function of the expected design life and for estimating the importance of random variables in response sensitivity. Nevertheless, this approach has following limitations when applied to the case of fatigue assessment of road bridges: 1) The critical value of the damage sum at failure, D_c is assumed to be equal to 1.0. This assumption does not allow to take into account the deviation effects related to loading history; 2) The accumulated damage is computed with a one-slope S-N curve having an asymptotic endurance limit, S_D ; the critical point related to the influence on the fatigue damage of stress range cycles below the CAFL, which is of primary importance in mechanical fatigue evaluation of welded joints, is not addressed; 3) In modelling the random number of cycles to failure ($\ln(N) = \lambda(S) + \sigma(S)\xi(\omega)$, where $\xi(\omega)$ is a standard Normal random

variable), the aleatory uncertainty of the fatigue limit is not taken into account: the ML-MCS approach presented in this thesis shows that the consideration of aleatory uncertainty of the CAFL is essential for computing quantiles of fatigue life (see Section 2.3.3).

In this Chapter a novel framework for fatigue reliability assessment of steel bridges under the long-term effect of traffic loading, is presented. WIM measurements are used to characterize traffic loading history. The fatigue reliability framework takes in account both the CAFL exceedance event and the critical damage accumulation event: failure probability and related reliability index are computed by estimating the joint failure probability of these two events. The S-N curves and the critical damage sum, D_c , are defined according to the ML-MCS approach, which has been presented in Chapters 2 and 3 .

The reliability framework which is presented in this Chapter was implemented in the Matlab Toolbox TB2 (see Appendix B). The Matlab Toolbox TB2 was validated using the structural reliability analysis software STRUREL [61].

The Chapter is organized as follows:

- In Section 4.2 the new framework for fatigue reliability analysis is presented;
- In Section 4.3 the fatigue reliability analysis framework is applied to the Venoge bridge study case;
- In Section 4.4 results of the fatigue reliability analysis of the Venoge bridge are presented and compared to Eurocode standards;
- In Section 4.5 results are discussed.

4.2 New framework for fatigue reliability analysis

In this Section the framework for the fatigue reliability analysis of road bridges under the long-term effect of traffic loading, is presented.

Welded joints in road bridges are subjected to VA fatigue loadings; hence fatigue life assessment is done by using linear damage accumulation rule (Miner's rule [53]):

$$D_d = \sum_i \frac{n_i}{\exp(Y(m_0, m_1, \sigma, V; S_i))} + \sum_j \frac{n_j}{\exp(Y(m_0, m_1, m_2, \sigma, V; S_j))} \leq D_c \quad (4.1)$$

where:

- D_d is the total accumulated damage;

- V is the natural logarithm of the CAFL;
- n_i is the i -cycle of the loading spectrum, which has nominal stress range S_i above the CAFL;
- n_j is the j -cycle of the loading spectrum, which has the nominal stress range S_j below the CAFL;
- m_1 is the slope of the S-N curve for a nominal stress range above the CAFL;
- $m_2 = m_1 - \Delta m$ is the slope of the S-N curve for a nominal stress range below the CAFL and it allows to take in account the gradual exceedance of the propagation threshold by lower stress ranges as the crack length increases;
- m_0 is the log-intercept of S-N curve having a slope equal to m_1 ;
- D_c is the critical value of the accumulated damage.

The variables listed above are defined in the S-N model.

The validity of Eq. 4.1 is conditioned to the fact that there is at least one cycle of the loading spectrum which exceeds the CAFL:

$$S_{max} \geq \exp(V) \quad (4.2)$$

where S_{max} is the maximum stress range of the loading spectrum.

Therefore the assessment of the fatigue failure probability of considered critical details asks for consideration of two events:

- E_1 : Critical damage accumulation
- E_2 : CAFL exceedance

To have fatigue failure, both events E_1 and E_2 must happen. From the definition of conditional probability:

$$P_f = P(E_1 \cap E_2) = P(E_1|E_2)P(E_2) = P(E_1^*)P(E_2) \quad (4.3)$$

where $E_1^* = E_1|E_2$ represents critical damage accumulation conditioned to CAFL exceedance; definition of limit state equations related to E_1^* and E_2 is discussed below.

Event E_1^* : critical damage accumulation conditioned to CAFL exceedance

Following from Equation 4.1, the limit state equation related to the conditioned event E_1^* may be written as:

$$g_1(\underline{X}_1) = D_c - \sum_i \frac{n_i}{\exp(Y(m_0, m_1, \sigma, V(\mu_V, \sigma_V); S_i))} - \sum_j \frac{n_j}{\exp(Y(m_0, m_1, \sigma, V(\mu_V, \sigma_V), m_2; S_j))} \quad (4.4)$$

The failure event E_1^* may be described in the following way:

$$E_1^* = \{g_1(\underline{X}_1) \leq 0\} \quad (4.5)$$

where \underline{X}_1 is the vector of basic random variables $(Y(m_0, m_1, m_2, \sigma, V(\mu_V, \sigma_V)), D_c(\mu_D, \sigma_D))$. It is noted that both the epistemic uncertainty of model parameters and the aleatory uncertainty of the CAFL, of the fatigue life and of the critical damage sum, are taken into account. Having defined the failure event E_1^* , the probability of failure $P(E_1^*) = P(E_1 \cap E_2)/P(E_2)$ may be defined as follows:

$$P(E_1^*) = \int_{g_1(\underline{X}_1) \leq 0} f_{\underline{X}_1}(\underline{x}_1) d\underline{x}_1 \quad (4.6)$$

where $f_{\underline{X}_1}(\underline{x}_1)$ is the pdf of \underline{X}_1 . The related reliability index is:

$$\beta_1 = -\Phi^{-1}(P(E_1^*)) \quad (4.7)$$

Since the limit state function $g_1(\underline{X}_1)$ is non linear in the basic random variables \underline{X}_1 , the β_1 index has to be computed using linearization approaches (First order reliability method, FORM, or Second order reliability form, SORM) or MCS technique.

Event E_2 : CAFL exceedance

The limit state equation related to the event E_2 is defined as follows:

$$g_2(\underline{X}_2) = \exp(V) - z_p \quad (4.8)$$

where \underline{X}_2 is the vector of basic random variables $(z_p, V(\mu_V, \sigma_V))$, with z_p indicating the p -return level of maximum stress range.

It is noted that both the epistemic uncertainty of S-N model parameters (μ_V, σ_V) and the aleatory uncertainty of the CAFL are taken into account.

In analogy with β_1 , the reliability index related to the event E_2 is:

$$\beta_2 = -\Phi^{-1}(P(E_2)) = -\Phi^{-1}\left(\int_{g_2(\underline{x}_2) \leq 0} f_{\underline{X}_2}(\underline{x}_2) d\underline{x}_2\right) \quad (4.9)$$

where $f_{\underline{X}_2}(\underline{x}_2)$ is the pdf of \underline{X}_2 . The reliability problem may be solved again using linearization approaches or MCS technique.

4.3 Study case

The framework presented in Section 4.2 was applied to the Venoge bridge, located on the A1 Swiss motorway between Lausanne and Geneva (see Figure 4.1). The Venoge bridge consists of two identical independent bridges (one for each direction) with a 219 meter length divided in four spans (see Figure 4.2). Each bridge was constructed in 1961 with two girders and then enlarged in 1995 to four girders (see Figure 4.3). Due to the slow lane (heavy traffic) location only the enlarged bridge section is considered in this study (see Figure 4.3).

The welded cover plate (see Figure 4.4) on the left lower flange, at the first mid span (Section A in Figure 4.2), was identified as the fatigue critical location. Two year-traffic induced stress history was generated using WIM measurements and a 3-dimensional finite element (FE) model of the bridge. The stress response influence line at the fatigue critical location was characterized with a refined three-dimensional (3-D) FE model which takes into account the effective transverse load repartition, the cracking of the concrete slab and the elastic stiffness of stud connectors; the FE model was calibrated and validated using experimental load-vs-strain results from bridge static tests [13]. MSC/Nastran [54] was used for the analysis. For the sake of brevity the reader is referred to [17] for complete information on the calibration of FE model of the bridge.



Figure 4.1: The Venoge bridge, Ecublens (Switzerland)

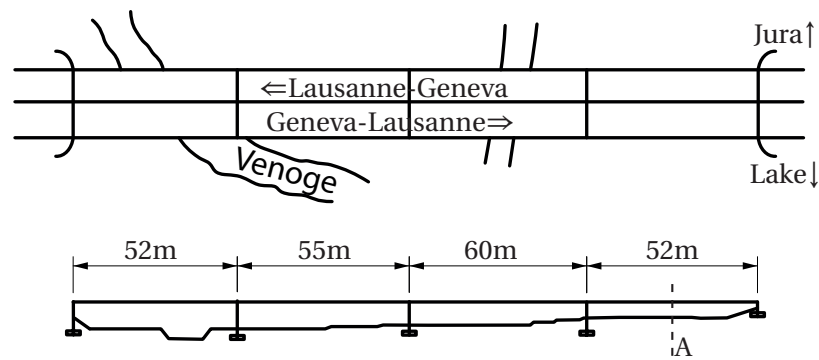


Figure 4.2: In-plane view and elevation of the Venoge bridge

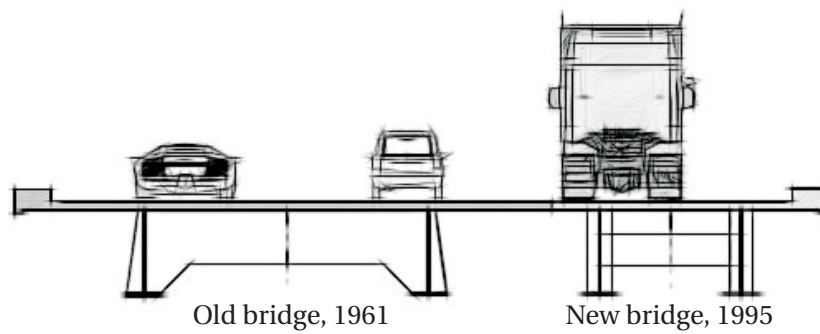


Figure 4.3: Lane configuration on the Venoge bridge



Figure 4.4: The critical detail: welded cover plate

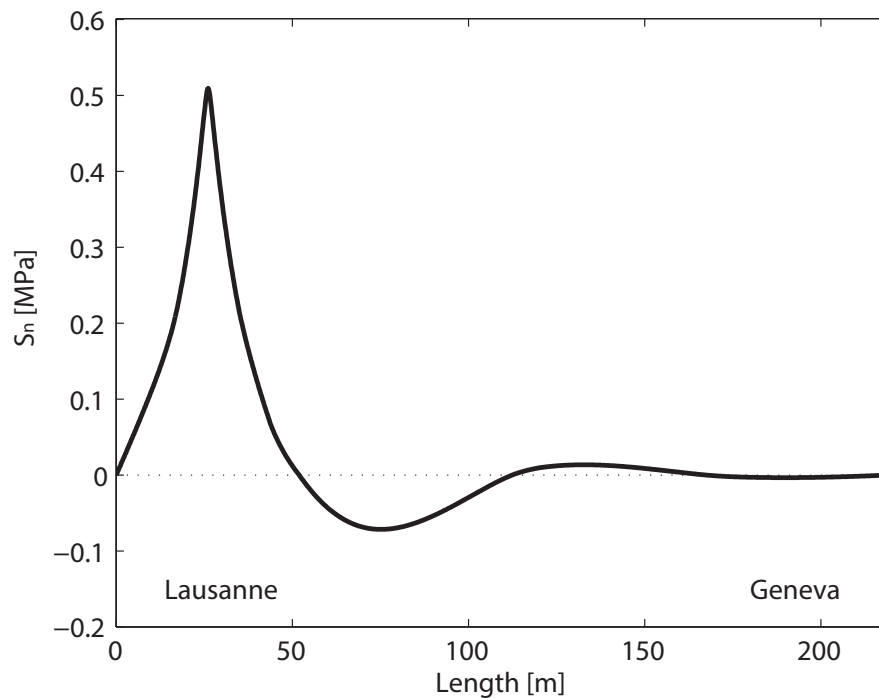


Figure 4.5: Influence line for nominal stress S_n at the critical section, 1 ton crossing axle

The influence line for the nominal stress S_n , at the critical section A , is shown in Figure 4.5. The bridge fatigue failure probability, during the 100-year design life, was computed by solving the reliability problem of Equation 4.3 at the critical location.

4.3.1 Traffic analysis

WIM recorded data of the Denges station (only 1km away from the bridge) over a 2 year period (1.01.2006 - 31.12.2007) were considered in order to reconstruct the time-history of bridge crossing heavy vehicles. Direction Lausanne-Geneva was analysed due to the unavailability of complete data for the opposite direction. WIM devices can capture static vehicle axle weights, which allow for characterization of traffic demand in terms of:

- time of passage
- vehicle speed
- number of axles
- gross total weight
- axles weight
- inter-axles distance

A code which reads recorded WIM data, classifies vehicles according to GR03-EUR13 classification [51] and produces the 2-year history of bridge crossing was implemented in the module TrafficAnalysis of Matlab Toolbox TB2 (see Appendix B). Only heavy vehicles with gross total weight (*GTW*) higher than 10 tons were considered herein and in fatigue calculation because lighter vehicles give a negligible contribution to the bridge fatigue damage [66].

Figure 4.6 shows that there is not a significant evolution of heavy traffic from the observed period (2006-2007) to year 2013, both in terms of observed/classified vehicles and of observed crossing axles. Figure 4.7 shows the comparison between the empirical pdf of *GTWs* for the observed period 2006-2007, and the empirical pdf of *GTWs* for the year 2013, confirming that there is not significant evolution from the observed period (2006-2007) to year 2013.

For the considered study case, the influence length of the critical detail is higher than 52m: the load dynamic amplification factor, ϕ_d , is set equal to 1.0, according to Brühwilher et al. [12] which recommended to use $\phi_d = 1.0$ for influence lengths longer than 40m.

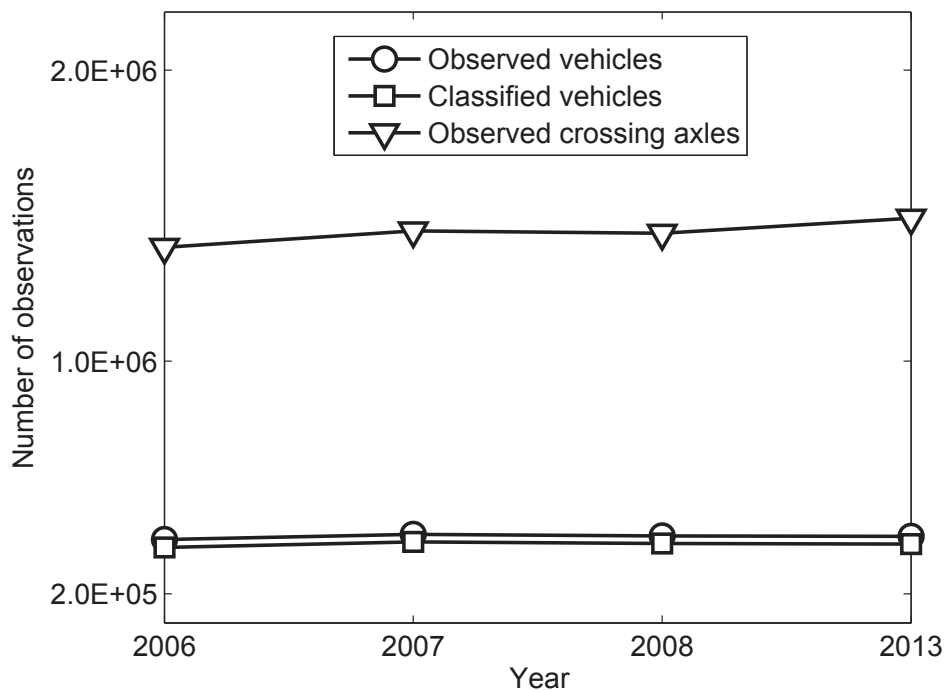


Figure 4.6: Heavy traffic observations (*GTW* > 10 tons)

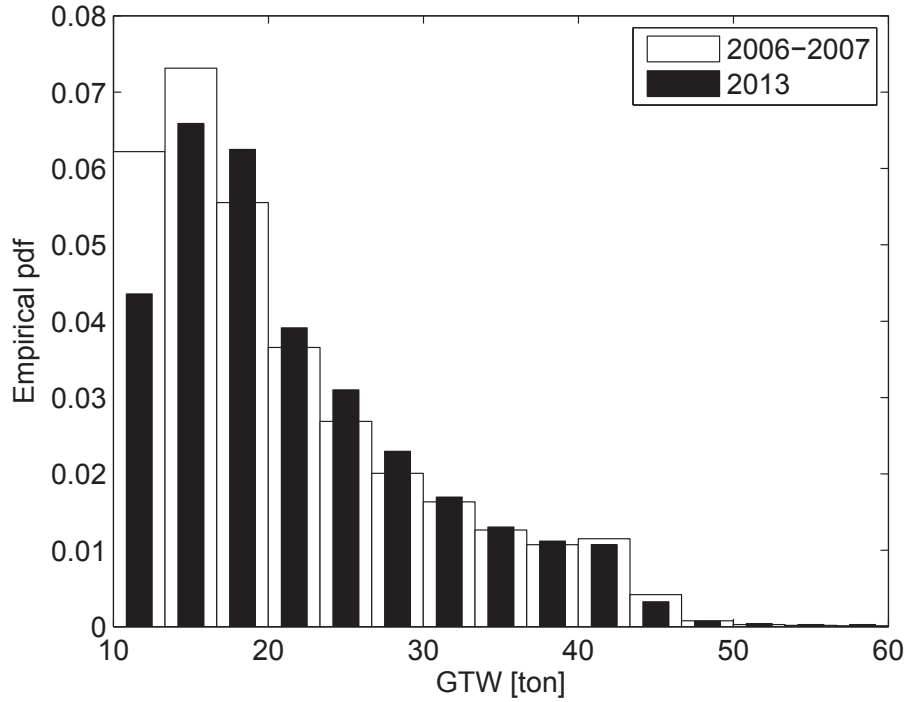


Figure 4.7: Empirical pdf of observed yearly GTWs

4.3.2 Fatigue resistance models

Two different S-N models were considered for the fatigue reliability analysis of the Venoge bridge:

1. ML-MCS-based VA S-N model for the cover-plate data-set with outlier disqualification, defined in Section 3.4;
2. Eurocode FAT45 S-N curve, with conventional hypothesis for critical damage D_c .

In the ML-MCS-based S-N model, the CA S-N curve is represented by a multivariate Normal vector, whose parameters are defined in Tables 3.4 and 3.5, while the critical value of damage sum, D_c , is a Log-Normal random variable, whose parameters are defined in Table 3.12.

In the Eurocode-based S-N model, the slopes and the CAFL of the CA S-N curve are deterministic values and the only source of fatigue scatter is represented by the Normal random variable m_0 , which is defined according to [73]ⁱⁱ; the critical value of damage sum, D_c , is a log-Normal

ⁱⁱThe location and the scale parameters of the m_0 Normal distribution are computed as follows:
 $\mu_{m_0} = \ln(\text{FAT}_{med}) = \ln\left(10^{\log_{10}(\text{FAT}) + 2 \cdot s_R}\right)$, with $s_R = 0.033$
 $\sigma_{m_0} = 0.5 \cdot (\mu_{m_0} - \ln(2 \cdot 10^6) - 3 \cdot \ln(\text{FAT}))$

random variable with mean equal to 0 and standard deviation equal to 0.3, according to JCSS PMC [41].

Values of S-N curve parameters and of D_c parameters are resumed in Table 4.1.

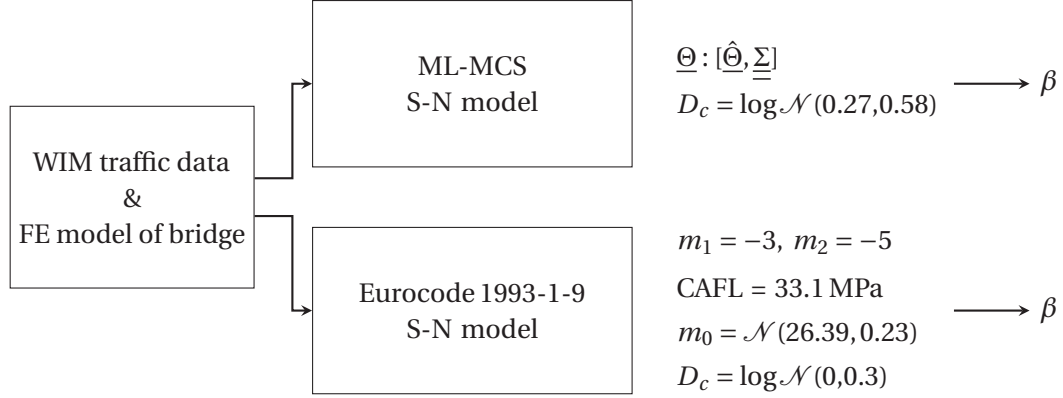


Table 4.1: Scheme for calculation of β reliability index

4.3.3 Resolution of reliability problem $P(E_1^*)$

ML-MCS S-N model

The limit state equation related to the event E_1^* has been formulated in Equation 4.4.

The S-N model variables $(m_0, m_1, m_2, \sigma, V(\mu_V, \sigma_V), D_c(\mu_D, \sigma_D))$ are defined in the ML-MCS VA S-N stochastic model for cover plate data-set with outlier disqualification (see Tables 3.4, 3.5 and 3.12).

In order to compute the weekly loading spectra, $(S_i, n_i)_{w=1, \dots, 104}$, the following scheme was followed:

1. The stress history at the critical section, $S_n(t)$, was obtained by using the crossing axle time history, $\mathcal{A}(t)$, and the influence line shown in Figure 4.5;
2. The 2-year stress history $S_n(t)$ was divided in 104 weekly blocks, $S_{n,w}(t)_{w=1, \dots, 104}$
3. From each block the stress range spectrum $(S_i, n_i)_{w=1, \dots, 104}$ was computed using a rain-flow algorithm [22].

This scheme has been implemented in the module `TrafficAnalysis` of Matlab Toolbox TB2 (see Appendix B).

The probability of failure $P(E_1^*)$ was computed by using MCS method:

$$P(E_1^*) = \int_{g_1(\underline{X}_1) \leq 0} f_{\underline{X}_1}(\underline{x}_1) d\underline{x}_1 = \frac{\eta_F}{\eta} \quad (4.10)$$

where η is the number of simulations performed and η_F is the number of failuresⁱⁱⁱ. During each simulation, one value of the limit state function $g_1(\underline{X}_1)$ (see Equation 4.4) is computed, by sampling a value of the multivariate Normal vector, $(m_0, m_1, m_2, \sigma, \mu_V, \sigma_V, \mu_D, \sigma_D)$ ^{iv}, and by taking $n_y \cdot 52$ stress range spectra, $(S_i, n_i)_w$, where n_y is the design life in years.

For high values of β the proposed MCS scheme would require a number of simulations too high (the estimation of $\beta = 6$ requires 10^{11} simulations): in this case the limit state function g_1 is re-written as follows:

$$g_1(\underline{X}_1) = D_c - D_d \quad (4.11)$$

and the probability of failure $P(E_1^*)$ is computed with FORM, after having characterized the random variable D_d with MCS (using 10^5 simulations^v).

The MCS resolution scheme proposed in this section has been implemented in the `E1definition` and `E1betacalc` modules of Matlab Toolbox TB2 (see Appendix B).

Eurocode S-N model

As discussed in Section 4.3.2, in the Eurocode S-N model, the only source of the fatigue scatter is represented by the normal random variable m_0 . In this case the simplified approach proposed by Chen et al. [14] is used for computing $P(E_1^*)$; the approach is presented below. The 104 weekly loading spectra $(S_i, n_i)_{w=1, \dots, 104}$ were computed by using the same scheme as previously presented for the ML-MCS S-N model. Then the weekly sum of m-power stress ranges was computed as:

$$r_{wk} = \sum_i n_i (s_i)^{-m_1} + \frac{1}{0.74 \text{FAT}^{m_1-m_2}} \sum_j n_j (s_j)^{-m_2} \quad \text{for } (k = 1, \dots, 104) \quad (4.12)$$

Within the assumption that the weekly sum of m-power stress ranges is a Normal random variable with location parameter μ_{R_w} and scale parameter σ_{R_w} , the observed sample r_{wk} was used to make inference about the distribution parameters. Under the assumption of no-traffic

ⁱⁱⁱIf MCS is asked to estimate a probability in the order of 10^{-y} , then approximately 10^{y+2} simulations are necessary to achieve an estimate with a coefficient of variance in the order of 10%

^{iv}At each simulation a different S-N curve and a different value of critical damage sum is considered, by taking into account the aleatory uncertainty of the S-N curve, of the CAFL and of the critical damage sum. The epistemic uncertainty of model parameters is also taken into account in repeated sampling of the multivariate Normal vector

^vIt was observed that 10^6 simulations give the same values of D_d distribution parameters as with 10^5 simulations

growth, the sum of m-power stress ranges over n_y year design life is:

$$R_d = \sum_{k=1}^{n_y \cdot 52} R_{w_k} \quad (4.13)$$

Location parameter μ_{R_d} and scale parameter σ_{R_d} were computed by making use of the central limit theorem [77]:

$$\begin{aligned} \mu_{R_d} &= n_y \cdot 52 \cdot \mu_{R_w} \\ \sigma_{R_d} &= \sqrt{n_y \cdot 52} \cdot \sigma_{R_w} \end{aligned} \quad (4.14)$$

The limit state equation g_1 was then re-written in function of the R_d random variable:

$$g_1(R_d, m_0, D_c) = D_c - \frac{R_d}{\exp(m_0)} = D_c - D_d \quad (4.15)$$

Since g_1 is a non-linear function of Normal random variables R_d, m_0, D_c , the probability of failure $P(E_1^*)$ was computed by using FORM with Hasofer-Lind approach [38].

4.3.4 Resolution of reliability problem P(E₂)

The limit state equation related to the event E_2 has been formulated in Equation 4.8. In order to characterize the random variable z_p (return level of maximum stress range), the stress history was analysed by following the classical extreme value (EV) theory approach.

EV theory approach for estimation of maximum stress range return levels z_p

The observed stress history was divided in 104 weekly blocks. Each weekly stress history block was transformed in a stress range weekly spectrum by using the rain-flow algorithm. From each weekly spectrum the maximum stress range, $s_{max,w}$, was extracted.

Within the assumption of constant pattern of variation, the observed $s_{max,w}$ can be modeled as independent observations from a GEV family distribution; the cdf of the GEV family distribution is defined as follows:

$$G(z) = \exp \left\{ - \left[1 + \xi \left(\frac{z - \tau}{\phi} \right) \right]^{\frac{-1}{\xi}} \right\} = Pr\{S_{max} \leq z\} \quad (4.16)$$

where τ is the location parameter, ϕ is the scale parameter, and ξ is the shape parameter.

The estimates of the extreme quantiles of the weekly maximum stress ranges were computed

by inverting the cdf of the GEV family distribution (see Equation 4.16):

$$z_p = G(z)^{-1} = \begin{cases} \tau - \frac{\phi}{\xi} \left\{ 1 - [-\ln(1-p)]^{-\xi} \right\} & \text{for } \xi \neq 0 \\ \tau - \phi \ln \{-\ln(1-p)\} & \text{for } \xi = 0 \end{cases} \quad (4.17)$$

with z_p representing the return level for the stress range, which is exceeded one time every p weeks. The plot $z_p - p$ is called return level plot.

The pdf of the GEV family distribution is defined as follows:

$$g(z) = \frac{1}{\phi} t(z)^{\xi+1} \exp(-t(z)) \quad (4.18)$$

where

$$t(z) = \begin{cases} \left(1 + \xi \frac{z - \tau}{\phi} \right)^{-\frac{1}{\xi}} & \text{for } \xi \neq 0 \\ \exp \left(-\frac{z - \mu}{\phi} \right) & \text{for } \xi = 0 \end{cases}$$

Under the assumption that observed maximum stress ranges are independent random variables which follow a GEV distribution, the negative log-Likelihood function is defined as the sum of $-\ln(g(z_i))$ over the 104 week observed period.

From Equation 4.18 it follows:

$$nLL(\tau, \phi, \xi) = 104 \ln(\phi) + \left(1 + \frac{1}{\xi} \right) \sum_{i=1}^{104} \ln \left[1 + \xi \left(\frac{z_i - \tau}{\phi} \right) \right] + \sum_{i=1}^{104} \left[1 + \xi \left(\frac{z_i - \tau}{\phi} \right) \right]^{-\frac{1}{\xi}}, \quad \text{for } \xi \neq 0 \quad (4.19)$$

provided that $1 + \xi \left(\frac{z_i - \tau}{\phi} \right) > 0$, for $i = 1 \dots 104$.

Or:

$$nLL(\tau, \phi, \xi) = 104 \ln(\phi) + \sum_{i=1}^{104} \frac{z_i - \tau}{\phi} + \sum_{i=1}^{104} \exp \left[-\left(\frac{z_i - \tau}{\phi} \right) \right], \quad \text{for } \xi = 0 \quad (4.20)$$

The ML estimate of GEV model parameters, $(\hat{\tau}, \hat{\phi}, \hat{\xi})$, was obtained by minimizing the negative log-Likelihood function (see Equations 4.19 and 4.20); since no analytical solution is available a numerical solution is needed for minimizing the negative log-Likelihood function.

In most cases $\xi > -0.5$ (the case $\xi \leq -0.5$ is rarely encountered since it corresponds to distributions with a very short bounded upper tail) and the vector $(\hat{\tau}, \hat{\phi}, \hat{\xi})$ follows a multivariate normal distribution with mean equal to (τ, ϕ, ξ) and covariance matrix equal to the inverse of the observed Fisher information matrix, $\underline{\underline{I}}((\tau, \phi, \xi))$ [19].

The assumption of approximate normality of ML estimators was verified and the variance of

the return level, $\text{Var}(z_p)$, was computed using the Δ method:

$$\text{Var}(z_p) = \left[\frac{\partial z_p}{\partial \tau}, \frac{\partial z_p}{\partial \phi}, \frac{\partial z_p}{\partial \xi} \right]^T \cdot \underline{\underline{\text{Cov}}}(\tau, \phi, \xi) \cdot \left[\frac{\partial z_p}{\partial \tau}, \frac{\partial z_p}{\partial \phi}, \frac{\partial z_p}{\partial \xi} \right] \quad (4.21)$$

where $\underline{\underline{\text{Cov}}}(\tau, \phi, \xi)$ is the covariance matrix of the vector $(\hat{\tau}, \hat{\phi}, \hat{\xi})$.

The validity of the extrapolation of stress range return levels, z_p , can be assessed using following diagnostic plots:

- Probability plot, which compares the empirical cumulative distribution function, $G^e(z_i) = i/(104 + 1)$, and the fitted distribution function, $G(z_i)$ (see Equation 4.16); deviation from diagonal indicates inaccuracy of the GEV fitting. Since for increasing i both $G^e(z_i)$ and $G(z_i)$ tend to unity, the probability plot is not very useful for large values of p , which is the zone of greatest interest in extreme value assessment problems;
- Quantile plot, which consists of points $[(G^{-1}(i/(104 + 1)), z_i), i = 1, \dots, 104]$; deviation from the diagonal indicates inaccuracy of the GEV fitting;
- Comparison of the pdf of the fitted GEV distribution with histogram of data. This plot is less useful then the probability and the quantile plots since the form of histogram varies with the choice of intervals.

It has to be noticed that the approach presented above is valid if:

1. The series $s_{max,w}$ is stationary: this assumption is realistic for the Venoge study case and can be verified by checking the diagram of observed maximum stress ranges;
2. The series $s_{max,w}$ is time-independent: this hypothesis is unrealistic for practical applications. Therefore in practical applications, provided that long-range dependence at extreme levels is weak, then $s_{max,w}$ follow the same distributional limit laws as those of independent series [15]. This means that $s_{max,w}$ may be fitted with GEV family distribution, provided that long-range dependence is eliminated; the GEV model parameters themselves are different from those that would have been obtained by considering an independent series, but since the parameters of the GEV family distribution have to be estimated anyway, this is not relevant.

ML estimation of GEV parameters, validation of z_p extrapolation by means of diagnostic plots and computation of $\text{Var}(z_p)$ were implemented in the module E2definition of the Matlab Toolbox TB2 (see Appendix B).

ML-MCS S-N model

The random variable $V(\mu_V, \sigma_V)$ was defined in the ML-MCS VA S-N stochastic model for cover plate data-set with outlier disqualification (see Tables 3.4 and 3.5).

Once the random variables V and z_p of the limit state equation g_2 (see Equation 4.8) were defined, the probability of failure $P(E_2)$ was computed with FORM. The FORM resolution scheme for computation of $P(E_2)$ was implemented in the module `E2betacalc` of Matlab Toolbox TB2 (see Appendix B).

Eurocode S-N model

According to the Eurocode S-N model, the CAFL is a deterministic value, which is determined by cutting the characteristic S-N curve at $5 \cdot 10^6$ cycles. In order to perform a reliability analysis on the failure event E_2 , the CAFL of the median S-N curve, $\exp(\mu_V)$, was computed by assuming a fatigue log-life standard deviation equal to 0.033 [73] (as for the computation of parameters of m_0 , see Table 4.1) and the standard deviation, σ_V , was determined by assuming a two-standard deviation difference between the mean and the characteristic value of the CAFL distribution:

$$V = \mathcal{N}(3.65, 0.08) \quad (4.22)$$

The probability of failure $P(E_2)$ was computed again with FORM.

4.4 Results

4.4.1 Event E_1^* : Critical damage accumulation

Eurocode S-N model

Observed weekly sum of m-power stress ranges and fitted normal distribution are plotted in Figure 4.8. The probability plot of observed weekly sums is shown in Figure 4.9.

The parameters of the Normal distribution R_w are:

$$\begin{aligned} \hat{\mu}_{R_w} &= 2.35 \cdot 10^6 \\ \hat{\sigma}_{R_w} &= 6.01 \cdot 10^5 \end{aligned} \quad (4.23)$$

The parameters of the Normal distribution R_d , over the design life, are:

$$\begin{aligned}\hat{\mu}_{R_d} &= 1.22 \cdot 10^8 \cdot n_y \\ \hat{\sigma}_{R_d} &= 4.33 \cdot 10^6 \cdot \sqrt{n_y}\end{aligned}\quad (4.24)$$

for $n_y = 1, \dots, 100$.

The coefficient of variation of R_w is equal to 0.256, while the coefficient of variation of R_d ranges from 0.256 (at beginning of design life) to 0.003 (at the end of design life). At the end of design life almost all randomness of accumulated damage is considered in the variable m_0 (see Equation 4.15).

After having defined all random variables in the limit state function g_1 (see Equation 4.15), the reliability index $\beta_1 = -\Phi^{-1}(P(E_1^*))$ was computed over the design life of the bridge, by using FORM (see Table 4.2). The results obtained by using FORM were checked by using SORM (see again Table 4.2): the difference in β_1 computation is negligible and use of SORM is not justified.

It is recalled here that $P(E_1^*)$ represents the probability of having critical damage accumulation (E_1), given that CAFL has been exceeded (E_2).

ML-MCS S-N model

The 104 weekly stress range spectra were generated by following the scheme presented in Section 4.3.3 (ML-MCS S-N model). The reliability index $\beta_1 = -\Phi^{-1}(P(E_1^*))$ was computed over the design life of the bridge, by using MCS (see Equation 4.10). Values of ML-MCS-based reliability index β_1 are compared to values of Eurocode-based reliability index β_1 in Table 4.3.

Years	FORM	SORM	Difference
25	12.028	12.030	<0.01%
50	10.196	10.190	<0.01%
75	9.124	9.122	<0.01%
100	8.363	8.361	<0.01%

Table 4.2: Calculation of β_1 : Eurocode S-N model

Years	Eurocode	ML-MCS
25	12.03	11.03
50	10.20	9.86
75	9.12	9.17
100	8.36	8.68

Table 4.3: Calculation of β_1 : Eurocode vs ML-MCS

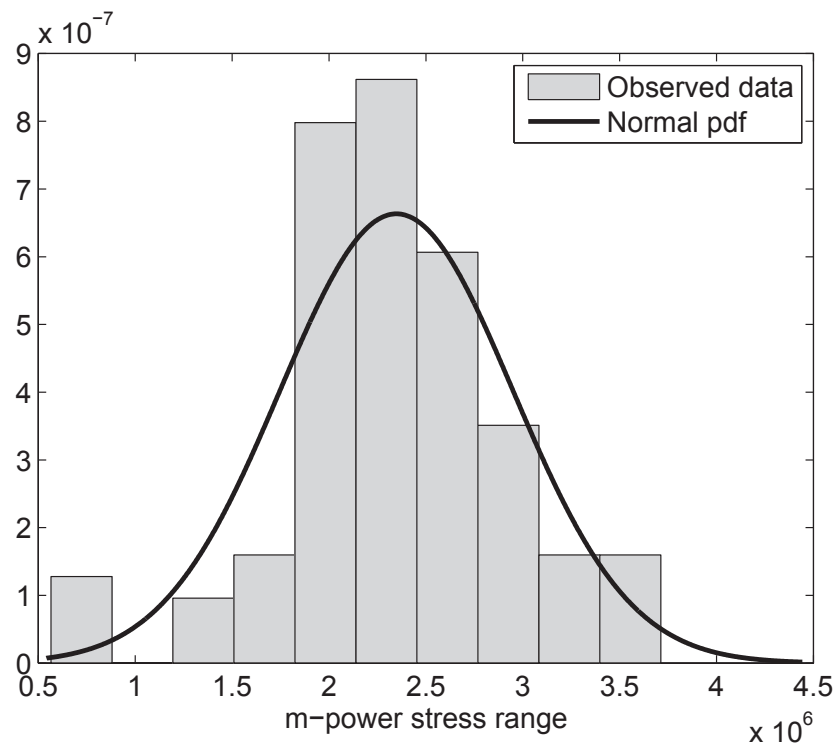


Figure 4.8: Observed weekly sum of m-power stress ranges

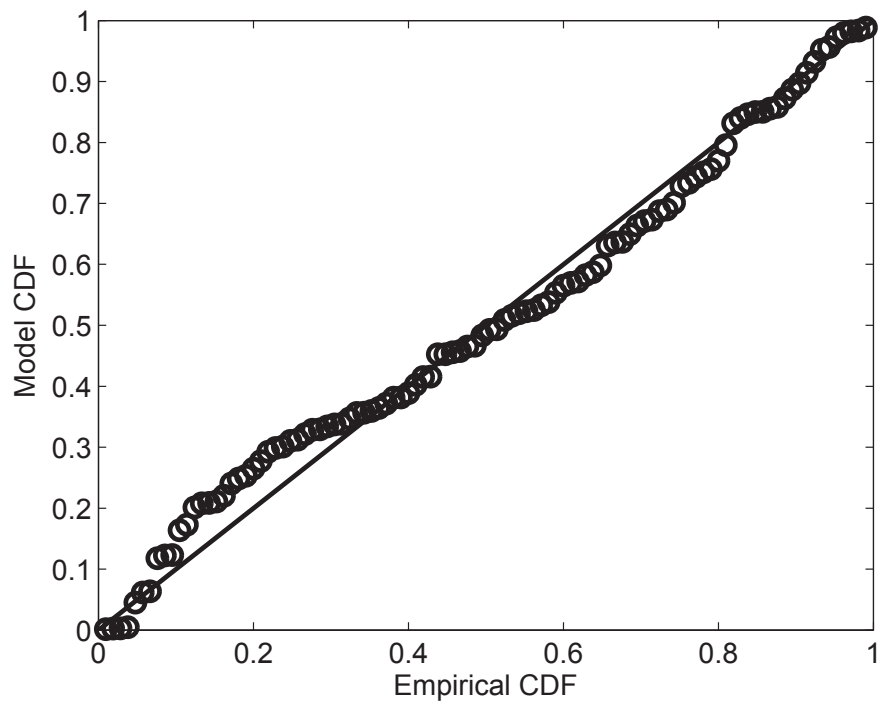


Figure 4.9: Probability plot of observed weekly sum of m-power stress ranges

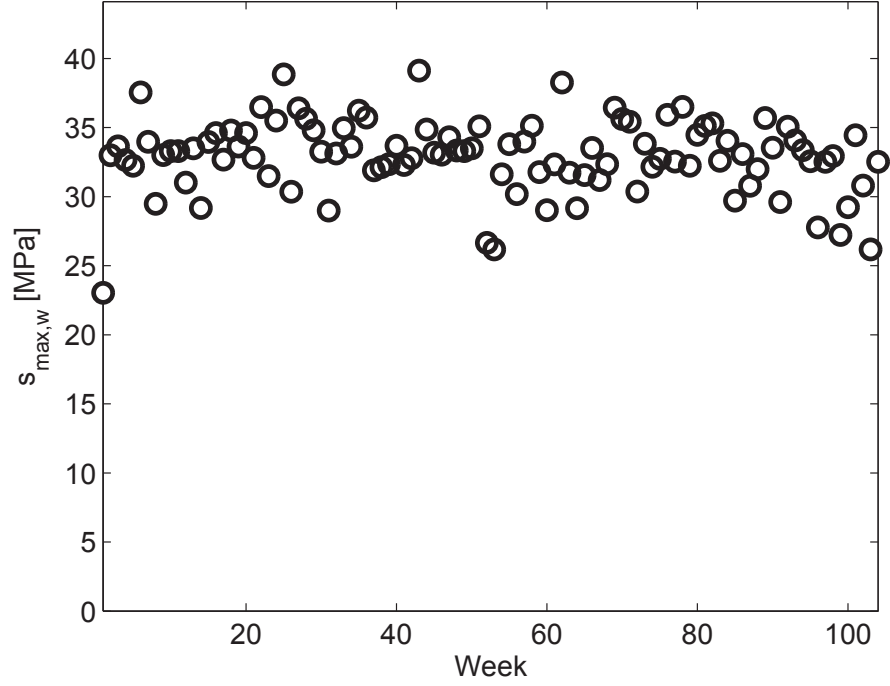


Figure 4.10: Observed weekly maximum stress ranges

4.4.2 Event E₂: CAFL exceedance

The observed weekly maximum stress ranges, $s_{max,w}$, over the period 2006-2007, are shown in Figure 4.10: the assumption of constant pattern of variation, which allows to model the observed $s_{max,w}$ as independent observations from a GEV family distribution, is supported. Fit of GEV distributions family to observed $s_{max,w}$ leads to the ML estimate:

$$(\hat{\mu}, \hat{\sigma}, \hat{\xi}) = (32.08, 2.88, -0.37) \quad (4.25)$$

$$\underline{\underline{\text{Cov}}}(\hat{\mu}, \hat{\sigma}, \hat{\xi}) = \begin{bmatrix} 1.7 \cdot 10^{-3} & 5.3 \cdot 10^{-3} & 4.3 \cdot 10^{-3} \\ \dots & 4.1 \cdot 10^{-2} & -1.2 \cdot 10^{-2} \\ \dots & \dots & 9.2 \cdot 10^{-2} \end{bmatrix} \quad (4.26)$$

Since the shape factor, ξ , is higher than -0.5, the hypothesis of asymptotic normality of ML estimators is supported.

Figure 4.11 represents \hat{z}_p against observed values (empirical return levels). The probability and quantile plots for assessing the accuracy of the GEV model fitted to the observed data

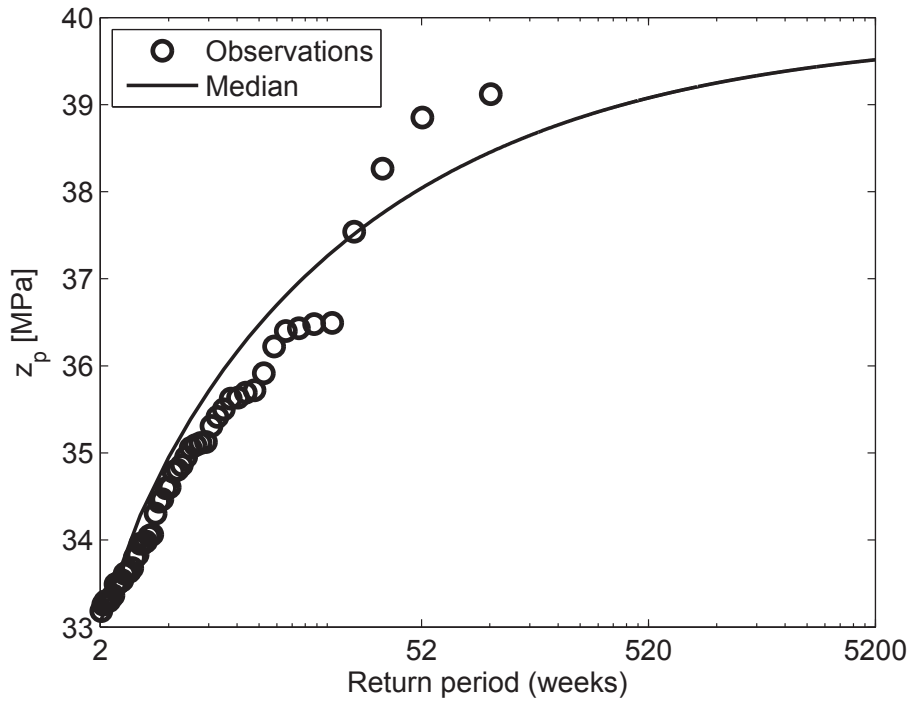


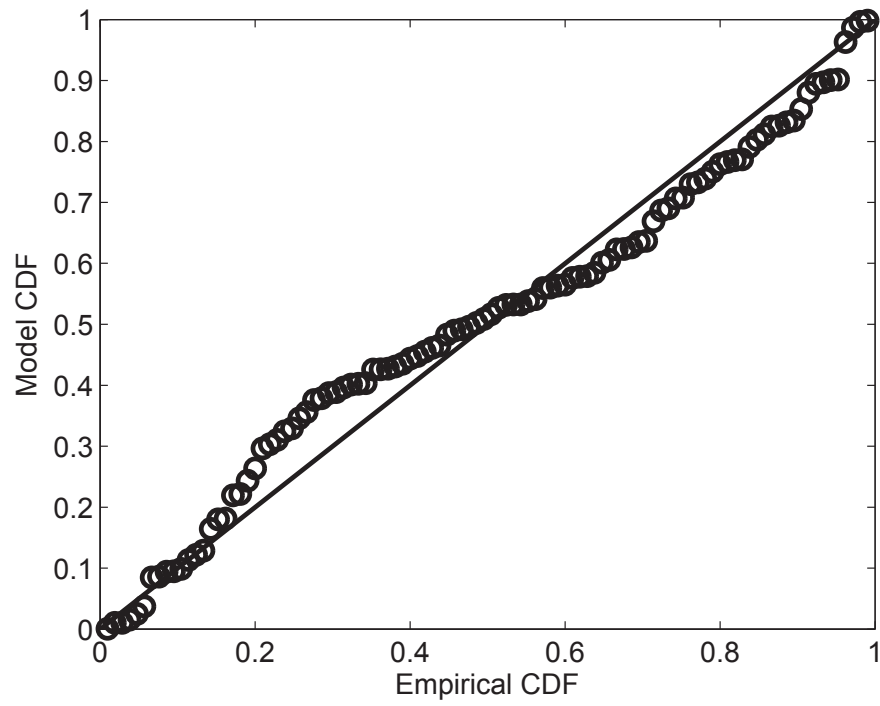
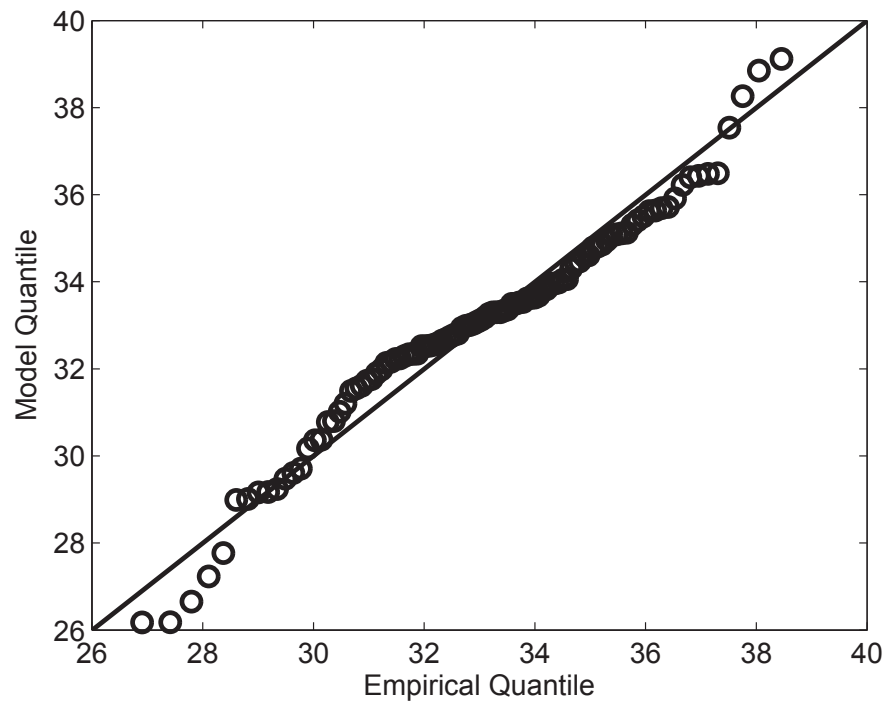
Figure 4.11: Return level plot of the weekly maximum stress range

Years	Eurocode	ML-MCS
25	-0.15	-0.94
50	-0.16	-0.94
75	-0.17	-0.94
100	-0.17	-0.94

Table 4.4: Calculation of β_2 : Eurocode vs ML-MCS

are shown in Figures 4.12 and 4.13. After having defined z_p random variable in limit state function g_2 (see Equation 4.8), the reliability index $\beta_2 = -\Phi^{-1}(P(E_2))$ was computed over the design life of the bridge, by using FORM for both Eurocode S-N model and ML-MCS S-N model.

Computed values of reliability index β_2 are presented in Table 4.4.

Figure 4.12: Probability plot of z_p Figure 4.13: Quantile plot of z_p

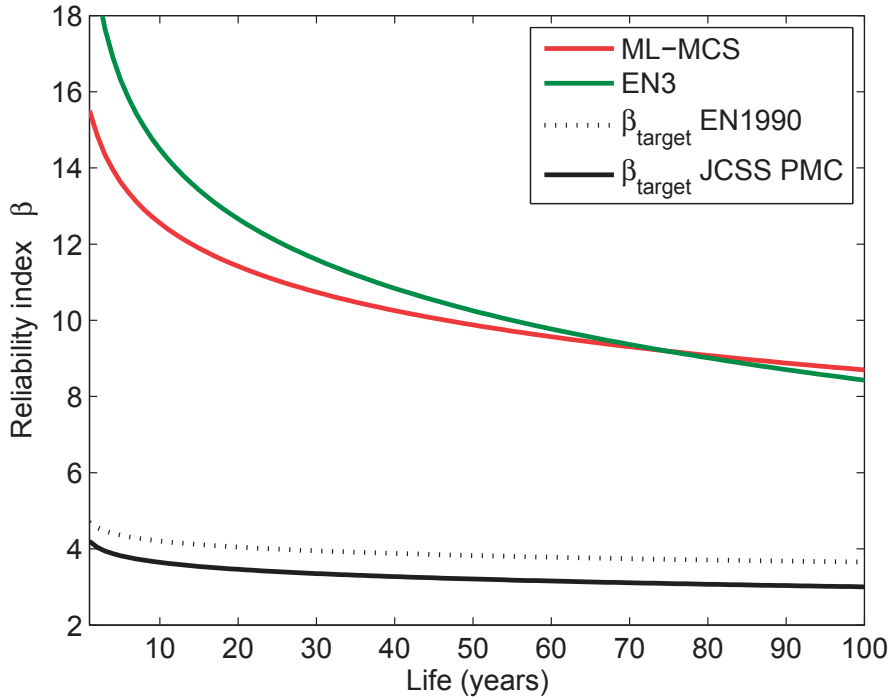


Figure 4.14: Evolution of reliability index β over the design life

4.4.3 Event $E_1 \cap E_2$: fatigue failure

According to Equation 4.3, the probability of fatigue failure is given by the product of probabilities $P(E_1^*)$ and $P(E_2)$; the fatigue reliability index $\beta = -\Phi^{-1}(P(E_1^* \cdot E_2))$ was computed using results of Sections 4.4.1 and 4.4.2.

The evolution of the fatigue reliability index β over the 100 year design life is shown in Figure 4.14, both for the Eurocode S-N model and the ML-MCS S-N model. Following reliability indexes are also plotted in Figure 4.14 for direct comparison:

- β_t EN1990, based on an annual failure probability equal to $1.3 \cdot 10^{-6}$, corresponding to a β annual equal to 4.7 (Reliability class RC2, assuming independency, [23] Annex C, Chapter C6);
- β_t JCSS, based on an annual failure probability equal to $1.3 \cdot 10^{-5}$, corresponding to a β annual equal to 4.2 (Normal relative cost of safety measure and moderate consequence of failure, assuming independency [41]).

S-N model	25y.	50 y.	75 y.	100 y.
EN 1993-1-9	12.03	10.20	9.12	8.36
ML-MCS [†]	11.03	9.86	9.17	8.68
ML-MCS [†] traffic growth 1	10.97	8.36	5.53	2.67
ML-MCS [†] traffic growth 2	11.35	7.44	3.53	1.76
Eurocode 1990	3.99	3.83	3.73	3.65
JCSS, PMC	3.40	3.21	3.09	3.00

([†]) S-N model with disqualification of outliers

Table 4.5: Calculation of β reliability index

Virtual traffic growth scenarios

In order to assess the impact of future traffic evolution on the fatigue analysis, the effect of increasing the weekly accumulated fatigue damage was studied (i.e. this effect could be caused by a change in repartition of vehicle classes or a change in axle weight distribution for a specific class). Two virtual scenarios were considered (see Figure 4.15): 1) Weekly accumulated damage, D_w , having a 7% yearly increment of the median value, $d_{w,0.5}$; and 2) Weekly accumulated damage, D_w , having a 500% discontinuous increment after 25 and 50 years of the median value, $d_{w,0.5}$, as well as a 3% yearly increment of the median value, $d_{w,0.5}$, starting from the first discontinuous increment. Furthermore, for both scenarios, it was assumed that the weekly accumulated damage, D_w , is constant for the first 20 years (from 1995 to now).

It is noted that the considered virtual traffic evolution scenarios take into account only an increase in number of vehicles and not in truck loads; this cause a change in $P(E_1^*)$, while $P(E_2)$ is not affected by the traffic evolution scenarios. The choice of considering only a change in $P(E_1^*)$ is due to the fact that, for the considered Venoge study case, the ML-MCS-based $P(E_2)$ is constantly higher than 80% over the bridge design life (see Table 4.4) and a change in $P(E_2)$ would not have a significant effect on the global probability of failure $P(E_1^*) \cdot P(E_2)$.

The evolution of the ML-MCS S-N model-based fatigue reliability index β over the 100 year-design life, for the two traffic growth scenarios, is shown in Figure 4.16. Figures 4.17 and 4.18 show the histograms and the density maps of sampled (d_d, d_c) , respectively for no traffic growth and traffic growth scenario 2 (for $t=100$ years). The MCS plot of sampled (d_d, d_c) is plotted with the limit state function $g_1 = D_c - D_d$ in Figures 4.19 and 4.20, respectively for no traffic growth and traffic growth scenario 2 (for $t=100$ years).

Table 4.5 shows all computed reliability indexes β and provides a comparison with target reliability indexes from Eurocode 1990 and JCSS PMC.

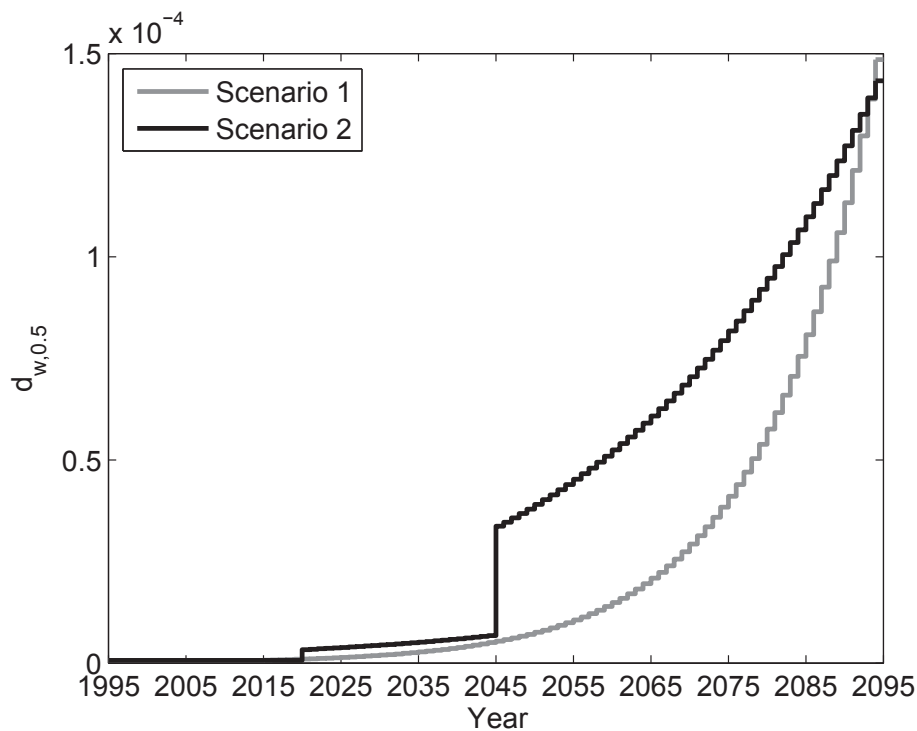


Figure 4.15: Weekly damage growth: Scenarios 1 and 2

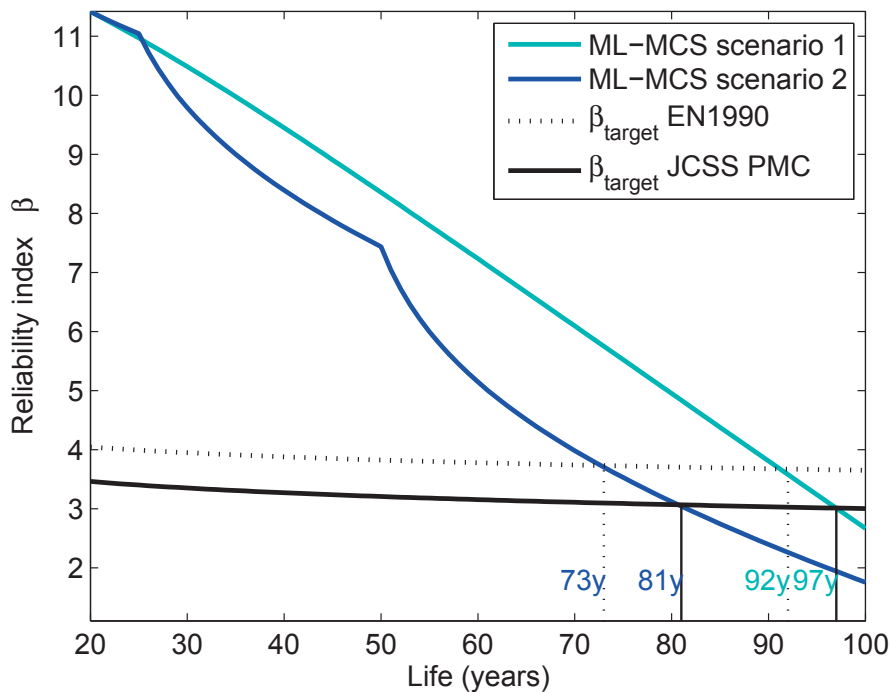


Figure 4.16: Evolution of reliability index β over the design life, considering traffic growth

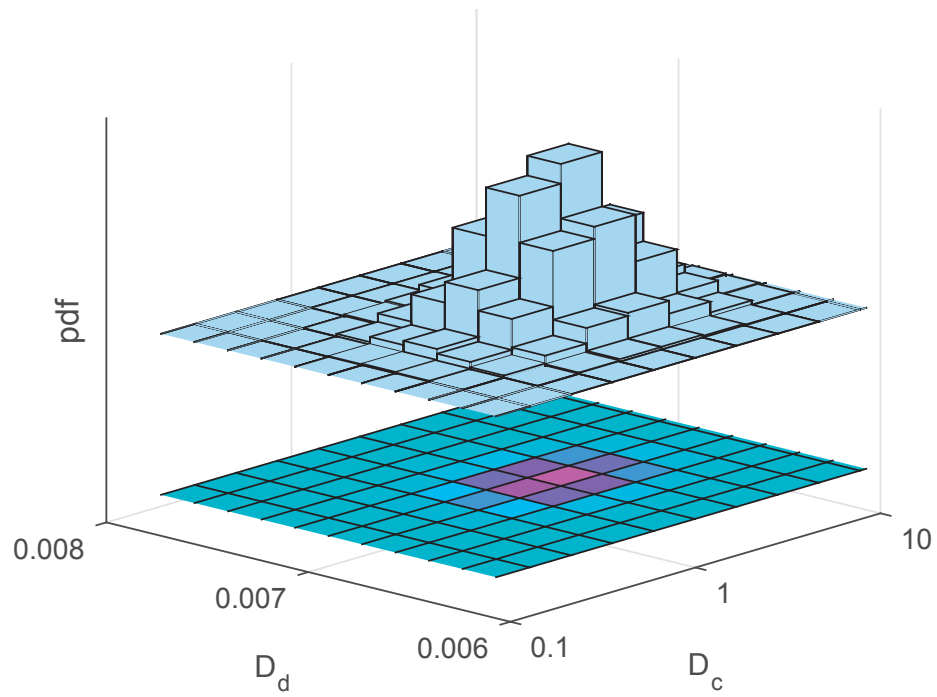


Figure 4.17: MCS data histogram and density map for $t=100$ years. No traffic growth

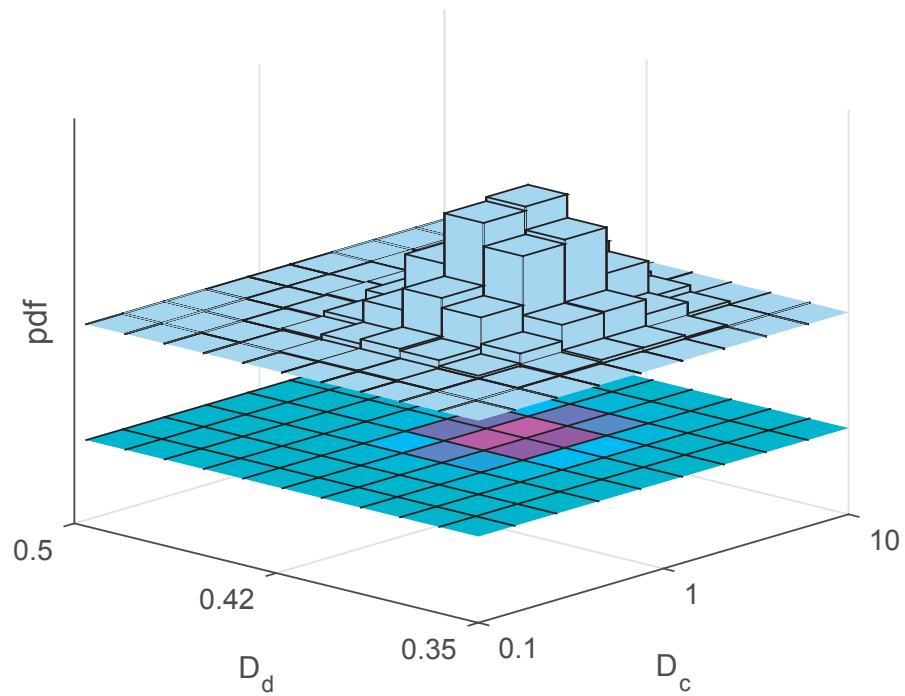


Figure 4.18: MCS data histogram and density map for $t=100$ years. Traffic growth scenario 2

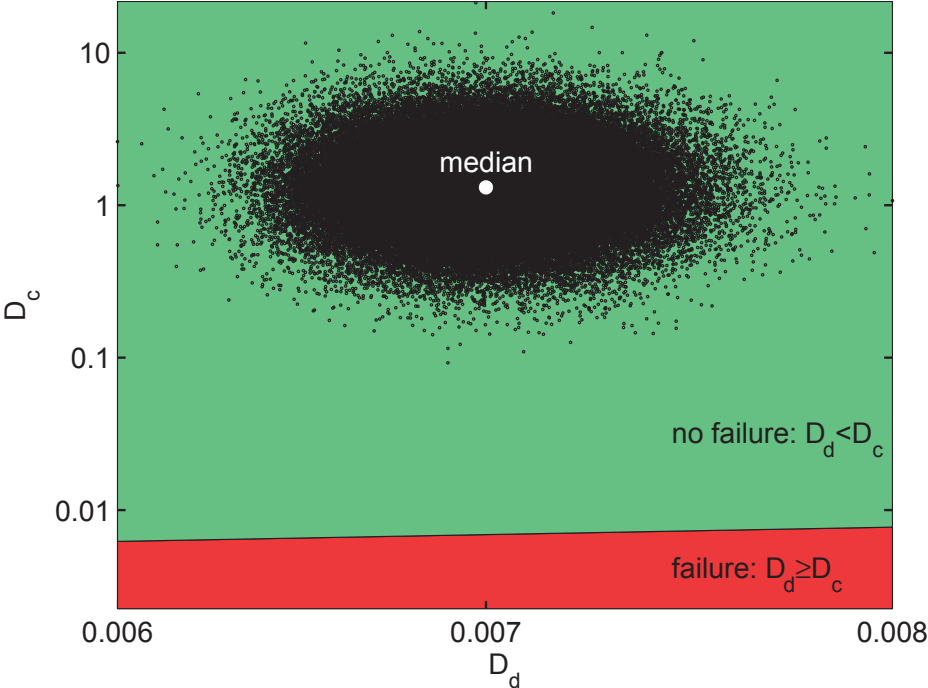


Figure 4.19: MCS plot for $t=100$ years. No traffic growth

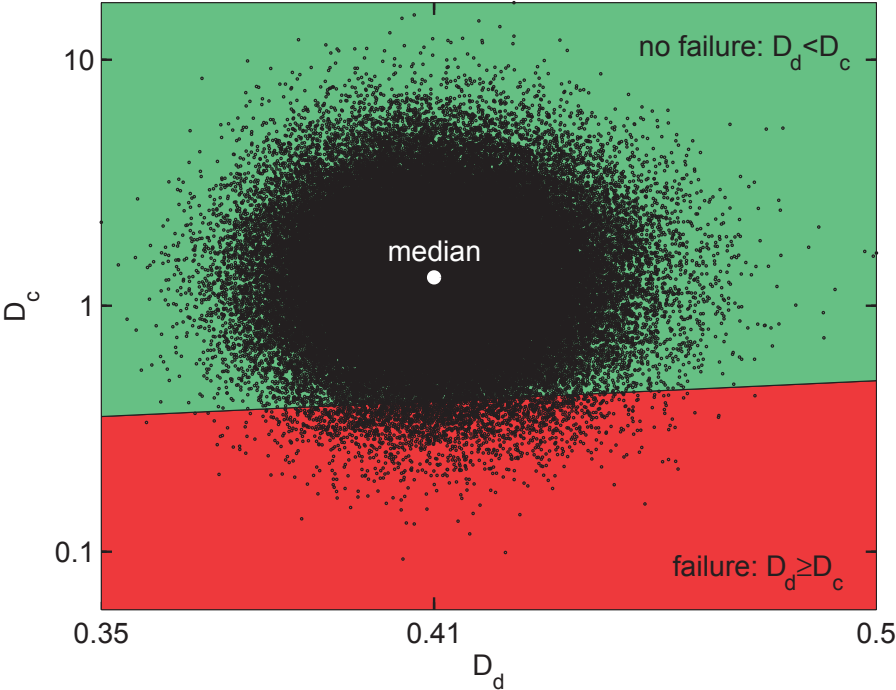


Figure 4.20: MCS plot for $t=100$ years. Traffic growth scenario 2

4.5 Conclusions and discussion

In this Chapter a new framework for fatigue reliability assessment of existing road bridges was presented, with application to Venoge bridge, a bridge part of the A1 Swiss Motorway.

A two year-continuous registration of WIM data and FE analysis were combined to compute the time-stress response at one fatigue critical location (welded cover plate, classified as FAT 45 in Eurocode standards [24]). The probability of failure, P_f , of the fatigue critical detail and related reliability index, β , were computed for a 100 year-design life. The failure probability P_f was computed as the product of $P(E_1|E_2)$ (probability of having critical damage accumulation conditioned on CAFL exceedance) and $P(E_2)$ (probability of CAFL exceedance). Two different S-N models were used to define fatigue strength of the critical detail: 1) Eurocode S-N model; and 2) ML-MCS S-N model (see Chapter 3).

Assessment of $P(E_1|E_2)$ and $P(E_2)$ asks respectively for the definition of limit state function g_1 and g_2 .

Concerning the Eurocode S-N model-based limit state function g_1 (see Equation 4.15), the random variables m_0 (log-intercept of S-N curve above the CAFL) and D_c (critical damage sum at failure), were defined according to [73] and [41]. The random variable R_d , representing the loading term of the limit state equation, was defined by fitting a Normal distribution R_w (weekly sum of m-power stress ranges) to 104 weekly observations and then applying central limit theorem in order to switch from S_w parameters to S_d parameters. The density plot (see Figure 4.8) and the probability plot (see Figure 4.9) provide support to the fitted Normal model. Concerning the ML-MCS S-N model-based limit state function g_1 (see Equation 4.11), the random S-N model multi-variate vector (including both S-N curve parameters and D_c random variable) was defined according to the results presented in Section 3.4.

Concerning the limit state function g_2 (see Equation 4.8), the random variable V was defined according to [73], for the Eurocode S-N model-based approach, and according to the results presented in Section 3.4, for the ML-MCS S-N model-based approach. The maximum stress range return level, z_p , representing the loading term of the limit state function, was defined by fitting a GEV family distribution to 104 weekly maximum stress ranges and then computing quantiles of the fitted distribution. Following three diagnostic plots provide support to the fitted GEV model: 1) The return level plot (see Figure 4.11); 2) The probability plot (see Figure 4.12); and 3) The quantile plot (see Figure 4.13).

Failure probability $P(E_1)$ and reliability index β_1 were computed by using FORM with Hasofer-Lind approach, for the Eurocode S-N model-based approach, and by using a MCS scheme, for the ML-MCS S-N model-based approach. Comparison of the Eurocode-based β_1 and the ML-MCS-based β_1 are shown in Table 4.3: for the first 75 years the Eurocode approach is under-conservative with respect to ML-MCS approach, while for the last 25 years the

Eurocode approach becomes over-conservative. This difference is due to the combination of three effects: 1) Different values of S-N curve intercept (see Figure 3.20); 2) Different position of CAFL (see again Figure 3.20); and 3) Approximation of Eurocode approach which uses the characteristic value of CAFL for computing m-power stress ranges (instead of considering CAFL as a random variable).

Failure probability $P(E_2)$ and related reliability index β_2 were computed for both S-N model approaches by using FORM with Hasofer-Lind approach. Comparison of Eurocode S-N model-based β_2 and ML-MCS S-N model-based β_2 are shown in Table 4.4: the Eurocode approach is highly unsafe with respect to ML-MCS approach due to the highly under-conservative estimation of CAFL (see Section 2.5). The probability of CAFL exceedance, $P(E_2)$, after 25 years, is equal to 56% according to Eurocode approach, while the ML-MCS approach gives $P(E_2) = 83\%$, which means that ML-MCS approach indicates the CAFL is closely to be surely exceeded after 25 years.

Figure 4.14 shows the evolution of the reliability index $\beta = -\Phi^{-1}(\Phi(-\beta_1) \cdot \Phi(-\beta_2))$ over the 100-year design life: for both Eurocode and ML-MCS S-N model-based approaches, the reliability index is greater than β_t EN1990 and β_t JCSS over whole bridge design life.

In order to assess the impact of future traffic evolution on the fatigue analysis, two very aggressive virtual traffic growth scenario were considered, the first one having a 7% yearly increment of the median value of weekly accumulated damage and the second one having a 3% yearly increment of the median value of weekly accumulated damage with two discontinuous 500% increments after 25 and 50 years. Figure 4.16 shows the evolution of the reliability index β over the 100 year-design life for the two traffic growth scenarios, based on the ML-MCS S-N model. The histograms and the density maps of sampled (d_d, d_c) in the ML-MCS S-N model-based β calculation are shown in Figure 4.17, for no-traffic growth, and in Figure 4.18, for the traffic growth scenario 2: the median of sampled d_d values increases from 0.007 (no traffic growth) to 0.4 (traffic growth), logically resulting in a significant reduction of β_1 . This reduction can be observed also in Figures 4.19 and 4.20, where β_1 is proportional to the distance from the median of sampled (d_d, d_c) to the limit state function (border between failure domain and no failure domain). The reduction of β_1 causes a decrease of β , that can be observed in Table 4.5.

Figure 4.16 reveals the importance of the choice of target reliability index:

- For the traffic growth scenario 1, the ML-MCS S-N model-based β becomes lower than β_t EN1990 after 92 years, while it becomes lower than β_t JCSS after 97 years;
- For the traffic growth scenario 2, the ML-MCS S-N model-based β becomes lower than β_t EN1990 after 73 years, while it becomes lower than β_t JCSS after 81 years.

From the two points above it follows that the limit date, at which an inspection of the critical detail would be recommended, is postponed by 5 years for the traffic growth scenario 1 and by 8 years for the traffic growth scenario 2, when adopting JCSS PMC-based target reliability index instead of the Eurocode 1990-based target reliability index.

In conclusion, the reliability analysis framework set up in this Chapter constitutes a powerful tool to perform fatigue reliability analyses of road bridges using WIM-based realistic characterization of traffic loadings. The use of ML-MCS-based S-N model gives more realistic characterization of the fatigue strength with respect to the standard approach and allows to improve the confidence in fatigue reliability analysis.

The considered Venoge bridge study case uses 2006-2007 WIM data and is based on stationary load sequences; however any additional WIM data-set can be used to update estimated model and to take in account possible future traffic growth (non-stationary loading sequences): in this case probability distributions having time-dependent parameters ($D_d(\mu_D(t), \sigma_D(t))$, $z_p(\tau(t), \phi(t), \xi(t))$) have to be used for reliability analysis.

5 Calibration of fatigue partial safety factors

5.1 Introduction

The safety and serviceability issues in structural design are addressed in structural codes by defining design equations which compare load effects and resistance. Due to the uncertain nature of load and resistance terms, these are modeled as random variables. Characteristic values of random variables and partial safety factors are introduced in order to achieve a target reliability level. The process of choosing design format, characteristic values, partial safety factors and target reliability level, by using some reliability methods, is called *code calibration*. The problem of reliability based code calibration has been addressed by many authors, [21], [60], [25] and it has also been implemented in Eurocode 1990 [23].

The typical design equation for the verification of a structural component (see Eurocode 1990) is:

$$G = \frac{zR_c}{\gamma_M} - (\gamma_{F1}E_{c1} + \dots + \gamma_{Fn}E_{cn}) = 0 \quad (5.1)$$

where:

- R_c is the characteristic value of resistance;
- z is the design factor;
- γ_M is the partial safety factor for resistance;
- E_{ci} is the characteristic value of the i^{th} action effect;
- γ_{Fi} is the partial safety factor for the i^{th} action effect.

Chapter 5. Calibration of fatigue partial safety factors

Application of partial safety factors together with characteristic values of resistance and loading effects ensures a certain level of reliability for the designed structural component.

According to the design Equation 5.1 a reliability analysis can be made with the following limit state equation:

$$g = zR - (E_1 + \dots + E_n) = 0 \quad (5.2)$$

For a given probabilistic model of the basis random variables R and E_i , and for an assigned value of target failure probability, the optimal design \hat{z} can be computed, which corresponds to the required level of target reliability. Having determined the optimal design \hat{z} , the corresponding design point (R_d, E_{di}) can be computed and the partial safety factors can be derived as follows:

$$\gamma_M = \frac{R_c}{R_d} \quad (5.3)$$

$$\gamma_{Fi} = \frac{E_{di}}{E_{ci}} \quad (5.4)$$

The relation between design values, characteristic values and partial safety factors is illustrated in Figure 5.1, for the simple case of only one action effect.

Resolution of the code calibration problem asks for: 1) Determination of target reliability level; and 2) Calibration of partial safety factors.

The choice of target reliability level is generally based on an economic decision theory approach; this issue is not addressed in this study.

The calibration of partial safety factors is a decision problem, in which partial safety factors are decision variables which are calibrated by maximizing an objective function. Faber et al.[25] proposed a practical approach for calibration of partial safety factors, in which the objective function is formulated as follows:

$$W(\gamma) = \sum_{j=1}^L w_j \cdot (\beta_j(\gamma) - \beta_t) \quad (5.5)$$

where:

- L is the number of load cases;
- w_j are the importance factors of different design load cases;
- β_t is the target reliability index.

Partial safety factors γ are computed by minimizing the objective function in Equation 5.5, in which the reliability index is computed by solving the limit state equation (see Equation 5.2), having determined the optimal design factor \hat{z} from the design equation (see Equation 5.1). It is noted that when partial safety factors are calibrated from Equation 5.5 they are not independent and in the case with one resistance factor and one loading factor only the product of them can be calculated.

General limit state Equation 5.2 and general design Equation 5.1 can be easily adapted to the fatigue design case.

In Eurocode standards, three verification schemes are proposed for fatigue design under VA loadings (see A.6 of EN-1993-1-9 [24]):

1. Verification scheme based on CAFL;
2. Verification scheme based on CA equivalent stress range at $2 \cdot 10^6$ cycles;
3. Verification scheme based on accumulated damage.

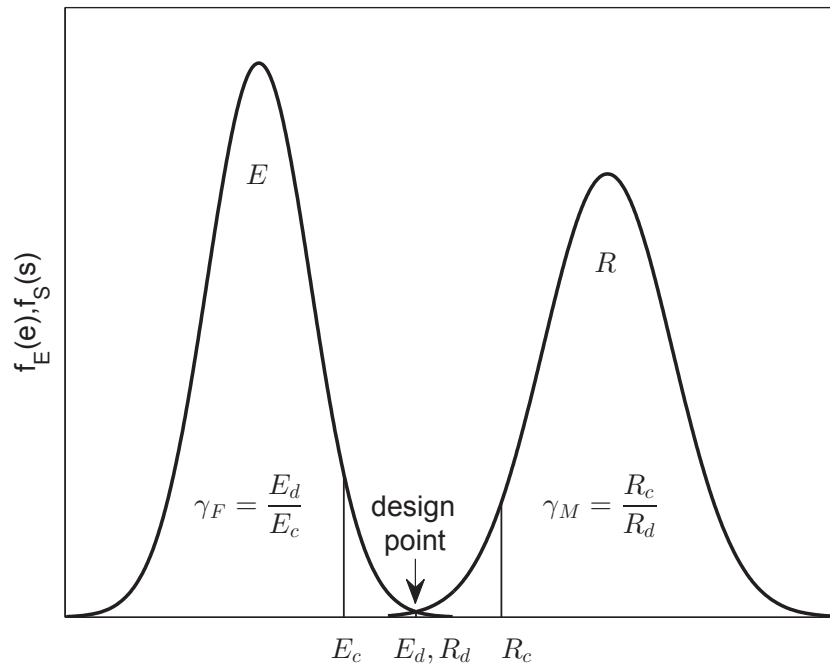


Figure 5.1: Relation between characteristic values, design values and partial safety factors

Verification scheme 1: based on CAFL

The fatigue design based on CAFL exceedance has to meet the following criterion:

$$\gamma_{Ff} \cdot S_{max_c} \leq \frac{CAFL}{\gamma_{Mf}} \quad (5.6)$$

where:

- CAFL is the characteristic value of the fatigue limit;
- S_{max_c} is the characteristic value of maximum loading stress range;
- γ_{Ff} is the loading partial safety factor, which is set to 1.0;
- γ_{Mf} is the resistance partial safety factor.

Verification scheme 2: based on CA equivalent stress range

The fatigue design based on CA equivalent stress range has to meet the following criterion:

$$\gamma_{Ff} \cdot S_{E,2} \leq \frac{S_c}{\gamma_{Mf}} \quad (5.7)$$

where:

- $S_{E,2}$ is the equivalent stress range, reported at $2 \cdot 10^6$ cycles, which is computed by using Fatigue Load Model (FLM) 3 and λ damage equivalent factors;
- S_c is the characteristic fatigue strength at $2 \cdot 10^6$ cycles (FAT).

Verification scheme 3: based on damage accumulation

The fatigue design based on damage accumulation has to meet the following criterion:

$$D_d = \sum_i^{N_{tot}} \frac{n_i}{N_i} \leq 1.0 \quad (5.8)$$

where:

- n_i is the number of cycles corresponding to the design loading stress range $\gamma_{Ff} \cdot S_i$;
- N_i is the number of cycles to failure obtained from the factored $\frac{S_c}{\gamma_{Mf}} - N$ curve.

5.2. New framework for partial safety factor calibration

Design method	Consequence of failure	
	Low consequence	High consequence
Damage tolerant	1.00	1.15
Safe life	1.15	1.35

Table 5.1: Recommended values for γ_{Mf} , by assuming $\gamma_{Ff} = 1$ (Table 3.1 of [24])

The definition of the partial resistance factor γ_{Mf} in EN 1993-1-9 (Section 1.4, pp. 9, [24]) is ambiguous because γ_{Mf} is strictly defined for fatigue strength at $2 \cdot 10^6$ cycles (therefore relevant only for verification scheme 2), but it is generically applied for fatigue strengths at any number of cycles (verification schemes 1 and 3).

Recommended values of partial factor γ_{Mf} are presented in Table 5.1. Proof of calibration of these values is not available and the real reliability level, β , corresponding to the values recommended in Table 5.1 is still under debate.

In this Chapter a new framework for calibration of fatigue partial safety factors is presented. The three different fatigue limit state (FLS) equations are formulated for direct comparison with the three fatigue design verification schemes proposed in Eurocode 1993-1-9. The VA S-N model used in this framework is defined using the new ML-MCS approach, which is presented in Chapters 2 and 3. The target reliability indexes for FLS are based on the recommendations of JCSS [41]. The Chapter is organized as follows:

- In Section 5.2 the new framework for calibration of fatigue partial safety factors using ML-MCS S-N model is presented;
- In section 5.3 an application of the framework to two typical bridge fatigue sensitive welded joints is considered;
- in Section 5.4 results of analyses of the two considered study cases are presented. A practical example, showing the impact of the choice of design S-N curves on fatigue design of a road bridge, is also given;
- in Section 5.5 results are discussed and comparison with partial safety factor values recommended in Eurocode 1993-1-9 is made.

5.2 New framework for partial safety factor calibration

In this section a new framework for calibration of fatigue partial safety factors using ML-MCS S-N model is presented. The framework includes the three verification schemes which have been presented in Section 5.1. One different limit state function is formulated for each of verification schemes.

Partial safety factors are calibrated for the three different design verification schemes, by using following general objective function (which is valid for all three verifications):

$$W(\gamma_{Ff}, \gamma_{Mf}) = \sum_{j=1}^L w_j \cdot (\beta_j(\gamma_{Ff}, \gamma_{Mf}) - \beta_t)^2 \quad (5.9)$$

where:

- γ_{Ff} is the partial safety factor for fatigue loading;
- γ_{Mf} is the partial safety factor for fatigue resistance;
- L is the number of load cases;
- w_j are the load case importance factors;
- β_j are the computed reliability indexes, for $j = 1, \dots, L$;
- $\beta_t = -\Phi^{-1}([\Phi(4.2)]^{100}) = 3.00$, is the target reliability index for a 100 year reference periodⁱ;

The reliability indexes β_j are computed by solving the limit state equation for different load cases ($j = 1, \dots, L$), after having determined the optimal design, \hat{z} , as solution of the design equation. Formulation of limit state and design equations for the three considered verification cases is discussed in following three subsections.

5.2.1 Verification scheme 1: based on CAFL

The design equation, for the generic load case j , is formulated as follows:

$$G_j = z_j \cdot \frac{\text{CAFL}}{\gamma_{Mf}} - \gamma_{Ff} \cdot S_{max_c, j} \quad (5.10)$$

where z_j is the design factor and $S_{max_c, j}$ is the characteristic value of the maximum stress range, $S_{max, j}$. The geometrical interpretation of the resistance partial safety factor γ_{Mf} is illustrated in Figure 5.2. S_{max} is modeled as a Gumbel random variable, $\mathcal{G}_1(\mu_{\mathcal{G}_1}, \sigma_{\mathcal{G}_1})$, having coefficient of variation equal to:

$$c_{v_{\mathcal{G}_1}} = \frac{1.28(\sigma_{\mathcal{G}_1} / \mu_{\mathcal{G}_1})}{0.58(\sigma_{\mathcal{G}_1} / \mu_{\mathcal{G}_1}) + 1} \quad (5.11)$$

ⁱbased on $\beta_t^{1y} = 4.2$ [41], assuming independency

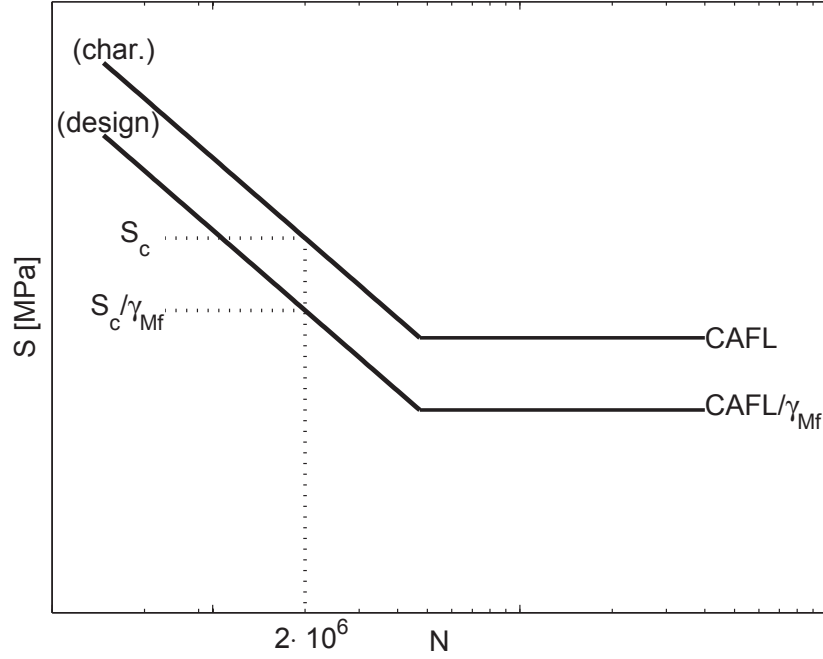


Figure 5.2: Resistance partial safety factor, verification schemes 1 and 2

In order to take into account both the effects of position and dispersion of loading term, 20 load cases are built by considering all possible combinations of the following values of $\mu_{\mathcal{G}_1}$ and $c_{\nu_{\mathcal{G}_1}}$:

$$\mu_{\mathcal{G}_1} = (\exp(\nu_{.05}), \dots, \Delta, \dots, \exp(\mu_V)) \quad \text{with } \Delta = (\exp(\mu_V) - \exp(\nu_{.05})) / 4 \quad (5.12)$$

$$c_{\nu_{\mathcal{G}_1}} = (0.20, 0.27, 0.33, 0.40) \quad (5.13)$$

The optimal design, \hat{z}_j , for the load case j , is computed by solving the design Equation 5.10, $G_j = 0$, for assigned values of partial safety factors.

The reliability index β_j is then computed by solving the following limit state equationⁱⁱ:

$$g_j = \hat{z}_j \cdot \exp(V) - S_{max,j} \quad (5.14)$$

ⁱⁱIt is noted that both the epistemic uncertainty of the model parameters and the aleatory randomness of the CAFL are taken into account in the definition of the fatigue limit state function

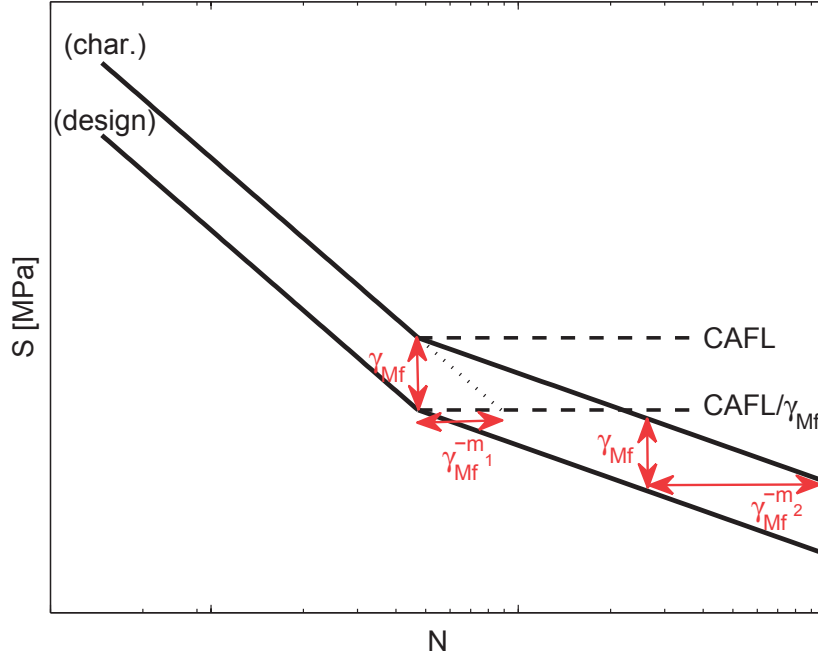


Figure 5.3: Resistance partial safety factor, verification scheme 3

Fatigue partial safety factors are calibrated by minimizing following objective function:

$$W(\gamma) = \sum_{j=1}^{20} w_j \cdot (\beta_j(\gamma) - 3.00)^2 \quad (5.15)$$

where $w_j = 1$ for $j = 1, \dots, 20$, since all load cases have the same importance.

It is noted that when γ_{Ff} and γ_{Mf} are determined with Equations 5.10, 5.14, and 5.15, they are not independent and only the product $\gamma_{Ff} \cdot \gamma_{Mf}$ is determined.

5.2.2 Verification scheme 2: based on CA equivalent stress range

The design equation, for the generic load case j , is formulated as follows:

$$G_j = z_j \cdot \frac{S_c}{\gamma_{Mf}} - \gamma_{Ff} \cdot S_{E,2c,j} \quad (5.16)$$

where z_j is the design factor, S_c is the characteristic value of fatigue strength at $2 \cdot 10^6$ cycles, and $S_{E,2c,j}$ is the characteristic value of equivalent stress range at $2 \cdot 10^6$ cycles, $S_{E,2,j}$.

The geometrical interpretation of the resistance partial safety factor is illustrated in Figure 5.2.

5.2. New framework for partial safety factor calibration

$S_{E,2}$ is modeled as a log-Normal random variableⁱⁱⁱ, $\log \mathcal{N}_2(\mu_{\mathcal{N}_2}, \sigma_{\mathcal{N}_2})$, having coefficient of variation equal to:

$$c_{v_{\mathcal{N}_2}} = \sqrt{\exp(\sigma_{\mathcal{N}_2}^2) - 1} \quad (5.17)$$

In order to take into account both the effects of position and dispersion of loading term, 20 load cases are built by considering all possible combinations of following values of $\mu_{\mathcal{N}_2}$ and $c_{v_{\mathcal{N}_2}}$:

$$\mu_{\mathcal{N}_2} = (3.40, 3.57, 3.75, 3.92, 4.10) \quad (5.18)$$

$$c_{v_{\mathcal{N}_2}} = (0.10, 0.13, 0.17, 0.20) \quad (5.19)$$

The optimal design, \hat{z}_j , for the load case j , is computed by solving the design Equation 5.16, $G_j = 0$, for assigned values of partial safety factors.

The reliability index β_j is then computed by solving the following limit state equation^{iv}:

$$g_j = \hat{z}_j \cdot S - S_{E,2,j} \quad (5.20)$$

Fatigue partial safety factors are calibrated by minimizing the following objective function:

$$W(\gamma) = \sum_{j=1}^{20} w_j \cdot (\beta_j(\gamma) - 3.00)^2 \quad (5.21)$$

where $w_j = 1$ for $j = 1, \dots, 20$, since all load cases have the same importance.

It is noted again that when γ_{Ff} and γ_{Mf} are determined with Equations 5.16, 5.20, and 5.21, they are not independent and only the product $\gamma_{Ff} \cdot \gamma_{Mf}$ is determined.

ⁱⁱⁱModeling the logarithm of the equivalent stress range as a Normal random variable allows for consideration of the variability on the maximum stress range obtained from fatigue load model as well as of the variabilities on different λ factors

^{iv}It is noted that both the epistemic uncertainty of the model parameters and the aleatory randomness of the fatigue life are taken into account in the definition of the fatigue limit state function

5.2.3 Verification scheme 3: based on damage accumulation

The design equation, for the generic load case j , is formulated as follows:

$$G_j = d_{c,5} - \left\{ \int_{\frac{CAFL}{\gamma_{Mf}}}^{\infty} \frac{n_{tot_{c,j}} \cdot \frac{s \cdot \gamma_{Ff}}{2\lambda_R^2} \exp\left(-\frac{(s \cdot \gamma_{Ff})^2}{2\lambda_R^2}\right)}{\frac{z_j \cdot N_c(s)}{(\gamma_{Mf})^{-m_1}}} ds + \int_0^{\frac{CAFL}{\gamma_{Mf}}} \frac{n_{tot_{c,j}} \cdot \frac{s \cdot \gamma_{Ff}}{2\lambda_R^2} \exp\left(-\frac{(s \cdot \gamma_{Ff})^2}{2\lambda_R^2}\right)}{\frac{z_j \cdot N_c(s)}{(\gamma_{Mf})^{-m_2}}} ds \right\} \quad (5.22)$$

where z_j is the design factor, $d_{c,5}$ is the characteristic value of the critical damage, $n_{tot_{c,j}}$ is the characteristic value of the total number of cycles and λ_R is the scale parameter of the Rayleigh loading spectrum.

The geometrical interpretation of the resistance partial safety factor is illustrated in Figure 5.3. n_{tot} is modeled as a Gumbel random variable, $\mathcal{G}_3(10^8, \sigma_{\mathcal{G}_3})$, having a coefficient of variation $c_{v_{\mathcal{G}_3}}$.

In order to take into account both the effects of uncertainty on loading spectrum stress ranges and uncertainty on total number of cycles, 32 load cases are built by considering all possible combinations of the following values of λ_R and $c_{v_{\mathcal{G}_3}}$:

$$\lambda_R : \quad \zeta = (0.05, 0.08, 0.11, \dots, 0.25) \quad (5.23)$$

$$c_{v_{\mathcal{G}_3}} = (0.20, 0.27, 0.33, 0.40) \quad (5.24)$$

where ζ is the percentage of stress range cycles exceeding the characteristic value of the CAFL (see Figure 5.4). Rayleigh distribution was chosen to model the loading spectrum since this probability distribution provides a quite accurate characterization of the upper tail of the spectrum, with only one distribution parameter.

The optimal design, \hat{z}_j , for the load case j , is computed by solving the design Equation 5.22, $G_j = 0$, for assigned values of partial safety factors. The reliability index β_j is then computed by solving the following limit state equation^v:

$$g_j = D_c - \left\{ \int_{\exp(V)}^{\infty} \frac{n_{tot_j} \cdot \frac{s}{\lambda_R^2} \exp\left(-\frac{s^2}{2\lambda_R^2}\right)}{\hat{z}_j \cdot N(s)} ds + \int_0^{\exp(V)} \frac{n_{tot_j} \cdot \frac{s}{\lambda_R^2} \exp\left(-\frac{s^2}{2\lambda_R^2}\right)}{\hat{z}_j \cdot N_c(s)} ds \right\} \quad (5.25)$$

^vIt is noted that both the epistemic uncertainty of the model parameters and the aleatory randomness of the CAFL, of the fatigue life and of the critical damage sum, are taken into account in the definition of the fatigue limit state function

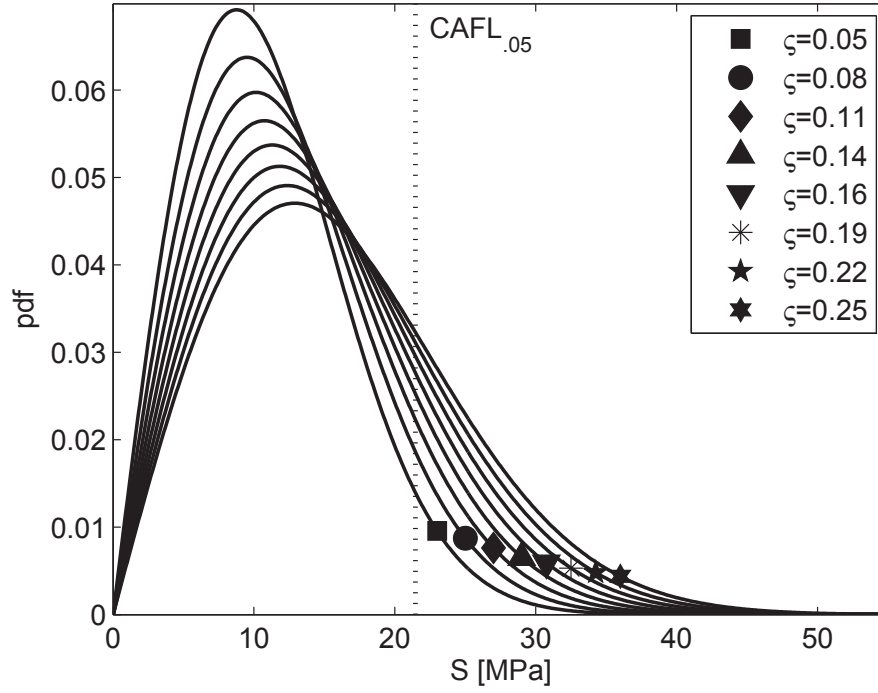


Figure 5.4: Rayleigh loading spectra, cover plate

Fatigue partial safety factors are calibrated by minimizing the following objective function:

$$W(\gamma) = \sum_{j=1}^{32} w_j \cdot (\beta_j(\gamma) - 3.00)^2 \quad (5.26)$$

where $w_j = 1$ for $j = 1, \dots, 32$, since all load cases have the same importance.

As for the previous two verification schemes, it is noted here that when γ_{Ff} and γ_{Mf} are determined with Equations 5.22, 5.25, and 5.26, they are not independent and only a combination of them is determined.

The framework presented in this Section was implemented in the Matlab Toolbox TB3 (see Appendix B). The Matlab Toolbox TB3 was validated using the structural reliability analysis software STRUREL [61].

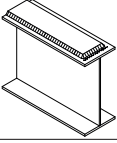
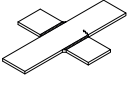
		
$Y V$	$\mathcal{N}(\mu_{Y V}, \exp(\sigma))$	$\mathcal{N}(\mu_{Y V}, \exp(\sigma))$
V	$\mathcal{N}(\mu_V, \exp(\sigma_V))$	$\mathcal{N}(\mu_V, \exp(\sigma_V))$
m_0	$\mathcal{N}(28.66, 2.85)$	$\mathcal{N}(25.77, 0.95)$
m_1	$\mathcal{N}(-3.42, 0.79)$	$\mathcal{N}(-2.67, 0.21)$
σ	$\mathcal{N}(-0.54, 0.20)$	$\mathcal{N}(-1.05, 0.14)$
μ_V	$\mathcal{N}(-3.45, 0.06)$	$\mathcal{N}(-3.86, 0.13)$
σ_V	$\mathcal{N}(-1.62, 0.41)$	$\mathcal{N}(-1.67, 0.50)$
Δm	6	5
D_c	$\log \mathcal{N}(0.27, 0.58)$	$\log \mathcal{N}(-0.31, 0.60)$
$d_{c,0.5}$	1.31	0.74
CAFL	21 MPa	30 MPa
a_{05}	27.58	25.14

Table 5.2: VA S-N model parameters

5.3 Study cases

The framework built in Section 5.2 was applied to the two fatigue sensitive details already studied in Chapters 2 and 3: 1) Welded cover plate; and 2) Welded in-plane gusset. The VA S-N stochastic model of the two considered details is given in Section 3.4.

The parameters of VA S-N curves are resumed in Table 5.2 for the convenience of the reader. It is recalled that the cover plate detail and the in-plane gusset detail were classified respectively as FAT45 and FAT50 in Eurocode 1993-1-9.

Verification scheme 1: based on CAFL

In Section 5.2.1 the procedure for calibrating fatigue partial safety factors for verification scheme 1 was presented. It was noted that only the product of $\gamma_{Mf} \cdot \gamma_{Ff}$ could be computed, since the resistance and load partial safety factors were not independent.

Moreover it is possible to set the load partial safety factor equal to 1.0 by proper choice of the return period of the characteristic value of the maximum stress range, $\rho_{S_{max}}$.

The resistance partial safety factor $\hat{\gamma}_{Mf}$ and the return period $\hat{\rho}_{S_{max}}$, corresponding to $\gamma_{Ff} = 1$, were computed using the following scheme:

1. The resistance partial safety factor $\hat{\gamma}_{Mf} = \gamma_{Mf}(\gamma_{Ff} = 1)$ was computed by minimizing the objective Equation 5.15, where the reliability indexes β_j were computed by setting $S_{max,j} = S_{max_c,j}$ in Equation 5.14;
2. The γ -characteristic return period plot (see Figure 5.5), which relates the product $\gamma_{Mf} \cdot \gamma_{Ff}$ to the return period of the characteristic value of the maximum stress range, $\rho_{S_{max}}$, was produced by minimizing the objective Equation 5.15, where the reliability indexes β_j were computed by considering $\rho_{S_{max}} = (250, 500, \dots, 2000)$ in Equation 5.14;
3. The return period $\hat{\rho}_{S_{max}}$ was computed by intersecting the γ -characteristic return period plot with the straight line $\gamma_{Ff} = 1$ (see again Figure 5.5).

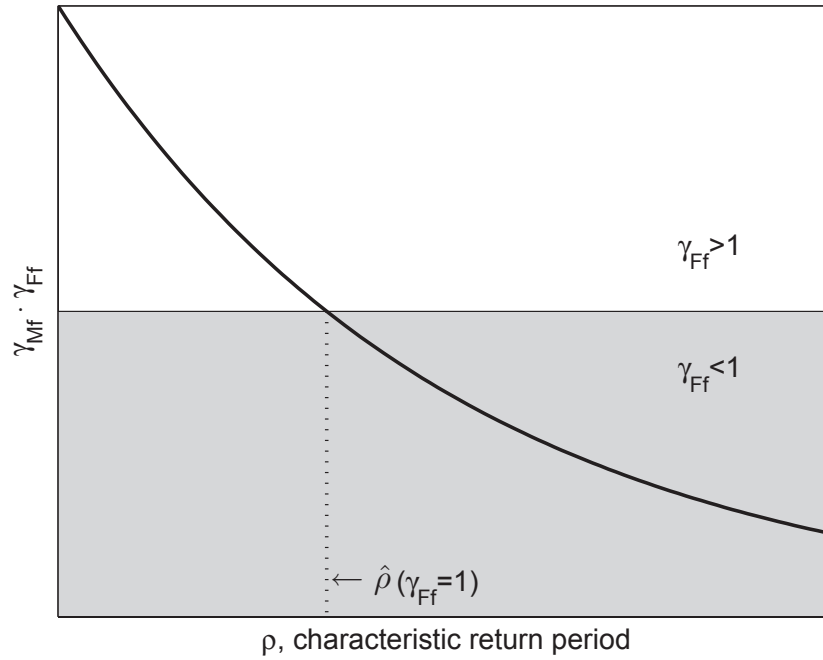


Figure 5.5: Illustration of γ – characteristic return period plot

Verification scheme 2: based on CA equivalent stress range

In Section 5.2.2 the procedure for calibrating fatigue partial safety factors for verification scheme 2 was presented. Also for this verification scheme, it was noted that only the product of $\gamma_{Mf} \cdot \gamma_{Ff}$ could be computed, since the resistance and loading safety factors were not independent.

Moreover, as for the verification scheme 1, a three step-scheme was set in order to compute the resistance partial safety factor $\hat{\gamma}_{Mf}$ and the return period $\hat{\rho}_{S_{E,2}}$, corresponding to $\gamma_{Ff} = 1$. The scheme is the same as the one used for the verification scheme 1, except for objective Equation 5.21 and limit state Equation 5.20 which were used in place of respectively objective Equation 5.15 and limit state Equation 5.14.

Verification scheme 3: based on damage accumulation

In Section 5.2.3 the procedure for calibrating fatigue partial safety factors for verification scheme 3 was presented. Also for this verification scheme, it was noted that only a combination of $\gamma_{Mf} \cdot \gamma_{Ff}$ could be computed, since the resistance and loading safety factors were not independent.

Moreover, as for the verification schemes 1 and 2, a three step-scheme was set in order to compute the resistance partial safety factor $\hat{\gamma}_{Mf}$ and the return period $\hat{\rho}_{S_{N_{tot}}}$, corresponding to $\gamma_{Ff} = 1$. The scheme is the same as the one used for the verification scheme 1, except for objective Equation 5.26 and limit state Equation 5.25 which were used in place of respectively objective Equation 5.15 and limit state Equation 5.14.

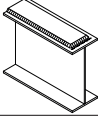
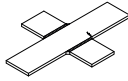
		
1	$S_{max} \leq \frac{CAFL}{\gamma_{Mf}}$ $\hat{\gamma}_{Mf} = 1.80$ $\hat{\rho}_{S_{max}} = 750 \text{ years}$	$S_{max} \leq \frac{CAFL}{\gamma_{Mf}}$ $\hat{\gamma}_{Mf} = 2.27$ $\hat{\rho}_{S_{max}} = 500 \text{ years}$
2	$S_{E,2} \leq \frac{S_c}{\gamma_{Mf}}$ $\hat{\gamma}_{Mf} = 1.33$ $\hat{\rho}_{S_{E,2}} = 750 \text{ years}$	$S_{E,2} \leq \frac{S_c}{\gamma_{Mf}}$ $\hat{\gamma}_{Mf} = 1.26$ $\hat{\rho}_{S_{E,2}} = 1000 \text{ years}$
3	$\sum_i^{n_{tot}} \frac{n_i}{N(\gamma_{Mf})} \leq 1.31$ $\hat{\gamma}_{Mf} = 1.37$ $\hat{\rho}_{n_{tot}} = 500 \text{ years}$	$\sum_i^{n_{tot}} \frac{n_i}{N(\gamma_{Mf})} \leq 0.74$ $\hat{\gamma}_{Mf} = 1.45$ $\hat{\rho}_{n_{tot}} = 500 \text{ years}$

Table 5.3: Resistance partial safety factors and related characteristic return periods ($\gamma_{Ff} = 1.0$)

5.4 Results

The resistance partial safety factor, $\hat{\gamma}_{Mf}$, and the characteristic return period, $\hat{\rho}$, which allow to set $\gamma_{Ff} = 1$, are shown in Table 5.3, for the three verification schemes.

An example of the graphical determination of the characteristic return period is given in Figure 5.6, for the cover plate, verification scheme 1. For each verification scheme, the fatigue verification criterion is also presented in Table 5.3. It has to be noted that for the verification scheme 3 (damage accumulation), the computed resistance partial safety factors refer to the characteristic VA S-N curve determined at $D_c = d_{c,.5} \neq 1$, and the critical damage used in the fatigue verification criterion is $d_{c,.5} \neq 1$. For this reason results for verification scheme 3 can not be directly compared to Eurocode standards, in which $d_{c,.5} = 1.0$.

In Table 5.4, results for verification schemes 1 and 2 are compared to Eurocode standards in terms of design value of CAFL and of design value of fatigue strength at $2 \cdot 10^6$ cycles. Since crack formation in the considered details could rapidly lead to structural failure, the case *Safe life, High consequences* is chosen in Table 3.1 of EN 1993-1-9 ($\gamma_{Mf} = 1.35$).

Results for verification scheme 3 are compared to Eurocode standards in terms of design VA S-N curves, in Figures 5.7 and 5.8. In order to make direct comparison with Eurocode design S-N curves, the ML-MCS design S-N curves were re-scaled at $d_{c,5} = 1.0$ (see Equation 3.10).

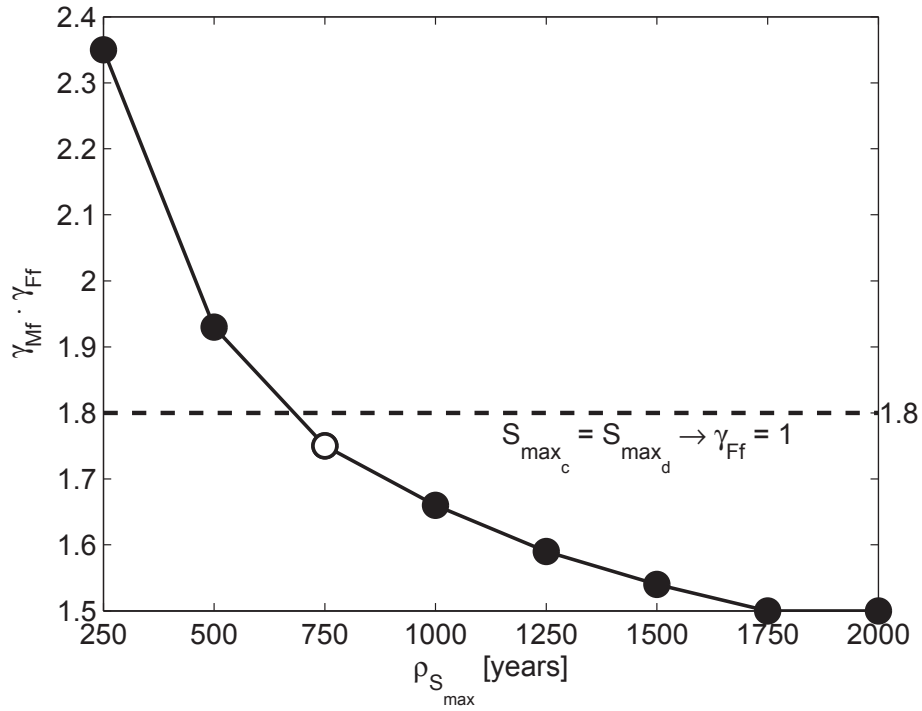


Figure 5.6: Return level plot, cover plate, verification scheme 1

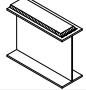
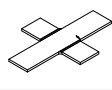
					
		ML-MCS	Eurocode	ML-MCS	Eurocode
1	CAFL [MPa]	21	33	31	29
	CAFL _d [MPa]	12	24	14	21
2	S _c [MPa]	46	45	53	40
	S _{c,d} [MPa]	35	33	42	30

Table 5.4: Comparison of design values for verification schemes 1 and 2

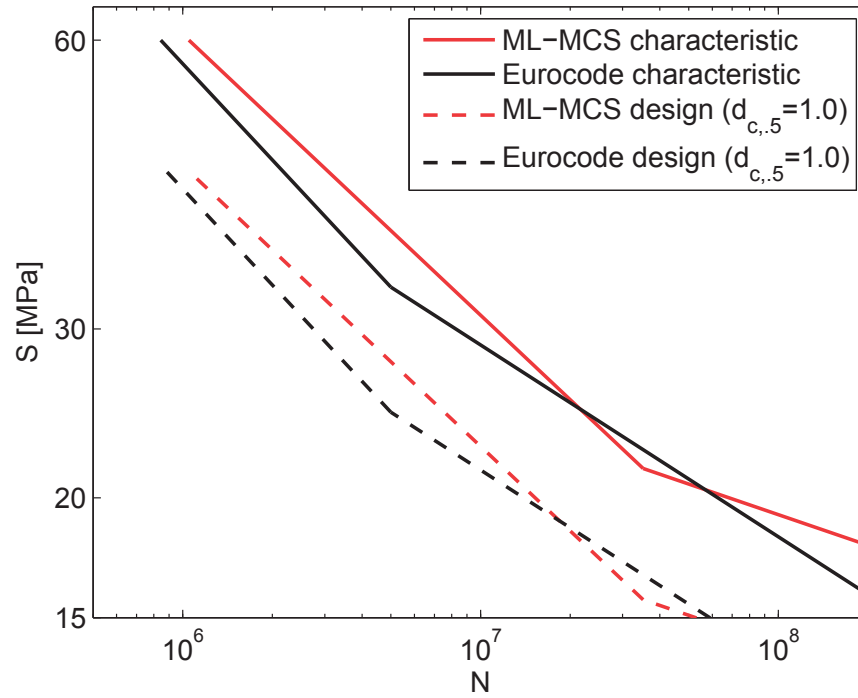


Figure 5.7: Comparison of VA design S-N curves for verification scheme 3, cover plate

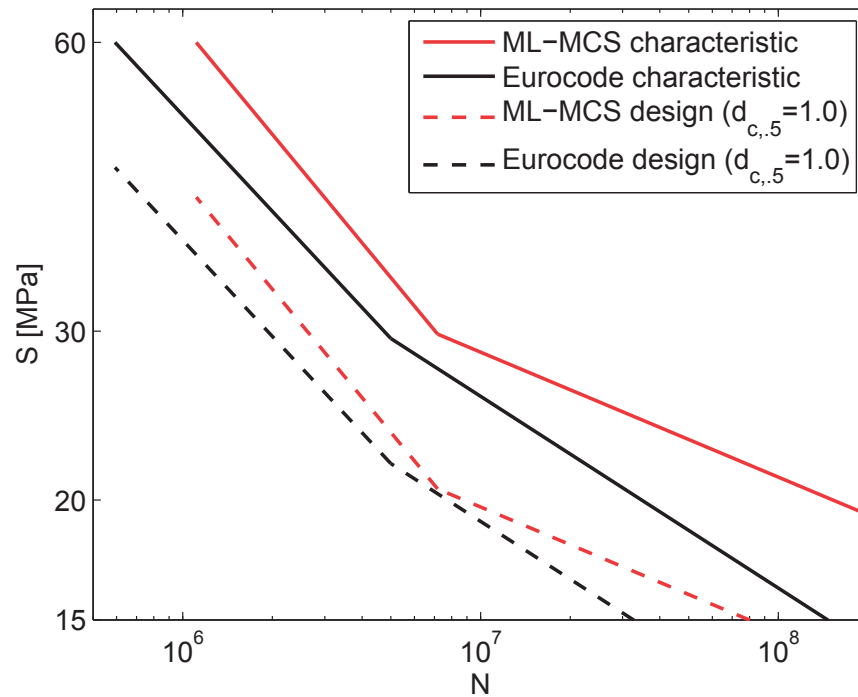


Figure 5.8: Comparison of VA design S-N curves for verification scheme 3, in-plane gusset

5.4.1 Example of fatigue design based on verification scheme 3

In this section a practical example of fatigue design of a road bridge using damage accumulation criterion (verification scheme 3) is given. This example allows to evaluate the impact of the choice of design S-N curves on the computed fatigue life.

The Venoge bridge, which was studied in Section 4.3, is considered again in this example.

Two critical details are considered:

1. Welded cover-plate, on the lower flange of the enlargement left bridge at the first mid-span;
2. In-plane welded gusset, on the lower flange of the enlargement left bridge at the first mid-span. This detail does not exist in reality and is considered for academic purpose only.

In order to define the stress range loading spectrum, a Rayleigh probability distribution is fitted to observed stress ranges at the critical section in the year 2006. The Rayleigh stress range spectrum, having scale parameter equal to 5.3, is shown in Figure 5.9 (a).

The design value of allowed number of cycles, n_d , is computed, for the two considered critical details, using following equation:

$$n_d = \frac{d_{c,.5}}{\int_0^\infty \frac{f_S(s)}{N(s)} ds} \quad (5.27)$$

where:

- $d_{c,.5}$ is the characteristic value of critical damage sum. When ML-MCS approach is used, $d_{c,.5}$ is equal to 1.31 for the cover plate detail and it is equal to 0.74 for the in-plane gusset detail; when Eurocode approach is used $d_{c,.5}$ is equal to 1.0 for both critical details;
- $f_S(s)$ is the Rayleigh loading stress range spectrum;
- $N(s)$ is the endurance obtained from the factored $\frac{S_c}{\gamma_{Mf}} - N$ curve. When ML-MCS approach is used γ_{Mf} is equal to 1.16 for the cover plate details and it is equal to 1.35 for the in-plane gusset detail (see Table 5.3); when Eurocode approach is used γ_{Mf} is equal to 1.35 for both critical details.

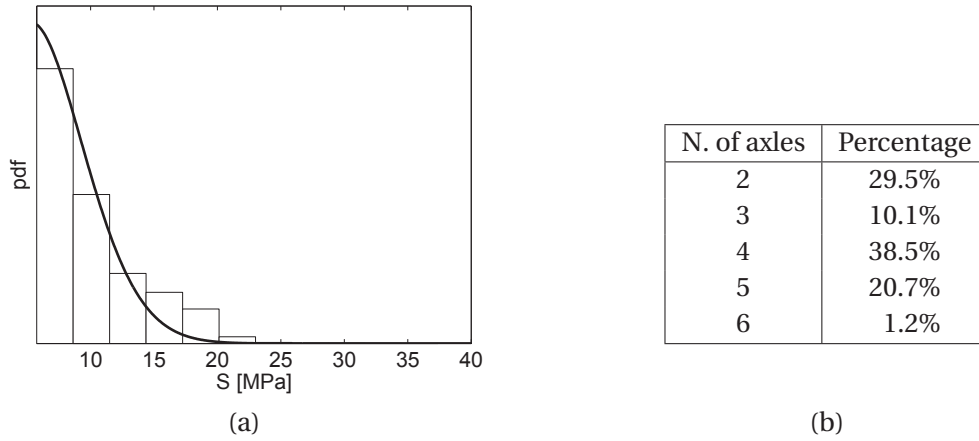


Figure 5.9: Loading model: (a) Stress range spectrum; (b) Traffic composition according to 2006 WIM measurements

The design value of allowed number of vehicles, n_{veh} , can be computed as follows:

$$n_{veh} = \frac{n_d}{\sum_{i=2}^6 i \cdot p_i} \quad (5.28)$$

where:

- i is the number of vehicle axles;
- p_i is the percentage of vehicles having i axles, according to Figure 5.9 (b).

The comparison between the ML-MCS-based design value of n_{veh} and the Eurocode-based design value of n_{veh} is presented in Figure 5.10 for the two considered details.

For the cover-plate detail the ML-MCS approach provides slightly higher estimate of design value of n_{veh} with respect to the Eurocode approach. However, both approaches predict a fatigue design life higher than 100 years, for a traffic volume, $n_{veh/year} \leq 2 \cdot 10^6$.

For the in-plane gusset detail the ML-MCS approach provides considerably lower estimate of design value of n_{veh} with respect to the Eurocode approach. Figure 5.11 shows the relationship between the design life in years and the number of crossing vehicles per year, $n_{veh/year}$, when the in-plane gusset is considered as the critical detail: it is noted that for $n_{veh/year} = 1.56 \cdot 10^6$, the Eurocode gives a design life equal to 100 years, which is about 60% of the design life predicted with ML-MCS approach. For $n_{veh/year} = 0.4 \cdot 10^6$ (which is the traffic volume measured by WIM on Venoge bridge in 2013, see Figure 4.6) the predicted design life increases from 390 years (Eurocode) to 710 years (ML-MCS).

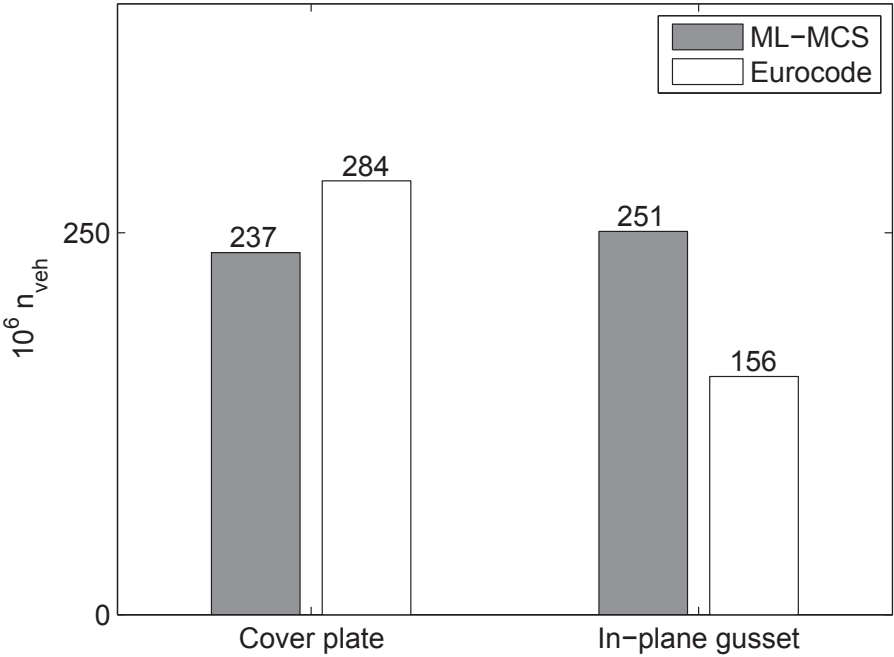


Figure 5.10: Comparison of design values of n_{veh} for verification scheme 3

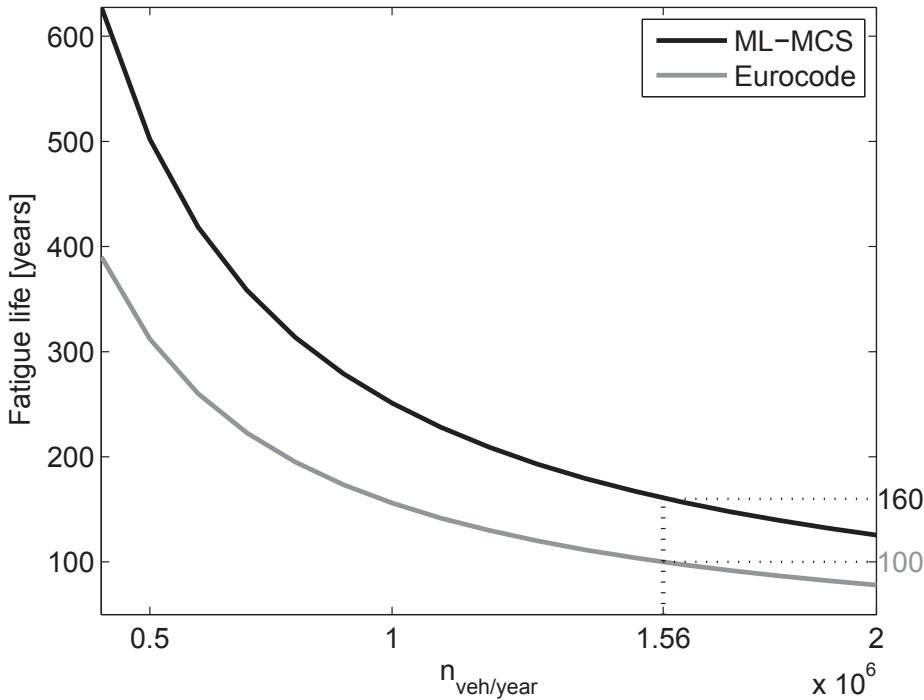


Figure 5.11: Relationship between design fatigue life and traffic volume, in-plane gusset

5.5 Conclusions and discussion

This Chapter presented a new framework for calibration of partial safety factors used in fatigue design of steel bridges.

The presented framework improves consistency in achieving target levels of safety by:

- Defining one different design equation for each of three design verification criteria proposed in Eurocode standards; this allows to distinguish three different resistance partial safety factors, γ_{Mf} , to be used in: 1) Fatigue design based on CAFL; 2) Fatigue design based on CA equivalent stress range at $2 \cdot 10^6$ cycles; and 3) Fatigue design based on accumulated damage;
- Defining a method to assess which is the characteristic return period of the load effect which allows to set $\gamma_{Ff} = 1.0$ in the design equation;
- Using ML-MCS-based S-N curves, which results in a more realistic consideration of the CAFL and of the fatigue strength in HCF region;
- Using ML-MCS-based VA S-N models, which results in a more realistic consideration of damage accumulation.

The study cases considered in this Chapter show that:

- Calibration of partial safety factors for verification scheme 1 (based on CAFL) gives higher values of $\hat{\gamma}_{Mf}$ with respect to the verification scheme 2 (based on equivalent stress range at $2 \cdot 10^6$ cycles), for both details (see Table 5.3). This is probably due to the higher fatigue life scatter in the HCF region with respect to the scatter in the finite life region;
- The $\hat{\gamma}_{Mf}$ for the verification scheme 1 is considerably higher for the in-plane gusset ($\hat{\gamma}_{Mf} = 2.27$) with respect to the cover plate ($\hat{\gamma}_{Mf} = 1.80$). This is probably due to the more dispersed CAFL distribution of the in-plane gusset detail with respect to the cover plate detail (see Figures 2.7 and 2.12);
- For all verification schemes the return period of characteristic load effect, $\hat{\rho}$, ranges between 500 and 1000 years (see Table 5.3);
- Eurocode standards give unsafe estimate of the design value of the CAFL, for both considered details (see Table 5.4). For the in-plane gusset detail this is due to the unsafe Eurocode-based calibration of resistance partial factor (see Tables 5.1 and 5.3), while

for the cover-plate gusset this is both due to the unsafe Eurocode-based calibration of resistance partial factor (see again Tables 5.1 and 5.3) as well as to the unsafe Eurocode-based estimate of the characteristic value of the CAFL (see Section 2.6);

- Eurocode standards and ML-MCS approach give similar values of $\hat{\gamma}_{Mf}$ for the verification scheme 2 (see Tables 5.1 and 5.3). The considerable difference on the design fatigue strength at $2 \cdot 10^6$ cycles (see Table 5.4), for the in-plane gusset detail, is due to the over-conservative Eurocode-based estimate of the characteristic fatigue strength (see Section 2.6);
- Figure 5.7 shows that the Eurocode-based VA design S-N curve of the cover-plate detail is over-conservative with respect to the ML-MCS-based S-N curve for stress ranges higher than 19MPa, while it becomes slightly under-conservative for stress ranges lower than 19MPa. Figure 5.8 shows that the Eurocode-based VA design S-N curve of the in-plane gusset detail is over-conservative with respect to the ML-MCS based S-N curve, at all stress ranges.

It is noted that the verification scheme 1 is the first mandatory step to carry out in fatigue design of new bridges (see Figure 5.12): considered study cases show that verification scheme 1 including Eurocode-based design value of CAFL is highly un-safe.

In order to show the impact of the choice of design S-N curves on the fatigue design of a road bridge, fatigue life was computed for the Venoge bridge, by considering both Eurocode-based design S-N curves and ML-MCS-based design S-N curves. Results show that, for the critical in-plane gusset detail, Eurocode standards give a prediction of the allowed number of crossing vehicles ($156 \cdot 10^6$) which is considerably lower than the value predicted by the ML-MCS approach ($251 \cdot 10^6$). For a traffic volume of $\approx 1.5 \cdot 10^6$ heavy vehicles per year, the design life increases from 100 years (Eurocode) to 160 years (ML-MCS).

The reliability framework for calibration of fatigue partial safety factors, set up in this paper and applied to two fatigue-sensitive details, constitutes a powerful tool that can be used to revise the Eurocode basis for fatigue design of structures. The three Eurocode formats for fatigue design and associated partial safety factors can be revised by considering different fatigue sensitive details and by further differentiating between: 1) Verification based on CAFL exceedance; 2) Verification based on equivalent stress range at $2 \cdot 10^6$ cycles, using lambda factors; and 3) Verification based on damage accumulation.

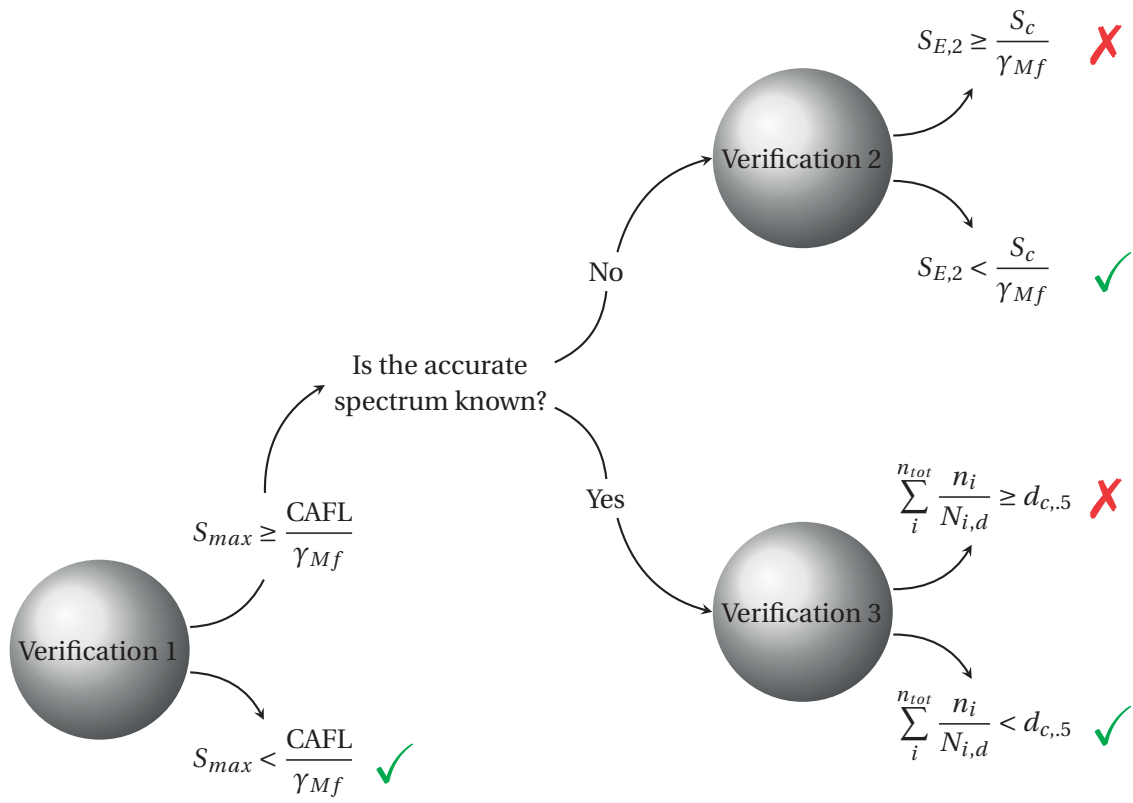


Figure 5.12: Fatigue design verification chart

6 Conclusions

The main target of this thesis is to provide a rigorous and reliable probabilistic approach for estimation of CA and VA fatigue S-N curves of welded joints.

A new method for estimation of CA S-N curves is provided, which gives more insight into realistic estimation of the CAFL and of the knee point. The novel idea of using MCS method for computing p quantiles of fatigue life provides characteristic S-N curves which give more reliable estimation of the fatigue life scatter in the HCF region with respect to existing standards. The re-definition of the CAFL and of the knee point in current standards is of primary importance since today, among in-service road steel bridges in Europe, there is a considerable amount of aged structures which operate in HCF region.

A new method is also provided for re-definition of m_2 and D_c variables in Miner's rule. The novel idea of re-simulating VA fatigue experimental tests and of using ML method to estimate the VA S-N stochastic model parameters gives experimental support to the choice of m_2 and D_c and allows to verify the conventional assumptions on Miner's rule variables which are made in current standards.

The ML-MCS approach for estimation of CA and VA S-N curves was integrated in the new reliability analysis framework for fatigue assessment of existing bridges. In the new framework the probability of fatigue failure is defined by taking into account both damage accumulation and CAFL exceedance critical events. The re-definition of the fatigue limit state function and the use of ML-MCS based S-N curves improves the confidence in computed fatigue reliability indexes.

The ML-MCS probabilistic approach for estimation of S-N curves was also integrated in the new framework for re-calibration of fatigue design partial safety factors. The new framework allows for re-visiting the Eurocode basis for fatigue design of new bridges and for re-calibrating the related partial safety factors, by further differentiating between the three design formats:

1) Based on CAFL; 2) Based on equivalent stress range at $2 \cdot 10^6$ cycles; 3) Based on damage accumulation.

6.1 General conclusions

In accordance with the objectives stated in Section 1.3, the main conclusions of this thesis are summarized as follows:

- The ML-MCS approach proposed in this thesis for estimation of CA S-N curves constitutes a powerful tool for re-definition of standard CA S-N curves of welded joints. Use of ML method allows to use run-out data for estimation of S-N curves. The novel idea of using MCS technique to estimate true p -quantiles of fatigue life gives more insight into realistic estimation of CAFL and knee point position.

According to considered study cases, arbitrarily fixing the CAFL at fixed number of cycles lead to an un-safe assumption which could be extremely dangerous for fatigue verifications based on CAFL.

It is recalled that the effectiveness of the proposed ML-MCS approach is conditioned to the use of experimental CA data-sets which have significant information in the HCF region. This issue is addressed in Section 6.2;

- The ML-MCS approach proposed in this thesis for estimation of VA S-N models constitutes a powerful tool for re-defining the second slope of S-N curves, m_2 , as well as the critical value of the damage sum used in Miner's rule, D_c . The novel idea of re-simulating experimental VA fatigue tests and to estimate m_2 and D_c with ML method allows to: 1) Give experimental support to the amount of the reduction of S-N curve slope, $\Delta m = m_1 - m_2$; 2) Give experimental support to the choice of probability distribution of D_c .

The considered study cases show that the ML-MCS approach gives the most realistic estimation of failure damage sum with respect to existing standards.

It is also noted that there is strong influence of load sequence on D_c probability distribution; it follows that realistic load histories should be used for producing VA experimental results, when the proposed ML-MCS approach is used for re-definition of m_2 and D_c in current standards;

- The reliability analysis framework set up in this thesis allows for performing fatigue reliability assessment of existing road steel bridges using WIM-based characterization of traffic load history. Use of ML-MCS-based S-N curves improves the confidence in fatigue reliability analysis. The novel contribution of the proposed framework consists

in computing the failure probability as joint probability of: 1) The CAFL exceedance event; and 2) The critical damage accumulation event.

The considered Venoge bridge study case shows the inaccuracy of Eurocode approach in assessment of reliability index during the 100 year-design life of the bridge. Additional study with consideration of two virtual traffic evolution scenarios reveals the importance of the choice of target reliability indexes, which can lead to a shift of the inspection delay of several years;

- The new framework set up in this thesis for calibration of fatigue partial safety factors allows for revising the Eurocode basis for fatigue design of new bridges. Use of ML-MCS-based VA S-N models gives more insights into realistic consideration of fatigue strength in HCF region as well as damage accumulation mechanism. New method is proposed to define the characteristic return period of load effect which allows to set the load partial factor, γ_{Ff} equal to unity in the design equation. Revision of resistance partial safety factor, γ_{Mf} , can be performed by differentiating between three verification schemes: 1) Based on CAFL exceedance; 2) Based on equivalent stress range at $2 \cdot 10^6$ cycles, using lambda factors; and 3) Based on damage accumulation.

Considered study cases do not support the Eurocode assumption of considering the same γ_{Mf} for all three verification schemes. Eurocode standards give highly unsafe estimate of design CAFL, for both study cases: fatigue design based on verification scheme 1, using Eurocode-based γ_{Mf} , could be highly dangerous.

It is recalled here that the verification scheme 1 is the first mandatory step in fatigue design of new bridges, which can be followed by schemes 2 or 3 according to the choice of the engineer (see Figure 5.12).

More detailed discussion on specific results of each Chapter as well as numerical results of considered study cases are presented at the end of each Chapter.

6.2 Future works

The results of this thesis provide a strong foundation for future work in fatigue verification of road steel bridges. The thesis has shown that there is a need of more CA and VA fatigue experimental results in the HCF region. Four areas of future work have been identified as follows:

- Re-definition of CA S-N curves in Eurocode standards;
- Re-definition of Miner's rule in Eurocode standards;

Chapter 6. Conclusions

- Revision of Eurocode formats for fatigue design and re-calibration of associated partial safety factors;
- Inclusion of the bi-linear CA S-N model without CAFL into the ML-MCS approach.

The following Section proposes future work in these four areas.

Re-definition of CA S-N curves in Eurocode standards

In order to re-define CA S-N curves of welded joints in Eurocode standards, a fatigue test program should be carried out according to following steps:

1. Choice of details to include in the re-definition of Eurocode standards (i.e. longitudinal attachment, transversal attachment, cover plate, T-joint, ...);
2. CA fatigue testing of selected details. It is recommended to use stress ranges varying from $1.5 \cdot \text{FAT}_{\text{EN}}$ to $0.5 \cdot \text{CAFL}_{\text{EN}}$, where FAT_{EN} and CAFL_{EN} are respectively the FAT and the CAFL of tested details, according to EN 1993-1-9. A minimum number of three data points is required for each stress range level. Experimental tests in which $N = 10^8$ will be reached without failure will be classified as run-outs. Use of the scheme recommended above will ensure to have significant CA experimental results in the HCF region;
3. Estimation of CA S-N stochastic models as well as characteristic S-N curves of considered details, using ML-MCS approach. Matlab Toolbox TB1 (see Appendix B) should be used.

Re-definition of Miner's rule in Eurocode standards

Once the CA S-N stochastic model has been estimated for the selected details, a VA fatigue test program needs to be carried out in order to re-define S-N curve second slope, m_2 , and critical damage, D_c . Following steps should be followed:

1. VA fatigue testing of selected details. Due to the strong influence of load history on the critical damage sum D_c , it is recommended to use realistic loading spectra for VA tests; one possibility would be to repeatedly apply real road bridge recorded load histories to the tested specimens.

It is recommended to use a number of cycles, \tilde{n}_{tot} , for each loading spectrum, such that:

$$\int_{\exp(\hat{\mu}_V)}^{s_{max}} \frac{\tilde{n}_{tot} \cdot \tilde{f}_S(s)}{N(s)} ds \leq 3.0 \quad (6.1)$$

where $\tilde{f}_S(s)$ is the loading spectrum, s_{max} is the maximum stress range of the loading spectrum, $\hat{\mu}_V$ is the ML estimate of median value of log-CAFL and $N(s)$ is the number of cycles to failure according to median CA S-N curveⁱ. Experimental tests in which n_{tot} will be reached without failure will be classified as run-outs. Use of the scheme recommended above will ensure to have significant VA experimental results in the HCF region.

It is recommended to use stress range loading spectra which have ζ varying from 0.5 to 0.05, where ζ is the percentage of stress range cycles exceeding the characteristic value of the ML-MCS based CAFL. A minimum number of five different load spectra should be used and a minimum number of three data points is required for each stress range loading spectrum;

2. Estimation of VA S-N stochastic models of considered details, which include $m_2 = (m_1 - \Delta m)$ and D_c , using ML-MCS approach. Matlab Toolbox TB1 (see Appendix B) should be used.

Revision of Eurocode formats for fatigue design and re-calibration of associated partial safety factors

Once the CA and VA S-N stochastic models of selected details have been estimated, the three Eurocode formats for fatigue design can be revised using the framework developed in Chapter 5. Matlab Toolbox TB3 (see Appendix B) should be used to re-calibrate partial resistance factors associated to the three verification formats.

A further improvement may be introduced in the developed framework, by considering realistic loading spectra instead of simple Rayleigh loading spectra.

Inclusion of the bi-linear CA S-N model without CAFL into the ML-MCS approach

The ML-MCS approach presented in this work is based on linear CA S-N curve having random CAFL. The existence of CAFL is still a topic for debate; Sonsino [68] suggests that CAFL does

ⁱAccording to results presented in Chapter 3, $d_c = 3.0$ is higher than the 0.9 quantile of D_c distribution for both cover-plate and in-plane gusset study cases: the choice of $d_c = 3.0$ in Equation 6.1 will then ensure to have a significant run-out if the experimental test ends without a failure after \tilde{n}_{tot} cycles

Chapter 6. Conclusions

not exist and that stress range cycles below the knee point should be accounted with a slope $m'_1 = -22$. The knee point is arbitrarily fixed at 10^7 cycles; due to the lack of experimental results in the HCF region, $m'_1 = -22$ is arbitrarily chosen in order to have a 10% constant stress range decrease with respect to the $\log(N)$ axis. The ML-MCS approach presented in this thesis can be adapted to a bi-linear S-N model having a slope $m'_1 = -22$ for stress range cycles below the knee point.

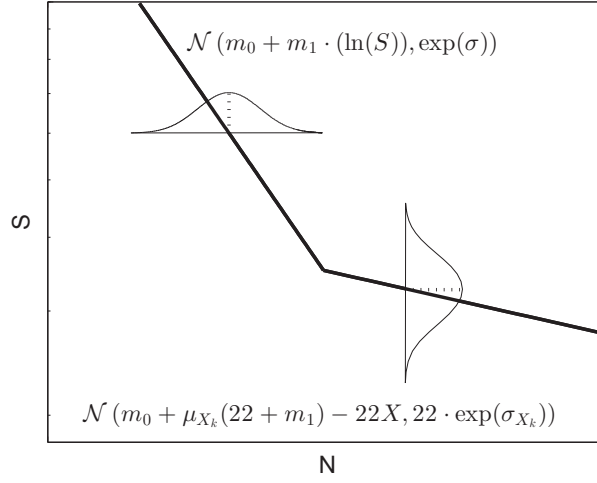


Figure 6.1: Bi-linear S-N curve without CAFL

The bi-linear model should be defined as follows:

$$Y = \begin{cases} m_0 + m_1 X + \epsilon(0, \exp(\sigma)), & \text{for } X > X_k \\ m_0 + \mu_{X_k}(22 + m_1) - 22X + \epsilon(0, 22 \cdot \exp(\sigma_{X_k})), & \text{for } X \leq X_k \end{cases} \quad (6.2)$$

where μ_K and $\exp(\sigma_K)$ are respectively the location and the scale parameters of the X_k random variable, which represents the natural logarithm of the stress range at the knee point (see Figure 6.1).

Thereafter, the model parameter vector, $\underline{\theta}$, relative to the S-N model with random CAFL, should be transformed as follows:

$$\underline{\theta} = (m_0, m_1, \sigma, \mu_V, \sigma_V) \rightarrow \underline{\theta} = (m_0, m_1, \sigma, \mu_{X_k}, \sigma_{X_k}) \quad (6.3)$$

As for the case of the S-N model with CAFL, the ML-MCS approach has the advantage of estimating the knee point instead of arbitrarily assuming its position.

Future work is required for: 1) Implementing the CA bi-linear S-N model into the ML-MCS approach; and 2) Validating it with experimental data-sets which contain significant information in the HCF region.

A Confidence and prediction bounds for fatigue S-N curves

A.1 Confidence intervals

In parameter inference, an interval estimator is a rule which specifies the method that we have to use to compute the bounds of the interval which will contain the target parameter. Ideally, the interval will have two properties: 1) It will contain the target parameter, θ ; 2) It will be relatively narrow. The bounds of the interval are computed from the sample measurements and will vary randomly from sample to sample; hence, the location and the length of the interval is a random quantity and we can not be certain that the target parameter, θ , will fall into the interval computed from one single sample. Interval estimators are commonly called *confidence intervals*; the probability that that θ will fall into a random confidence interval is called *confidence level*. The confidence level gives the fraction of time, in repeated sampling, that the computed confidence intervals will contain θ .

Let θ_l and θ_u denote the random lower and upper confidence interval bounds, respectively for the parameter, θ .

Then, if:

$$P(\theta_l \leq \theta \leq \theta_u) = 1 - \alpha \quad (\text{A.1})$$

the probability $(1 - \alpha)$ is the confidence level associated with the confidence interval $[\theta_l, \theta_u]$.

A.2 Large sample confidence intervals

A.2.1 Confidence interval for the mean

Let (Y_1, \dots, Y_n) be a random sample of size n from a normal distributions with mean, μ and standard deviation, σ .

Then the sample mean:

$$\bar{Y} = \frac{1}{n} \sum_{i=1}^n Y_i \quad (\text{A.2})$$

is normally distributed with mean, $\mu_{\bar{Y}}$ and standard deviation, $\sigma_{\bar{Y}} = \sigma / \sqrt{n}$.

Then the random variable:

$$Z = \frac{\bar{Y} - \mu_{\bar{Y}}}{\sigma_{\bar{Y}}} = \frac{\bar{Y} - \mu}{\sigma / \sqrt{n}} \quad (\text{A.3})$$

has a standardized normal distribution, with:

$$P\left(\bar{Y} + z_{\frac{\alpha}{2}} \frac{\sigma}{\sqrt{n}} \leq \mu \leq \bar{Y} + z_{\frac{1-\alpha}{2}} \frac{\sigma}{\sqrt{n}}\right) = 1 - \alpha \quad (\text{A.4})$$

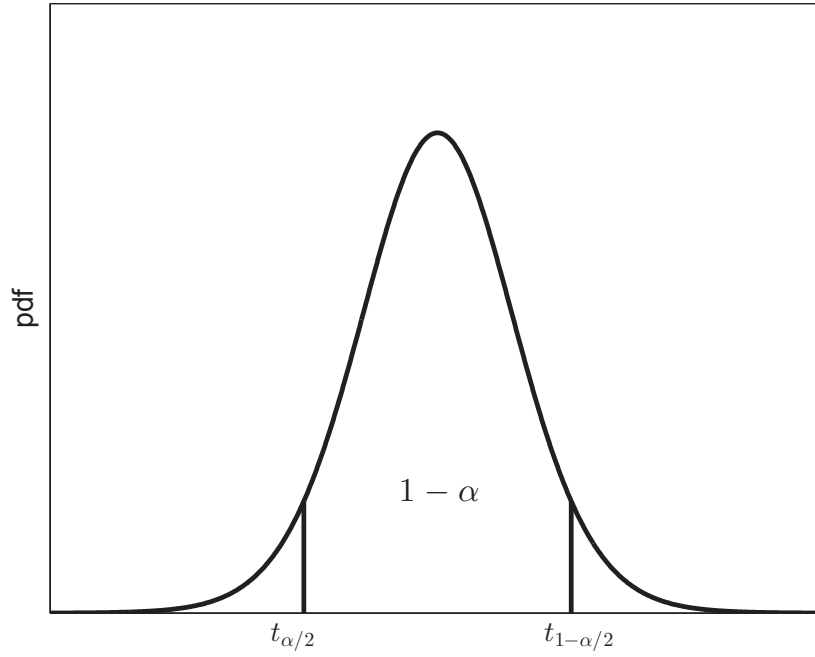


Figure A.1: Student's T probability density function

The $(1 - \alpha) \cdot 100\%$ confidence interval for μ is:

$$\left(\bar{Y} + z_{\frac{\alpha}{2}} \frac{\sigma}{\sqrt{n}}, \bar{Y} + z_{\frac{1-\alpha}{2}} \frac{\sigma}{\sqrt{n}} \right) \quad (\text{A.5})$$

If the parameter σ is unknown we can substitute σ for the sample standard deviation, $\hat{\sigma}$:

$$\hat{\sigma} = \frac{1}{n-1} \sum_{i=1}^n (Y_i - \bar{Y})^2 \quad (\text{A.6})$$

In this case the random variable:

$$T = \frac{\bar{Y} - \mu}{\hat{\sigma} / \sqrt{n}} \quad (\text{A.7})$$

has a Student's T distribution (see Figure A.1) with n degrees of freedom and the $(1 - \alpha) \cdot 100\%$ confidence interval for μ is:

$$\left(\bar{Y} + t_{\frac{\alpha}{2}} \frac{\hat{\sigma}}{\sqrt{n}}, \bar{Y} + t_{\frac{1-\alpha}{2}} \frac{\hat{\sigma}}{\sqrt{n}} \right) \quad (\text{A.8})$$

A.2.2 Confidence interval for the standard deviation

Let (Y_1, \dots, Y_n) be a random sample of size n from a normal distribution with mean, μ , and standard deviation, σ .

Then the random variable:

$$\frac{(n-1)\hat{\sigma}^2}{\sigma^2} = \frac{1}{\sigma^2} \sum_{i=1}^n (Y_i - \bar{Y})^2 \quad (\text{A.9})$$

has a Chi-squared distribution with $n - 1$ degrees of freedom (see Figure A.2). The $(1 - \alpha)100\%$ confidence interval for σ is:

$$\left(\frac{(n-1)\hat{\sigma}^2}{\chi_{1-\frac{\alpha}{2}, n-1}^2}, \frac{(n-1)\hat{\sigma}^2}{\chi_{\frac{\alpha}{2}, n-1}^2} \right) \quad (\text{A.10})$$

The central limit theorem

The results given in Section A.2 are valid if (Y_1, \dots, Y_n) is a random sample of size n from a Normal distribution; what happens if random variables (Y_1, \dots, Y_n) are not normally distributed? We can invoke the *central limit theorem* (see [77], p. 370). Let (Y_1, \dots, Y_n) be independent and identically distributed random variables, with $E(Y_i) = \mu$, and $\text{Var}(Y_i) = \sigma^2$.

If we define the random variable:

$$Y^* = \frac{\bar{Y} - \mu}{\frac{\sigma}{\sqrt{n}}} \quad (\text{A.11})$$

the distribution function of Y^* converges to the standard Normal distribution as $n \rightarrow \infty$ (usually $n > 30$ is accepted). In that case results shown in Section A.2 remain valid.

A.3 Confidence intervals of S-N curves - IIW approach

S-N curves are estimated using experimental results from CA fatigue experimental tests. Each experimental test is represented by a couple $(x_i = \ln(S_i), y_i = \ln(N_i))$, where S_i is the nominal applied stress range and N_i is the number of cycles until the failure (or run-out if the test has been stopped without failure). Within the assumption that the logarithm of number of cycles $Y(X)$ is a Normal random variable, then each experimental result $y_i(x_i)$ can be seen as a realization of the Normal random variable $Y(X)$.

The information contained in the experimental dataset can be used to make inferences about the random variable $Y(X)$ from which the sample is taken. The Normal random variable $Y(X)$ is defined by the location parameter, μ_Y , and by the scale parameter, σ_Y .

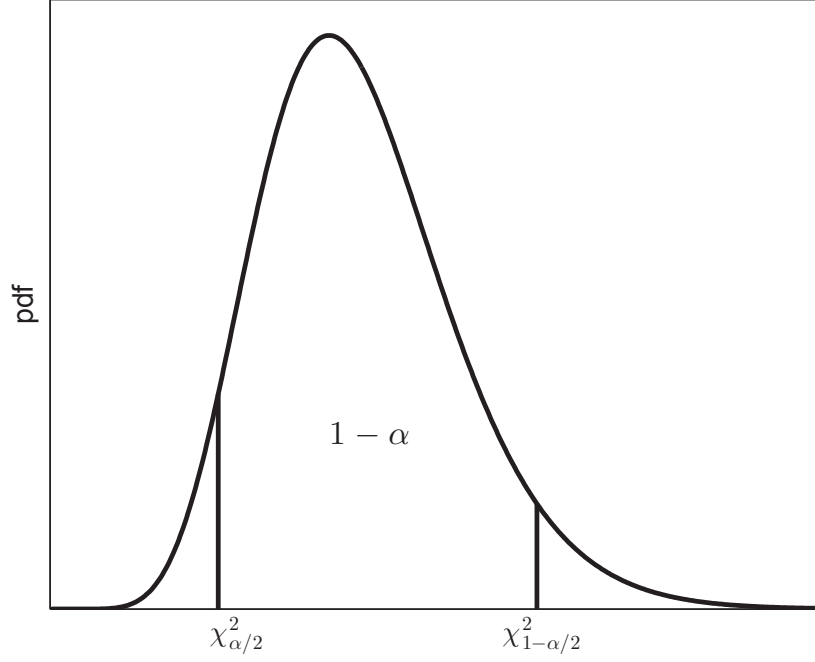


Figure A.2: Chi-squared probability density function

According to IIW recommendations [40] the linear model:

$$Y(x) = m_0 + m_1 x + \varepsilon(0, \sigma) \quad (\text{A.12})$$

represents the response function traced by Y over the experimental region of interest.

The sample mean:

$$\hat{y}(x) = \hat{m}_0 + \hat{m}_1 x \quad (\text{A.13})$$

is a point estimator of $\mu_Y(x)$ and can be computed using a least-squares (LS) approach: the sum of differences between the observed y_i and the predicted $(\hat{m}_0 + \hat{m}_1 x_i)$ is minimized. Only the failure points are considered.

The LS unbiased estimators of model parameters are:

$$\hat{m}_1 = \frac{n \cdot \sum_{i=1}^n (x_i \cdot y_i) - \sum_{i=1}^n x_i \cdot \sum_{i=1}^n y_i}{n \cdot \sum_{i=1}^n (x_i)^2 - \left(\sum_{i=1}^n x_i \right)^2} \quad (\text{A.14})$$

$$\hat{m}_0 = \bar{y} - \hat{m}_1 \bar{x} \quad (\text{A.15})$$

Appendix A. Confidence and prediction bounds for fatigue S-N curves

The sample standard deviation:

$$\hat{\sigma} = \sqrt{\frac{1}{n-2} \sum_{i=1}^n (y_i - \hat{y}(x_i))^2} \quad (\text{A.16})$$

is an unbiased point estimator of σ_Y and is independent of both \hat{m}_0 and \hat{m}_1 , under the assumption of normality of error term, $\varepsilon(0, \sigma)$ (see p.582 in [77]).

As shown in Section A.2.1, the 75% two-side confidence interval for $\mu_Y(x)$ is:

$$\left(\hat{y}(x) + t_{.125, n-2} \frac{\hat{\sigma}}{\sqrt{n}}, \hat{y}(x) + t_{.875, n-2} \frac{\hat{\sigma}}{\sqrt{n}} \right) \quad (\text{A.17})$$

Note that Student's T distribution with $n-2$ degrees of freedom is used since the mean function is defined using two independent parameters, m_0 , and m_1 .

As shown in Section A.2.1, the 75% two-side confidence interval for σ_Y^2 is:

$$\left(\frac{(n-2)\hat{\sigma}^2}{\chi_{.875, n-2}^2}, \frac{(n-2)\hat{\sigma}^2}{\chi_{.125, n-2}^2} \right) \quad (\text{A.18})$$

Note that the Chi-squared distribution with $n-2$ degrees of freedom is used.

According to IIW recommendations the characteristic S-N curve is obtained by translating the median S-N curve (coincident with mean S-N curve) at the .05 quantile of the $Y(x)$ Normal distribution, by using the lower bound of the 75% two-side confidence interval of $\mu_Y(x)$ and the upper bound of the 75% two-side confidence interval of σ_Y .

The equation of the characteristic S-N curve is then:

$$y = \hat{m}_0 + \left(\frac{t_{.125, n-2}}{\sqrt{n}} + -1.645 \sqrt{\frac{n-2}{\chi_{.125, n-2}^2}} \right) \cdot \hat{\sigma} + \hat{m}_1 x \quad (\text{A.19})$$

The issue of the estimation of the CAFL position is not addressed.

A.4 Prediction intervals

Let's consider the linear model expressed by the Equation A.12. In the previous section we discussed the method to estimate confidence intervals for μ_Y and σ_Y .

Now we discuss a different problem: the distribution of the random variable $Y(x) = \mathcal{N}(m_0 + m_1 x, \sigma)$ being known, we want to predict the particular response $Y(x)$ that we will observe if the experiment is run at some time in the future; we are interested in predicting the value of Y when $x = x^*$, called Y^* . It is possible to show (proof is omitted in this document) that the interval:

$$\left(\hat{m}_0 + \hat{m}_1 x^* + t_{\frac{\alpha}{2}, n-2} \hat{\sigma} \cdot \sqrt{1 + \frac{1}{n} + \frac{(x^* - \bar{x})^2}{\sum_{i=1}^n (x_i - \bar{x})^2}}, \hat{m}_0 + \hat{m}_1 x^* + t_{\frac{1-\alpha}{2}, n-2} \hat{\sigma} \cdot \sqrt{1 + \frac{1}{n} + \frac{(x^* - \bar{x})^2}{\sum_{i=1}^n (x_i - \bar{x})^2}} \right) \quad (\text{A.20})$$

in repeated sampling will contain the actual value of Y^* with probability $1 - \alpha$. Equation A.20 represents a $100 \cdot (1 - \alpha)\%$ hyperbolic prediction interval for Y^* .

A.5 Prediction intervals of S-N curves - Eurocode approach

Statistical method for assessment of mean S-N curve, that is discussed in section A.3, is used again in Commentary to Eurocode 3 document [29].

The characteristic S-N curve is then obtained by translating the median S-N curve at the 5% lower hyperbolic prediction bound of Y , in correspondence of $N = 2 \cdot 10^6$ cycles:

$$\hat{m}_0 + \hat{m}_1 x_{c_{LS}} + t_{.05, n-2} \cdot \hat{\sigma} \cdot \sqrt{1 + \frac{1}{n} + \frac{(x_{c_{LS}} - \bar{x})^2}{\sum_{i=1}^n (x_i - \bar{x})^2}} \quad (\text{A.21})$$

where $x_{c_{LS}}$ is the LS estimate of log-strength at $2 \cdot 10^6$ cycles.

The equation of the characteristic S-N curve is then:

$$y = \hat{m}_0 + t_{.05, n-2} \cdot \hat{\sigma} \cdot \sqrt{1 + \frac{1}{n} + \frac{(x_{c_{LS}} - \bar{x})^2}{\sum_{i=1}^n (x_i - \bar{x})^2}} + \hat{m}_1 x \quad (\text{A.22})$$

A.6 Discussion

Two different statistical methods for assessment of characteristic S-N curves are recommended from IIW and Eurocode. According to the Commentary to Eurocode 3 Part 1-9, the characteristic S-N curve is obtained by translating the median S-N curve at the .05 lower hyperbolic prediction bound of Y , in correspondence of $N = 2 \cdot 10^6$ cycles; instead according to IIW recommendations the characteristic S-N curve is obtained by translating the median S-N curve at .05 quantile of the $Y(x)$ Normal distribution, by using the lower bound of the 75% confidence interval of $\mu_Y(x)$ and the upper bound of the 75% confidence interval of σ_Y .

If we compare characteristic values $Y_{c,IIW}$ and $Y_{c,EN3}$ at a reference log-stress range, x^* , we have:

- $Y_{c,IIW}$ is the .05 quantile of the Normal distribution $\tilde{Y}(x^*)$ with parameters $\mu_{Y,l}$ and $\sigma_{Y,u}$, where $\mu_{Y,l}$ is the lower bound of the 75% confidence interval for μ_Y (that is the interval which in repeated sampling will contain the actual value of μ_Y with probability 75%) and $\sigma_{Y,u}$ is the upper bound of the 75% confidence interval for σ_Y (that is the interval which in repeated sampling will contain the actual value of σ_Y with probability equal to 75%);
- $Y_{c,EN3}$ is the lower bound of the 95% prediction interval for $Y(x^*)$; it represents the lower bound of the interval that will contain the value $Y(x^*)$ with probability equal to 95%, if the experiment at $x = x^*$ is run at some time in the future.

Following numerical example shows the difference between the IIW-based statistical approach and the Eurocode-based statistical approach in estimation of the characteristic strength at $2 \cdot 10^6$ cycles.

S [MPa]	N [MPa]	$x = \log(S)$	$y = \log(N)$	$x \cdot y$	x^2	y^2	$(x - \bar{x})^2$
108	1077000	2.0334	6.0322	12.2661	4.1348	36.388	0.0486
108	800000	2.0334	5.9031	12.0035	4.1348	34.8465	0.0486
139	597000	2.1430	5.7760	12.3780	4.5925	33.3619	0.0123
139	537000	2.1430	5.7300	12.2794	4.5925	32.8326	0.0123
202	204000	2.3054	5.3096	12.2406	5.3146	28.1922	0.0027
202	188000	2.3054	5.2742	12.1588	5.3146	27.8167	0.0027
202	107000	2.3054	5.0294	11.5945	5.3146	25.2947	0.0027
265	79000	2.4232	4.8976	11.8682	5.8721	23.9868	0.0287
265	70000	2.4232	4.8451	11.7409	5.8721	23.4750	0.0287
265	42000	2.4232	4.6231	11.2033	5.8721	21.3744	0.0287
Sum →		22.5387	53.4204	119.7331	51.0149	287.5684	0.2158

Table A.1: Numerical table

A.6.1 Numerical example

Fatigue test results from the numerical example in Section 5.3 of Commentary to Eurocode 3 Part 1-9 (p.122 in [29]) are considered; the experimental stress ranges, S , and number of cycles to failure, N , are presented in the first two columns of Table A.1.

The S-N curve parameters and the sums of square deviations are computed by using numerical results presented in Table A.1:

$$\hat{m}_1 = \frac{n \cdot \sum_{i=1}^n (x_i \cdot y_i) - \sum_{i=1}^n x_i \cdot \sum_{i=1}^n y_i}{n \cdot \sum_{i=1}^n (x_i)^2 - \left(\sum_{i=1}^n x_i \right)^2} = \frac{10 \cdot 119.7331 - 22.5387 \cdot 53.4204}{10 \cdot 51.0149 - 22.5387^2} = -3.102$$

$$\hat{m}_0 = \bar{y} - \hat{m}_1 \bar{x} = 12.334$$

$$S_{xx} = \sum_{i=1}^n x_i^2 - \frac{\left(\sum_{i=1}^n x_i \right)^2}{n} = 51.0149 - \frac{22.5387^2}{10} = 0.216$$

$$S_{yy} = \sum_{i=1}^n y_i^2 - \frac{\left(\sum_{i=1}^n y_i \right)^2}{n} = 287.5684 - \frac{53.4204^2}{10} = 2.194$$

$$S_{xy} = \sum_{i=1}^n x_i \cdot y_i - \frac{\sum_{i=1}^n y_i \cdot \sum_{i=1}^n x_i}{n} = 119.7331 - \frac{22.5387 \cdot 53.4204}{10} = -0.669$$

where $n = 10$ is the sample size.

The logarithm of the stress range at $2 \cdot 10^6$ cycles, on the mean regression line, is:

$$x_{cLS} = \frac{\log(2 \cdot 10^6) - \hat{m}_0}{\hat{m}_1} = \frac{\log(2 \cdot 10^6) - 12.334}{-3.102} = 1.945$$

The sample standard deviation is:

$$\hat{\sigma} = \sqrt{\frac{S_{yy} - \hat{m}_1 \cdot S_{xy}}{n-2}} = \sqrt{\frac{2.194 + 3.102 \cdot (-0.669)}{8}} = 0.1214$$

IIW approach

By using $t_{.125,8} = -1.240$ and $\chi^2_{.125,8} = 3.797$ in Equation A.19, the characteristic S-N curve for the considered data-set is obtained:

$$y = \hat{m}_0 + \left(\frac{t_{.125,n-2}}{\sqrt{n}} - 1.645 \sqrt{\frac{8}{\chi^2_{.125,8}}} \right) \cdot \hat{\sigma} + \hat{m}_1 x = 12.334 - 0.338 - 3.102 \cdot x$$

The characteristic value of the logarithm of the stress range at $2 \cdot 10^6$ cycles is:

$$x_c = \frac{\log(2 \cdot 10^6) - 12.334 + 0.338}{-3.102} = 1.836$$

It follows:

$$S_c = 10^{x_c} = 68.53 \text{ MPa}$$

Eurocode approach

By using $t_{.05,8} = -1.860$ in Equation A.22, the characteristic S-N curve for the considered data-set is obtained:

$$y = \hat{m}_0 + t_{.05,n-2} \cdot \hat{\sigma} \cdot \sqrt{1 + \frac{1}{n} + \frac{(x_{CLS} - \bar{x})^2}{\sum_{i=1}^n (x_i - \bar{x})^2}} + \hat{m}_1 x = 12.334 - 0.280 - 3.102 \cdot x$$

The characteristic value of the logarithm of the stress range at $2 \cdot 10^6$ cycles is:

$$x_c = \frac{\log(2 \cdot 10^6) - 12.334 + 0.280}{-3.102} = 1.854$$

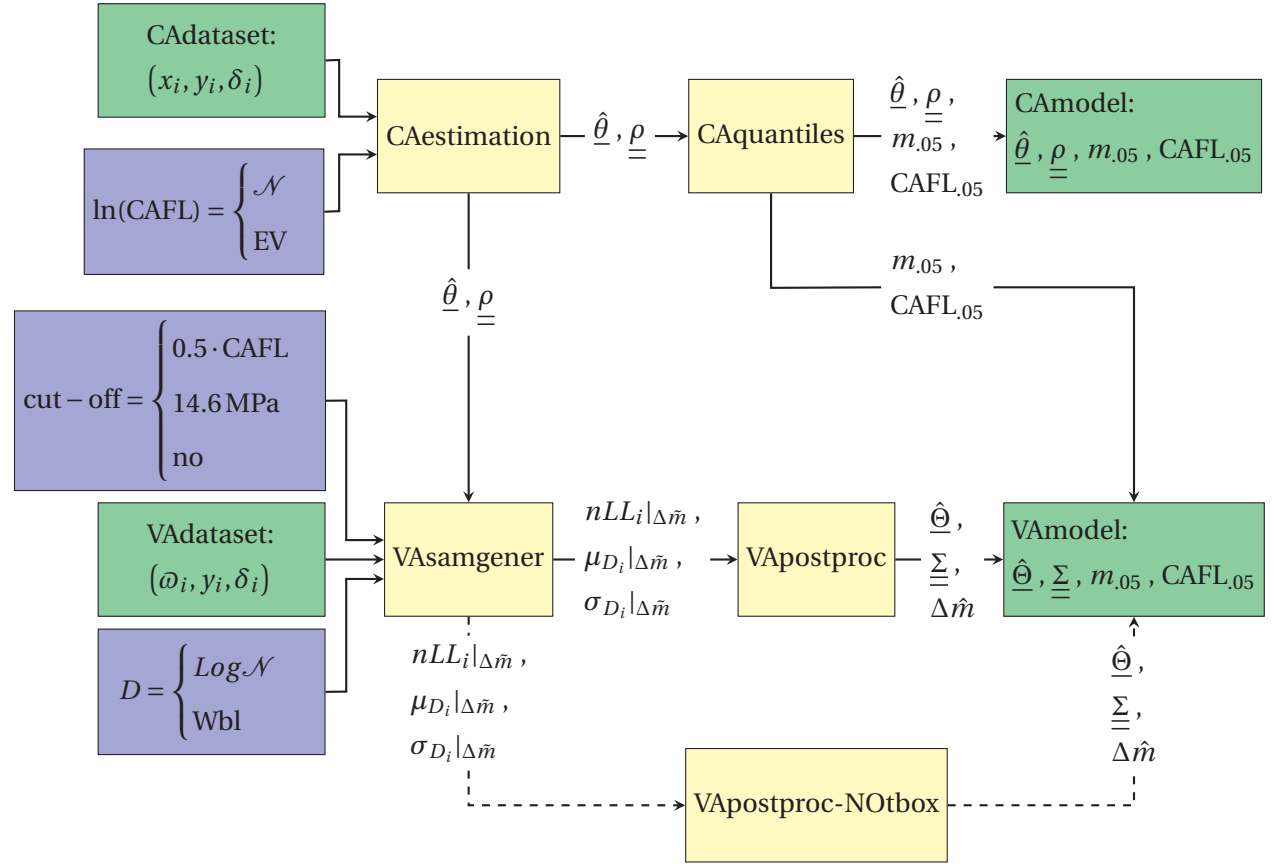
It follows:

$$S_c = 10^{x_c} = 71.50 \text{ MPa}$$

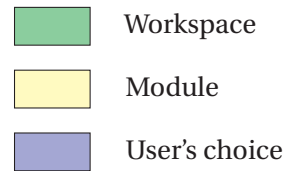
In this case Eurocode approach gives slightly higher estimate of the characteristic strength at $2 \cdot 10^6$ cycles, with respect to IIW approach (+ 4.4%).

B Matlab Toolboxes

B.1 Toolbox TB1

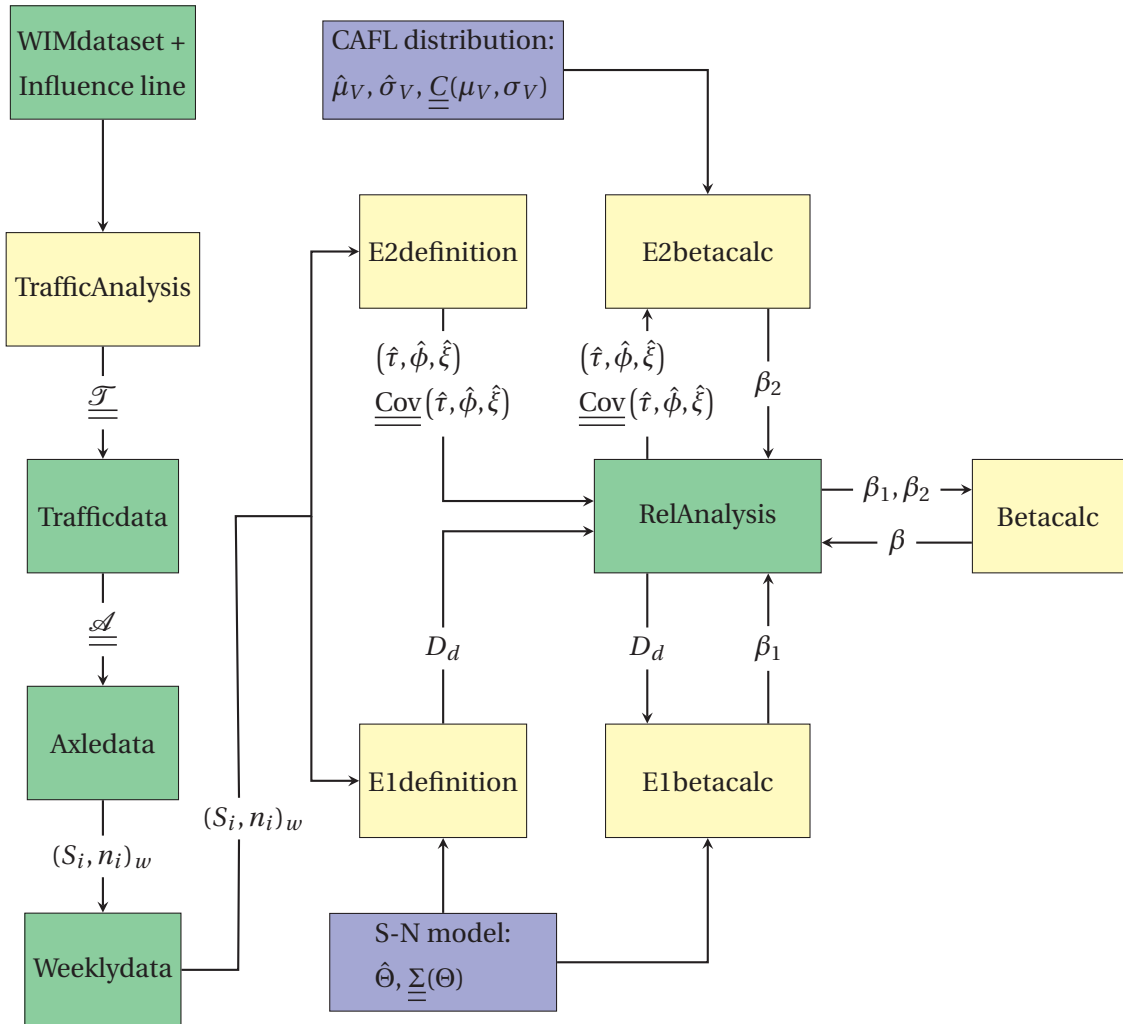


Legend:

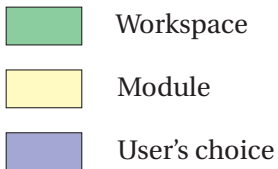


This Toolbox is available for download at: <https://infoscience.epfl.ch/record/213809?ln=en>

B.2 Toolbox TB2

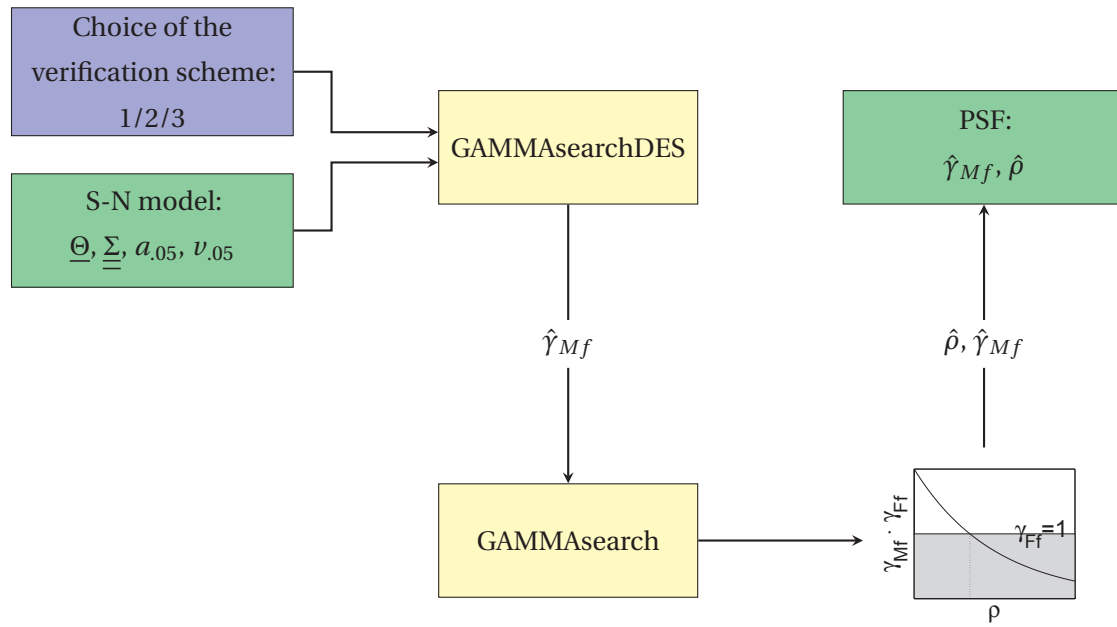


Legend:

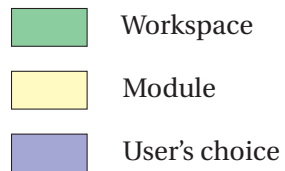


This Toolbox is available for download at: <https://infoscience.epfl.ch/record/213809?ln=en>

B.3 Toolbox TB3



Legend:



This Toolbox is available for download at: <https://infoscience.epfl.ch/record/213809?ln=en>

Bibliography

- [1] ASTM Standard E1049, 2001. In R F Allen, N C Baldimi, E L Gutman, E Keefe, C M Leinweber, V A Mayer, P A McGee, K A Peters, T J Sandler, A Whealen, and R F Wilhelm, editors, *Annual Book of ASTM Standards*, pages 739–748. ASTM, Lausanne, 2001.
- [2] AASHTO. AASHTO LFRD Bridge Design Specifications Customary U.S. Units, 2012.
- [3] P Albrecht, H Lu, K Jung, H J Liu, and J G Cheng. Long life variable-amplitude fatigue strength of welded steel bridge details. Technical report, Federal Highway Administration, Lausanne, 1994.
- [4] P Albrecht and K Yamada. Simulation of service fatigue loads for short span highway bridges. In *ASTM STP 671*, Lausanne, 1979.
- [5] Pedro Albrecht and Akhrawat Lenwari. Variable-Amplitude Fatigue Strength of Structural Steel Bridge Details: Review and Simplified Model. *Journal of Bridge Engineering*, 14(4):226–237, 2009.
- [6] Doobyong Bae. Experimental study on fatigue strength of in-plane welded gusset joints. *KSCE Journal of Civil Engineering*, 8(1):89–93, 2004.
- [7] S F Bailey. *Basic principles and load models for the structural safety evaluation of existing road bridges*. PhD thesis, Ecole Polytechnique Fédérale de Lausanne, Lausanne, 1996.
- [8] Claudio Baptista. *Multiaxial Fatigue In Welded Steel Bridge Analysis. DRAFT November 2015*. PhD thesis, Lausanne, 2015.
- [9] D Benoit, H P Lieurade, and M Truchon. Fatigue behaviour under programmed loading of welded cruciform and butt joints in steel E355. ECSC Report 6210. Technical report, Lausanne, 1977.
- [10] S Berge. Residual stress and stress interaction in fatigue testing of welded joints. Report SK/R55. Technical report, University of Trondheim, Lausanne, 1981.

Bibliography

- [11] J Bogren and L Lopez Martinez. Spectrum fatigue testing and residual stress measurements on non-load carrying fillet welded test specimens. In A.F. Blom, editor, *Proceedings of the Nordic Conference on Fatigue*, Lausanne, 1993. EMAS.
- [12] E Brühwiler and Jean-Paul Lebet. Updating of traffic loads on existing bridges. In IABSE, editor, *Codes in Structural Engineering Developments and Needs for International Practice*, Lausanne, 2010.
- [13] O Burdet. Pont sur la Venoge (VD) côté Jura , après la solidarisation, Rapport d’essai de charge statique. Technical Report Vd, EPFL, IBAP, Lausanne, 1997.
- [14] Z. W. Chen, Y. L. Xu, and X. M. Wang. SHMS-Based Fatigue Reliability Analysis of Multi-loading Suspension Bridges. *Journal of Structural Engineering*, 138(3):299–307, 2012.
- [15] Stuart G. Coles. *An introduction to Statistical Modeling of Extreme Values*. Lausanne, 2001.
- [16] C Crespo-Minguillón and JR Casas. A comprehensive traffic load model for bridge safety checking. *Structural Safety*, 19(4):339–359, 1997.
- [17] L D’Angelo. Calibration of Finite Element Model of Venoge Bridge. EPFL-REPORT-210514. Technical report, EPFL, Lausanne, 2013.
- [18] L D D’Angelo, A Nussbaumer, M Fénart, and A Dumont. Fatigue life assessment of existing motorway bridge. In A Zigoni, editor, *Proceedings of 5th International Conference on Structural Engineering, Mechanics and Computation, Cape Town, September 2-5, 2013*, volume 5, pages 757–761, Lausanne, 2013.
- [19] T de Oliveira. *Threshold methods for sample extremes*. Reidel Dordrecht, Lausanne, 1984.
- [20] Elber W. Fatigue Crack Closure Under Cyclic Tension. *Engineering Fracture Mechanics*, 2(1):37–45, 1970.
- [21] B Ellingwood, James G MacGregor, T V Galambos, and C A Cornell. Load Factors and Load Combinations. *Journal of the Structural Division*, 108(5):978–997, 1982.
- [22] T Endo, K Mitsunaga, K Takahashi, K Kobayashi, and M Matsuishi. Damage evaluation of metals for random or varying loading: three aspects of rain flow method. In *Proceedings of Symposium on Mechanical Behaviors of Materials*, pages 371–380, Lausanne, 1974.
- [23] European Committee for Standardization. Eurocode EN 1990 - Basis of structural design, 2001.

-
- [24] European Committee for Standardization. Eurocode 3: Design of steel structures - Part 1-9: Fatigue, 2005.
- [25] M H Faber and J D Sørensen. Applications of Statistics and Probability in Civil Engineering. In A Der Kiureghian, S Madanat, and J M Pestana, editors, *Proceedings of the 9th International Conference on Applications of Statistics and Probability in Civil Engineering*, pages 927–935, Lausanne, 2003. Millpress.
- [26] John W Fisher, A Nussbaumer, Peter B Keating, and B T Yen. Resistance of Welded Details Under Variable Amplitude Long-Life Fatigue Loading. Technical report, National Cooperative Highway Research Program, Lausanne, 1993.
- [27] John W Fisher and Robert E Slockbower. Fatigue resistance of full scale cover-plated beams. Technical report, Fritz Engineering Laboratory, Lausanne, 1977.
- [28] N E Frost, K J Marsh, and L P Pook. *Metal fatigue*. Dover, Lausanne, 1999.
- [29] Sedlacek G, A Hobbacher, A Nussbaumer, J Stotzel, and D Schafer. Commentary to Eurocode 3. Part 1-9 - Fatigue, 2014.
- [30] E Gassner. Endurance stresses and fatigue life of a mild steel weld under different types of load spectra. *Welding Research Abroad*, 11(4):23–477, 1965.
- [31] Z Guédé, B Sudret, and M Lemaire. Life-time reliability based assessment of structures submitted to thermal fatigue. *International Journal of Fatigue*, 29(7):1359–1373, 2007.
- [32] Tong Guo, Dan M. Frangopol, and Yuwen Chen. Fatigue reliability assessment of steel bridge details integrating weigh-in-motion data and probabilistic finite element analysis. *Computers and Structures*, 112-113:245–257, 2012.
- [33] Tim Gurney. *Fatigue of welded structures*. Cambridge University Press, Lausanne, 2nd edition, 1979.
- [34] Tim Gurney. Fatigue tests on fillet welded joints under variable amplitude loading. TWI Research Report, No. 293/1985. Technical report, Lausanne, 1985.
- [35] Tim Gurney. Fatigue tests on fillet welded joints in steel under simulated wide band type loading. TWI Research Report, No. 365/1988. Technical report, Lausanne, 1988.
- [36] E Haibach. *Modifizierte lineare Schadensakkumulations-Hypothese zur Berücksichtigung des Dauerfestigkeitsabfalls mit fortschreitender Schädigung*. , Juli 1970, TM Nr. 50/70. Laboratorium für Betriebsfestigkeit, Lausanne, 1970.

Bibliography

- [37] E Haibach. The allowable stresses under variable amplitude loading of welded joints. In The Welding Institute, editor, *Proceedings of the conference on fatigue of welded structures*, pages 328–346, Lausanne, 1971.
- [38] A M Hasofer and N C Lind. An exact and invariant first order reliability format. *Journal of the Engineering Mechanics Division ASCE*, 100:111–121, 1974.
- [39] Hirt and M Crisinel. La resistance à la fatigue des poutres en âme pleine composées-soudées. Technical report, École Polytechnique Fédérale de Lausanne, Lausanne, 1975.
- [40] A Hobbacher. IIW document IIW-xxxx-13 Recommendations for fatigue design of welded joints and components, 2013.
- [41] Joint Committee Structural Safety. JCSS Probabilistic Model Code: Resistance Models, 2013.
- [42] W. S. Kim and I. Lotsberg. Fatigue Test Data for Welded Connections in Ship-Shaped Structures. *Journal of Offshore Mechanics and Arctic Engineering*, 127(4):359, 2005.
- [43] A Kondo. Fatigue under Variable Amplitude Loading. In R O Ritchie and Y Murakami, editors, *Comprehensive Structural Integrity*, chapter 4.10, pages 253–278. Lausanne, 2003.
- [44] A Kondo and K Yamada. Variable amplitude fatigue tests of in-plane gussets in long life region. *Journal of Structural Engineering*, 48A, 2002.
- [45] T Lassen, Ph Darcis, and N Recho. Fatigue Behavior of Welded Joints Part 1 — Statistical Methods for. *Supplement to the Welding Journal*, (December):183–187, 2005.
- [46] T Lassen and N Recho. *Fatigue Life Analyses of Welded Structures*. Wiley-ISTE, Lausanne, 2006.
- [47] S J Maddox. Influence of Tensile Residual Stresses on the Fatigue Behavior of Welded Joints in Steel. *ASTM STP 776*, pages 63–96, 1982.
- [48] G Marquis. Long life spectrum fatigue of carbon and stainless steel. *Fatigue & Fracture of Engineering Materials and Structures*, 19(6):739–753, 1996.
- [49] MATLAB. *version R2014a*. The Mathworks Inc., Lausanne, 2010.
- [50] R C McClung. A literature survey on the stability and significance of residual stresses during fatigue. *Fatigue & Fracture of Engineering Materials and Structures*, 30(3):173–205, 2007.

-
- [51] Thierry Meystre and Manfred A Hirt. Evaluation de ponts routiers existants avec un modèle de charge de trafic actualisé, Mandat de recherche AGB 2002/005, 2006.
- [52] Russell B Millar. *Maximum Likelihood Estimation and Inference: With Examples in R, SAS and ADMB*. Lausanne, 2011.
- [53] M A Miner. Cumulative damage in fatigue. *Journal of Applied Mechanics*, 12:159–164, 1945.
- [54] MSC Software. MSC Nastran Quick Reference Guide, 2012.
- [55] Wayne Nelson. Fitting of Fatigue Curves with Nonconstant Standard Deviation to Data with Runouts. *Journal of Testing and Evaluation*, 12:69–77, 1984.
- [56] Wayne Nelson. *Accelerate Testing: Statistical Models, Test Plans, and Data Analyses*. Lausanne, 1990.
- [57] P Paris and F Erdogan. A critical analysis of crack propagation laws. *Journal of Basic Engineering*, 85:528–534, 1960.
- [58] Francis G Pascual and William Q Meeker. Estimating Fatigue Curves With the Random Fatigue-Limit Model. *Technometrics*, 1999.
- [59] H Polezhayeva. Fatigue testing on welded panels. MPD/10/05, 2010.
- [60] M K Ravindra and T V Galambos. Load and Resistance Factor Design for Steel. *Journal of the Structural Division*, 104(9):1337–1353, 1978.
- [61] Reliability Consulting Programs (RCP). STRUREL, a Structural Reliability Analysis Program-System, COMREL & SYSREL: Users Manual, 2004.
- [62] J. Rörup and Fricke. Mean compressive stresses - Experimental and theoretical investigations into their influence on the fatigue strength of welded structures. *The Journal of Strain Analysis for Engineering Design*, 40(1):631–642, 2005.
- [63] J. Rörup and H Petershagen. The effect of compression mean stresses on the fatigue strength of welded structures. *Welding in the World*, 44(5):20–25, 2000.
- [64] C Sanger, R McDonald, and P Kurath. Prediction of Welding Residual Stresses and Redistribution/Relaxation due to Cyclic Loading. In *SAE 2006 World Congress and Exhibition*, Lausanne, 2005.
- [65] J Schijve. The analysis of random load-time histories with relation to fatigue tests and life calculations. In W Barrois and E L Ripley, editors, *Fatigue of aircraft structures*, page 115. Pergamon, Lausanne, 1966.

Bibliography

- [66] C G Schilling. Variable amplitude load fatigue, Task A - Literature Review. Volume I. Traffic loading and bridge response. Interim report, 1990.
- [67] C G Schilling, K Klippenstein, J M Barsom, and G T Blake. Fatigue of welded steel bridge members under variable amplitude loadings, NCHRP Final Report 12. Technical report, Lausanne, 1975.
- [68] C Sonsino. Course of SN-curves especially in the high-cycle fatigue regime with regard to component design and safety. *International Journal of Fatigue*, 29(12):2246–2258, December 2007.
- [69] C Sonsino, S J Maddox, and A Hobbacher. Fatigue life assessment of welded joints under variable amplitude loading. State of the present knowledge and recommendations for fatigue design regulations. In *IIW International Conference on Technical Trends and Future Prospectives of Welding Technology for Transportation, Land, Sea, Air and Space 2004. Osaka, Japan*, pages 84–99, Lausanne, 2004.
- [70] J Spindel and E Haibach. The method of maximum likelihood applied to the statistical analysis of fatigue data. *International Journal of Fatigue*, 1(April):81–88, 1979.
- [71] B Sudret and Z Guede. Probabilistic assessment of thermal fatigue in nuclear components. *Nuclear Engineering and Design*, 235(17-19):1819–1835, 2005.
- [72] S Suresh. *Fatigue of Materials*. Cambridge University Press, Lausanne, 2004.
- [73] Technical European Convention for Constructional Steelwork - TC6. Recommendations for the fatigue design of steel structures, 1985.
- [74] The British Standards Institution. BS7608:1993 Code of practice for fatigue design and assessment of steel structures, 1993.
- [75] Mark Anthony Treacy. *The use of monitored data in the verification of structural and fatigue safety of existing post-tensioned concrete highway bridges*. PhD thesis, Lausanne, 2014.
- [76] M Vormwald and T Seeger. Consideration of fatigue damage below the endurance limit in life predictions for variable amplitude loadings. In *Proceedings of the Fourth International Conference on Fatigue and Fatigue Thresholds*, pages 517–523, Lausanne.
- [77] Dennis D Wackerly, William Mendenhall, and Richard L Scheaffer. *Mathematical Statistics, with Application*. Thomson, Lausanne, 7th edition.

- [78] Welding Institute. *Fatigue performance of welded high strength steels: a compendium of reports from a sponsored research programme*. Report series. Welding Institute, Lausanne, 1974.
- [79] C H Whang. *Introduction to fracture mechanics*. DSTO Aeronautical and Maritime Research Laboratory, Lausanne, 1996.
- [80] A Wöhler. Theorie rechteckiger eiserner Brückenbalken mit Gitterwänden und mit Blechwänden. *Zeitschrift für Bauwesen*, 5:121–166, 1855.
- [81] Y Zhang and S Maddox. Investigation of fatigue damage to welded joints under variable amplitude loading spectra. *International Journal of Fatigue*, 31(1):138–152, 2009.

Luca D'Angelo | MSc

Passage F.-L. Bocion 4 – 1007, Lausanne, Switzerland
☎ +41 (0) 78 6486135 • ✉ luca.dangelo@outlook.com
🌐 <https://ch.linkedin.com/in/lucadangelo83>

Work Experience

EPFL, ICOM <i>PhD Candidate</i> Thesis: Probabilistic approach for fatigue evaluation of welded connections with focus on road steel bridges	Lausanne, Switzerland 02/2012–12/2015
Sky Aircraft <i>Stress Engineer</i> SKYLANDER SK105 program (new twin turboprop light skyaircraft)	Base Aérienne de Chambley, Onville, France 03/2010–01/2012
DTU, MEKANIK <i>Research Assistant</i> Micro alloyed high strength net shape components	Kgs. Lyngby, Denmark 09/2008–02/2010
IMAST Technological district <i>Training course</i> Polymers and composite materials	Naples, Italy 04/2008–08/2008

Education

Phd in Civil Engineering <i>EPFL, ICOM</i> Thesis: Probabilistic approach for fatigue evaluation of welded connections with focus on road steel bridges	Lausanne, Switzerland 02/2012–12/2015
MSc in Aerospace and Astronautic Engineering <i>University Federico II, Summa cum Laude</i> Thesis: High fidelity structural analysis of aircraft engine and wind turbine blades	Naples, Italy 11/2005–01/2008
Exchange student, Erasmus project <i>Aerospace Dept., University of Glasgow</i>	Glasgow, Scotland 01/2007–06/2007
BSc in Aerospace Engineering <i>University Federico II, Summa cum Laude</i> Thesis: New method for prediction and calculation of fracture mechanism	Naples, Italy 11/2002–11/2005

PhD Thesis

Title: Probabilistic approach for fatigue evaluation of welded connections with focus on road steel bridges

Supervisor: Prof. Alain Nussbaumer

Description: Re-definition of fatigue resistance S-N curves using Maximum Likelihood method and Monte-Carlo Simulations approach. New framework for fatigue reliability assessment of road bridges under the long-term effect of traffic. Calibration of fatigue partial safety factors for fatigue design.

Languages

Italian: Mother tongue

English: Full professional proficiency

French: Full professional proficiency

Technical skills

- o Structural reliability analysis
- o Probabilistic models
- o Risk assessment
- o Finite element analysis
- o Numerical analysis
- o Simulations

Softwares

- o Matlab
- o MSC Nastran, Patran
- o Abaqus
- o R, C++
- o MS Office package
- o LaTeX

Honors and awards

- o EDCE Mobility award, EPFL, Lausanne (Switzerland), November 2013
- o PIROS Industrial fellowship, IMAST technological district, Naples (Italy), April 2008
- o Top degree in MSc, January 2008
- o Top degree in BSc, November 2005

References

Prof. Alain Nussbaumer

Director of Steel Structures Laboratory (ICOM)
EPFL, Lausanne, Switzerland
✉ alain.nussbaumer@epfl.ch

Joseph Bartholomé

Head of structures
SONACA, Gosselies, Belgium
✉ jbartholome@skynet.be

Prof. Niels Skat Tiedje

Associate Professor
DTU, Kgs. Lyngby, Denmark
✉ nsti@mek.dtu.dk

Prof. Michael Havbro Faber

Head of Civil Engineering Dept.
DTU, Kgs. Lyngby, Denmark
✉ mihf@byg.dtu.dk

Maurice Elkaim

Technical Director
GECI Systems, Paris, France
✉ maurice.elkaim@geci.net

Prof. Leonardo Lecce

Full Professor
University Federico II, Naples, Italy
✉ leonardo.lecce@unina.it

Journal Publications

- D'Angelo, L. and A. Nussbaumer (2015). "Reliability based fatigue assessment of existing motorway bridge". In: *Structural Safety* 57, pp. 35–42.
- Pasquier, R., L. D'Angelo, J.-A. Goulet, C. Acevedo, A. Nussbaumer, and I.F.C. Smith (2015). "Measurement, data interpretation and uncertainty propagation for fatigue assessments of structures". In: *Journal of Bridge Engineering* xx, pp. xx–xx.

Conference Publications

- D'Angelo, L., M. H. Faber, and A. Nussbaumer (2015). "Calibration of partial safety factors for fatigue design of steel bridges". In: *12th International Conference on Applications of Statistics and Probability in Civil Engineering (ICASP12)*.
- D'Angelo, L., M. Rocha, A. Nussbaumer, and E. Brühwiler (2014). "S-N-P Fatigue Curves using Maximum Likelihood". In: *7th European Conference on Steel and Composite Structures (EUROSTEEL)*.
- D'Angelo, L., A. Nussbaumer, M.-A. Fénart, and A.-G. Dumont (2013). "Fatigue Life Assessment of Existing Motorway Bridge". In: *5th International Conference on Structural Engineering, Mechanics and Computation (SEMC)*.